WELL-DEFINED ULTRATHIN Pd FILMS ON Pt(111): ELECTROCHEMICAL PREPARATION AND INTERFACIAL CHEMISTRY

A Dissertation

by

YEON SU PARK

Submitted to the Office of Graduate Studies of
Texas A&M University
in partial fulfillment of the requirements for the degree of

DOCTOR OF PHILOSOPHY

May 2005

Major Subject: Chemistry

WELL-DEFINED ULTRATHIN Pd FILMS ON Pt(111): ELECTROCHEMICAL PREPARATION AND INTERFACIAL CHEMISTRY

A Dissertation

by

YEON SU PARK

Submitted to Texas A&M University
in partial fulfillment of the requirements
for the degree of

DOCTOR OF PHILOSOPHY

Approved as to style and content by:

Manuel P. Soriaga (Chair of Committee)	Gyula Vigh (Member)
D. Wayne Goodman (Member)	Donald G. Naugle (Member)
	Emile A. Schweikert (Head of Department)

May 2005

Major Subject: Chemistry

ABSTRACT

Well-Defined Ultrathin Pd Films on Pt(111):

Electrochemical Preparation and Interfacial Chemistry. (May 2005)

Yeon Su Park, B.S., Korea University; M.S., Korea University

Chair of Advisory Committee: Dr. Manuel P. Soriaga

Well-defined ultrathin films of palladium, with coverages ranging from submonolayer, Θ_{Pd} = 0.5 monolayer (ML), to multilayer, Θ_{Pd} = 8 ML, were electrochemically deposited on Pt(111) using potentiostatic and potentiodynamic methods. In both methods, between the coverage regimes studied, the growth of the Pd films follows the Stranski-Krastanov mechanism.

The interfacial electrochemical properties associated with the film-to-bulk transition were characterized by conventional voltammetric techniques in combination with low-energy electron diffraction (LEED) and Auger electron spectroscopy (AES). The voltammetric peaks associated with H-atom adsorption and desorption on terrace sites indicate that the Pd electrodeposit starts to exhibit bulk-like properties at a coverage of 3 ML.

Voltammetric cycling, in sulfuric acid solution, between the hydrogen evolution and the double-layer regions, was found to exert minimal influence on the annealing (smoothening) of the electrodeposited Pd films. However, cycling within the same potential region in the presence of bromide anions (at which Br^- adsorption/Br

desorption takes place) smoothens the initially rough Pd films essentially as well as high-temperature annealing.

The influence of chemisorbed bromine on the anodic dissolution of Pd was also studied; this was for comparison with previous work on the anodic dissolution of Pd, in inert electrolyte, catalyzed by chemisorbed iodine. The present studies indicated that a small but measurable amount of bromine was desorbed along with dissolution of the Pd step atoms; bromine at the Pd terrace behaved identically to iodine in that the coverage of iodine is maintained regardless of the amount or origin of the of anodically stripped Pd.

Atomically smooth, well-defined ultrathin Pd films were prepared by a constant potential deposition (CPD) method followed by multiple potential cycles, in dilute Br^- solution, within the double-layer region and reductive removal of Br_{ads}, by simple emersion at a potential just before the hydrogen evolution reaction potential (E_{HER}). A previously adapted method for the same purpose involved the chemisorption of iodine onto ultrathin Pd_{CPD} films, from dilute I^- solution, followed by reductive desorption of I_{ads} in iodide-free solution at pH 10 and at a potential just before E_{HER}.

ACKNOWLEDGMENTS

My unceasing gratitude goes to Dr. M. P. Soriaga, my advisor and committee chair, for his support, guidance, and encouragement during my stay at Texas A&M University. I gratefully acknowledge all the instructive comments and advice provided by my committee members: Dr. W. Goodman, Dr. Gy. Vigh and Dr. D. Naugle.

To the previous and current members of Dr. Soriaga's research group, specifically Dr. Y.-G. Kim, Dr. C. Wang, Dr. X. Chen, Jean Sanabria-Chinchilla, Juan Cruz, and Ding Li, thank you for embodying an excellent example of *esprit de corps*. Special thanks go to Jack Hess Baricuatro and Mohammad Akhtar Hossain for all the help in conducting my experiments. The writing of this manuscript would have been unbearably arduous without Jack's unsolicited editorial assistance.

The successful completion of this dissertation thrives upon the inspiration coming from my wife, Kyoungok Min, and my son, Sangmin Park. Love and respect go to my parents, brother, sister, and parents-in-laws.

This research was financially supported by the National Science Foundation and the Robert A. Welch Foundation.

TABLE OF CONTENTS

Page

LIST OF FIGURES

FIGURE Page

FIGURE Page

FIGURE Page

FIGURE Page

FIGURE Page

INTRODUCTION

Many interesting processes occur at the electrode-electrolyte interface. Notable examples include metal electrodeposition, metal corrosion, molecular adsorption, oxygen reduction, and methanol oxidation. These processes are associated with many important technologies and industrial applications such as electroplating, batteries, fuel cells, semiconductors, corrosion inhibition, and electroanalytical sensors. Controlling these processes requires the knowledge of the interfacial structure and composition, and their correlation to interfacial reactivity.

A classical description of the electrode-electrolyte interface is shown in Figure 1 [1]. This model describes the electrode surface as the topmost layer of atoms on the electrode and the ensemble of adsorbed solvent and specifically adsorbed species. Between the electrode surface and the bulk solution is an interfacial region of interest. The electrode side of the interface is a narrow region of charge that extends a few angstroms into the bulk. The solution side of the interface is composed of two regions: (i) the compact layer where field-oriented adsorbed water molecules, specifically adsorbed anions and solvated cations exist, and (ii) the diffuse layer where the solvated ions interact with the charged metal surface.

This dissertation follows the style and format of The Journal of Electroanalytical Chemistry.

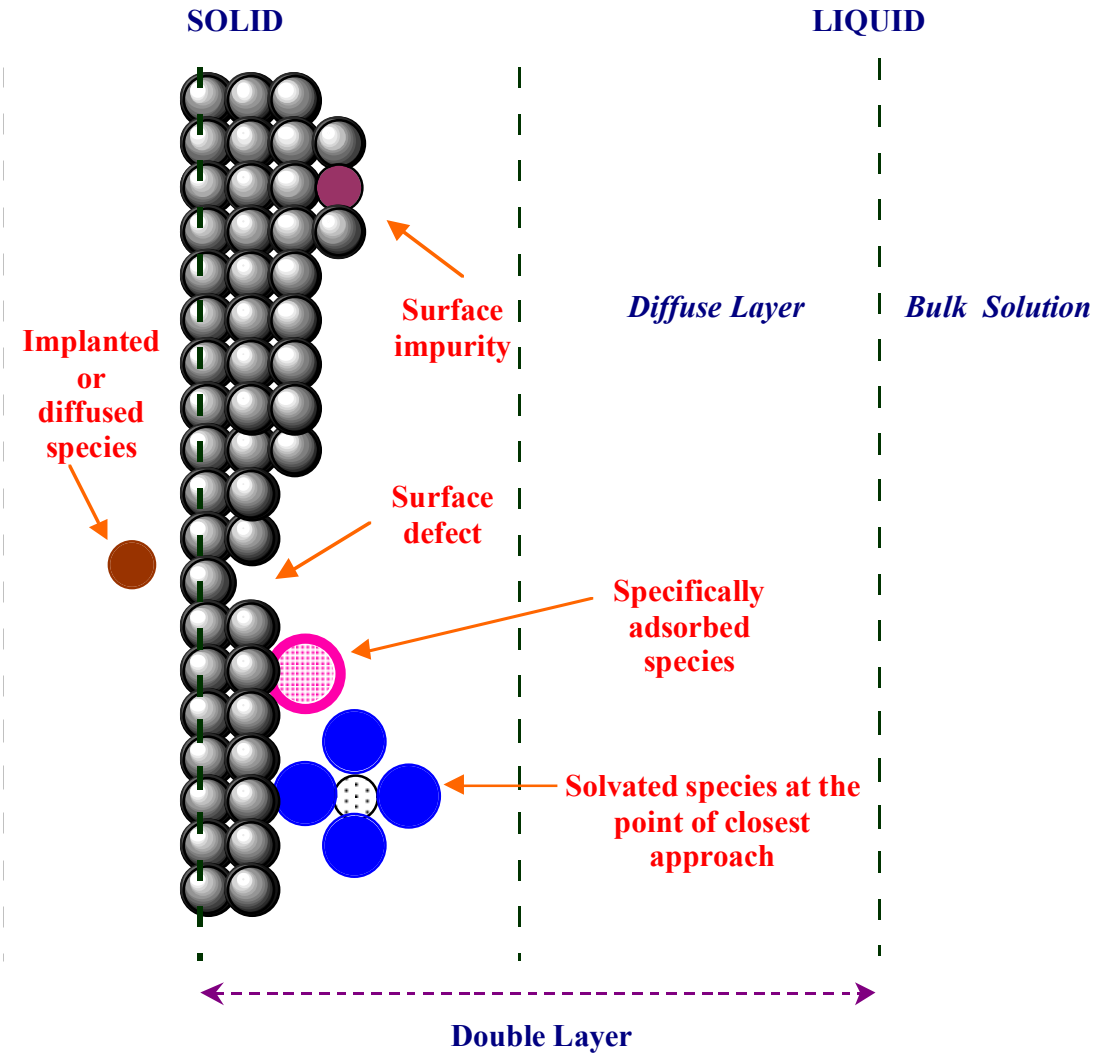

Figure 1. A classical description of the electrode-electrolyte interface: Gouy-Chapman-Stern model [1].

Electrochemical Surface Science

Traditionally, electrochemical techniques such as voltammetry and coulometry have been adapted to study the electrode-electrolyte interface. These techniques rely on the measurement of electric signals associated with oxidation and reduction reactions. The data acquired from these techniques have led to the successful development of thermodynamic description of electrochemical systems. However, the information obtained from traditional electrochemical approaches lacks molecular specificity and, hence, represents only the macroscopic properties of the electrode-electrolyte interface. Such methods are unable to provide detailed information regarding substrate-adlayer interactions or specific chemical changes by the adsorption process. To obtain an atomic-resolved view of electrochemical processes, the use of other interfacial analytical techniques is necessary. In this regard, the union of conventional electrochemistry (EC) and ultrahigh vacuum (UHV) surface analytical techniques (referred to as "UHV-EC approach") has been of great importance.

UHV-EC Approach

One of the primary concerns of electrochemical surface science is to correlate, at the atomic level, surface composition and structure to electrochemical reactivity. In order to minimize ambiguities in the interpretation of empirical data, experimental protocols necessitate the use of: (i) electrode surfaces that are structurally and compositionally well-characterized, (ii) analytical techniques that are surface sensitive, and (iii) a contaminant-free environment.

The experimental approach employed in this study meets the aforementioned requirements by the use of a well-defined Pt single-crystal electrode, ultrahigh vacuum-based modern surface analysis techniques, and high purity reagents and gases. The experimental methodology includes: (1) electrochemistry (EC), (2) Auger electron spectroscopy (AES), and (3) low energy electron diffraction (LEED).

Metal Thin Films on Foreign Metal Substrates

The properties of metal thin films on foreign metal substrates are of great importance in surface science and heterogeneous catalysis [2-4]. These bimetallic systems usually exhibit physicochemical properties that are significantly different from their bulk counterparts [5-6].

Pd thin films deposited on noble metal surfaces have received great attention in recent years due to prospects of catalysis enhancement [5]. Of particular interest is the combination of Pd and Pt which have identical lattice structure, similar atomic radii, comparable lattice energy but different cohesive energy [7]. The relatively low surface energy of Pd favors its deposition onto Pt [8]; epitaxial film growth with minimal lattice strain is expected [9-12]. Structurally bulk-like thin films provide an opportunity to study Pd without perturbation from hydrogen absorption [10]. Surface electrochemistry has been widely adapted in studying the electrochemical and structural properties of these thin films [5-6,11,13-17].

Literature Review

Early studies of Pd thin films on Pt surfaces focused on the influence of underlying polycrystalline substrates on the electrosorption properties of Pd thin films [18]. Pd thin film studies using Pt single crystalline substrates were conducted by Attard and Bannister [19]. The authors investigated voltammetric features of Pd submonolayer and monolayer films electrodeposited on Pt(111) electrodes and reported the observation of reversible hydrogen adsorption peak which was not observed in bulk Pd. Shortly thereafter, Clavilier and co-workers observed a second hydrogen adsorption peak appearing at a slightly positive potential from the first hydrogen adsorption peak [20]. Other studies have shown the existence of hydrogen adsorption peaks for Pd films less than a few monolayer (ML) coverage [6,10-11].

Early studies using electron spectroscopies under ultrahigh vacuum conditions suggested a Frank-van der Merwe (layer-by-layer) growth mode of Pd thin films on Pt(111) [5]. However, recent surface X-ray scattering [6] and electrochemical scanning tunneling microscopic [21] studies revealed evidences of a pseudomorphic Stranski-Krastanov Pd growth mode. Kolb and co-workers [21-22] recently showed that the Pd growth mode and Pd film morphology were very sensitive to electrodeposition conditions such as overpotential and electrolyte composition. For instance, a transition from three-dimensional cluster growth to two-dimensional growth was observed when overpotential was decreased. The presence of sulfate in solution promotes three-dimensional island formation while chloride favors quasi layer-by-layer growth on a pseudomorphic monolayer.

Kinetic properties of Pd thin films formed on Pt single-crystal surfaces have been recently investigated by monitoring some important catalytic processes such as oxidation of formic acid [17,23-24], oxidation of CO [14-15], oxygen reduction reaction (ORR) [24], and hydrogen evolution reaction (HER) [13]. Compared to bulk Pd or unmodified Pt single-crystal surfaces, Pd thin films on Pt single-crystal surfaces generally have enhanced electrocatalytic activity towards formic acid oxidation probably due to a high resistance of the Pd surfaces against CO poisoning [24]. The strong interaction between Pd film and adsorbed hydrogen has been shown to alter the energetics of HER [13]. The low potential of zero charge (pzc) of Pd, along with some anion effects, has been demonstrated to inhibit the ORR [25]. Enhancement of the CO oxidation reaction [14] on Pd thin films is ascribed to the adsorption of hydroxyl anions due to the highly oxophilic nature of Pd thin films.

The presence of strongly adsorbed anions, such as halides, can dramatically alter the properties of noble metals such as Pd and Pt [26]. The structure, composition and electrochemical reactivity of the Pd-halogen interface are influenced by the nature of anions in electrolyte solution, solution pH, and electrode potential [26-28]. Oxidative chemisorption of halides onto Pd surfaces occur from acidic and neutral solutions of halides. Spontaneous chemisorption of iodide [28-29] and potential-controlled chemisorption of bromide and chloride [27-28] have been reported in literature. Chemisorbed halogens form $(\sqrt{3}\times\sqrt{3})R30°$-X (X = I, Br, Cl) adlattices on Pd(111) surfaces in the double-layer region [28-31]. Positive excursion of the adsorption potential generally leads to an increase in the coverage of chemisorbed halogens on bulk

Pd [27-28]. The presence of strongly adsorbed sulfate ions leads to a much narrower potential window for the formation of the $(\sqrt{3}\times\sqrt{3})R30^{o}$-X (X = Br, Cl) adlattices [28].

Exposure of electrochemically disordered Pd(111) surface to dilute aqueous solution of iodide results in well-ordered and highly stable $(\sqrt{3}\times\sqrt{3})R30°$-I structure [32-34]. Subsequent reductive desorption of the chemisorbed iodine regenerates an ordered Pd(111)-(1×1) surface [32-34].

Chemisorption of an iodine monolayer on Pd thin films electrodeposited on Pt(111) electrode has been investigated [31]. For Pd films with thickness less than 2 ML, iodine assumes a (3×3) LEED pattern which is the same adlattice geometry exhibited by iodine on bare Pt(111). Mixed (3×3) and $(\sqrt{3}\times\sqrt{3})$ structures are obtained from Pd films with 2 ML coverage. These results reveal that, using iodine as a surface probe, the Pt(111) substrate influences the Pd adlattice structure up to 2 ML coverage.

Halides in acidic and neutral solutions catalyze Pd dissolution [27-28,31]. Chemisorbed iodine also facilitates the dissolution of Pd in its bulk and thin film states [31]. Chemisorberd bromine, however, has little effect on the dissolution of bulk Pd [27].

Lafferty and co-workers studied the adsorbed iodine-catalyzed anodic stripping of Pd thin films on Pt substrates in dilute sulfuric acid solution [35]. The authors reported selective and quantitative removal of the Pd films and proved the validity of using this method for the coverage determination of Pd thin films on Pt substrates.

Objective

The objectives of this research are: (i) to prepare ultrathin Pd films on Pt(111) surfaces by an electrochemical method, and (ii) to investigate the interfacial structure and electrochemistry of the Pd thin films in inert electrolyte (sulfuric acid) and in the presence of a strongly surface-active anion (bromide). The interfacial chemistry imparted by chemisorbed bromine is to be compared with that induced by chemisorbed iodine; an example of the latter is the layer-by-layer anodic dissolution of Pd catalyzed by a single monolayer of zerovalent iodine atoms. Experimental measurements will be based upon the combination of traditional electrochemical methods, such as cyclic voltammetry, and non-traditional (ultrahigh-vacuum) surface analytical techniques.

METHODOLOGY

Ultrahigh Vacuum (UHV) Surface Analysis

The surface characterization techniques employed in this study use electrons of low kinetic energy either as surface-sensitive probes or signals. At kinetic energies between 10 and 150 eV, the mean free paths of the electrons within a solid lie between 4 to 20 Å, as shown in Figure 2 [36]. These electrons penetrate only the topmost surface layers of the solid and provide unique surface sensitivity. Hence, the techniques that involve low-energy electrons are most suitable for the study of the solid surfaces [36].

Low Energy Electron Diffraction (LEED)

LEED is one of the most commonly adapted techniques to obtain surface crystallographic information. LEED data were acquired with a PE 15-120 LEED Optics and PE 11-020 LEED Electronics system (Perkin-Elmer, Eden Prairie, MN). Figure 3 shows a schematic diagram of the LEED optics system. The optics consists of an electron gun and a display system. The electron gun delivers a monoenergetic electron beam of 10 to 150 eV kinetic energy to the sample surface. The display system is composed of a four-grid retarding field analyzer (RFA) and a concentric phosphor-coated collector screen. The RFA allows only elastically diffracted electrons to be detected at the collector screen. The first grid (G1) is grounded to act as a shield between the negatively biased second (G2) and third grids (G3). These grids block out inelastically diffracted electrons. The elastically diffracted electrons pass through

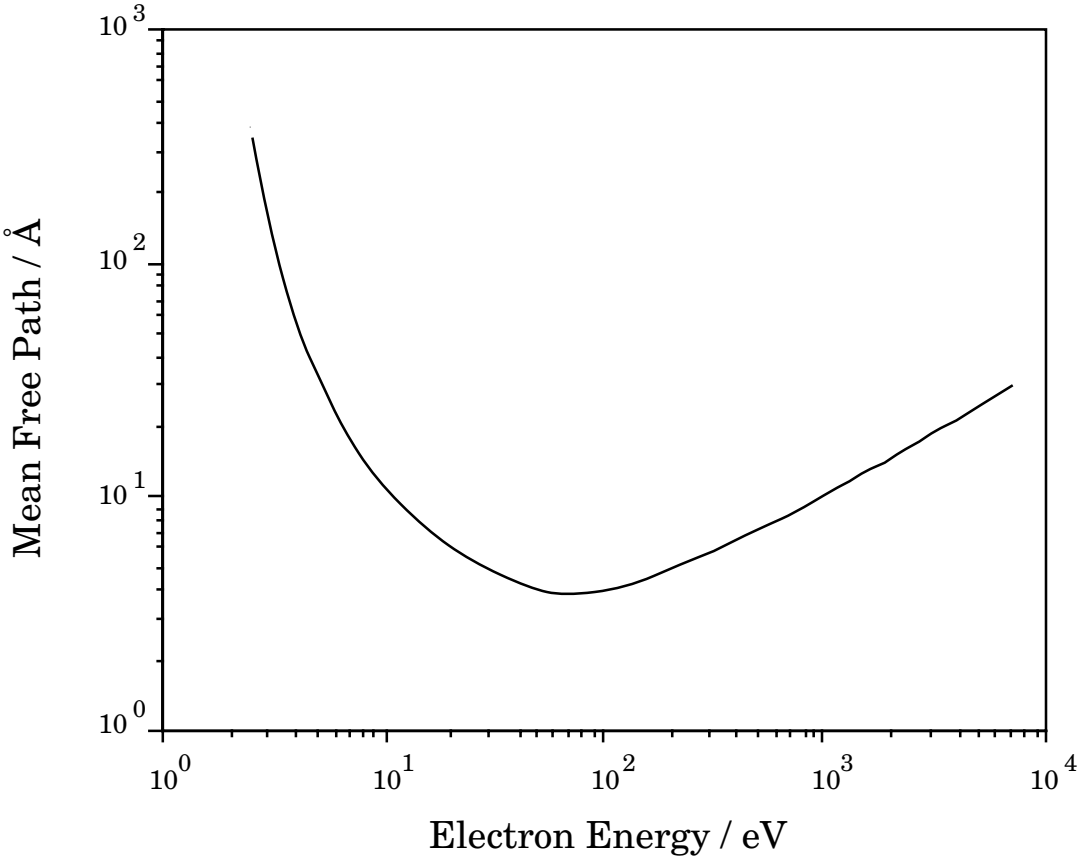

Figure 2. “Universal curve.” Electron mean-free-path as a function of electron kinetic energy [36].

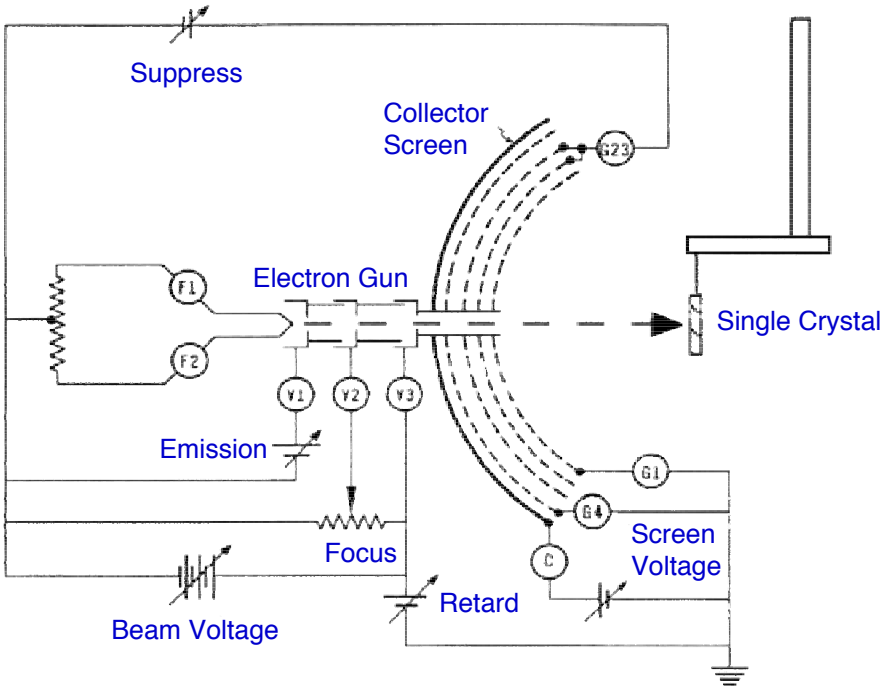

Figure 3. Schematic diagram of the LEED optics.

another shielding grid (G4) and are accelerated by a large potential (2 – 5 kV) onto a phosphor-coated collector screen. A pattern of bright spots is generated on the screen. A Sony DSC 31 digital camera (Sony Electronics, Tokyo, Japan) was used to take photographs of LEED patterns.

LEED takes advantage of the low escape depth of low-energy electrons to produce a diffraction pattern characteristic of the two-dimensional interfacial order. The in-phase elastic scattering of monoenergetic electrons from a periodic array of surface atoms causes constructive interference of the scattered electrons along specific directions. The elastically diffracted electron beams pass through RFA and generate a pattern of the bright spots on a phosphor-coated screen. The pattern produced by the spots varies with the periodicity of the surface lattice and can give information about interfacial structure of the sample. The diffraction pattern is related to the atomic spacing of the sample surface according to the following equation:

$$\sin(\theta) = n\lambda/a \qquad (1)$$

where θ is the angle between the surface normal and the diffracted electron, n is the number of diffracted electron beams, λ is the wavelength of the diffracted electron, and a is the atomic spacing of the solid. This equation indicates that the spacing of the diffraction spots is inversely related to the spacing of the atoms in the surface lattice. Hence, the LEED pattern is in reciprocal space with respect to the surface lattice and must be converted to real space to obtain geometrical information about the unit cell.

The real space lattice can be reconstructed from the LEED pattern using the following vector relationships:

$$\vec{a}^{*} = \frac{\vec{b} \times \vec{z}}{\vec{a} \cdot \vec{b} \times \vec{z}} \tag{2}$$

$$\vec{b}^{*} = \frac{\vec{z} \times \vec{a}}{\vec{a} \cdot \vec{b} \times \vec{z}} \tag{3}$$

where $\vec{a}^{*}$ and $\vec{b}^{*}$ are the reciprocal unit cell vectors, $\vec{a}$ and $\vec{b}$ the real space unit cell vectors, and $\vec{z}$ the surface normal.

The electrode-surface unit mesh was initially established by visual inspection of the diffraction spots. Subsequently, the LEED patterns were compared with those obtained from calculations [37]. Wood's notation [38] was used to describe the structural information derived from the LEED patterns. Figure 4 shows a typical (1×1) LEED pattern for a clean and well-ordered Pt(111) electrode surface.

Auger Electron Spectroscopy (AES)

AES is widely used in probing surface elemental composition. A set of PE AES system (Perkin Elmer, Eden Prairie, MN), which included PE 10-155 Cylindrical-Auger Electron Optics, PE 32-150 Digital AED Control, PE 32-100 Electron Multiplier Supply, PE 11-010 Electron Gun Control, and PE 96B V/f Preamplifier, was used for the surface elemental analysis of the single-crystal electrode. Figure 5 shows the schematic diagram of the AES system. The Optics consists of a cylindrical mirror analyzer (CMA) for electron energy discrimination, a coaxial normal-incidence electron gun, and a variable-

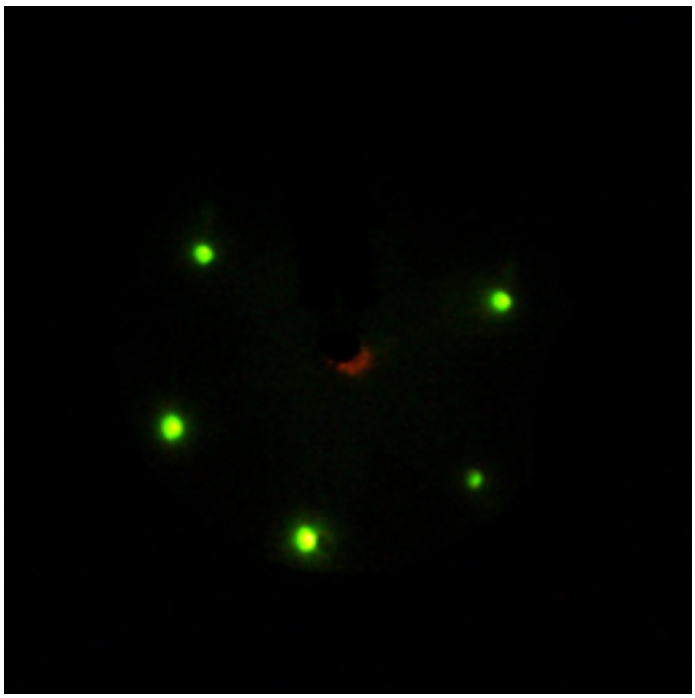

Figure 4. LEED pattern for a clean and well-ordered Pt(111) electrode. Beam energy = 62.0 eV; beam current = 2 μA.

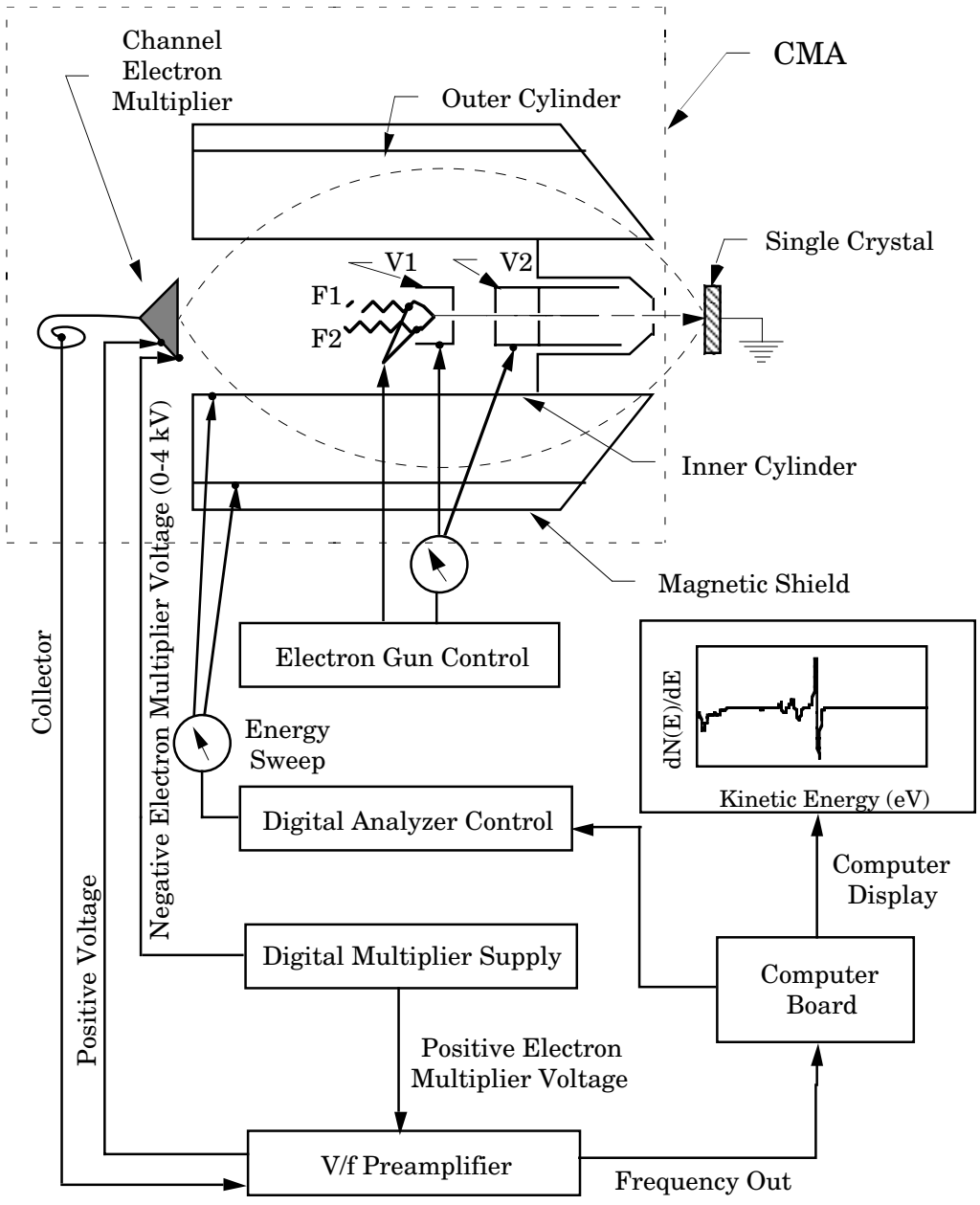

Figure 5. Schematic diagram of the AES system.

gain electron multiplier detector. A beam of monoenergetic electrons (Ep = 2 keV) produced by the electron gun is scattered off the sample surface. The scattered electrons enter the CMA and are repelled from the outer cylinder by a negative DC voltage. The DC voltage is ramped during the data collection scan. Depending upon the specific voltage, only those electrons with the appropriate kinetic energy pass through the exit slit and strike the electron multiplier.

The CMA is designed to operate at high throughput with a constant electron kinetic energy resolution of 0.6%. The resolution of the CMA defines the width of the bandpass window of the analyzed electrons. The band pass window was scanned at 2 eV/s. The electron gun beam current was adjusted to 1 μA above the background current. Low incident currents were selected to minimize electron-beam-induced surface damage.

The Auger process was discovered by Pierre Auger in 1925 while working with X-rays [39]. Figure 6 depicts the Auger process. A high energy electron beam (typically 2 to 10 keV) is directed at the solid surface causing a core-level (K) electron to be ejected. In the decay process, an electron from higher energy level (L_I) fills the vacancy produced. The energy released from this transition can be radiative (X-ray) or nonradiative (Auger). The Auger process occurs when the energy is transferred to another electron in higher energy level (L_{III}) causing this electron ejected. This process is designated as KL_IL_{III} and the ejected electron is called an Auger electron. The kinetic energy E_A of the Auger electron is given by the following equation [40]:

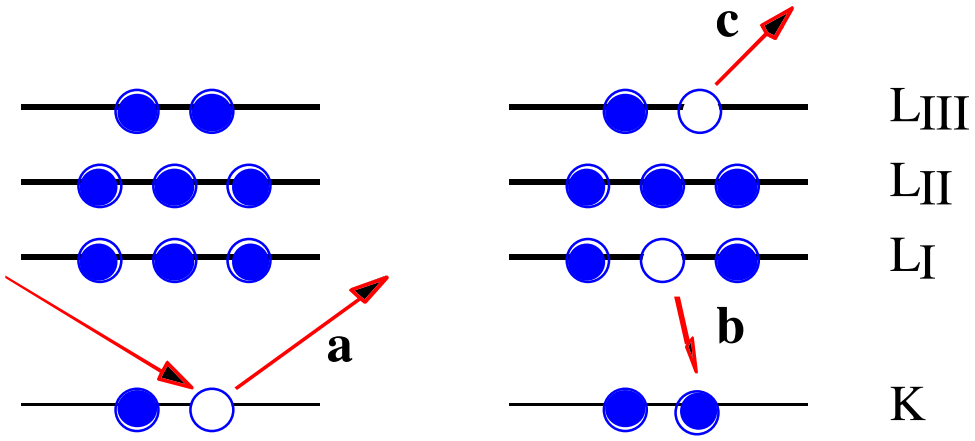

Figure 6. The Auger process. (a) A core level electron is ejected. (b) Electron decays to fill the vacancy. (c) Auger electron is emitted with a kinetic energy related to the binding energies of K, L_I and L_{III}.

$$E_A = E_K - E_{LI} - E_{LIII} - e\Phi_{sp} \quad (4)$$

where E_K, E_{LI} and E_{LIII} are the electron binding energies at the respective electronic levels, e is the electronic charge, and Φ_{sp} is the work function of the spectrometer.

In the Auger process, at least three electrons must be involved; thus, hydrogen and helium cannot be analyzed by AES. Although incident electrons have high energies, emitted Auger electrons generally have much lower kinetic energies so the escape depths of the Auger electrons are within a few angstroms of the solid surface. Hence, AES is still a surface-sensitive technique.

The kinetic energies of the Auger electrons are independent of the incident beam energy used to produce them and are characteristic of their parent atoms. They can, therefore, be used to identify the elemental composition of solid surfaces. The Auger signal from a sample surface is superimposed on a large continuous background of secondary electrons originating from the inelastic scattering of the incident electron beam. The Auger signal-to-noise ratio can be improved through the use of electronic differentiation [40]. In this method, the Auger signal voltage is measured along with the background voltage during the scan of the outer cylinder potential. The resulting signal is converted from voltage to frequency, pre-amplified, and converted to a pulse train. The computer collects the data directly in the N(E) vs. E integral mode and then mathematically differentiates to give the derivative spectrum (dN(E)/dE vs. E). In this mode AES can detect surface contaminants down to 0.1% of a monolayer [41]. Figure 7 is a typical AES spectrum of a clean Pt(111) single crystal.

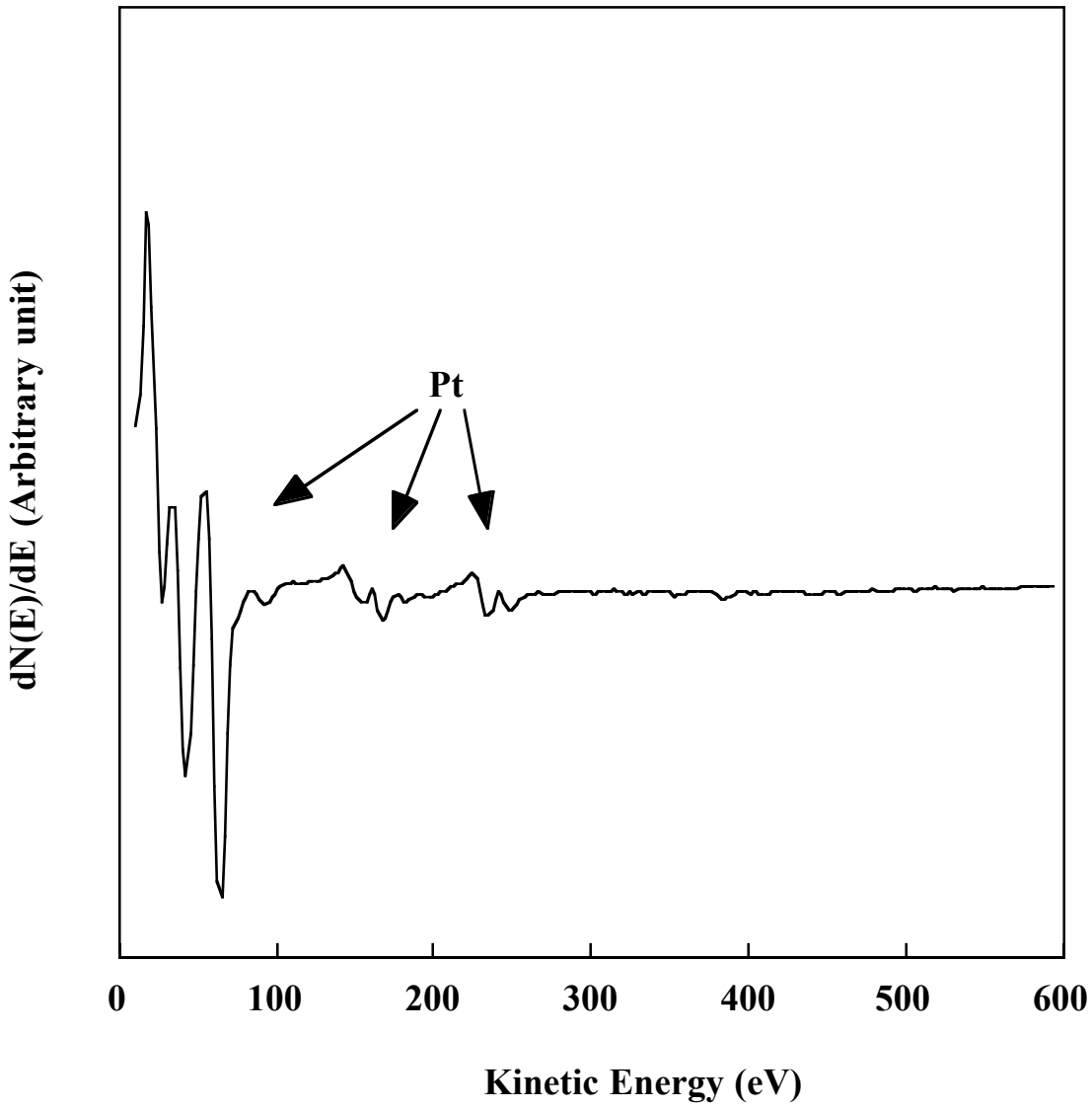

Figure 7. AES spectrum of a clean Pt(111) electrode surface. Incident beam energy = 2 keV; beam current = 1 μA.

Surface coverage of the adsorbate can be extracted from the AES data based upon the following equation [36]:

$$\Gamma_a = \frac{I_a}{I_p \phi_c G_a} \tag{5}$$

where Γ_a is the absolute packing density of the adsorbate (mole/cm^2); I_a, the Auger current for the adsorbate; I_p, the primary beam current; ϕ_c, the measured collection efficiency of the Auger spectrometer; and G_a, the calculated Auger electron yield factor. I_a is obtained from the derivative spectra by double integration of the adsorbate second-harmonic amplitude, A_2, corrected for the clean surface signal, A_{2c} [36]:

$$I_a = \frac{4}{k^2}\int_0^{E_p}\int_0^{E} (A_2 - \Phi_b A_{2c})\, dE'dE \tag{6}$$

where Φ_b compensates for any observed adsorbate-induced attenuation of the substrate signal, and k is the modulation amplitude. The assumption that the clean surface signal provides an appropriate background cannot always be made and several different methods have been proposed for background subtraction. Their advantages and shortcomings are discussed elsewhere [42].

If an independent surface characterization technique is available for calibration purposes, equation 5 can be expressed in purely empirical terms which may be obtained directly from the derivative energy spectra:

$$Q_X = (I'_X/I'_S)B'_X \tag{7}$$

where Q_X is the relative surface coverage (Γ_X/Γ_S), I'_X is the peak height of the adsorbate Auger transition, I'_S is the peak height of an Auger transition for the metal substrate, and B'_X is an empirical calibration factor.

Electrochemistry

Electrochemical experiments were performed using a CV-27 Voltammograph (Bioanalytical Systems, West Lafayette, IN). In this conventional three-electrode potentiostat, potential was applied between a working electrode and a reference electrode and the resulting current flowed through an auxiliary electrode. A Ag/AgCl (1 mM NaCl) electrode was used as the reference electrode. A piece of Pt wire served as the auxiliary electrode. The current or charge (the integration of current) was recorded using a VP-6414S X-Y recorder (Soltec, Sun Valley, CA).

Voltammetry

Voltammetry is an electrochemical method in which current is recorded as a function of applied potential. In linear sweep voltammetry (LSV), electrode potential is changed from an initial (E_i) to a final value (E_f) at a constant rate where $E_i \neq E_f$. In cyclic voltammetry (CV), the applied potential is scanned from E_i to E_f and then returned to E_i at the same rate. A typical voltammogram of a clean and well-ordered Pt(111) bead electrode in 100 mM H_2SO_4 is shown in Figure 8.

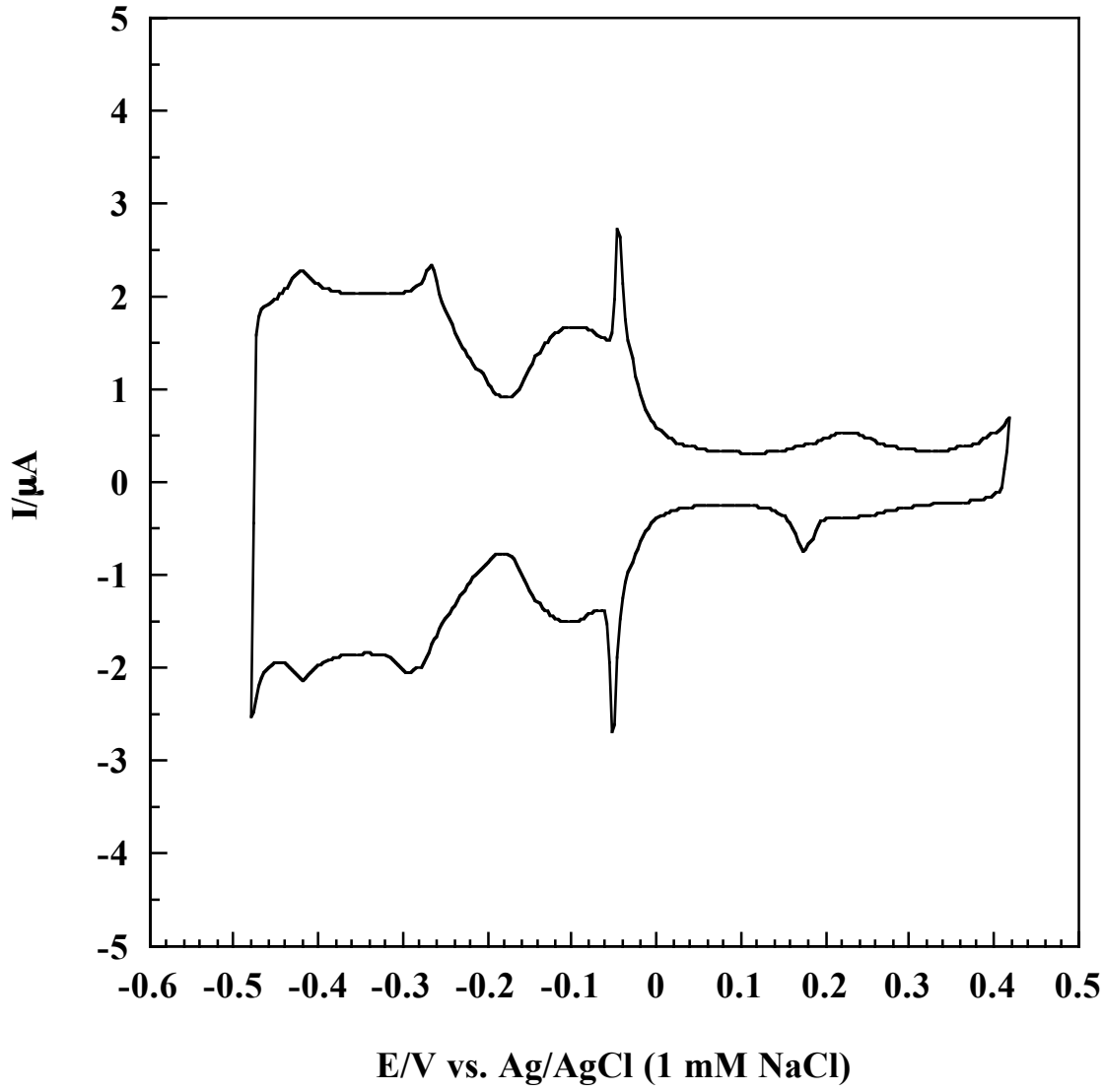

Figure 8. Cyclic voltammogram of a Pt(111) electrode in 100 mM H_2SO_4. Sweep rate = 50 mV/s. Electrode area = 0.28 cm^2.

Coulometry

In coulometry, the electrolytic charge associated with an electron transfer is measured over a predetermined time as the potential is stepped from one value, at which no faradaic process takes place, to another at which a faradaic process occurs. This technique can be used to determine surface packing density (Γ, nmol/cm^2) for an adsorbed electroactive species using Faraday's law:

$$Q - Q_b = nFA\Gamma \qquad (8)$$

where Q is total charge of the electrochemical process, Q_b is the background charge obtained in the absence of adsorbate, F is Faraday's constant, A is the area of the electrode, and n is the number of electrons transferred.

UHV-EC Instrumentation

The UHV-EC instrument employed in this study was based on a commercial stainless steel UHV chamber (Perkin-Elmer, Eden Prairie, MN). A photograph of the instrument is shown in Figure 9. The main chamber of the apparatus consists of three major compartments: (i) an electrochemistry (EC) chamber, (ii) a gate-valve (MDC Vacuum Products, Hayward, CA) isolable surface analysis chamber, and (iii) a valve-isolable ion pump well. The single-crystal electrode was transferred by means of an X-Y-Z manipulator (Varian, Lexington, MA) mounted on a linear positioning table

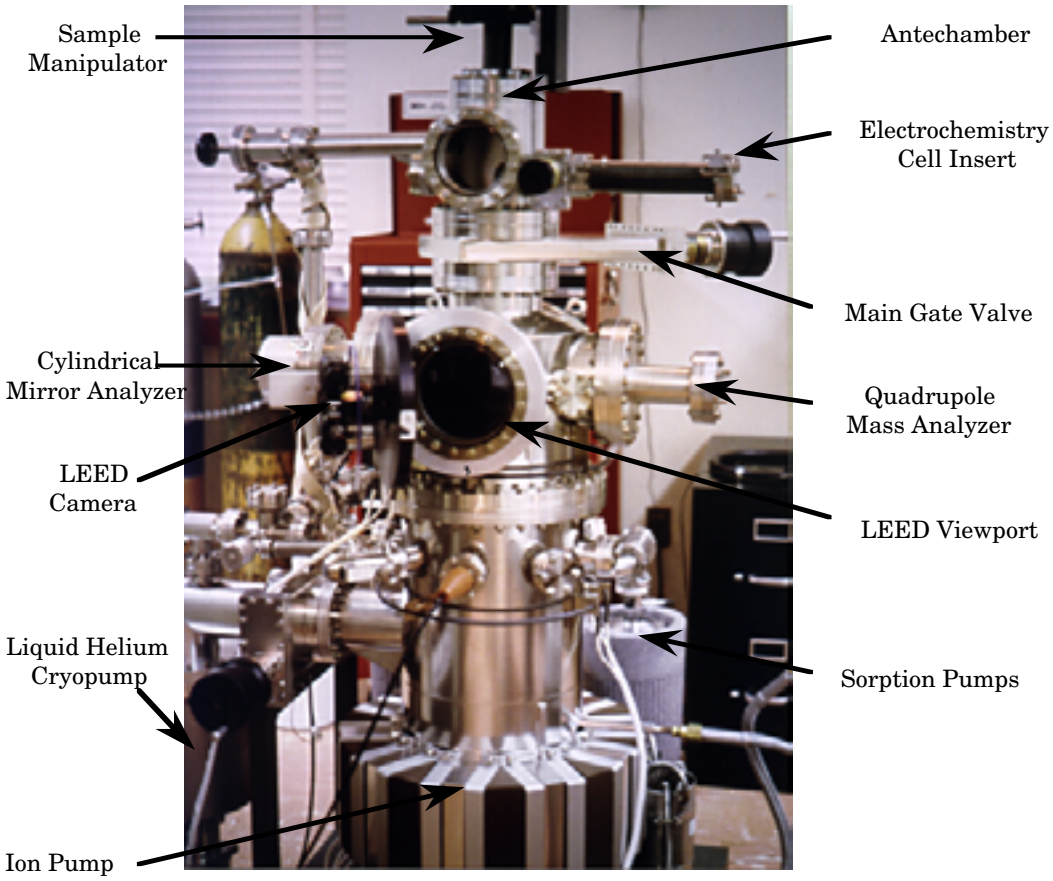

Figure 9. Photograph of the UHV-EC instrument.

(LinTech, Los Angeles, CA). This configuration allowed sample transfer and manipulation under a controlled environment.

Figure 10 shows a top-view schematic diagram of the UHV-EC chamber. The EC chamber had a gate-valve (MDC Vacuum Products) isolable electrochemical cell port through which an electrochemical cell assembly can be inserted. The surface analysis chamber used for the preparation and analysis of the sample electrode was equipped with the modules for LEED, AES, and temperature-programmed desorption-mass spectrometry (TPD-MS) instrumentation. Two variable leak valves (Varian, Lexington, MA) allowed the introduction of ultra-high purity gases. A custom-built ion gun was used for Ar^+-sputtering. With the use of a manipulator the electrode could be placed in front of each instrument for characterization.

Initial pumping of the chamber from ambient pressure down to 10^{-3} torr was accomplished by liquid nitrogen-cooled sorption pumps. A turbomolecular pump (Balzers TPU 060, Hudson, NH) was used to lower the pressure further to 10^{-6} torr. The final pumping stage consisted of using an ion pump (Perkin-Elmer TNBX Series 1000, Eden Prairie, MN) and a cryogenically cooled titanium sublimation pump. The UHV-EC system was periodically baked at 200°C for up to 4 days to maintain a base pressure of 10^{-9} torr.

Experiments

A single-crystal Pt(111) disc electrode of 99.999% purity, 7.5 mm in diameter and 1.0 mm in thickness, was used for UHV-EC experiments. The disc electrode, oriented to

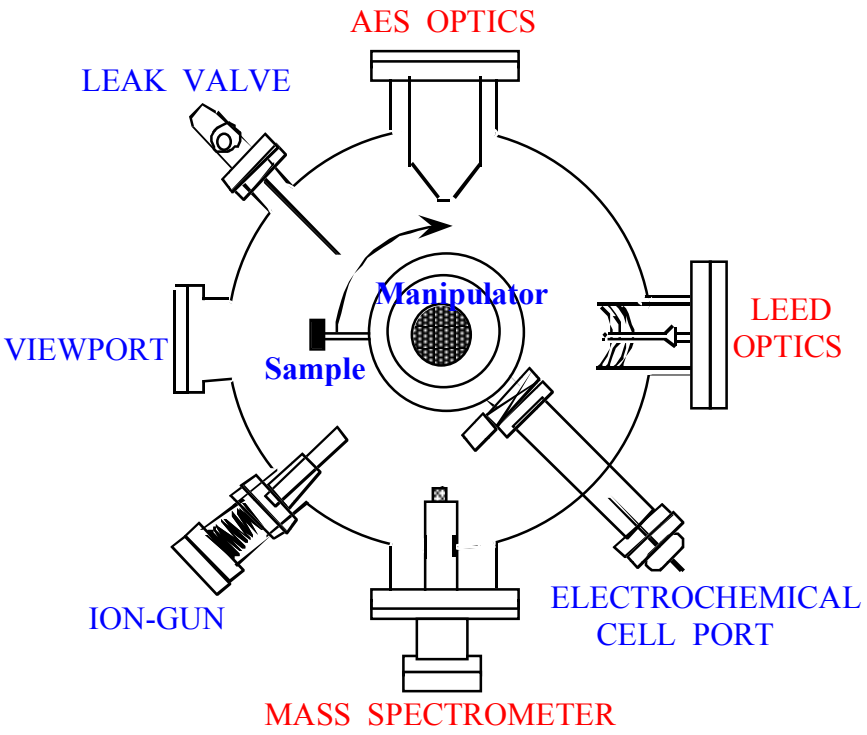

Figure 10. Top-view schematic diagram of the surface analysis chamber.

within ± 0.5° of the (111) plane and metallurgically polished to a mirror finish, was purchased from Aremco Products (Ossining, NY). Two Pt wires of 0.5 mm thickness (99.99% purity, Johnson-Matthey Inc., Seabrook, NH) were spot-welded to the edges of the disc to provide electrical contact and mechanical support. Two Pt-10% Rh/Pt thermocouple wires (Omega Engineering, Stanford, CT) were spot-welded to the top edge of the disc for temperature measurement and feedback control of a crystal temperature controller (Omega Engineering). The electrode area exposed to the electrochemical cell was measured, based on hydrogen underpotential deposition-desorption charge on Figure 8, to be 1.12 cm^2, which is very close to the calculated geometric electrode area of 1.1192 cm^2.

Electrochemistry experiments in the UHV-EC apparatus were performed using a custom-built two-compartment glass cell, a Ag/AgCl (1 mM NaCl) reference electrode, and a Pt-wire counter electrode (Figure 11). A low concentration of Cl^- in the reference electrode was used to minimize Cl^- contamination of the working electrode.

A typical UHV-EC experiment consists of three steps: (1) preparation of a clean and well-ordered Pt(111) electrode surface under UHV; (2) electrochemical experiments; and (3) surface analyses.

The Pt(111) electrode was cleaned before each set of experiments. The cleaning consisted of the following procedures: (i) Ar^+-bombardment (4 -10 μA Ar^+ current) to obtain contaminant-free surface. (ii) Thermal annealing at 550 °C in 5×10^{-6} torr oxygen to remove surface carbon and sulfur contamination; this procedure did not result in a layer of thermal Pt oxide. (iii) Thermal annealing to 750 °C under UHV to restore long-

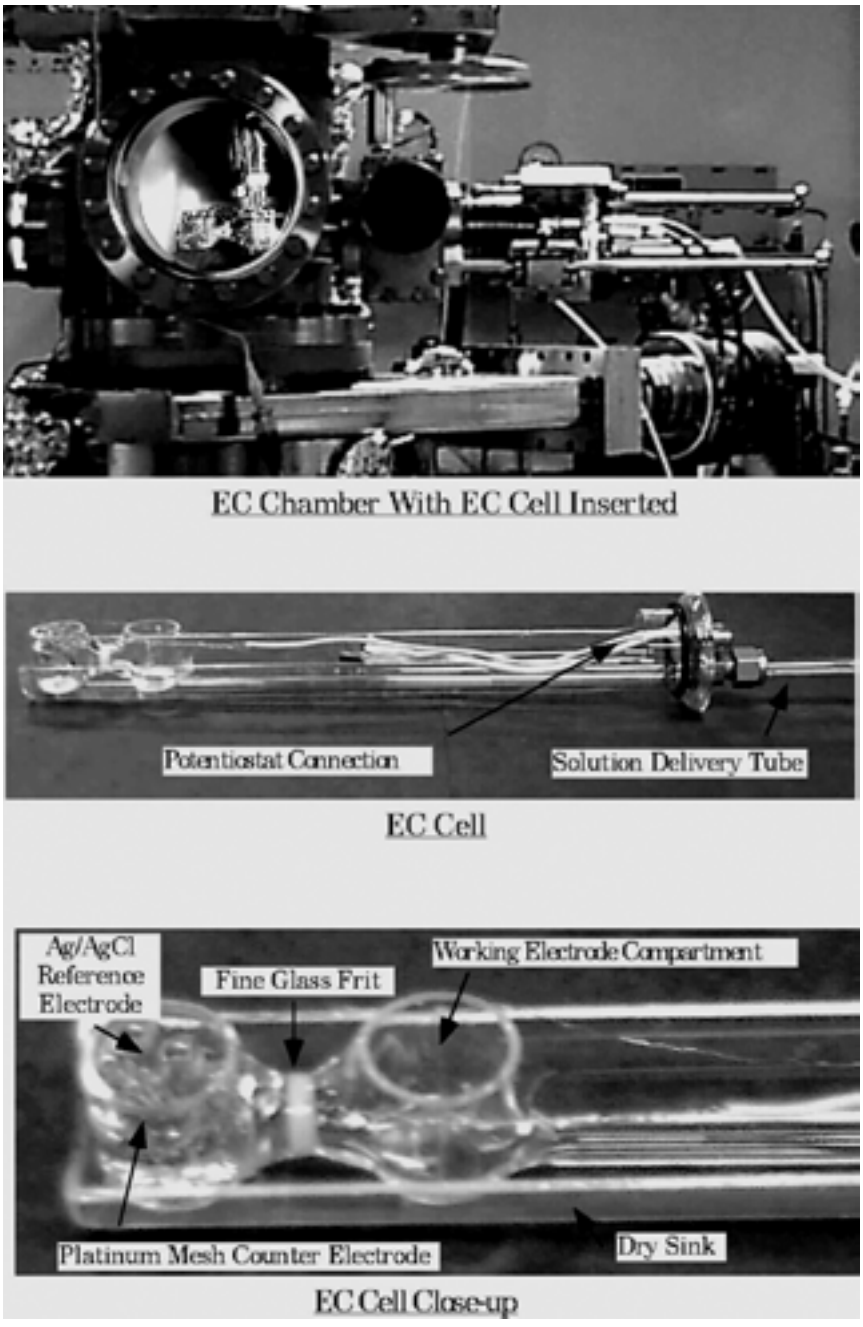

Figure 11. Photograph of the electrochemical ante-chamber and the electrochemical cell.

range order of Pt(111) surface which was roughened by Ar^+-bombardment. Figure 12 shows the effect of Ar^+-bombardment on the LEED patterns for Pt(111). Even a one-minute Ar^+-bombardment results in a rough surface, as can be inferred from slightly diffuse LEED pattern. Two-minute or longer Ar^+-bombardment makes the surface very rough resulting to profoundly diffuse LEED patterns. LEED and AES were used to verify surface order and purity, respectively. The cleaning procedures were repeated until satisfactory surface order and purity were attained.

Pd Deposition and Coverage Measurements

Pd Deposition

Two different electrochemical methods were adapted for preparing ultrathin Pd films onto the Pt(111) surface: potentiostatic and potentiodynamic depositions. For the potentiostatic deposition, a clean and well-ordered Pt(111) crystal was immersed into a solution of 0.50 mM $PdSO_4$ in 100 mM H_2SO_4 at open circuit potential (0.42 V); a constant potential between 0.230 and –0.400 V was then applied for 2 minutes. For the potentiodynamic deposition, a clean and well-ordered Pt(111) crystal was immersed into a solution of 0.50 mM $PdSO_4$ in 100 mM H_2SO_4 at open circuit potential. The potential was scanned very slowly (0.1 mV/s) toward more negative values until a desired electrolytic charge for Pd deposition was accumulated. When corrected for the background charge, the deposition charge provides a direct measure of the surface coverage, based on Faraday's Law.

(A) 1 minute

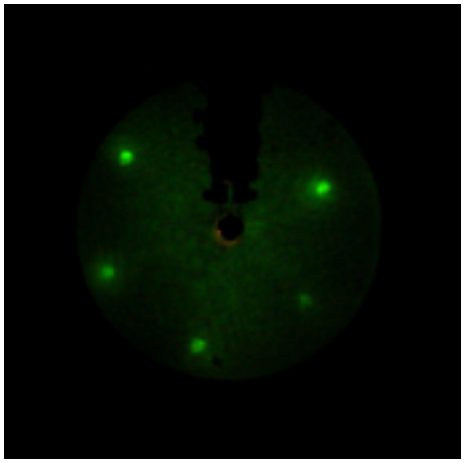

(B) 2 minutes

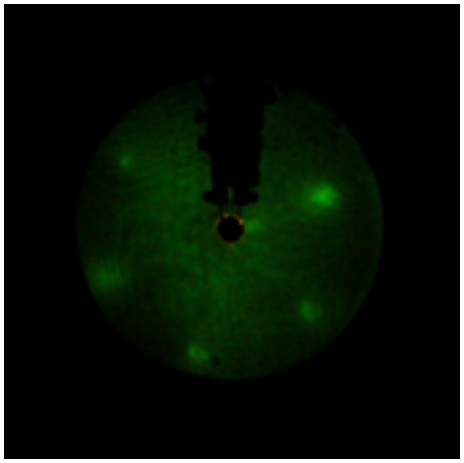

(C) 5 minutes

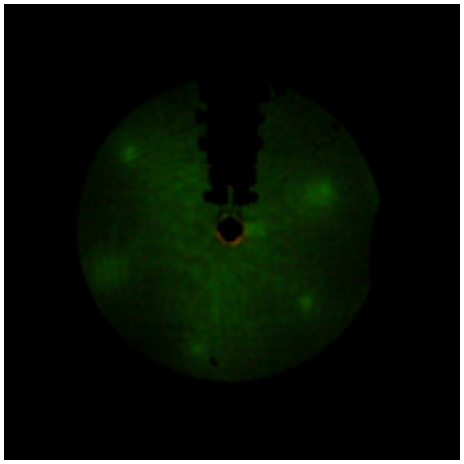

(D) 12 minutes

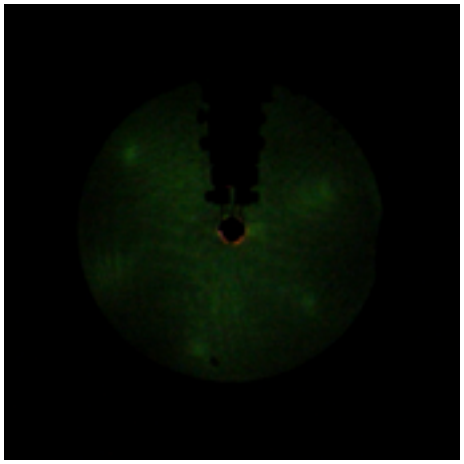

Figure 12. LEED patterns for Pt(111) after Ar^+-bombardment with a beam current of 4 μA. Bombardment time = (A) 1, (B) 2, (C) 5, and (D) 12 minutes. Beam energy = 62.0 eV; beam current = 2 μA.

Pd Coverage Measurement

As an independent method to determine the coverage of Pd films on Pt(111) surface, chemisorbed iodine ($I_{(ads)}$)-catalyzed Pd dissolution method was adapted [31]. This method is based on the fact that the $I_{(ads)}$ catalyzes the dissolution of Pd in acidic media, especially in sulfuric acid. Figure 13 shows the voltammograms for I-catalyzed dissolution of Pd. The $I_{(ads)}$-catalyzed Pd dissolution occurs even in the absence of corrosive agents such as chloride or bromide in the electrolyte solution. In the $I_{(ads)}$-catalyzed Pd dissolution method, electrolytic charge for the anodic stripping of Pd was measured, from which the coverage of Pd was determined. Regression analysis of the Pd stripping charge versus Pd deposition charge yields a line with a slope of 0.98 indicating the close agreement between the coverages determined by the two methods.

In order to ascertain at which electrodeposition condition the Pt(111) is completely covered by Pd, Cu underpotential deposition (UPD) experiments were performed. This method is based on the fact that the Cu UPD peaks on Pt occur at potentials different from Pd: hence, the progress of Pd deposition from submonolayer to monolayer coverages could be monitored [26].

Bromine Adsorption and Coverage Measurements

Bromine was adsorbed onto ultrathin Pd films from a solution of 1 mM NaBr in 100 mM NaF, which was adjusted to pH 4 with tetrafluoroacetic acid (CF_3COOH; TFA), at controlled potentials between –0.300 and 0.800 V for 3 minutes. In order to determine

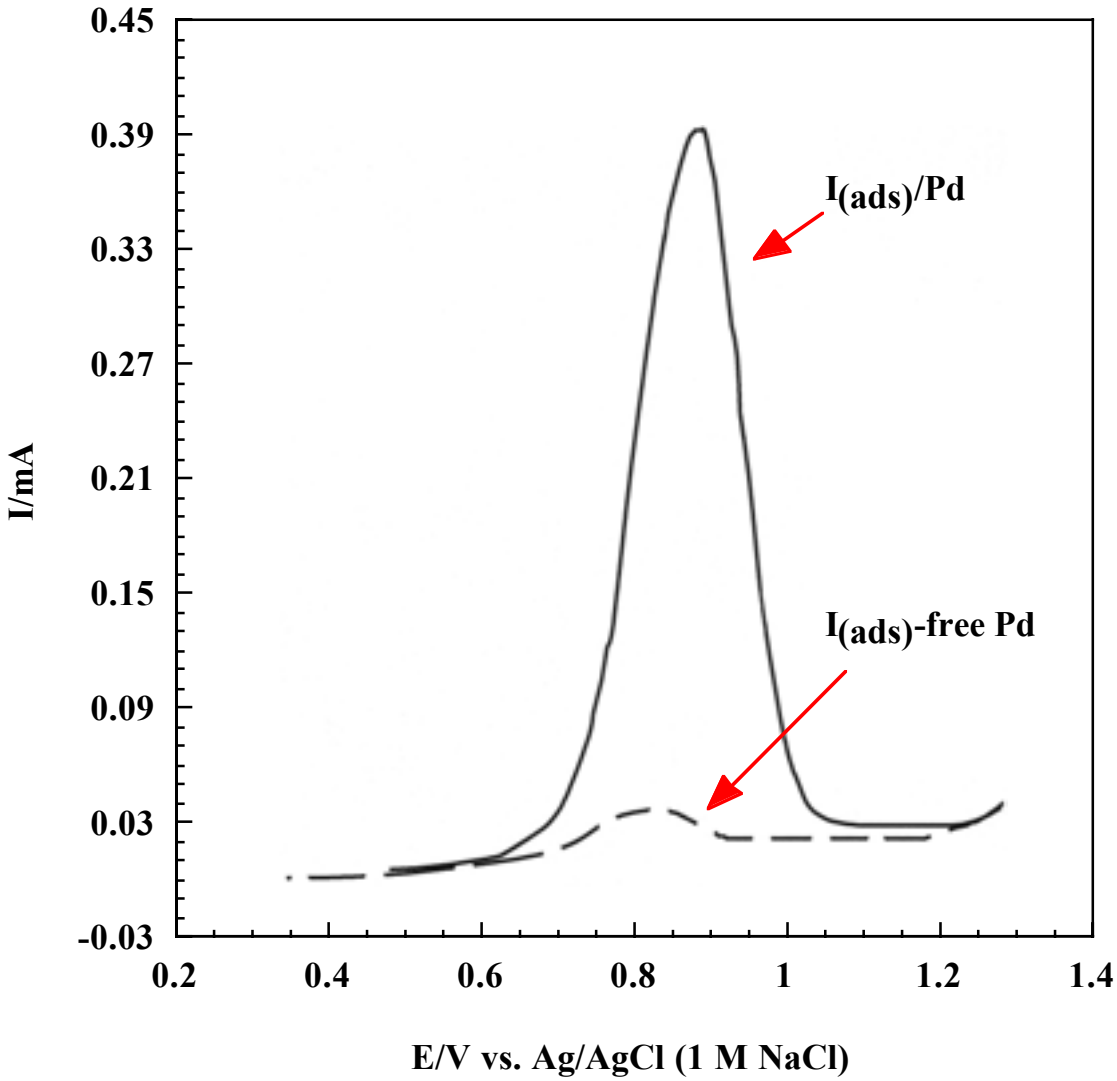

Figure 13. Voltammograms of clean (dashed line) and iodine-coated (solid line) polycrystalline electrode in 0.5 mM H_2SO_4. Electrode area = 1 mm^2. Sweep rate = 10 mV/s.

the bromine coverage on ultrathin Pd films, AES spectra were obtained. Equation 7 was used to obtain the bromine coverage on ultrathin Pd films.

Reagents and Gases

All solutions were made up using 18.2 Ω Millipore water (Millipore Systems, Houston, TX). This water delivery system consists of a prefilter, two ion exchangers, a trap to remove trace organics, and a 0.2 micron particulate filter. All glassware was cleaned using hot chromic acid (3% $K_2Cr_2O_7$ dissolved in 10 M H_2SO_4). The following high-purity reagents were used to prepare all solutions: fuming H_2SO_4 (Aldrich, Milwaukee, WI), $PdSO_4$ (Aldrich), NaI (Curtin Matheson Scientific, Houston, TX), NaBr (Johnson Mathey, England), NaCl (Johnson Mathey), $Cu(ClO_4)_2$ (Aldrich), NaF (Aldrich), CF_3COOH (Aldrich), and $K_2Cr_2O_7$ (EM Science, Gibbstown, NJ). High purity gases, specifically nitrogen (BOTCO, Bryan, TX), argon (BOTCO), and oxygen (Proxair, Dunbury, CT), were used in the experiments.

RESULTS

Spontaneous Deposition of Pd

At open circuit potential (typically 0.42 V) Pd can be spontaneously deposited onto the Pt(111) surface. Figure 14 shows the Auger electron spectrum and LEED pattern (insert) of the Pt(111) electrode immersed in Pd^{2+}-containing solution for 2 minutes. The Auger electron spectrum reveals a small Pd peak at 330 eV along with Pt peaks at 64, 168, and 237 eV. Under the current experimental condition, submonolayer coverages of Pd (less than 0.2 ML) were typically obtained; this result concurs with those observed by other groups [17]. A bright, sharp (1×1) pattern, comparable to that of the clean substrate itself, was obtained after the spontaneous deposition.

Potentiostatic Deposition of Pd

The amount of Pd that can be electrodeposited at a chosen potential is an interplay of the Pd^{2+}-ion concentration and deposition time. To find the highest deposition potential which affords a surface coverage of 1 ML Pd using 0.5 mM $PdSO_4$ at a fixed deposition time of 2 minutes, Cu UPD experiments were performed after depositing Pd at various potentials. Figure 15 shows a series of voltammograms for the Cu UPD on Pt(111) precoated with Pd at (A) 0.222 V, (B) 0.221 V, and (C) 0.220 V, respectively. The coexistence of both the Pd adlayer and the pristine Pt(111) surface at 0.222 V gives rise to two distinctive potential regions: Cu UPD onto and stripping from

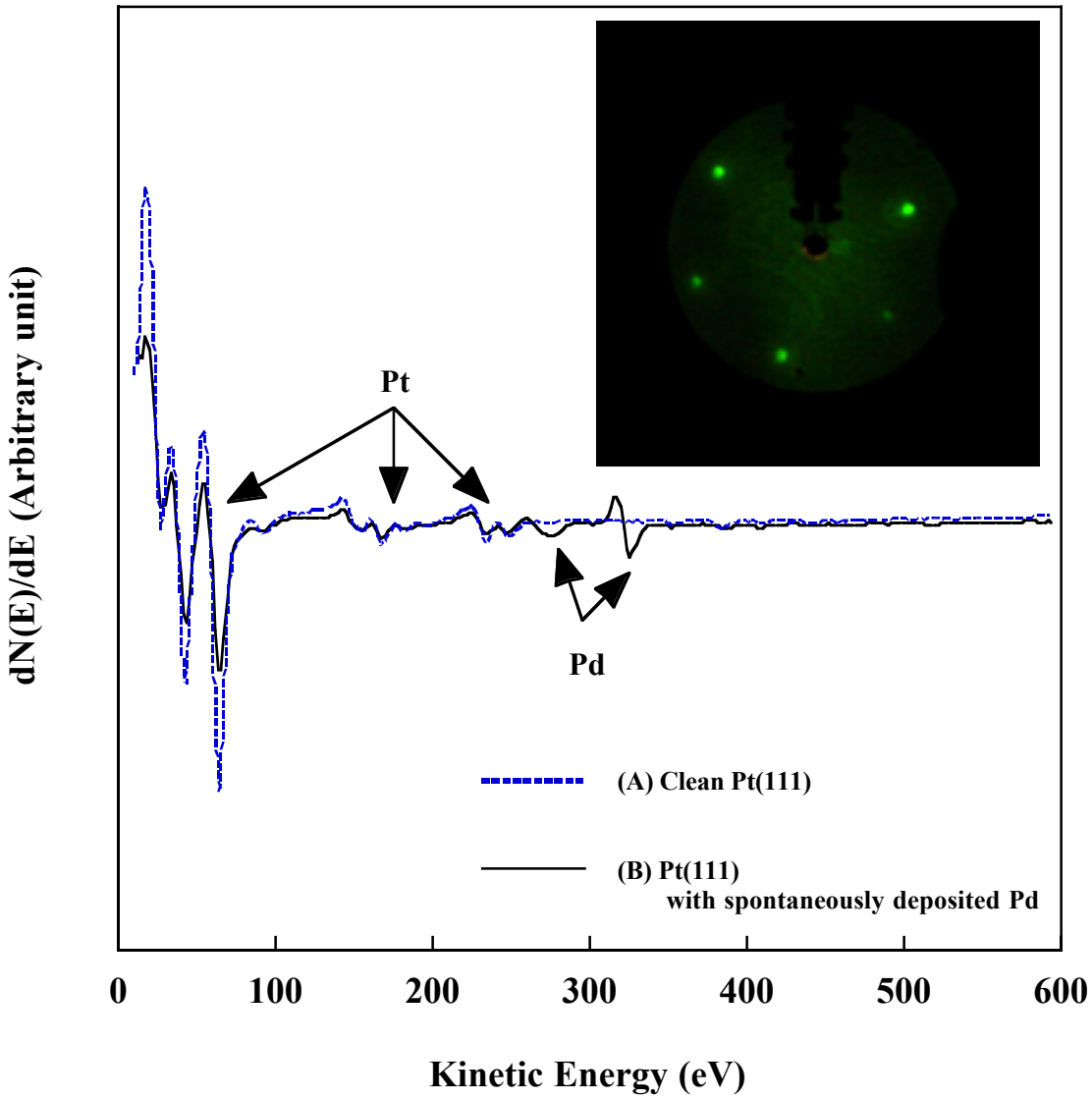

Figure 14. Auger electron spectra for (A) clean Pt(111) and (B) Pt(111) coated with spontaneously deposited Pd. Deposition was done at open circuit potential for 2 minutes using a solution of 0.5 mM $PdSO_4$ and 100 mM H_2SO_4. Incident beam energy = 2 keV; beam current = 1 μA. Insert shows the corresponding LEED pattern: Beam energy = 62.0 eV; beam current = 2μA.

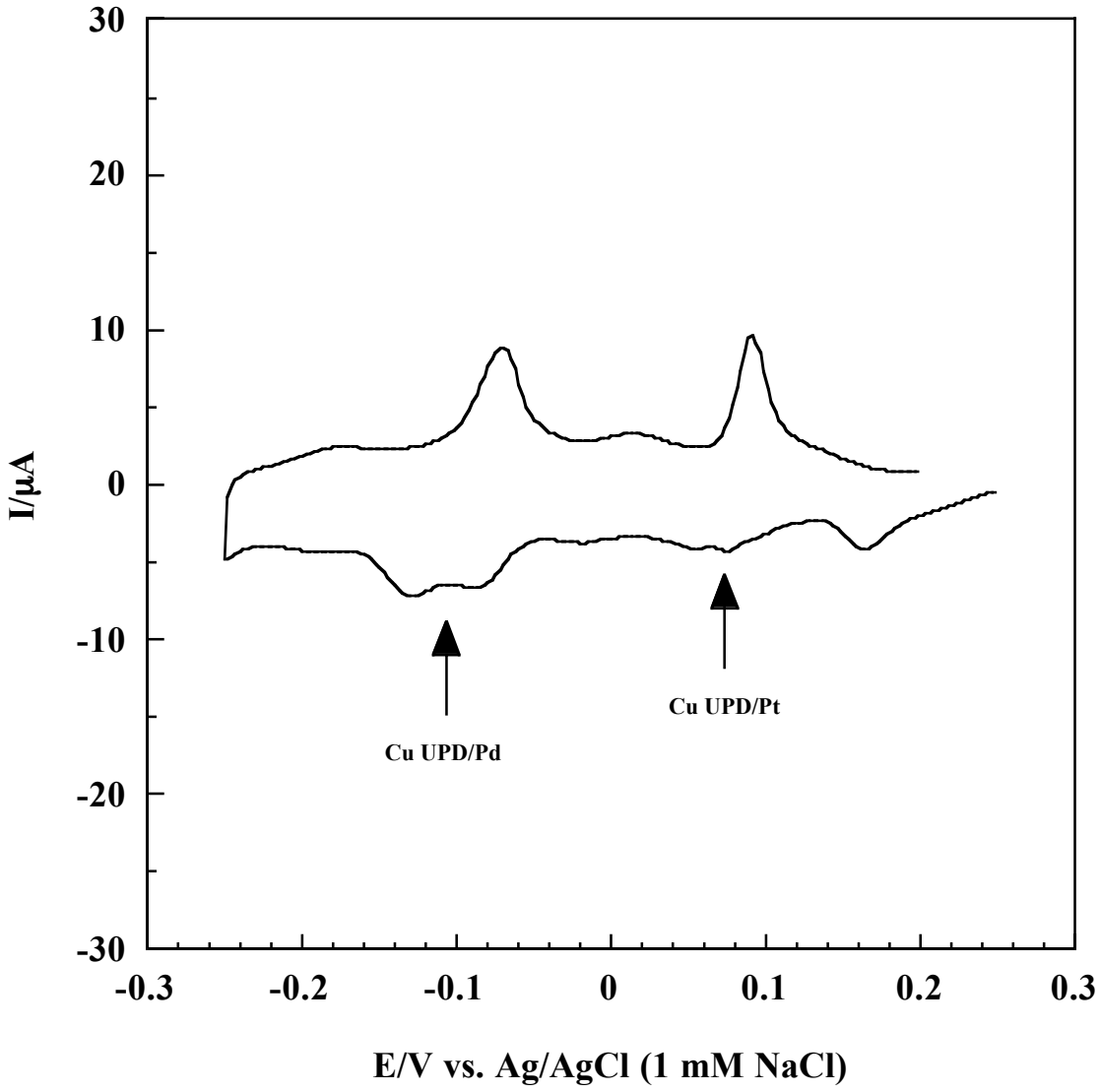

Figure 15. Voltammograms of Cu UPD on Pd thin film formed on Pt(111). (A) At 0.222 V. The voltammogram was obtained in the solution of 10 mM $CuSO_4$ and 100 mM H_2SO_4. Pd was deposited from 0.5 mM $PdSO_4$ in 100 mM H_2SO_4 for 2 minutes. Sweep rate = 2 mV/s. Electrode area = 1.12 cm^2.

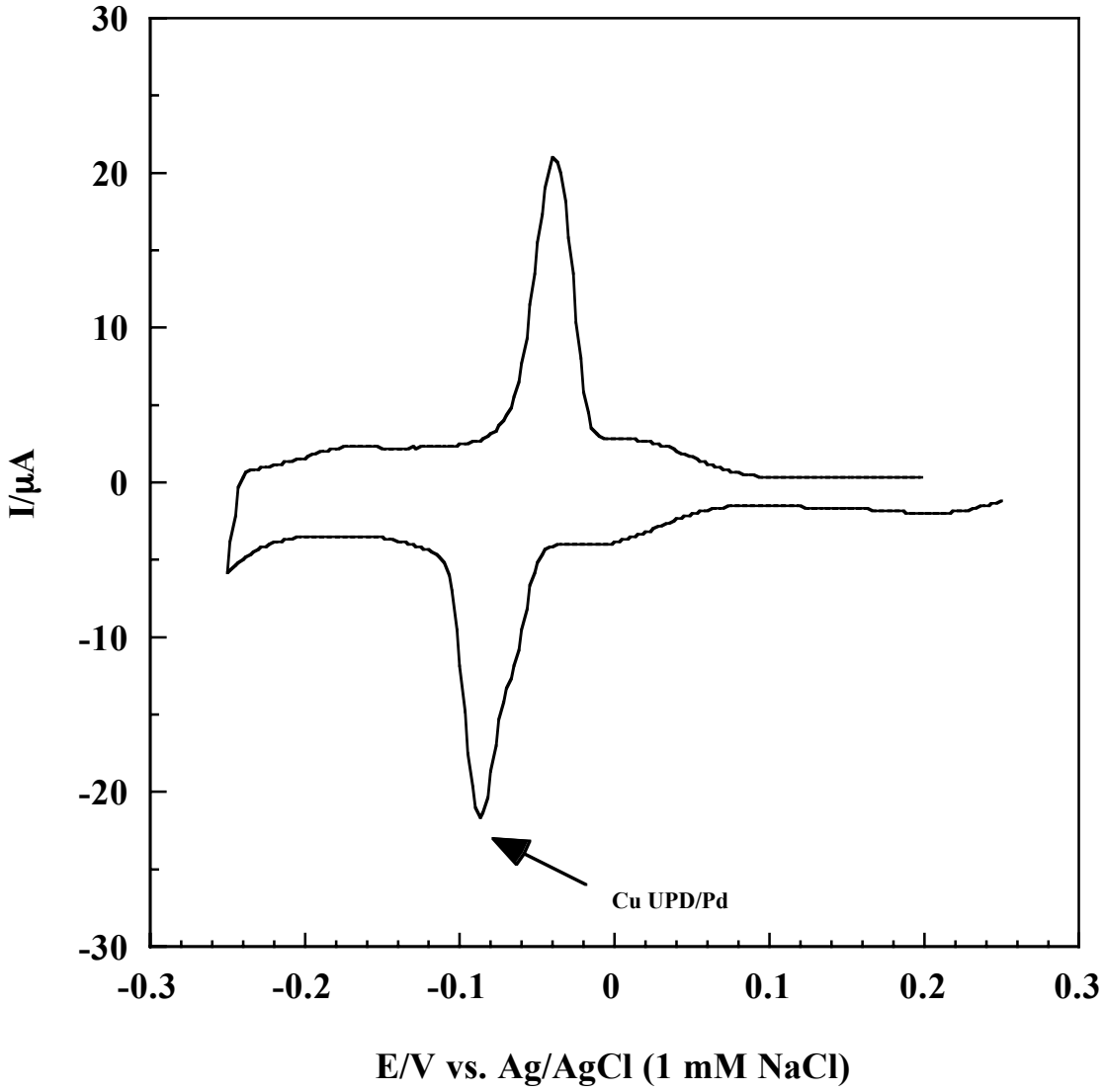

Figure 15 Continued. (B) At 0.221 V.

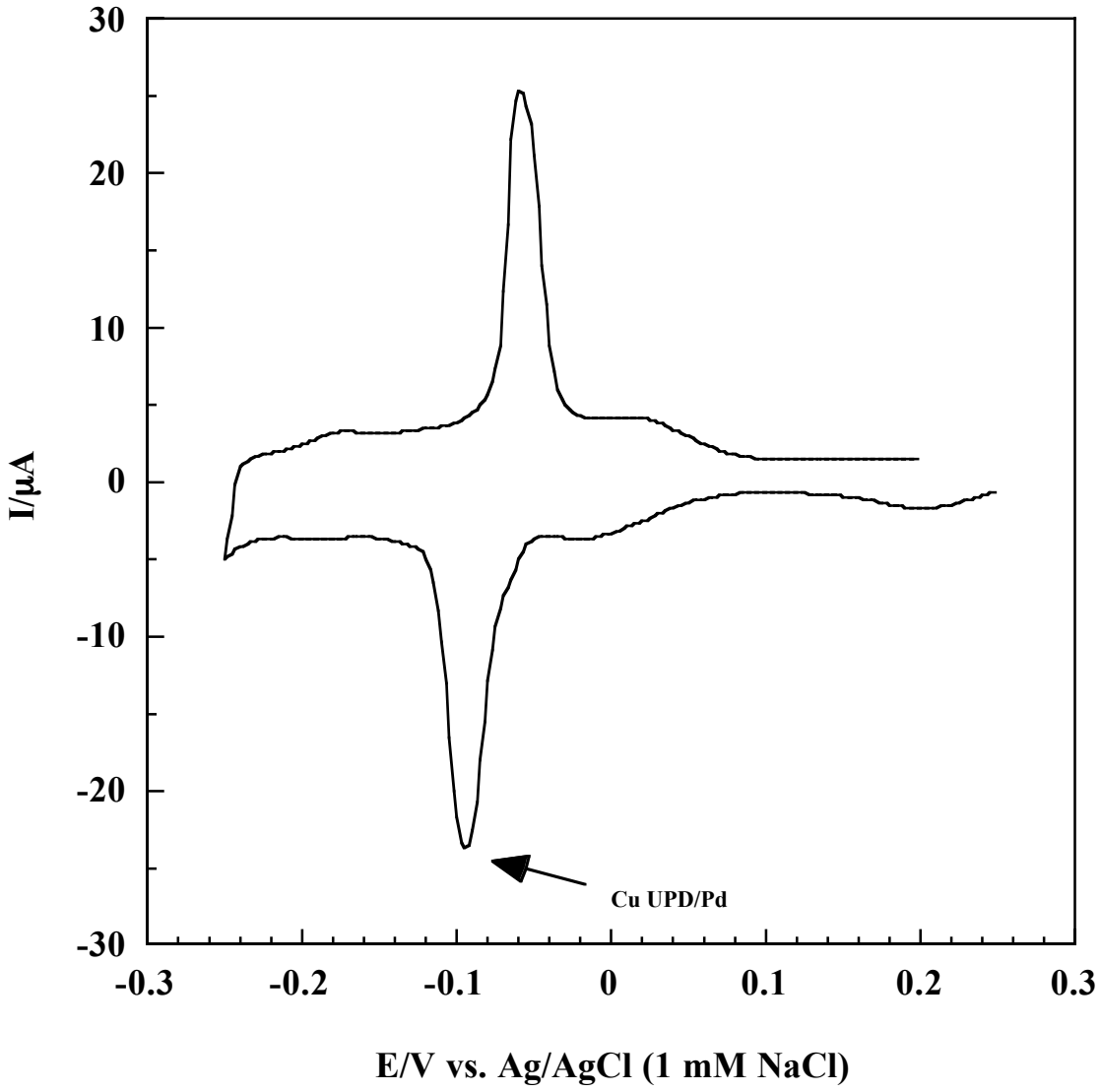

Figure 15 Continued. (C) At 0.220 V.

(i) Pd film between –0.16 and –0.05 V and (ii) Pt(111) surface between 0.02 and 0.13 V.

Pd film formation at 0.221 V led to the extinction of voltammetric peaks due to Cu UPD and stripping on the Pt(111) surface; the Pd film, therefore, fully covers the Pt(111) surface at this deposition condition. Similar voltammograms were obtained from Pd films deposited at 0.220 V.

The amount of Pd deposited at the pre-selected potentials can be quantitatively assayed using I_{ads}-catalyzed dissolution of Pd [31]. The I_{ads}-catalyzed Pd stripping charges for the Pd films deposited at 0.222, 0.221, and 0.220 V were found to be 455.4, 547.2, and 644.6 μC, respectively. Based on the Cu UPD results in Figure 15 and the I_{ads}-catalyzed Pd stripping charges, it can be claimed that complete coverage of Pt(111) surface by Pd occurs at ca. 0.221 V under the present experimental condition.

The calculated stripping charge for 1 ML Pd on the Pt(111) surface is 538.5 μC; this value is essentia1ly the same as the deposition charge (539 μC) and I_{ads}-catalyzed stripping charge for Pd film formed at the highest potential (0.221 V) where the complete coverage of Pt(111) surface by Pd occurs. Thus, a charge of 538.5 μC can be taken to represent the charge corresponding to 1 ML Pd stripped from the Pt(111) electrode with the surface area of 1.12 cm^2. All Pd coverages reported in this study are based on the value of 538.5 μC/ML.

Ultrathin Pd films of various coverages can be prepared by applying constant potential; this method is, from hereon, referred to as *constant potential deposition*

(CPD). The amount of Pd deposited was ascertained from the I_{ads}-catalyzed Pd stripping charge.

Figure 16 shows voltammograms for the I_{ads}-catalyzed anodic stripping of ultrathin Pd films prepared at various potentials. All the voltammograms display distinctive oxidation peaks at 0.43 and 0.73 V. The magnitude of the anodic stripping peaks at 0.43 V is directly proportional to the amount of Pd initially deposited; hence, the peak at 0.43 V is assigned to the oxidative dissolution of Pd to Pd^{2+}. The peak at 0.73 V is independent of the quantity of electrodeposited Pd. Based upon previous works with clean and I-coated Pd(111) electrode [29,43], the peak at 0.73 V is attributed to the oxidation of I_{ads} to IO_3^-. The amounts of the Pd films prepared at 0.230, 0.221, 0.185, 0.150, 0.110, and -0.200 V correspond to 0.5, 1, 2, 3, 4, and 8 ML, respectively.

Figure 17 shows a plot of the amount of elecrodeposited Pd, expressed as equivalent monolayers, versus applied potential. As the Pd deposition potential ($E_{Pd\ deposition}$) decreases, the Pd coverage per unit charge increases almost linearly between 0.23 and 0.00 V. Between 0.00 and –0.20 V, the increase in Pd coverage with $E_{Pd\ deposition}$ becomes less steeper; the Pd coverage decreases gradually below –0.20 V. This observation is ascribed to the hydrogen evolution reaction (HER) which competitively inhibits further Pd deposition as $E_{Pd\ deposition}$ goes more negative.

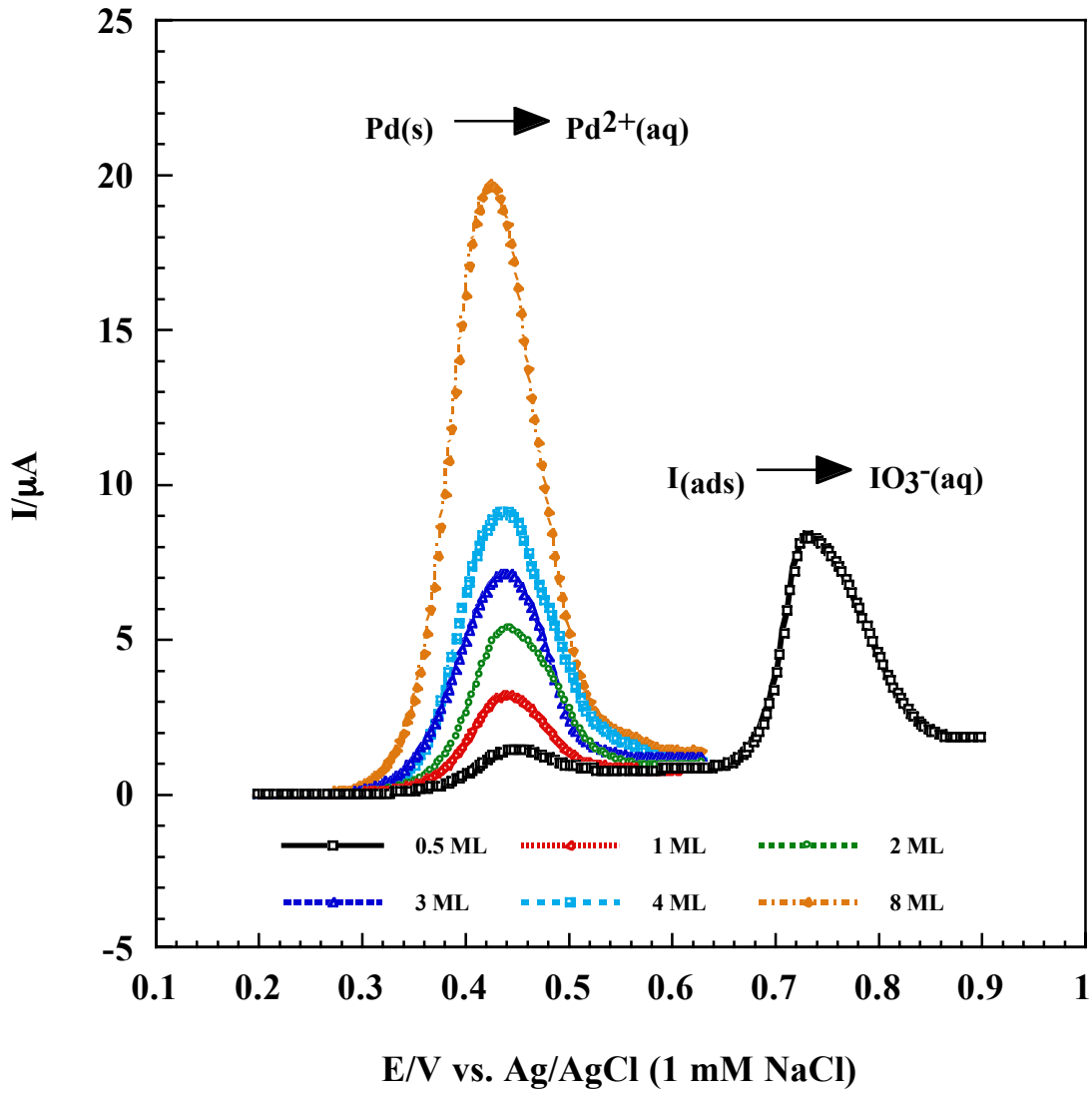

Figure 16. Voltammograms of the I_{ads}-catalyzed anodic stripping of Pd_{CPD} films from Pt(111) surface in 100 mM H_2SO_4. Submonolayer to 8 ML of Pd_{CPD} films were deposited from 0.5 mM Pd SO_4 in 100 mM H_2SO_4 by potentiostatic deposition. Sweep rate = 0.5 mV/s.

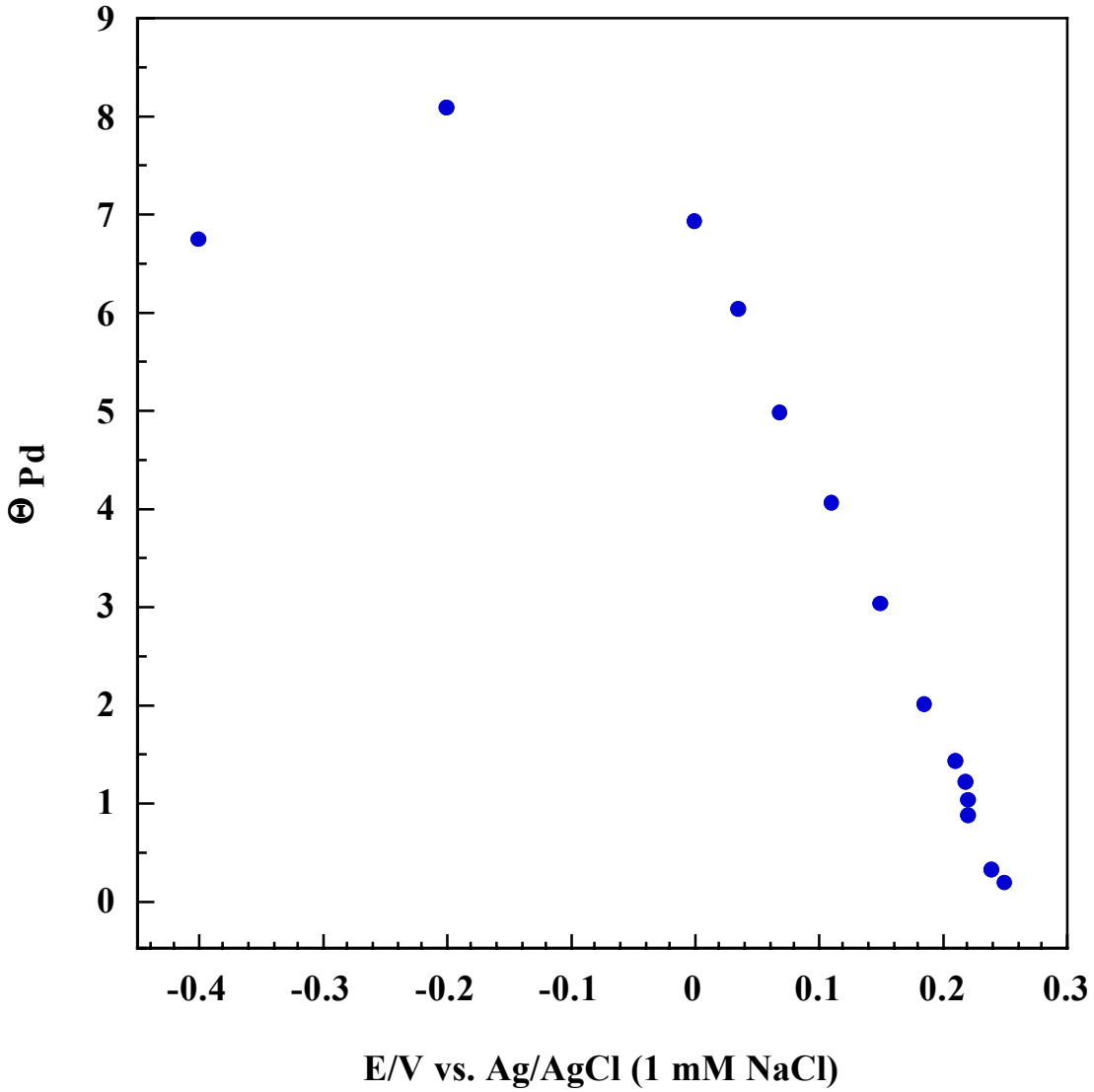

Figure 17. Pd coverage as a function of Pd deposition potential. Pd was deposited from 0.5 mM $PdSO_4$ in 100 mM H_2SO_4. Deposition time = 2 minutes.

Interfacial Structure and Composition

The structure and composition of ultrathin Pd films prepared by CPD (hereafter referred to as *Pd_{CPD} films*) were probed using LEED and AES. The following coverages of Pd_{CPD} films were explored: 0.5, 1, 2, 3, 4, and 8 ML.

All the Pd_{CPD} films investigated yield LEED spectra (Figure 18) that show (1×1) patterns. Depending upon the Pd coverage, the brightness of the LEED spots changes a lot while the sharpness of the spots remains almost constant. The LEED pattern for 1 ML Pd_{CPD} film in Figure 18 (B) shows the brightest spots, probably due to the formation of a complete well-ordered monolayer of Pd on the Pt(111) surface. LEED spots for 0.5 ML Pd_{CPD} film in Figure 18 (A) are less brighter than those for 1 ML Pd_{CPD} film; the difference in spot brightness results from the higher step density on the Pt(111) surface with submonolayer coverages of Pd. The LEED pattern for 2 ML Pd_{CPD} film in Figure 18 (C) has slightly less brighter spots compared with those for 1 ML Pd_{CPD} film. At Pd coverages higher than 2 ML, the LEED spot brightness decreases as Pd coverage increases; such trend can be gleaned from Figures 18 (D)-(F). These observations suggest that surface order of the Pd_{CPD} film decreases with increasing Pd coverage.

The Auger electron spectra (Figure 19) for Pd_{CPD} films reveal that the intensity of the Pd signal at 330 eV increases with Pd coverage. The Pt signal intensity at 168 eV, however, decreases with Pd coverages up to 1 ML and becomes negligible above that Pd coverage.

(A) 0.5 ML Pd_{CPD} film

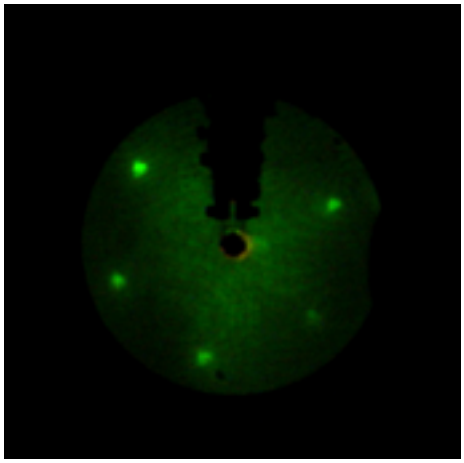

(B) 1 ML Pd_{CPD} film

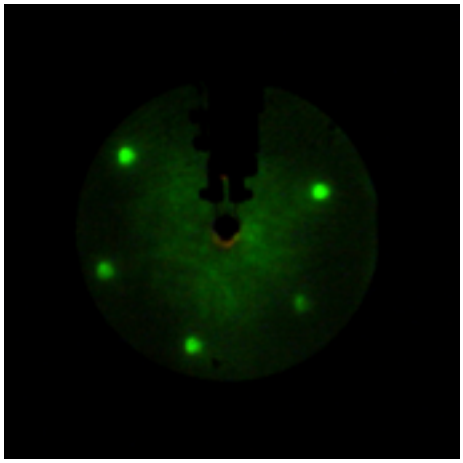

(C) 2 ML Pd_{CPD} film

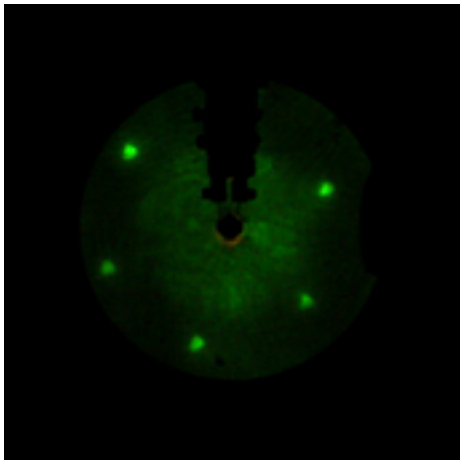

(D) 3 ML Pd_{CPD} film

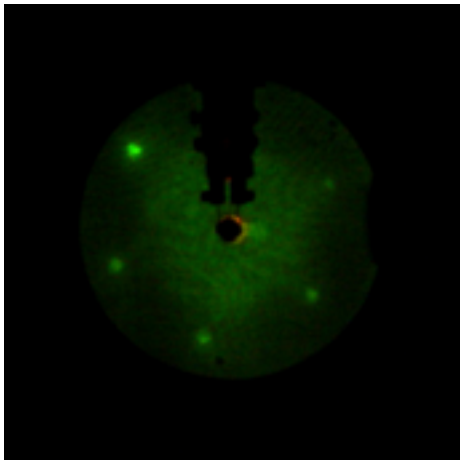

Figure 18. LEED patterns for Pd_{CPD} films on Pt(111) at different Pd coverages. (A) 0.5, (B) 1, (C) 2, and (D) 3 ML. Pd films were prepared by potentiostatic deposition. Beam energy = 62.0 eV; beam current = 2 μA.

(E) 4 ML Pd_{CPD} film

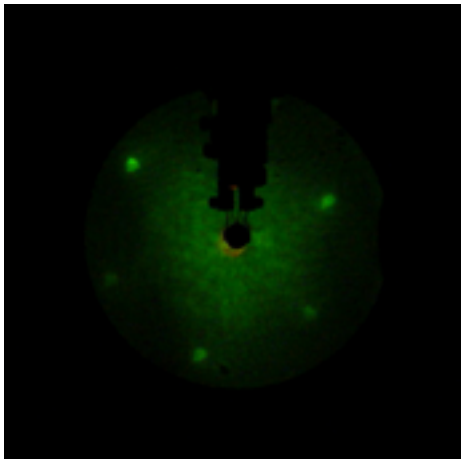

(F) 8 ML Pd_{CPD} film

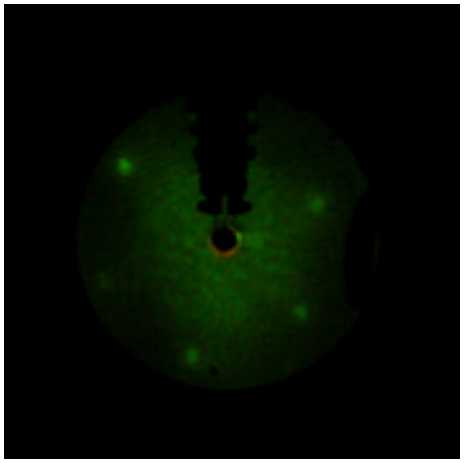

Figure 18 Continued. (E) 4 and (F) 8 ML.

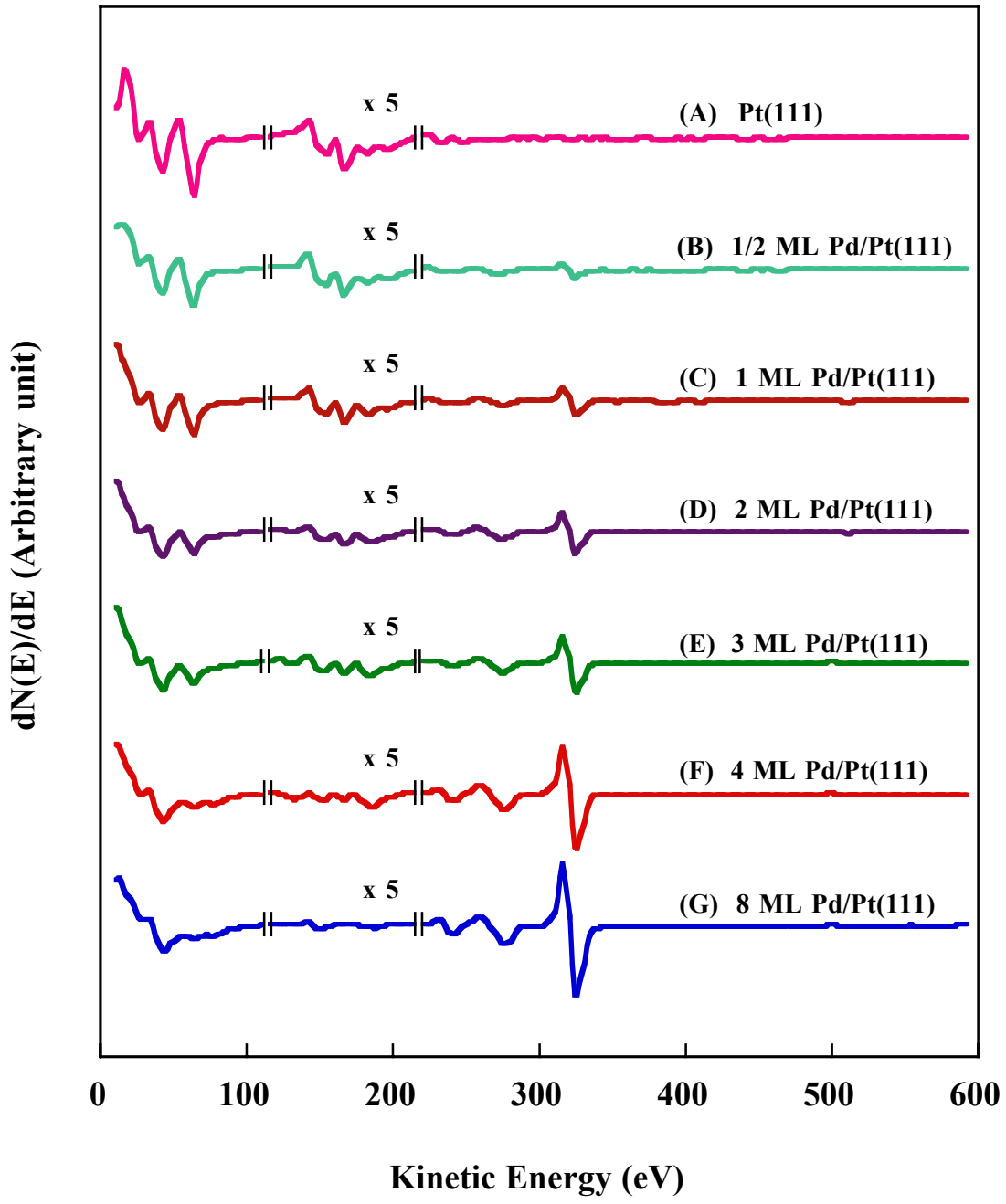

Figure 19. AES spectra of Pd_{CPD} films on Pt(111). Pd films were prepared by potentiosatic deposition. Incident beam energy = 2 keV; beam current = 1 μA.

Electrochemical Behavior

Cyclic voltammograms for Pt(111) substrate and ultrathin Pd_{CPD} films were obtained in 100 mM H_2SO_4. Figure 20 depicts typical voltammetric features for a clean and ordered Pt(111): (i) broad hydrogen adsorption/desorption region between -0.45 and –0.17 V; (ii) the so-called butterfly peaks between –0.17 and 0.00 V, which are claimed to be related with (bi)sulfate desorption/adsorption [6,25]; (iii) sharp redox peaks at ca. –0.06 V, which are characteristic of clean and well-ordered Pt(111) surface; the origin of these peaks is not yet clearly understood; (iv) a large surface Pt oxidation peak at 0.78 V, along with small oxidation features starting at 0.17 V; and (v) a Pt reduction peak at 0.24 V.

The voltammogram for 0.5 ML Pd_{CPD} film in Figure 21 (A) shows two pairs of redox peaks at ca. –0.34 and –0.29 V, which are related to hydrogen underpotential deposition/desorption (hereafter referred to as *H_{upd} adsorption/desorption*) on ultrathin Pd films [11,20]. These features are not observed in bulk Pd because hydrogen readily diffuses from the surface to the internal matrix of the solid [7,44].

Adsorption/desorption of H_{upd} and HSO_4^-/SO_4^{2-} on ultrathin Pd films are known to be surface-site specific [6,21,25]. Reversible peaks centered at –0.33 V are associated with redox processes at terrace sites while the analogous set at –0.29 V is voltammetric signature of step sites [6,25]. Some researchers [21] have claimed that the redox peaks at –0.29 V may be due to similar desorption/adsorption process on terrace sites of Pd *bulk* deposits.

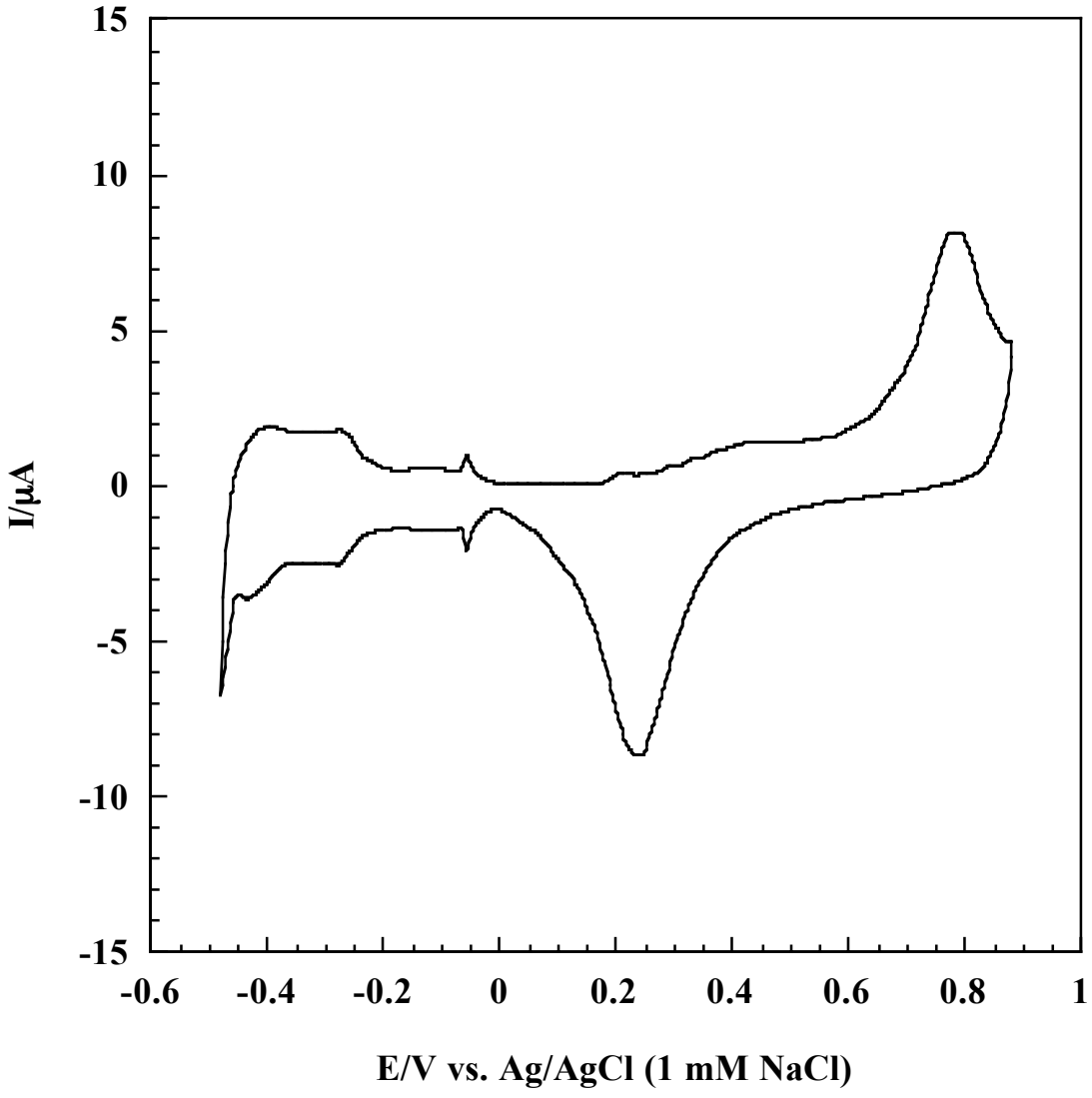

Figure 20. Cyclic voltammogram of a Pt(111) disc electrode in 100 mM H_2SO_4. Sweep rate = 2 mV/sec. Electrode area = 1.12 cm^2.

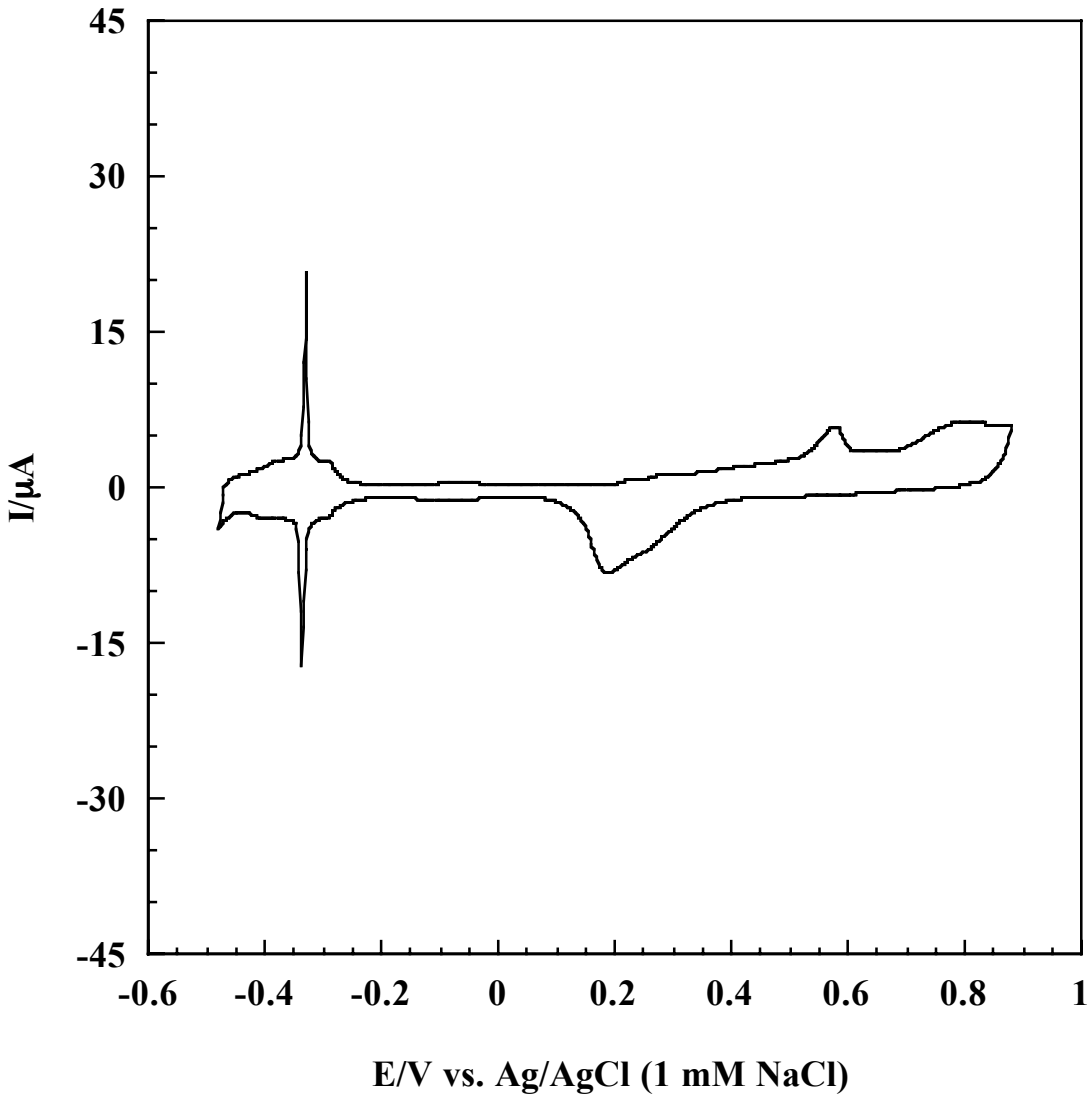

Figure 21. Cyclic voltammogram of n Pd_{CPD} film on Pt(111) in 100 mM H_2SO_4. (A) n = 0.5 ML. Pd was deposited by potentiostatic deposition. Sweep rate = 2 mV s^{-1}. Electrode area = 1.12 cm^2.

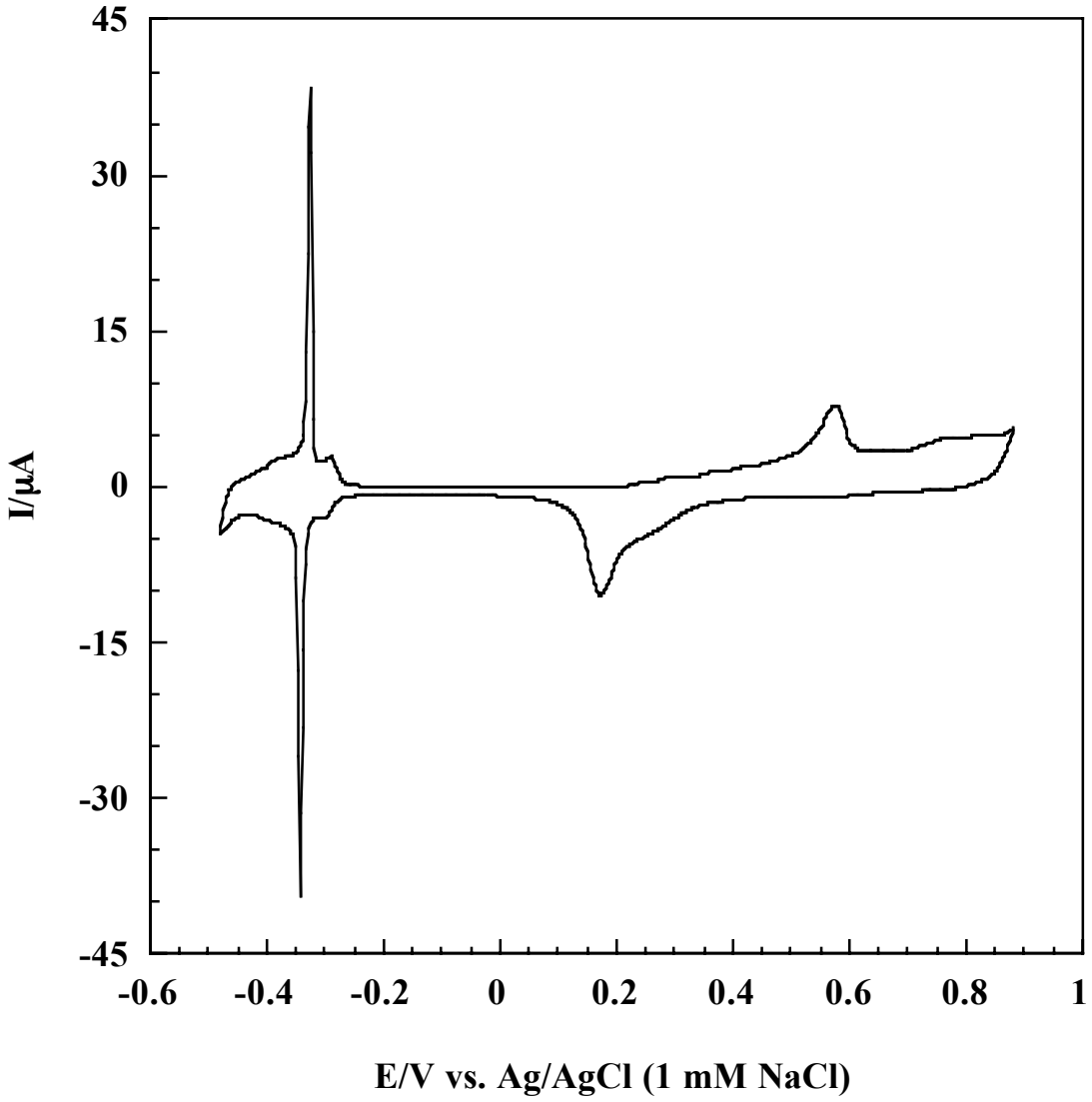

Figure 21 Continued. (B) n = 1 ML.

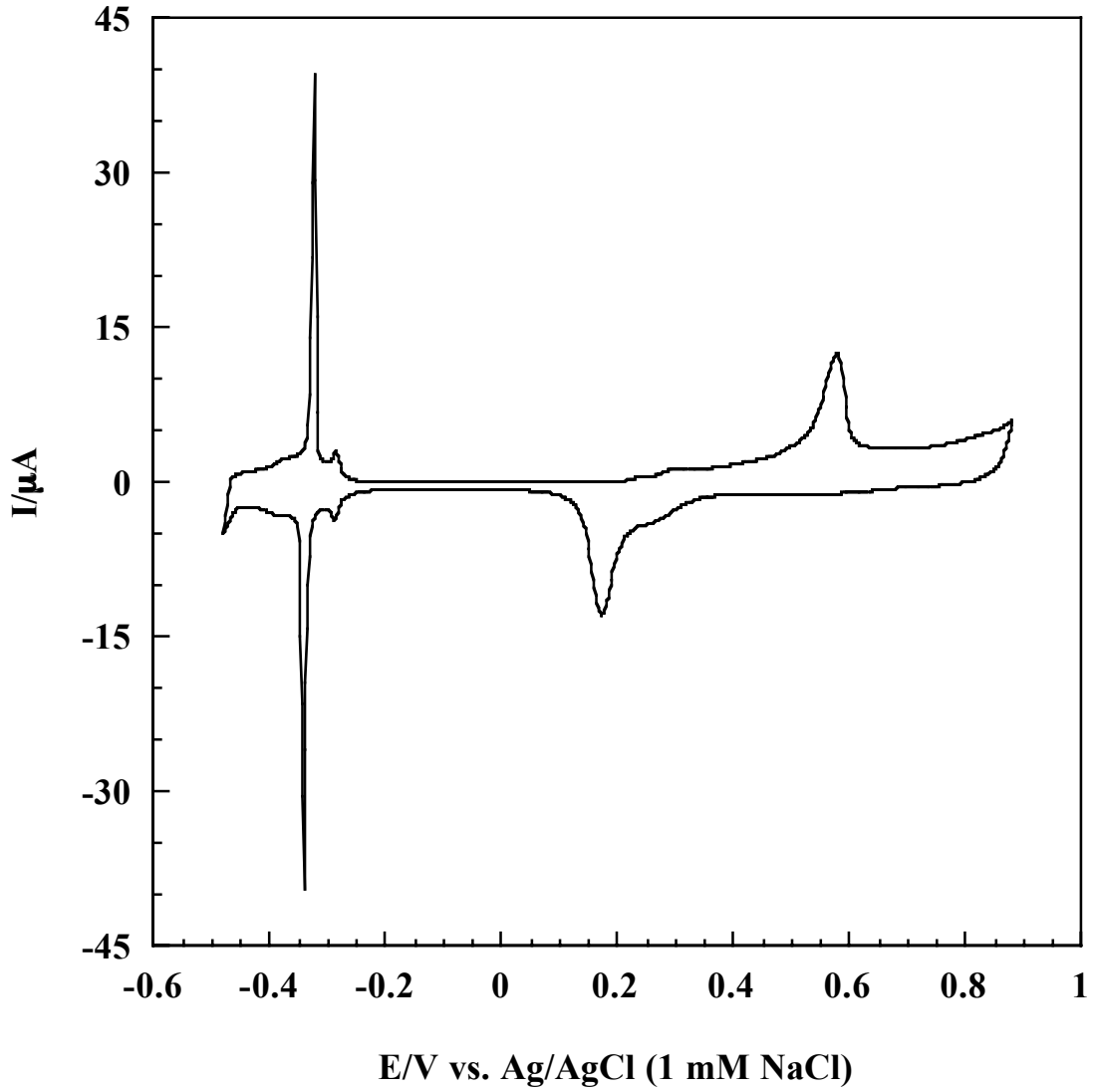

Figure 21 Continued. (C) n = 2 ML.

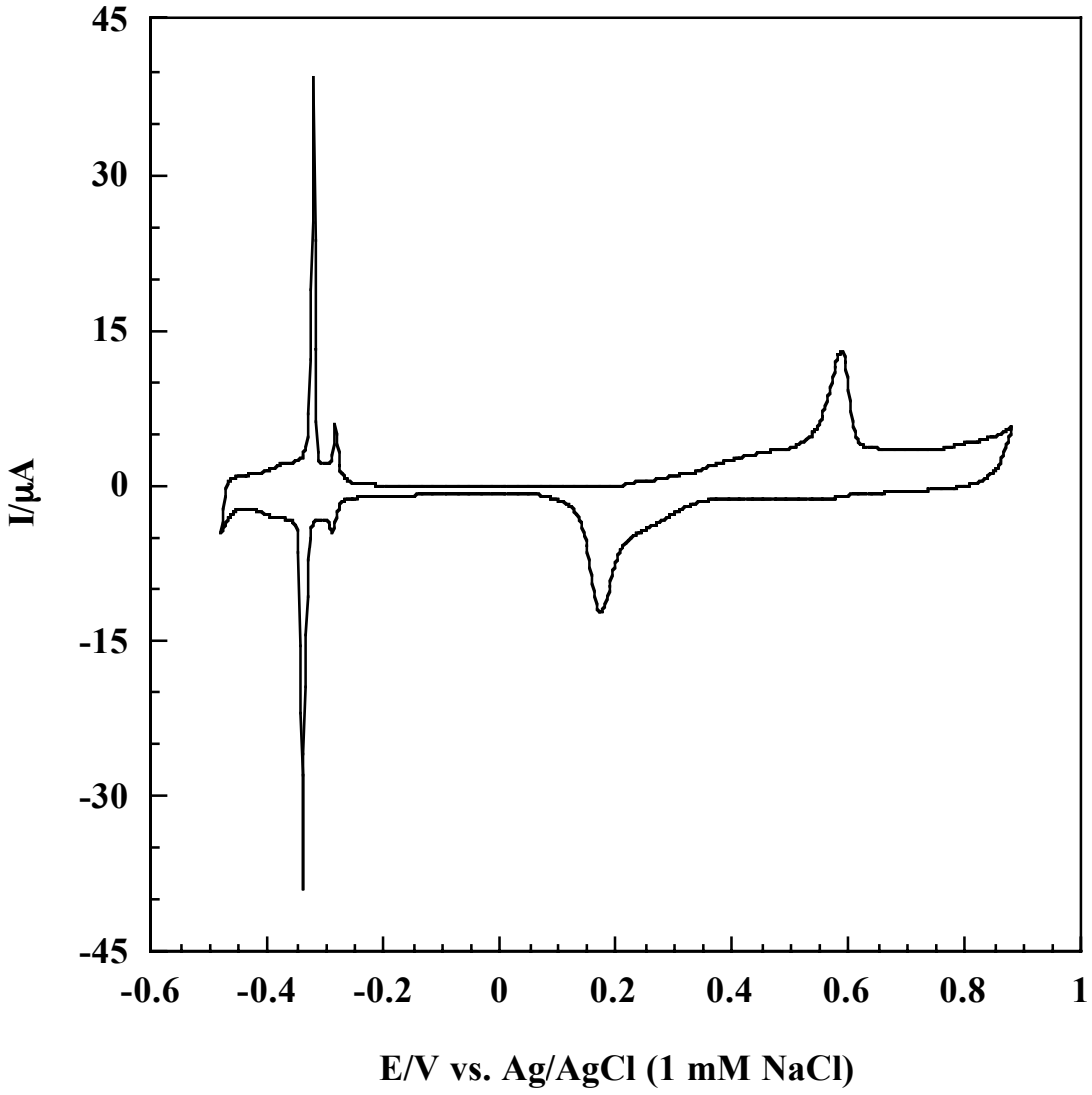

Figure 21 Continued. (D) n = 3 ML.

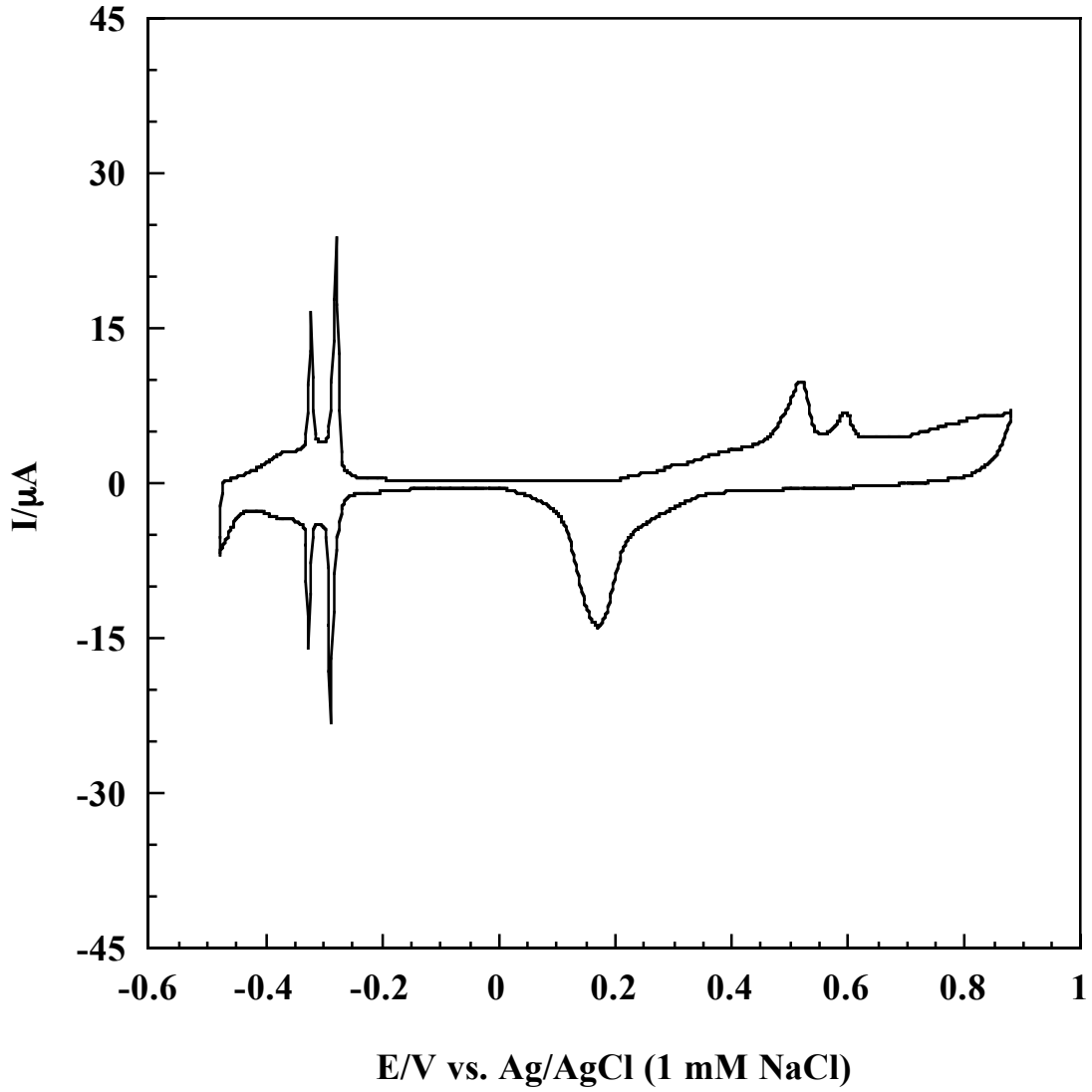

Figure 21 Continued. (E) n = 4 ML.

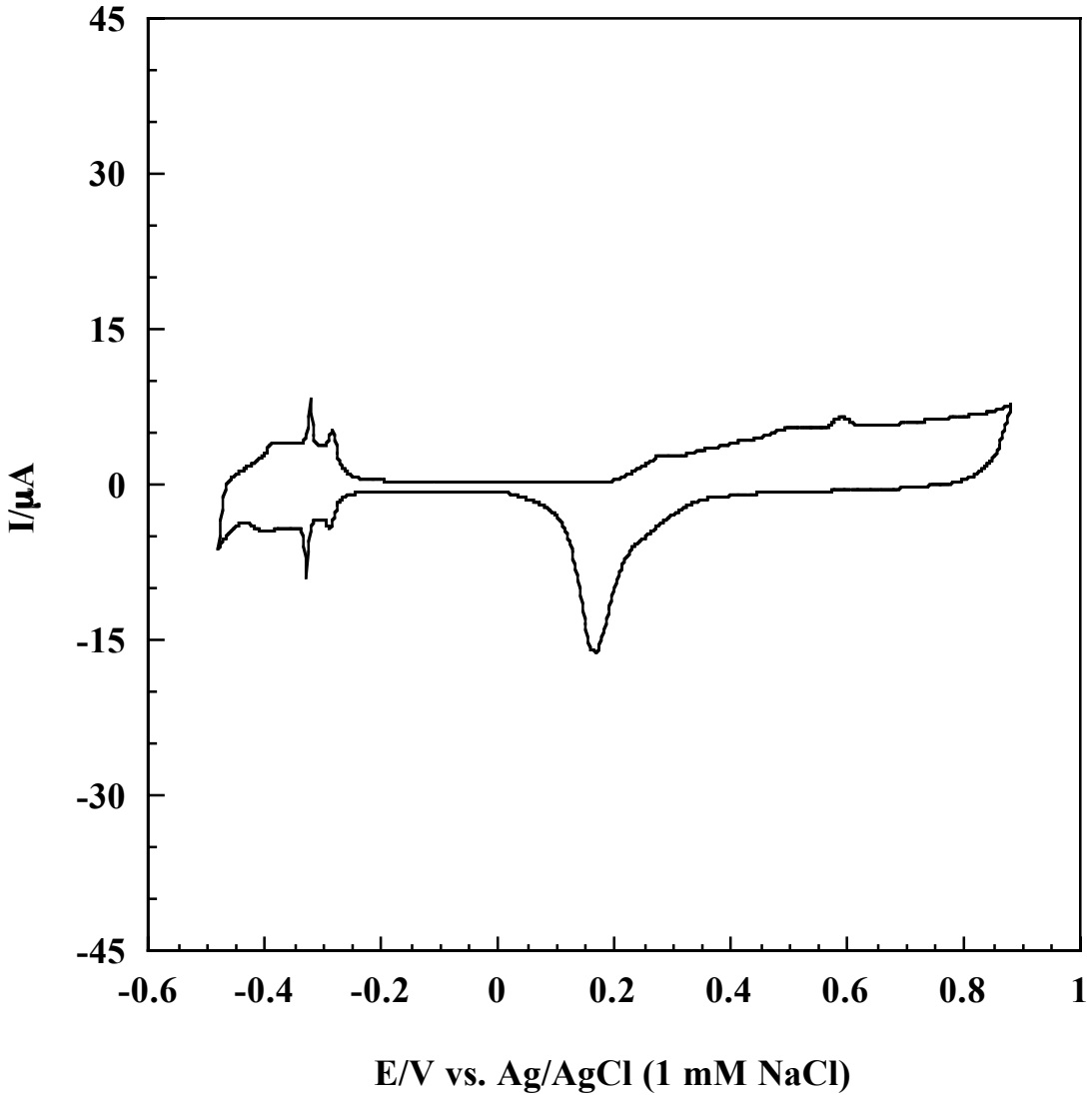

Figure 21 Continued. (F) n = 8 ML.

Beyond the double layer potential region, two sets of oxidation and reduction peaks are evident. In sulfuric acid medium, Pd redox peaks appear at more negative potential than Pt redox peaks [45,46]. Based on the voltammogram of bare Pt(111) and the established redox peak positions for ultrathin Pd films [11-13,19,20,25,26] and bulk Pt [45,46] reported in literature, the peaks at 0.58 and 0.78 V in Figure 21 (A) correspond to the oxidation of Pd thin film and uncovered Pt substrate, respectively. The peak at 0.18 V is assigned to Pd reduction. At submonolayer coverages of Pd, it is not surprising to detect voltammetric signals from the exposed Pt substrate, such as the nondescript features found between –0.17 and 0.00 V and the broad reduction peak at 0.24 V.

A comparison of the voltammogram of 0.5 ML Pd_{CPD} film with that of 1 ML Pd_{CPD} film in Figure 21 (B) shows: (i) The increase in the signal intensities of the terrace and step H_{upd} adsorption/desorption peaks, with the growth of the terrace-related peak much more dramatic than the step counterpart; (ii) The enhancement of the Pd redox peak and the weakening of Pt redox peak signal. As the Pt(111) surface becomes fully covered with the Pd film, characteristic Pt voltammetric features between –0.17 and 0.00 V are not observed.

Voltammetric features of 2 and 3 ML Pd_{CPD} films, as shown in Figures 21 (C) and (D), respectively, resemble those of 1 ML Pd_{CPD} film, except for the small differences in peak size; as Pd coverage increases, terrace H_{upd} adsorption/desorption and Pt redox peaks become slightly smaller while the Pd redox peaks slightly larger.

Interestingly, the voltammogram of 3 ML Pd_{CPD} film shows a tiny new oxidation peak at 0.52 V while no Pt redox peaks are noticeable.

Compared to Pd_{CPD} films of lower coverages, the voltammogram of 4 ML Pd_{CPD} film in Figure 21 (E) shows much larger step H_{upd} adsorption/desorption peaks and much smaller terrace H_{upd} adsorption/desorption peaks. It is interesting to note that Pd oxidation peak at 0.52 V becomes larger than that at 0.58 V. The fact that the step H_{upd} adsorption/desorption peaks are much larger than the terrace H_{upd} adsorption/desorption peaks suggests the existence of a lot of Pd islands on 4 ML Pd_{CPD} film.

As the film coverage is increased to 8 ML, the Pd island density seems to be lower than that of 4 ML Pd_{CPD} film. Apparently, this observation is borne out of the fact that the peak intensities of the terrace H_{upd} and step H_{upd} adsorption/desorption dramatically decreases. The terrace H_{upd} adsorption/desorption peaks are smaller than those of the 0.5 ML Pd_{CPD} film while step H_{upd} adsorption/desorption peaks are comparable to those of the 3 ML Pd_{CPD} film. Very small Pd oxidation peaks are observed at 0.52 and 0.58 V, even though the total Pd oxidation charge is larger than that for 4 ML Pd_{CPD} film.

The peaks at 0.52 and 0.58 V are ascribed to Pd oxidation at steps and terraces, respectively. These peak assignments are based on the concomitant changes in the peak sizes that coincide with the characteristic voltammetric nuances of the H_{upd} adsorption/desorption processes at the step and terrace sites.

As can be seen Figures 21 (B)-(F), H_{upd} deposition/desorption peak size, along with electrolytic charge, is strongly dependent upon Pd coverage. Figure 22 shows plots

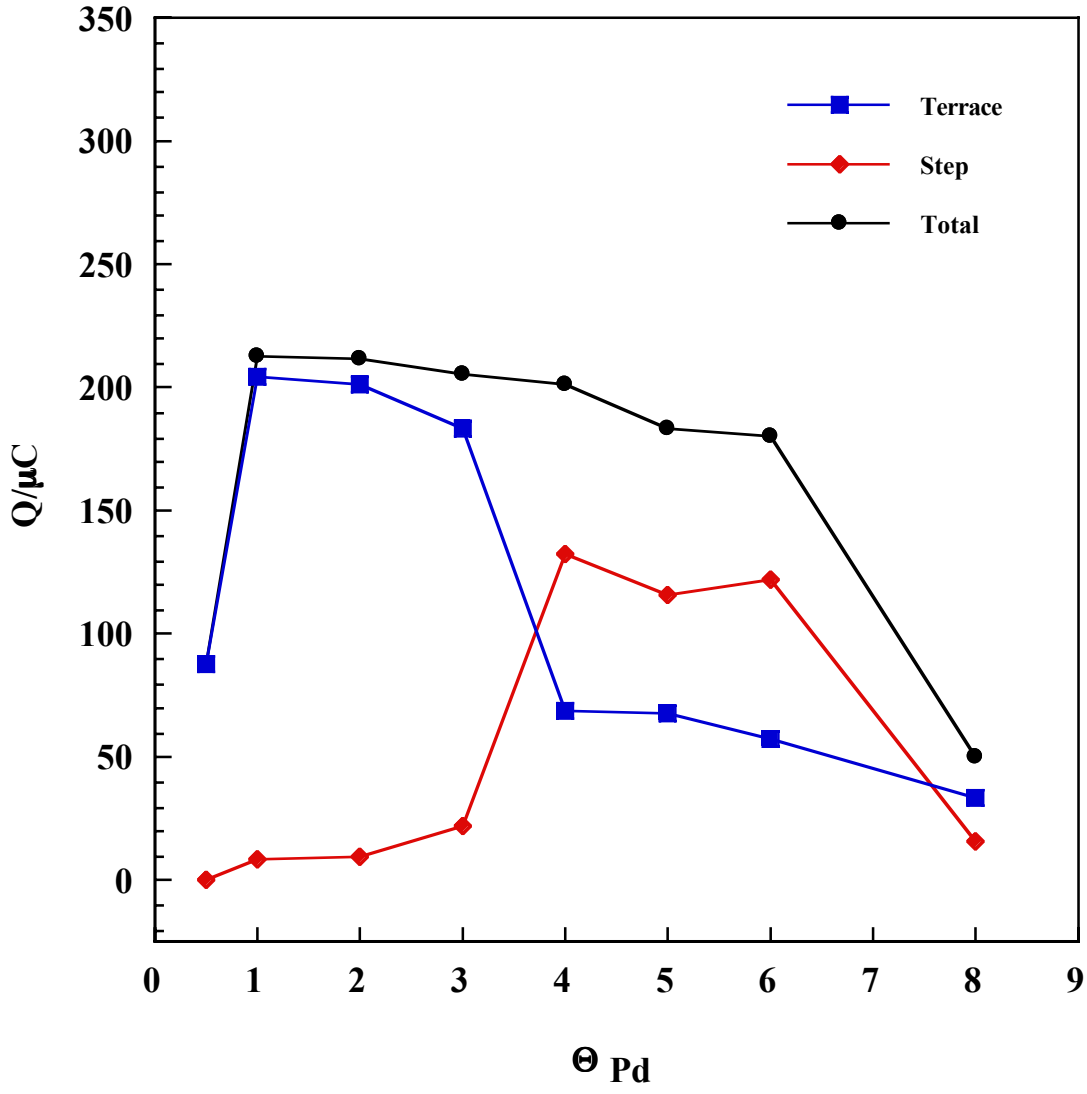

Figure 22. H_{upd} desorption charge of Pd_{CPD} films versus Pd coverage. Pd films were prepared by potentiostatic deposition. Electrode area = 1.12 cm^2.

of H_{upd} desorption charge as a function of Pd coverage. Up to 3 ML, terrace H_{upd} desorption charge is much larger than step H_{upd} desorption charge. Between 4 and 6 ML, terrace H_{upd} desorption charge is, however, smaller than step H_{upd} desorption charge. At 8 ML, terrace H_{upd} desorption charge is slightly larger than step H_{upd} desorption charge.

Compared with 1 ML Pd_{CPD} film, 0.5 ML Pd_{CPD} film shows much smaller terrace H_{upd} desorption charge. Between 1 and 3 ML, as Pd coverage increases, terrace H_{upd} desorption charge decreases slightly while step H_{upd} desorption charge marginally increases. When Pd coverage increases from 3 to 4 ML, terrace H_{upd} desorption charge becomes much smaller while step H_{upd} desorption charge becomes much larger. Between 4 and 8 ML Pd, both terrace and step H_{upd} desorption charges decrease gradually with Pd coverage.

Total H_{upd} desorption charge decreases gradually as Pd coverage increases from 1 to 6 ML. Total H_{upd} desorption charge for 8 ML Pd coverage is 54 μC, which is much smaller than the values obtained with Pd coverages less than 8 ML.

Potentiodynamic Deposition of Pd

Potential sweep deposition (PSD) involves initiating the scan at open circuit potential (0.42 V) and terminating the scan at a more negative potential until the desired charge has been accumulated. The scan rate employed is 0.1 mV/s. The prepared films were characterized using LEED, AES, and electrochemistry.

Interfacial Structure and Composition

LEED patterns for ultrathin Pd films prepared by PSD (hereafter referred as *Pd_{PSD} films*) are shown in Figure 23. Up to 3 ML, Pd_{PSD} films show sharp and bright (1×1) patterns. At Pd coverage higher than 3 ML, Pd_{PSD} films show somewhat diffuse (1×1) patterns. Compared with LEED patterns for Pd_{CPD} films of corresponding coverage, LEED spots for Pd_{PSD} films are sharper, but less bright. AES spectra for Pd $_{PSD}$ films in Figure 24 are very similar to those for Pd_{CPD} film with corresponding Pd coverage. Intensity of Pd signal at 330 eV increases while that of Pt signal at 168 eV decreases, as Pd coverage increases. The Pt signal becomes negligible at Pd coverage higher than 3 ML, unlike for Pd_{CPD} films.

Electrochemical Behavior

At a submonolayer Pd-coverage of 0.5 ML, the following voltammetric features in Figure 25 (A) are noticeable: (i) the peak at ca. –0.34 V represents H_{upd} adsorption/desorption on terraces; no equivalent signals from step sites are discernible; (ii) peaks at 0.58 and 0.78 V correspond to the oxidation of the Pd_{PSD} film and the uncovered Pt substrate, respectively; (iii) a broad redox feature for Pt(111) between –0.17 and 0.00 V; (iv) reduction of Pd and Pt at 0.18 and 0.24 V, respectively.

The voltammogram of 1 ML Pd_{PSD} film in Figure 25 (B) shows the growth of the terrace H_{upd} adsorption/desorption peaks while the peaks associated with steps remain absent. The electrodeposited Pd film completely covers the Pt(111) surface as indicated by the disappearance of the voltammetric features between –0.17 and 0.00 V. Even

(A) 0.5 ML Pd_{PSD} film

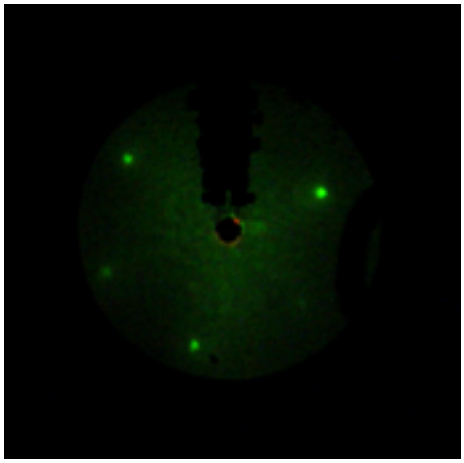

(B) 1 ML Pd_{PSD} film

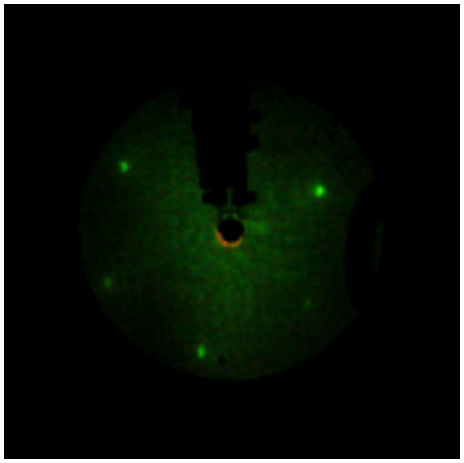

(C) 2 ML Pd_{PSD} film

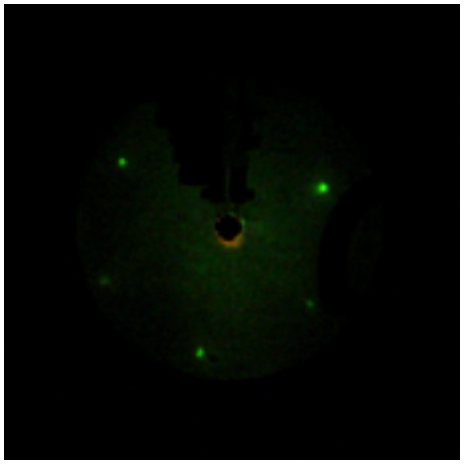

(D) 3 ML Pd_{PSD} film

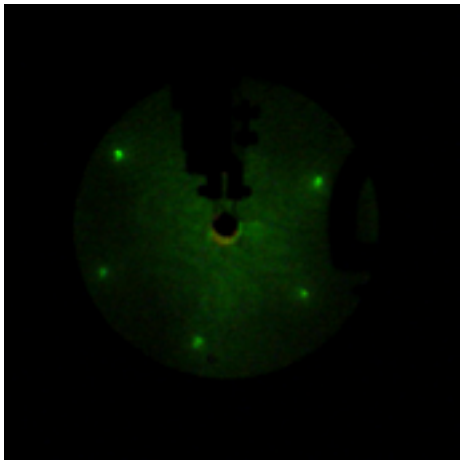

Figure 23. LEED patterns for Pd_{PSD} films on Pt(111). Pd coverage = (A) 0.5, (B) 1, (C) 2, and (D) 3 ML. Pd films were prepared by potentiodynamic deposition. Beam energy = 62.0 eV; beam current = 2 μA.

(E) 4 ML Pd_{PSD} film

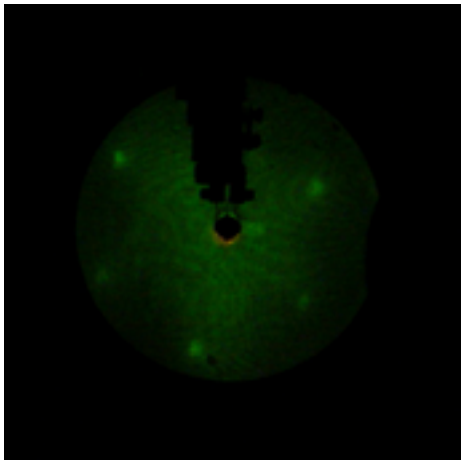

(F) 8 ML Pd_{PSD} film

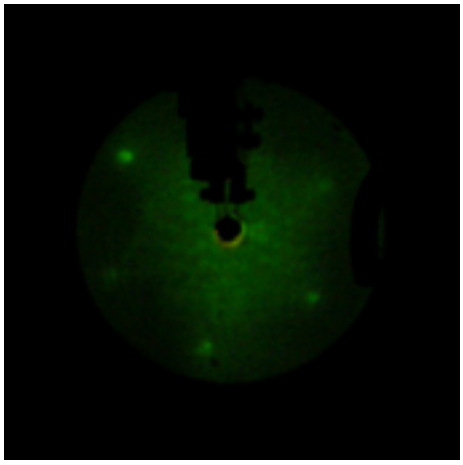

Figure 23 Continued. LEED patterns for Pd_{PSD} films on Pt(111): Pd coverage = (E) 4 and (F) 8 ML.

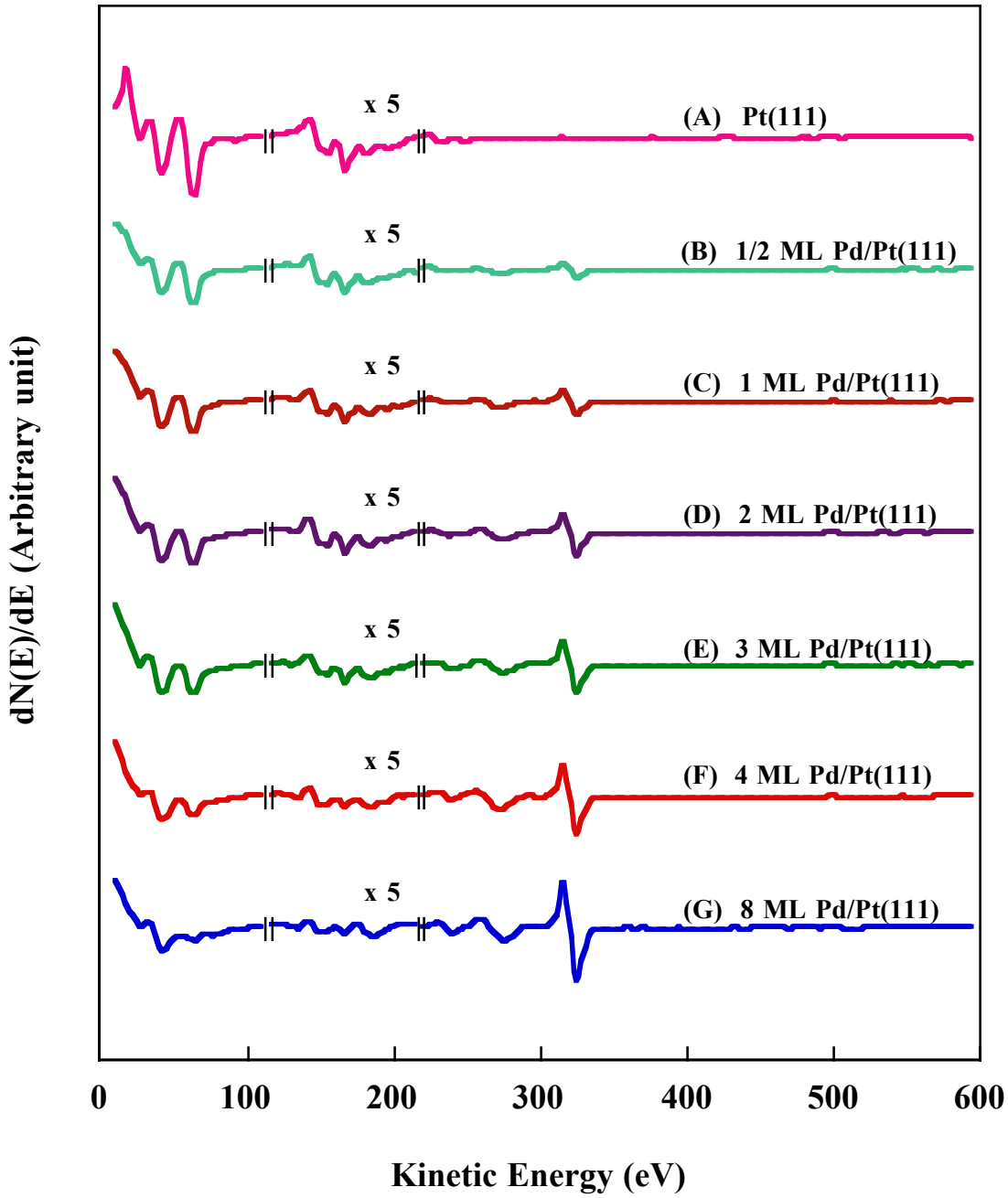

Figure 24. AES spectra for Pd_{PSD} films on Pt(111). Pd films were prepared by potentiodynamic deposition. Incident beam energy = 2 keV; beam current = 1 μA.

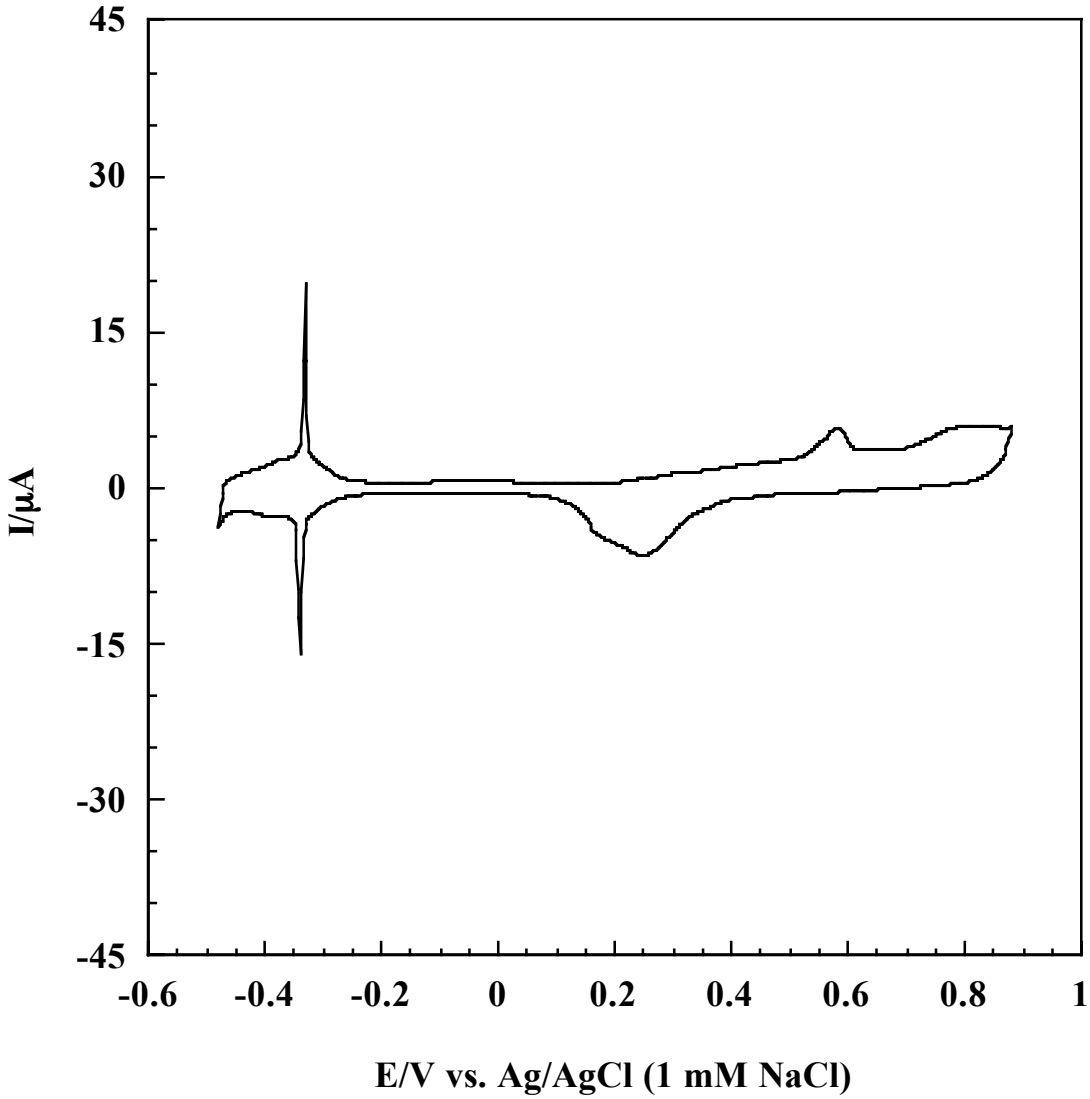

Figure 25. Cyclic voltammogram for n Pd_{PSD} films on Pt(111) in 100 mM H_2SO_4. (A) n = 0.5 ML. Pd was deposited by potentiodynamic deposition. Sweep rate = 2 mV/s. Electrode area = 1.12 cm^2.

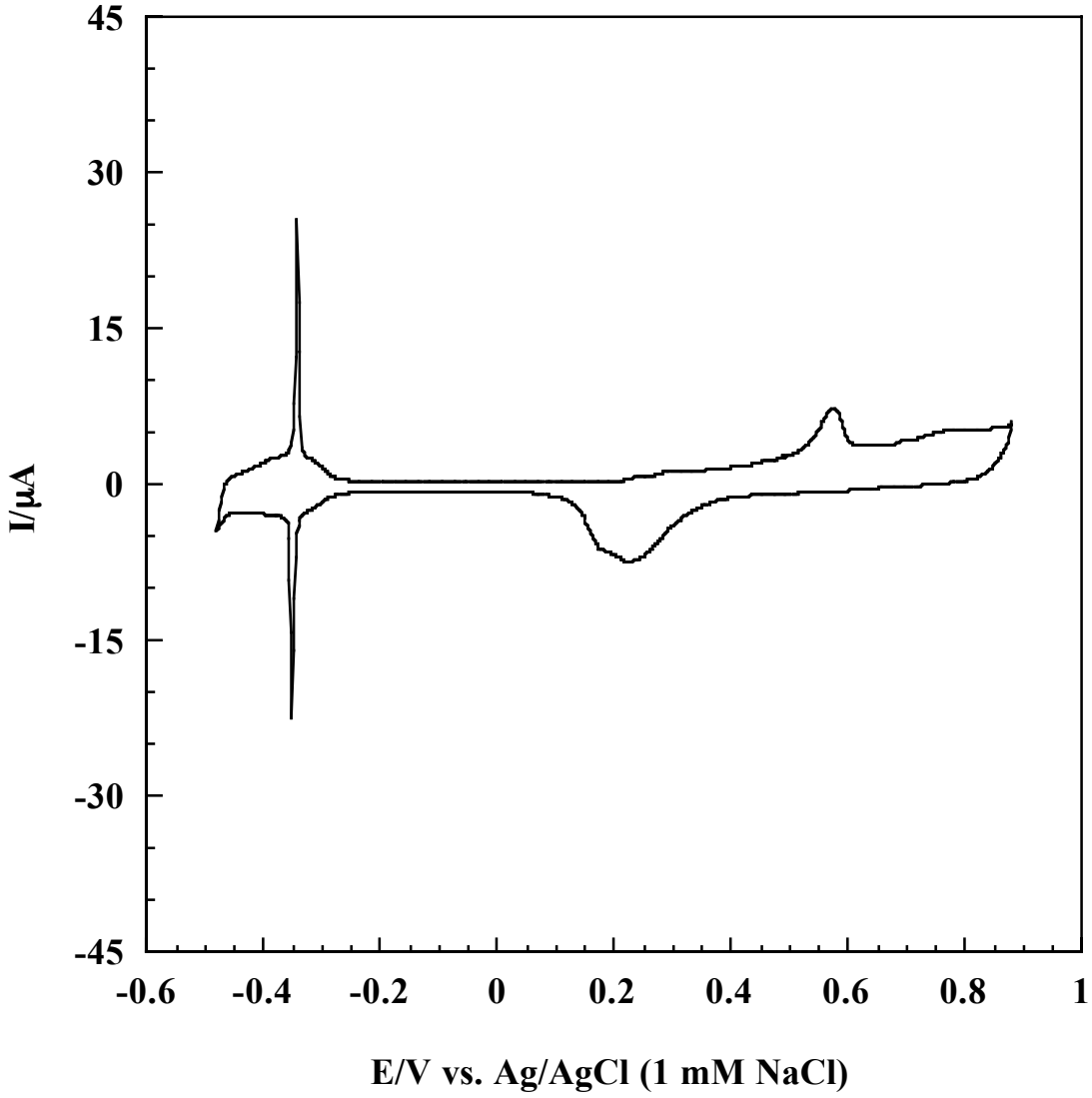

Figure 25 Continued. (B) n = 1 ML.

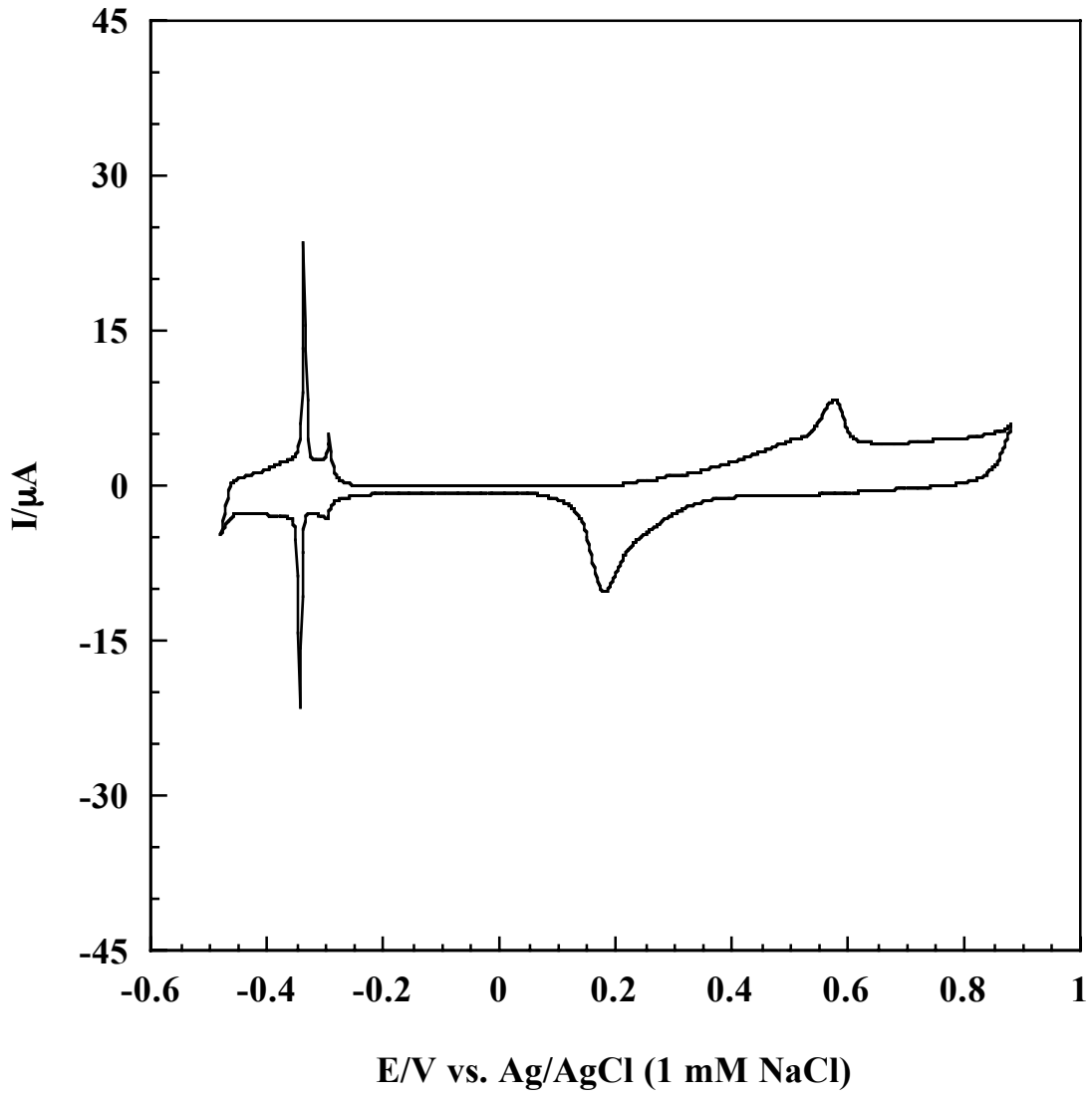

Figure 25 Continued. (C) n = 2 ML.

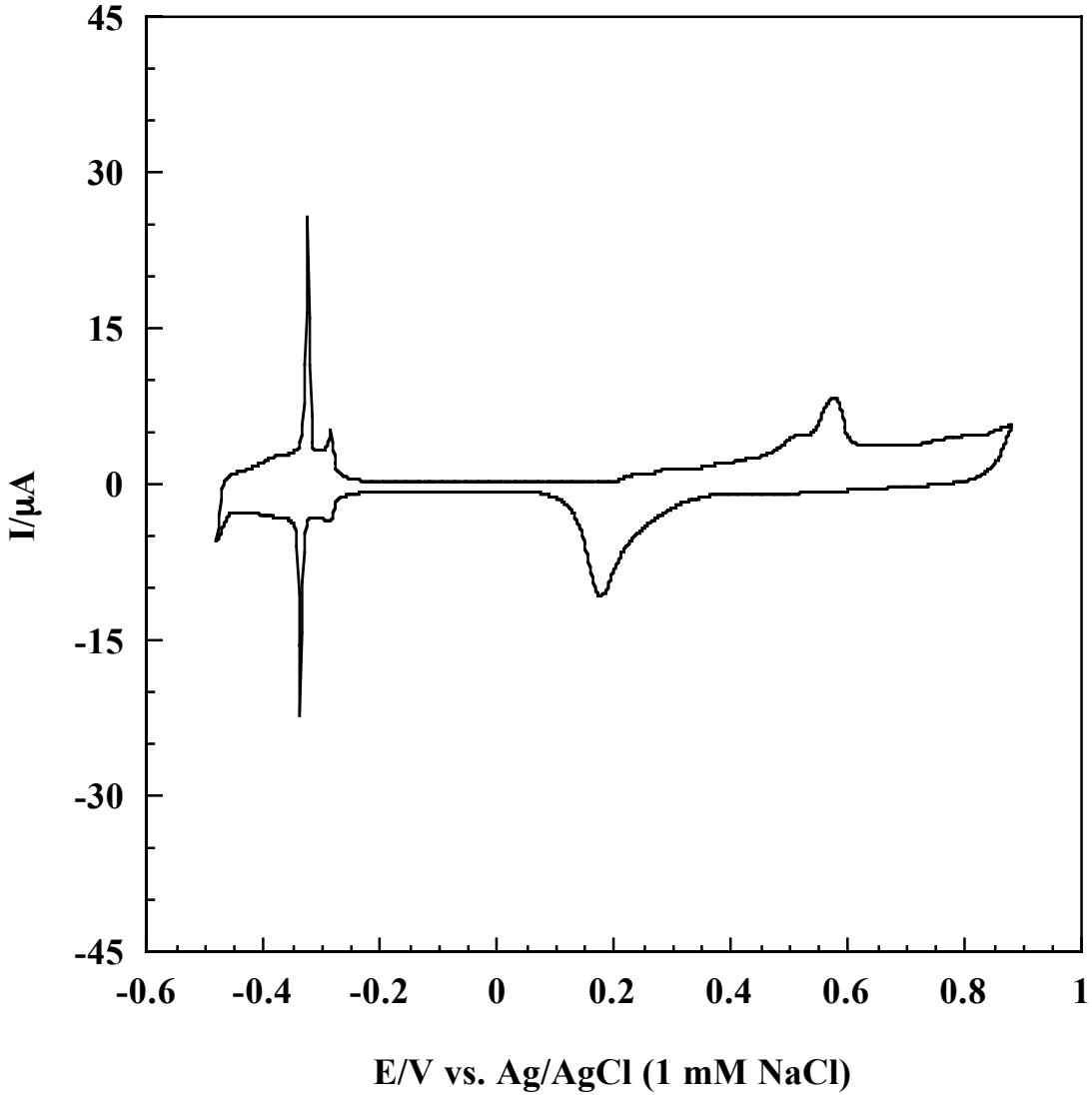

Figure 25 Continued. (D) n = 3 ML.

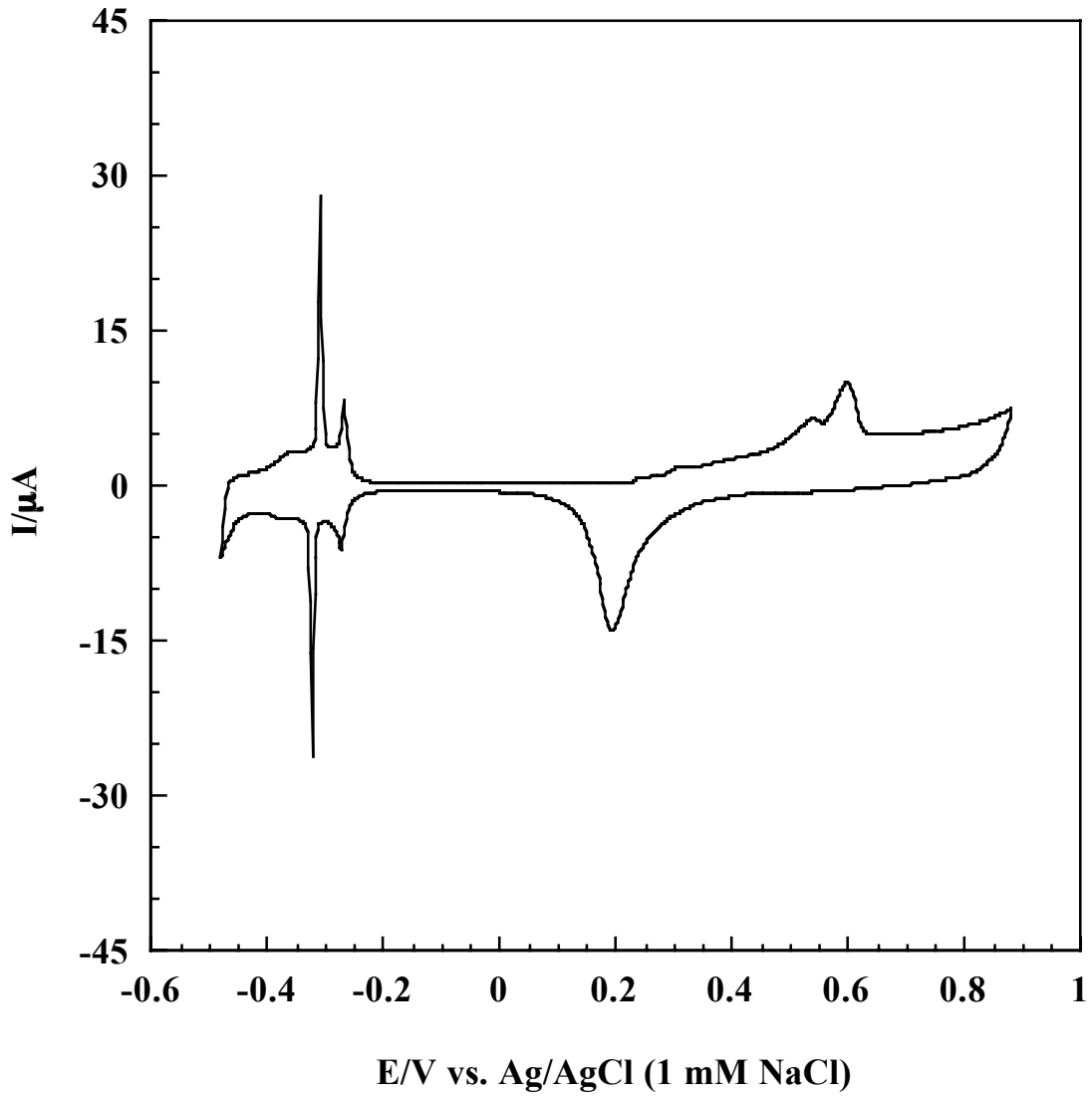

Figure 25 Continued. (E) n = 4 ML.

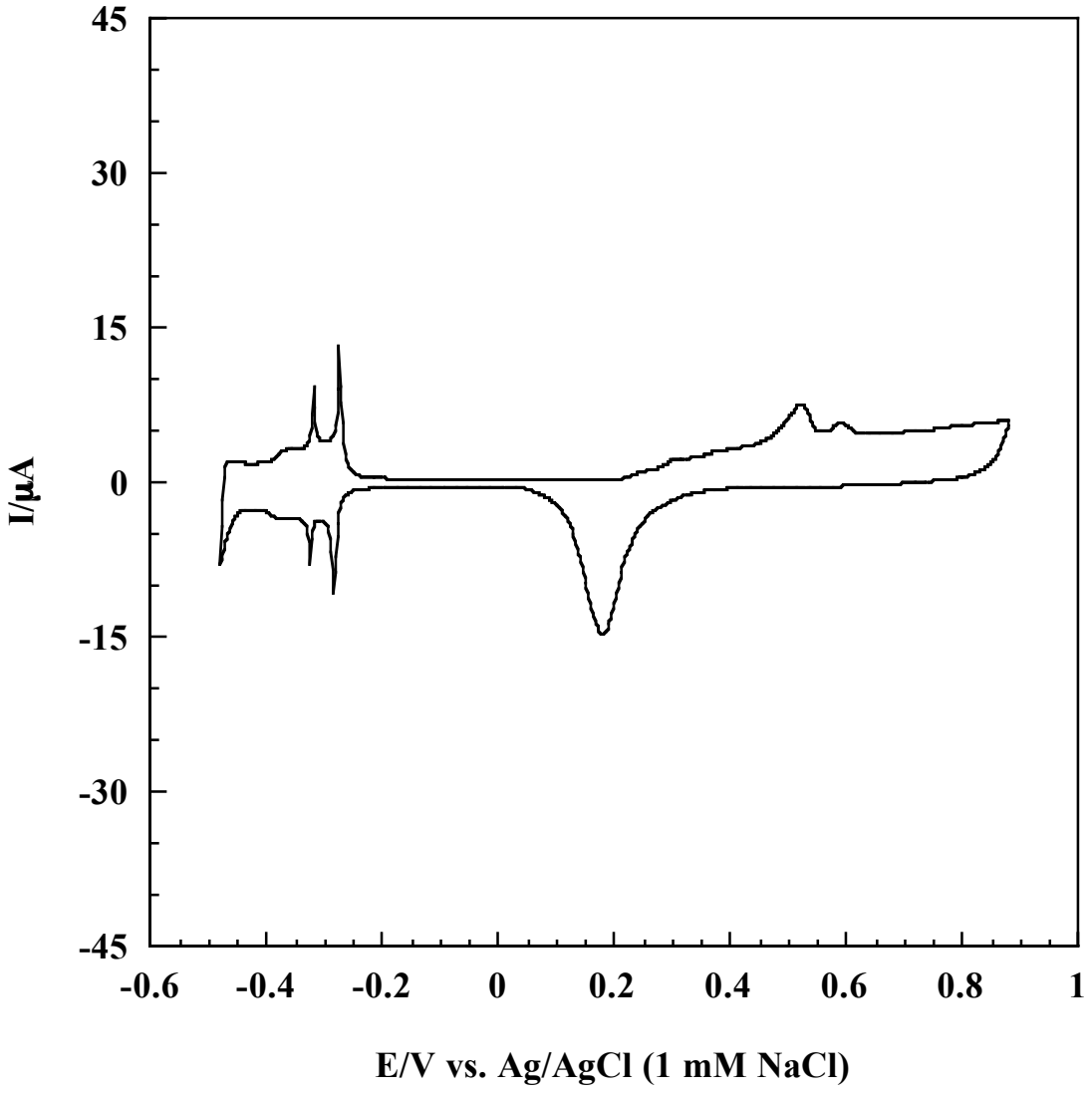

Figure 25 Continued. (F) n = 8 ML.

though the Pt substrate appears to be fully covered with the Pd adlayer, the Pt oxidation peak at 0.78 V is still present and its reduction counterpart becomes larger than the Pd reduction peak.

At a Pd coverage of 2 ML, step H_{upd} adsorption/desorption peaks emerge (Figure 25 (C)). The size and shape of the terrace H_{upd} adsorption/desorption peaks closely resemble those of a 1 ML Pd_{PSD} film. A new broad step Pd oxidation peak is seen at 0.48 V which is slightly more negative with respect to the peak position for terrace Pd oxidation. The Pt reduction peak finally disappeared.

The voltammogram of the 3 ML Pd_{PSD} film (Figure 25 (D)) is very similar to that of the 2 ML Pd_{PSD} film, except for a slightly larger step Pd oxidation peak at 0.51 V.

As shown in Figure 25 (E), at a Pd coverage of 4 ML, peaks for step H_{upd} adsorption/desorption and step Pd oxidation become more prominent while the peak intensity for the terrace H_{upd} adsorption/desorption remained virtually the same.

Figure 25 (F) reveals that, for the 8 ML Pd_{PSD} film, the step-related voltammetric peaks for H_{upd} adsorption/desorption and Pd oxidation become larger than their terrace counterparts.

Figure 26 shows plots of the site-dependent H_{upd}-desorption charge as a function of Pd coverage. Up to 4 ML Pd, the terrace H_{upd} desorption charge is much larger than the step H_{upd} desorption charge. As Pd coverage increases from 1 to 4 ML, the step H_{upd} desorption charge increases gradually while the terrace-related charge remains almost unchanged. At 8 ML Pd, the step H_{upd} desorption charge exceeds the terrace H_{upd} desorption charge.

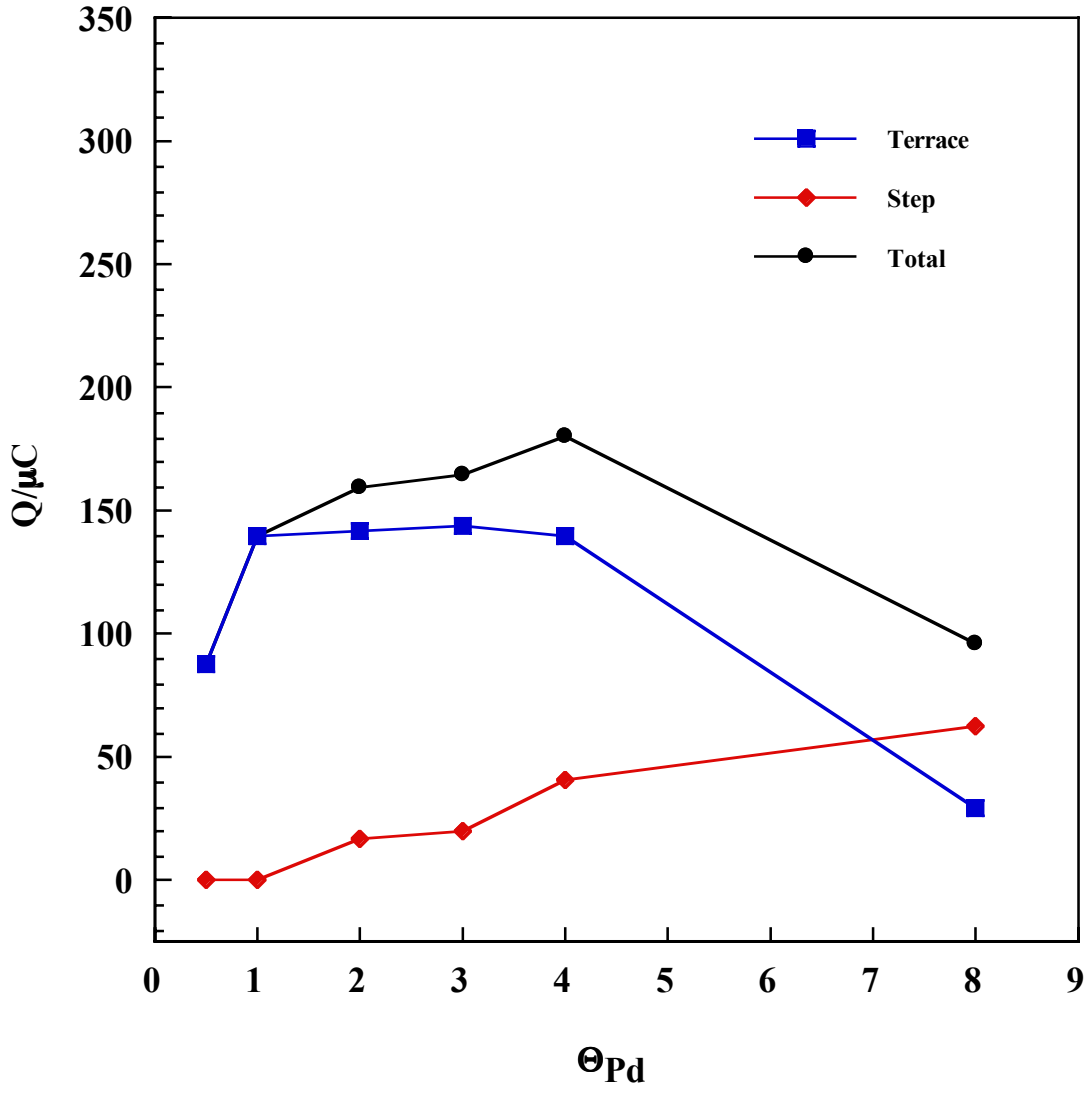

Figure 26. H_{upd} desorption charge of Pd_{PSD} films versus Pd coverage. Pd films were prepared by potentiodynamic deposition. Electrode area = 1.12 cm^2.

The total H_{upd} desorption charge gradually increases up to 4 ML Pd coverage and then decreases at 8 ML Pd coverage. Reasons remain unclear as to why the total H_{upd} desorption charge increases with Pd coverage up to 4 ML while the terrace H_{upd} desorption charge appears to level off.

Thermal Annealing of Ultrathin Pd films

Thermal annealing has been conventionally used to induce smoothening of metal electrode surfaces. To investigate the effects of thermal annealing on the electrodeposited Pd films, various Pd_{CPD} films were heated to 250 °C for 15 minutes under UHV conditions and then slowly cooled to room temperature.

Post-annealing LEED spectra in Figure 27 indicate that thermal annealing enhances the brightness and sharpness of the spots, implying that the Pd film surface becomes more ordered and smoother after thermal treatment. At Pd coverages of 3 ML or higher, a diffuse $(\sqrt{3}\times\sqrt{3})R30°$ adlayer structure is typically obtained after the thermal annealing.

Voltammograms for thermally annealed Pd_{CPD} films are displayed in Figure 28. Up to 2 ML Pd coverage, no step H_{upd} adsorption/desorption peaks are discernible. The fact that only terrace-related peaks are observed suggests that thermal annealing induces smoothening of Pd films surfaces. It is interesting to note that, for thermally treated Pd_{CPD} films with coverages of 3 ML or higher, the characteristic adsorption/desorption peaks associated with H_{upd} disappear, suggesting the onset of bulk-like behavior of the Pd film.

(A) 0.5 ML Pd_{CPD} film

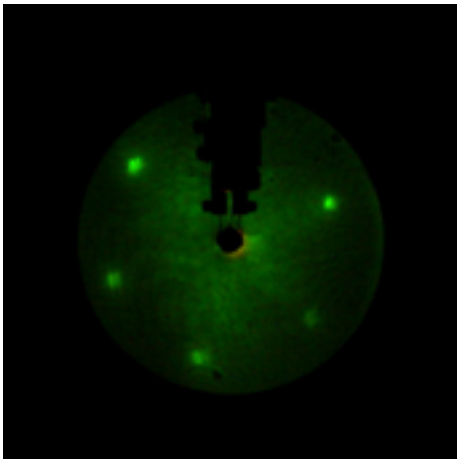

(B) 1 ML Pd_{CPD} film

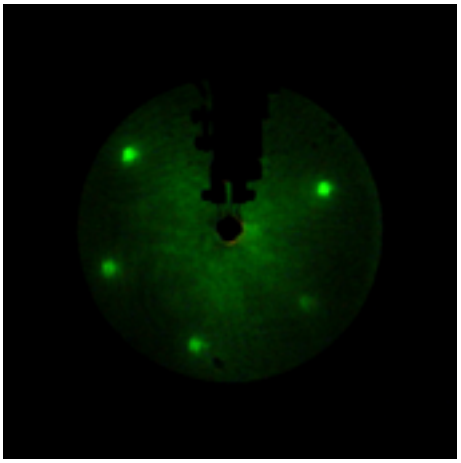

(C) 2 ML Pd_{CPD} film

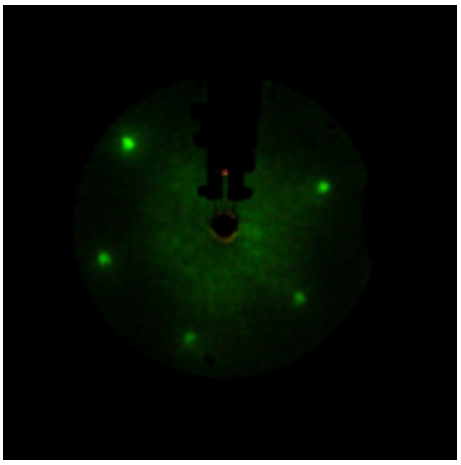

(D) 3 ML Pd_{CPD} film

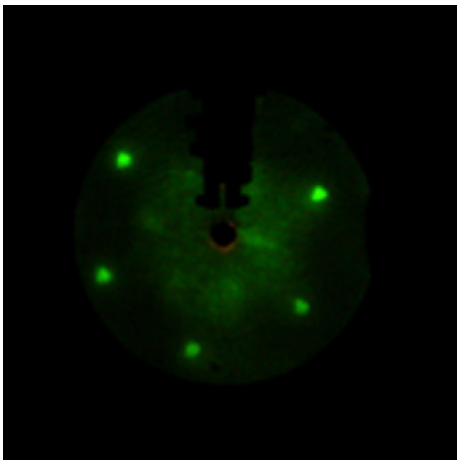

Figure 27. LEED patterns for thermally annealed Pd_{CPD} films on Pt(111). Pd coverage = (A) 0.5, (B) 1, (C) 2, and (D) 3 ML. Thermal annealing was performed at 250 °C for 15 minutes under UHV conditions. Pd films were prepared by potentiostatic deposition. Beam energy = 62.0 eV; beam current = 2 μA.

(E) 4 ML Pd_{CPD} film

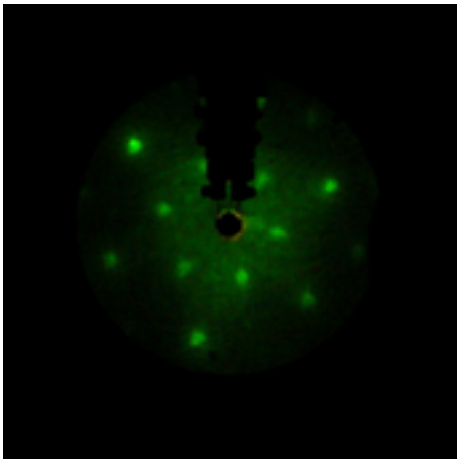

(F) 8 ML Pd_{CPD} film

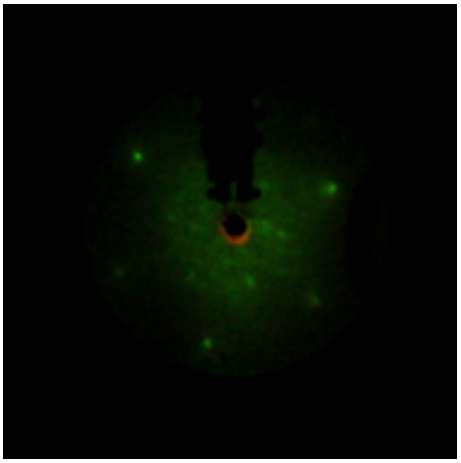

Figure 27 Continued. (E) 4 and (F) 8 ML Pd_{CPD} films on Pt(111).

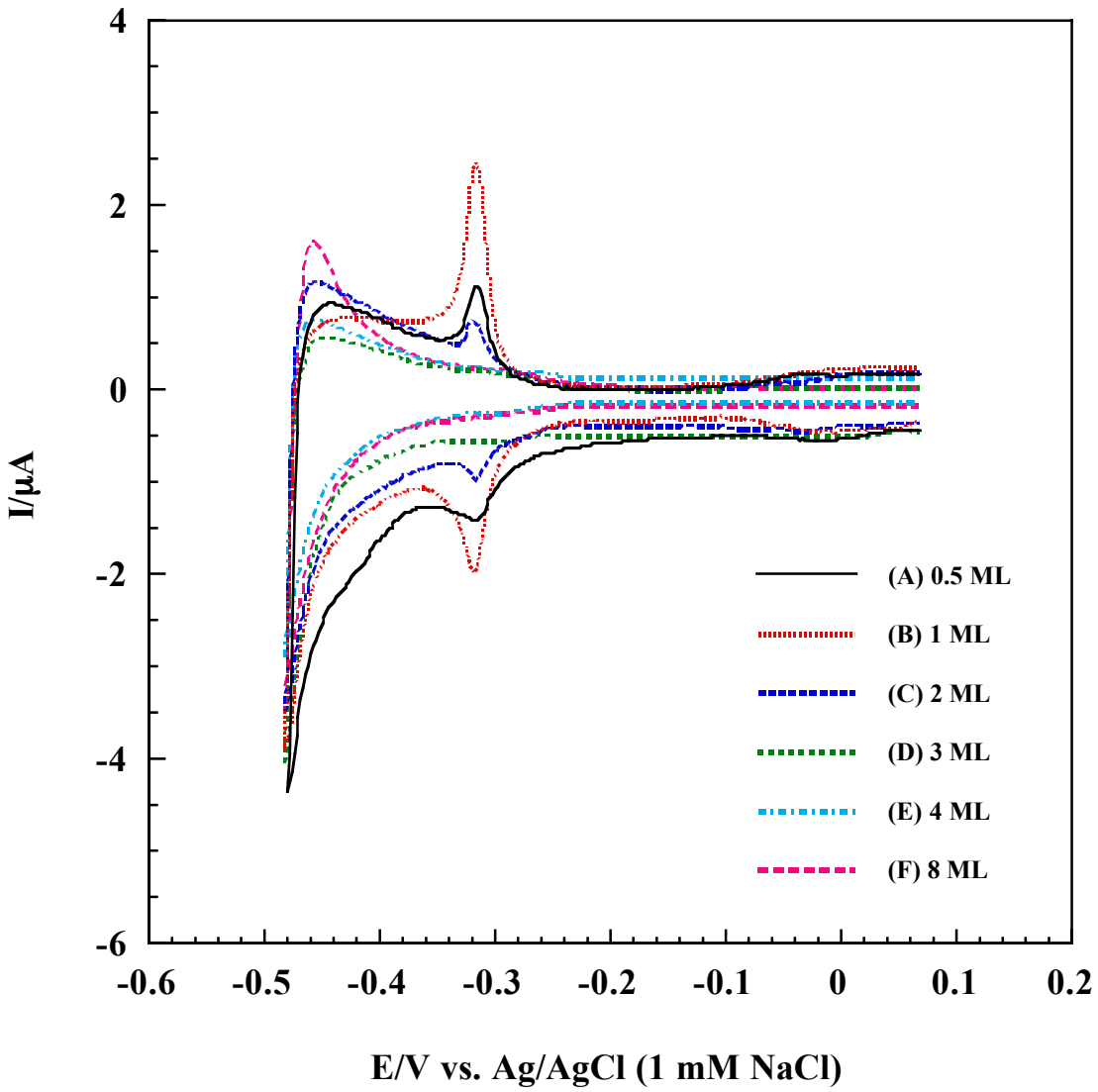

Figure 28. Voltammograms for thermally annealed Pd_{CPD} films on Pt(111) in 100 mM H_2SO_4. Thermal annealing was performed at 250 °C for 15 minutes under UHV conditions. Pd films were prepared by potentiostatic deposition. Sweep rate = 2 mV s^{-1}. Electrode area = 1.12 cm^2.

Electrochemical Annealing of Ultrathin Pd films

Programmed electrode-potential excursions to regions bordering dramatic surface perturbation can be considered an electrochemical analog to thermal annealing. Under the present study, two different potential windows were explored: (i) the region between the inception of the hydrogen evolution reaction (HER) and double-layer charging; and (ii) the region between HER and Pd film-surface oxidation. Potential cycling within these pre-defined regions is dubbed as electrochemical annealing (EC annealing).

Potential Cycling at Potentials Prior to Pd Surface Oxidation

A 4 ML Pd_{CPD} film was cycled between the early onset of HER at –0.48 V and at the double-layer region, –0.02 V. As shown in Figure 29 (A), the 1st potential cycle yields two pairs of redox peaks: terrace and step H_{upd} adsorption/desorption peaks at –0.34 and –0.30 V, respectively. Step voltammetric peaks are slightly larger than those of the terrace. The 2nd potential cycle in Figure 29 (B) gives rise to slightly sharper terrace and step H_{upd} adsorption/desorption peaks. Further potential cycling leads to minimal change in voltammetric features, as shown by the results of the 5th potential cycle (Figure 29 (C)).

When the same series of potential cycling was performed on 4 ML Pd_{PSD}, Figure 30 (A) shows that, after the 1st cycle, large terrace and small step H_{upd} adsorption/desorption peaks are observed at -0.34 and –0.30 V, respectively. The 2nd potential cycle (Figure 30 (B)) produces sharper peaks for both terrace and step H_{upd}

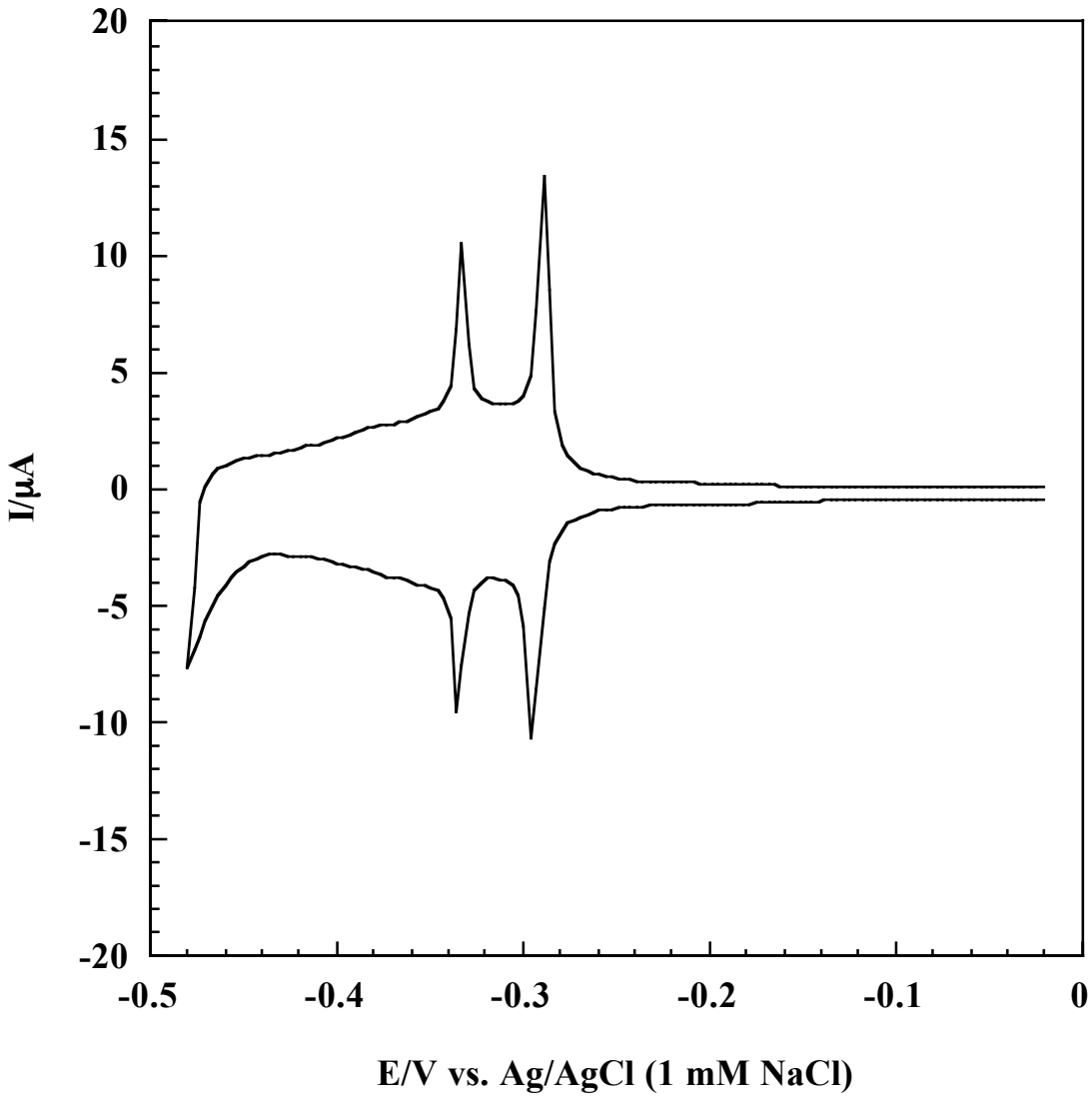

Figure 29. Voltammogram for 4 ML Pd_{CPD} film on Pt(111) during potential cycling in 100 mM H_2SO_4 between the double layer and hydrogen evolution regions after Pd deposition. (A) First potential cycle. Pd film was prepared by potentiostatic deposition. Sweep rate = 2 mV/sec. Electrode area = 1.12 cm^2.

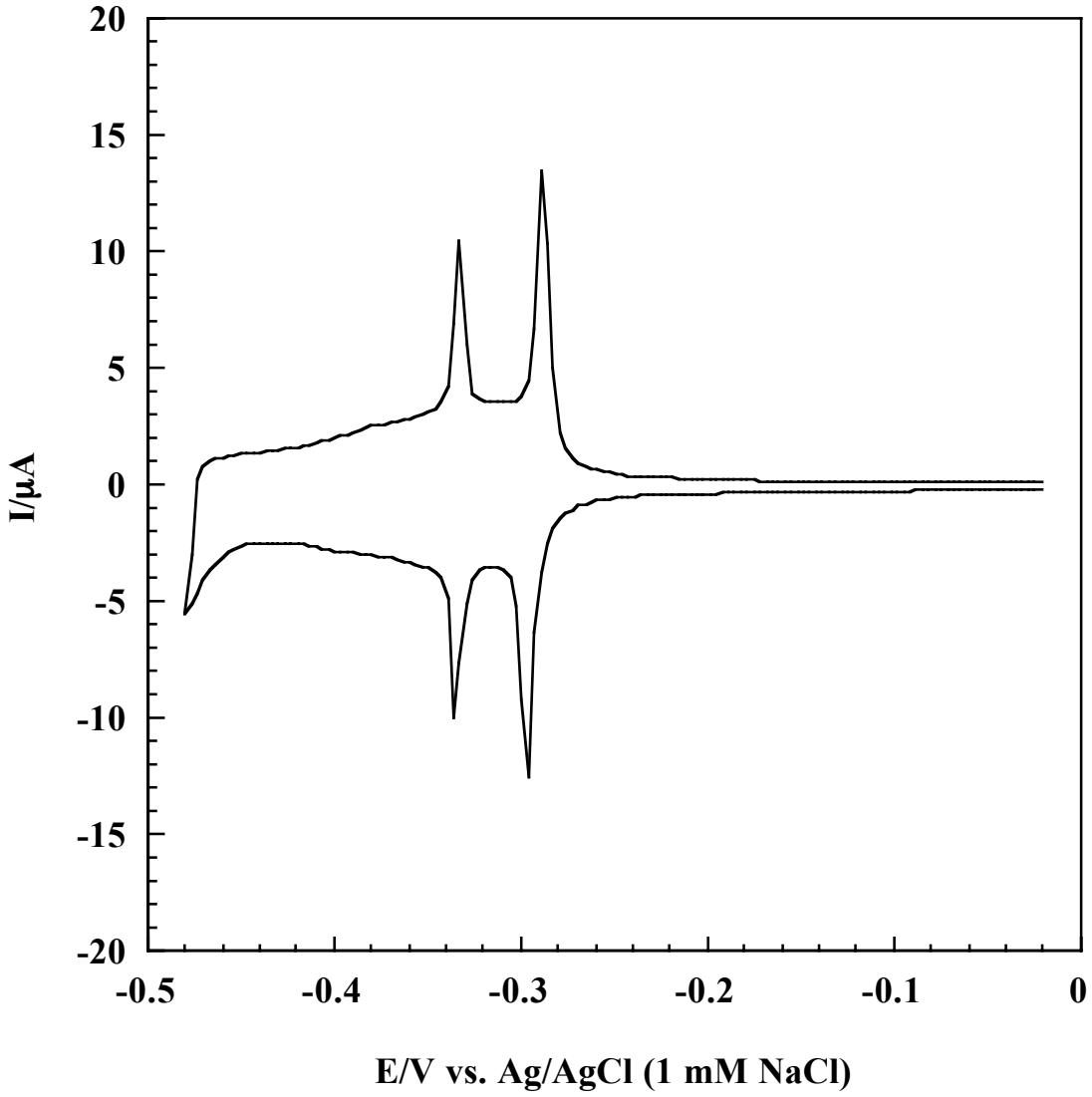

Figure 29 Continued. (B) Second potential cycle.

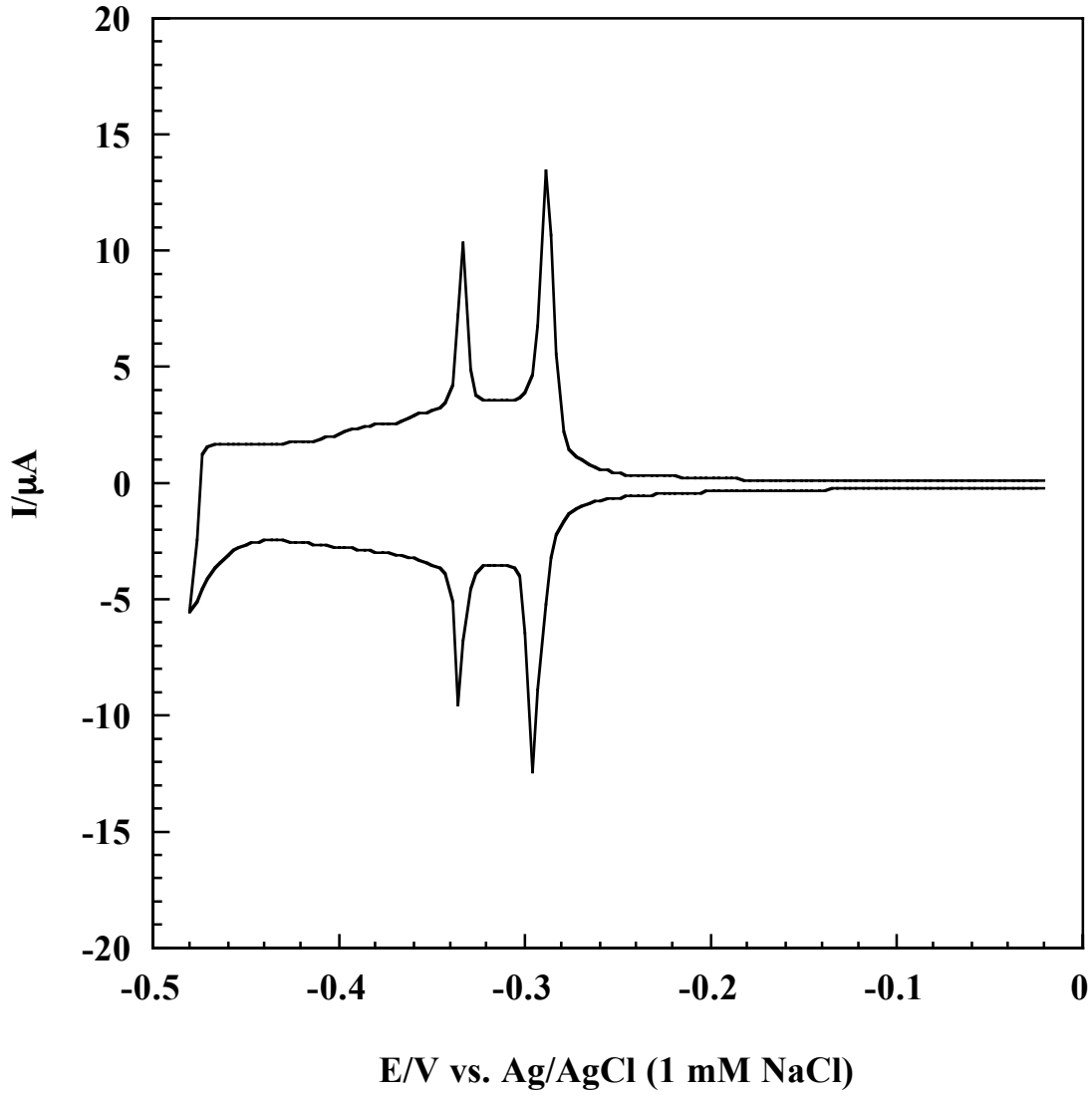

Figure 29 Continued. (C) Fifth potential cycle.

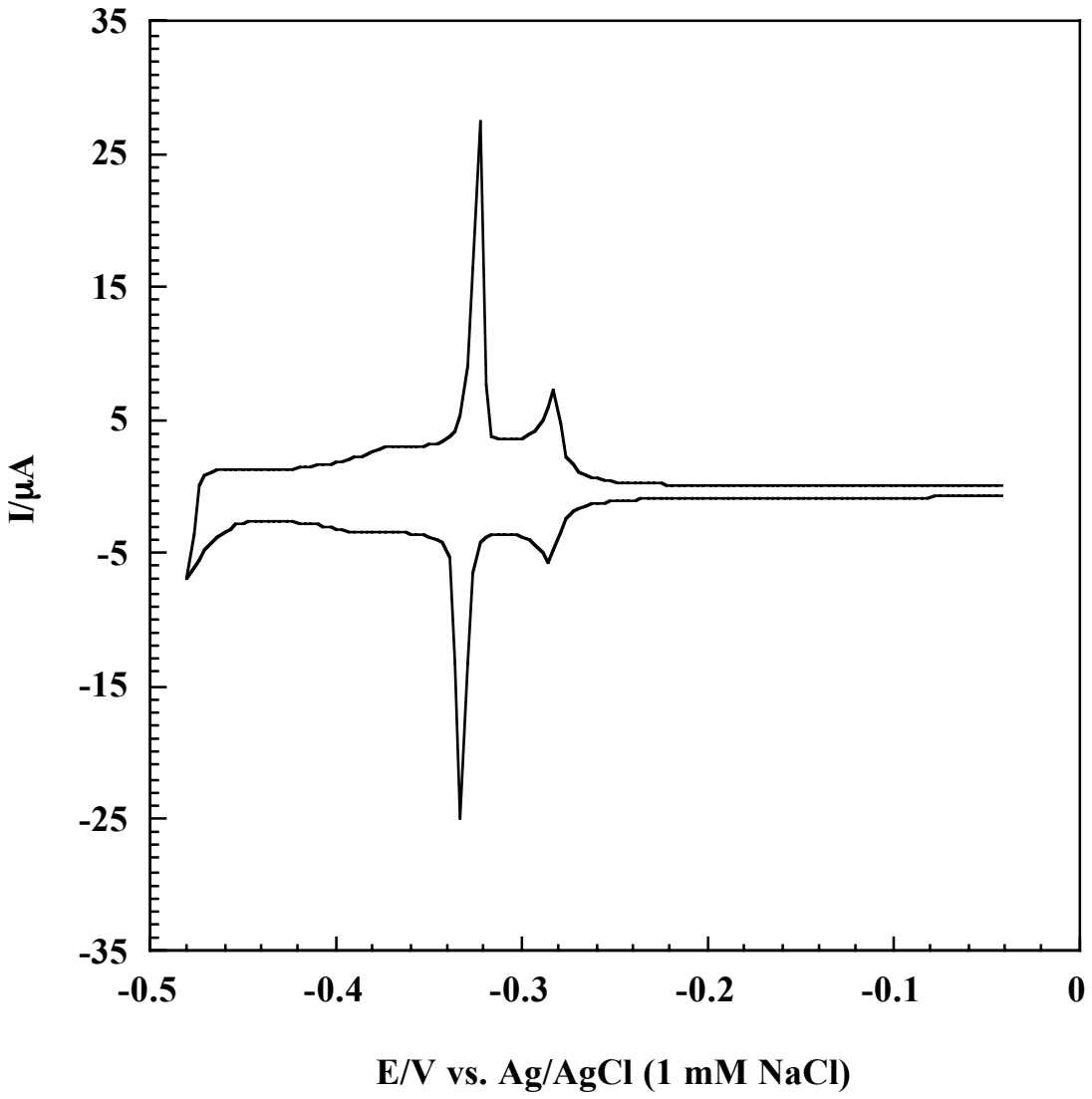

Figure 30. Voltammogram for 4 ML Pd_{PSD} film on Pt(111) during potential cycling in 100 mM H_2SO_4 between the double layer and hydrogen evolution regions after Pd deposition. (A) First potential cycle. Pd film was prepared by potentiodynamic deposition. Sweep rate = 2 mV/s. Electrode area = 1.12 cm^2.

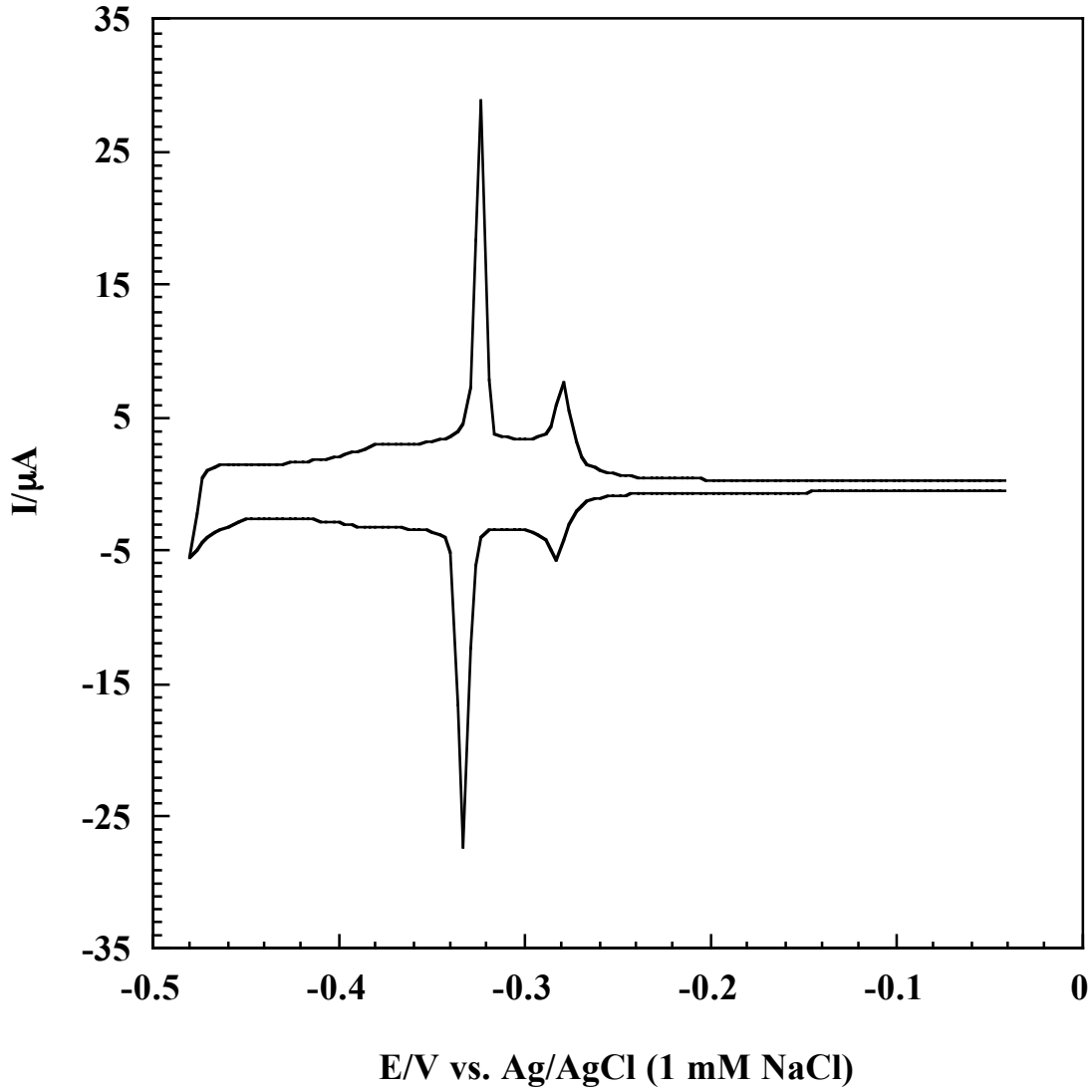

Figure 30 Continued. (B) Second potential cycle.

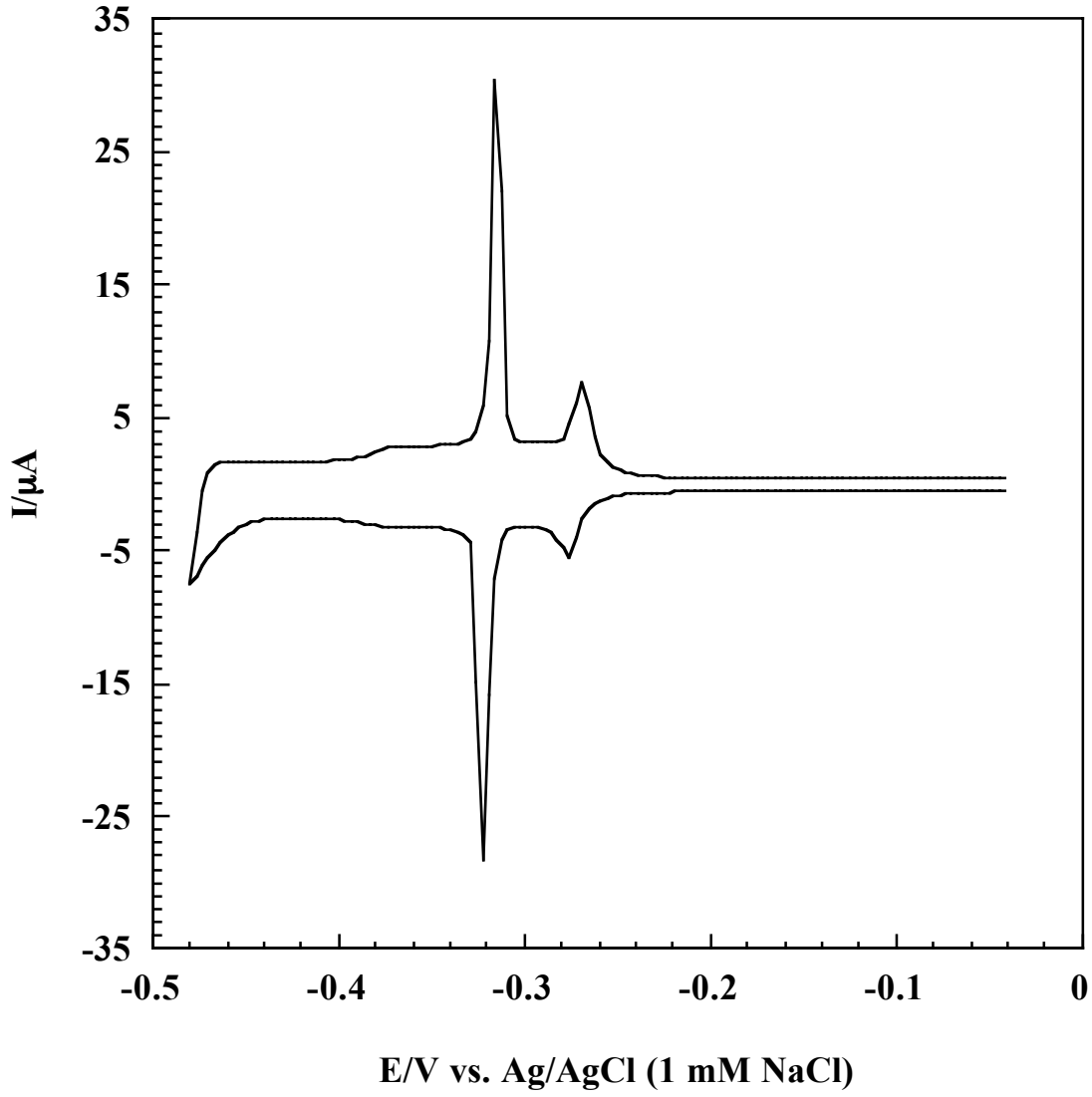

Figure 30 Continued. (C) Fifth potential cycle.

adsorption/desorption. The 5th potential cycle (Figure 30 (C)) reveals no drastic changes in the voltammetric features.

The above observations imply that, for both Pd_{CPD} and Pd_{PSD} films, the 1st potential cycling between the hydrogen evolution and double-layer regions induces only slight smoothening effects on the Pd films. Further potential cycling does not lead to significant morphological changes in Pd film surface.

Electrochemical Cycling up to Anodic-oxidation Potentials

The potential window for electrochemical annealing was extended to 0.88 V at which Pd surface oxidation transpires. For 4 ML Pd_{CPD} film, the 1st potential cycle in Figure 31 (A) shows that the voltammetric features at –0.30 V and 0.48 V, associated with step H_{upd} adsorption/desorption and step Pd oxidation, respectively, are much larger than those of the terrace-related processes. A large Pd reduction peak is observed at 0.18 V. The 2nd potential cycle in Figure 31 (B), marks the growth of the terrace and step H_{upd} adsorption/desorption peaks; both peak sizes appear nearly the same. A slight reduction in the peak sizes for the step Pd oxidation and Pd reduction is observed.

Step-related peaks continue to diminish in intensity during the 3rd and 5th potential cycles (Figure 31 (C) and (D), respectively) while, conversely, the peaks associated with the terrace become more pronounced. Interestingly, Figure 31(D) shows a small broad Pt reduction peak at 0.24 V.

At the 8th potential cycle in Figure 31 (E), the signal intensity decreases for the voltammetric peaks representing H_{upd} adsorption/desorption on both terraces and steps;

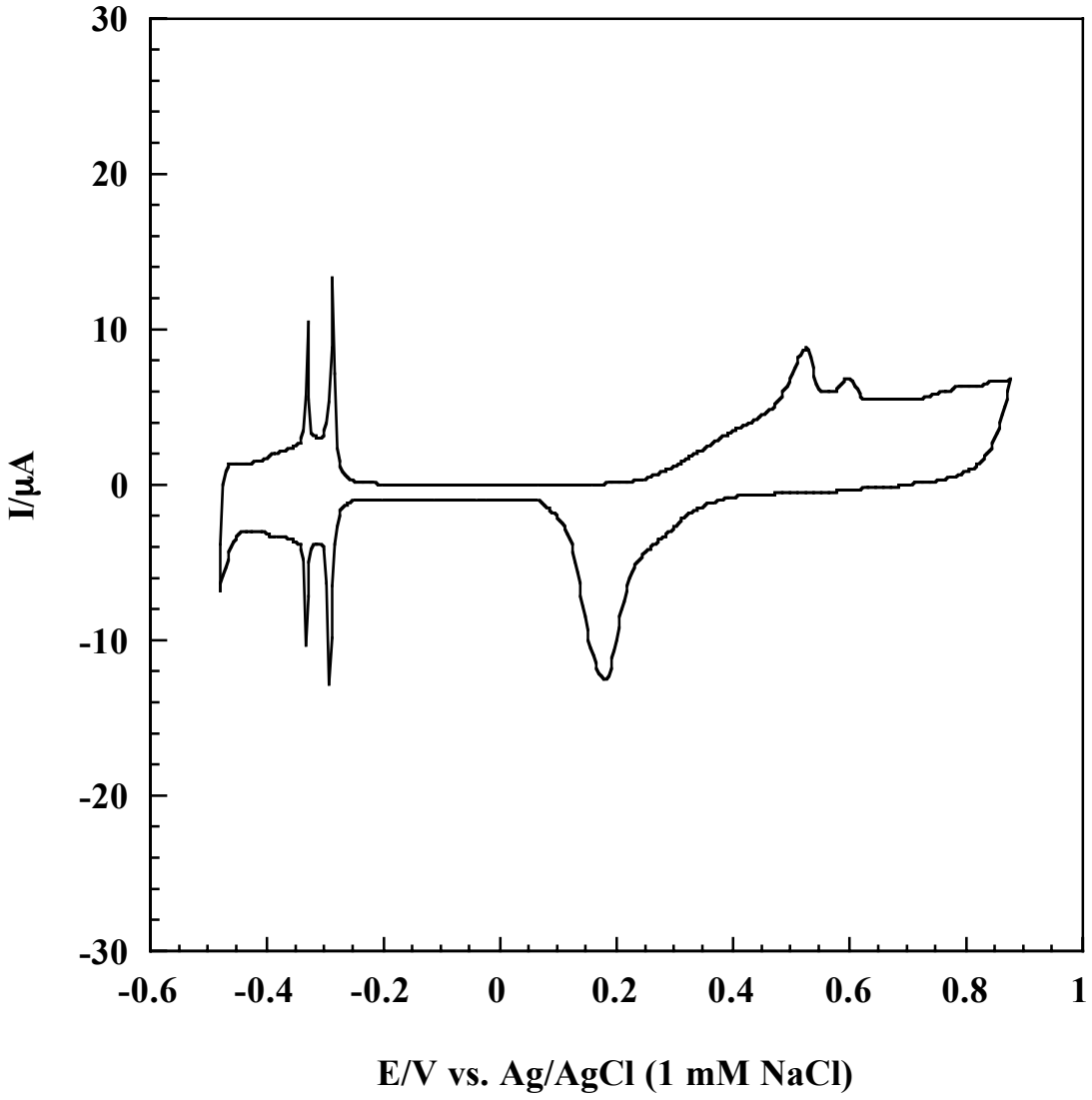

Figure 31. Cyclic voltammogram for 4 ML Pd_{CPD} film on Pt(111) during potential cycling in 100 mM H_2SO_4 between the hydrogen evolution and Pd oxidation regions. (A) First potential cycle. Pd film was prepared by potentiostatic deposition. Sweep rate = 2 mV/sec. Electrode area = 1.12 cm^2.

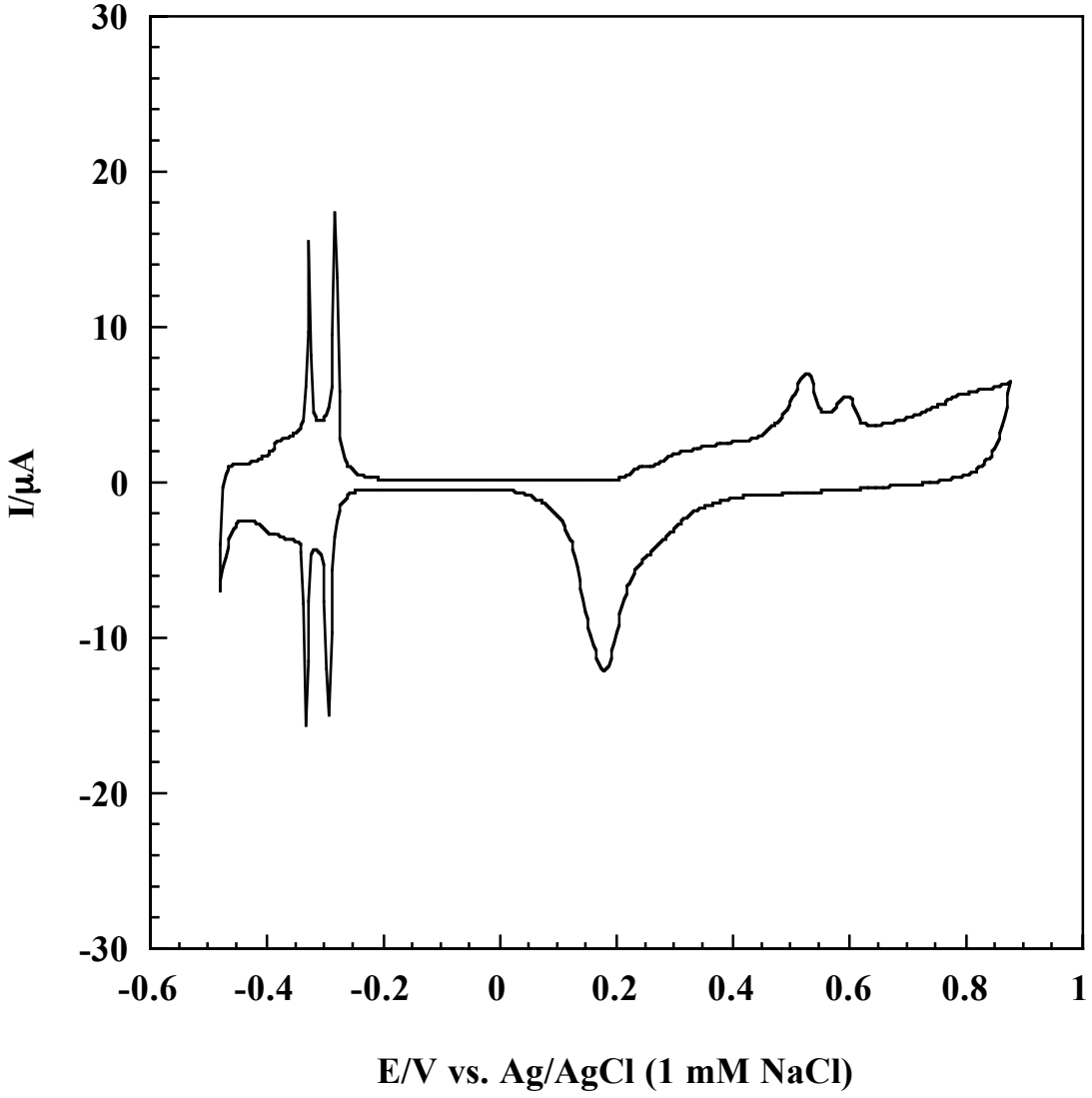

Figure 31 Continued. (B) Second potential cycle.

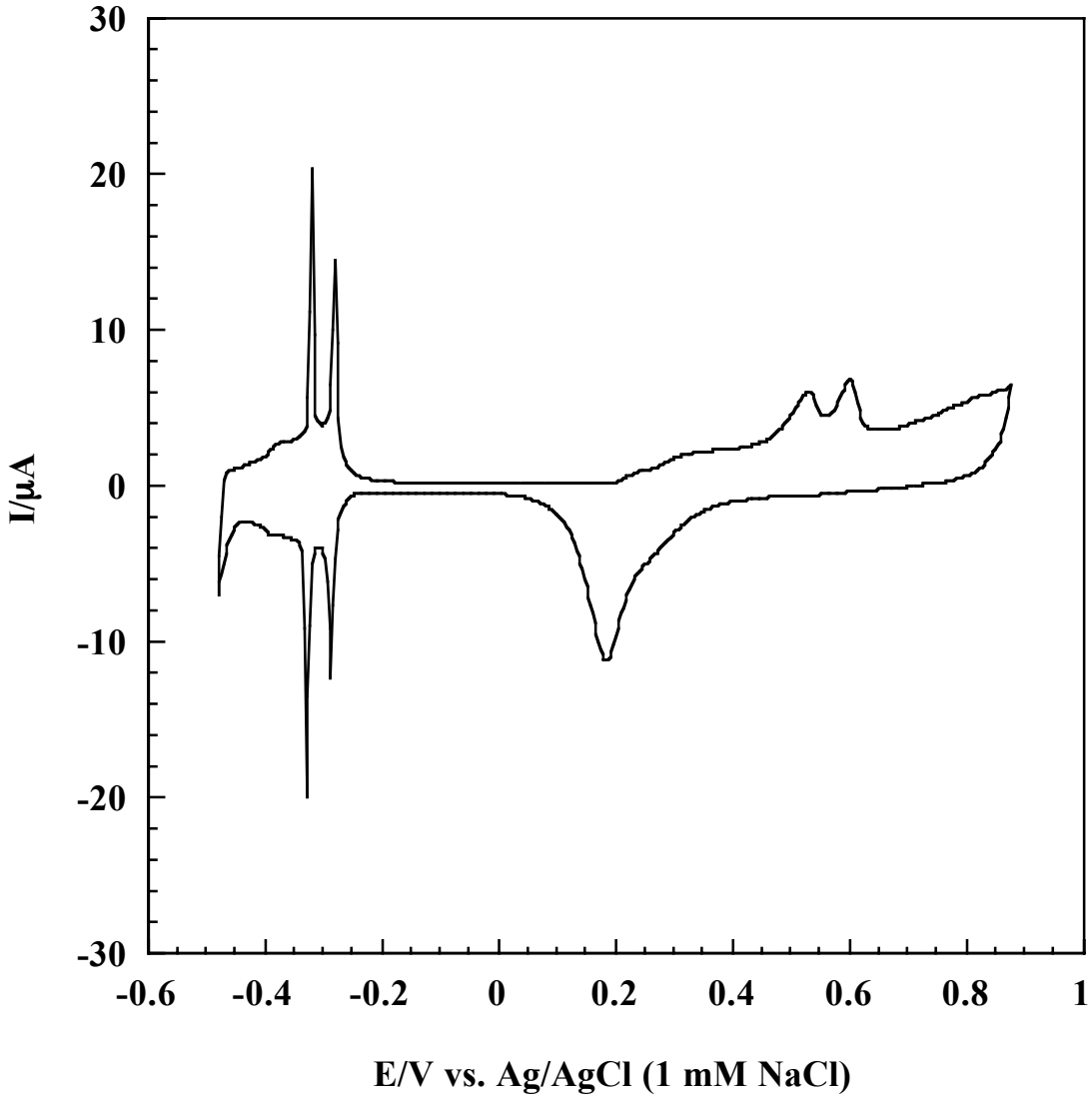

Figure 31 Continued. (C) Third potential cycle.

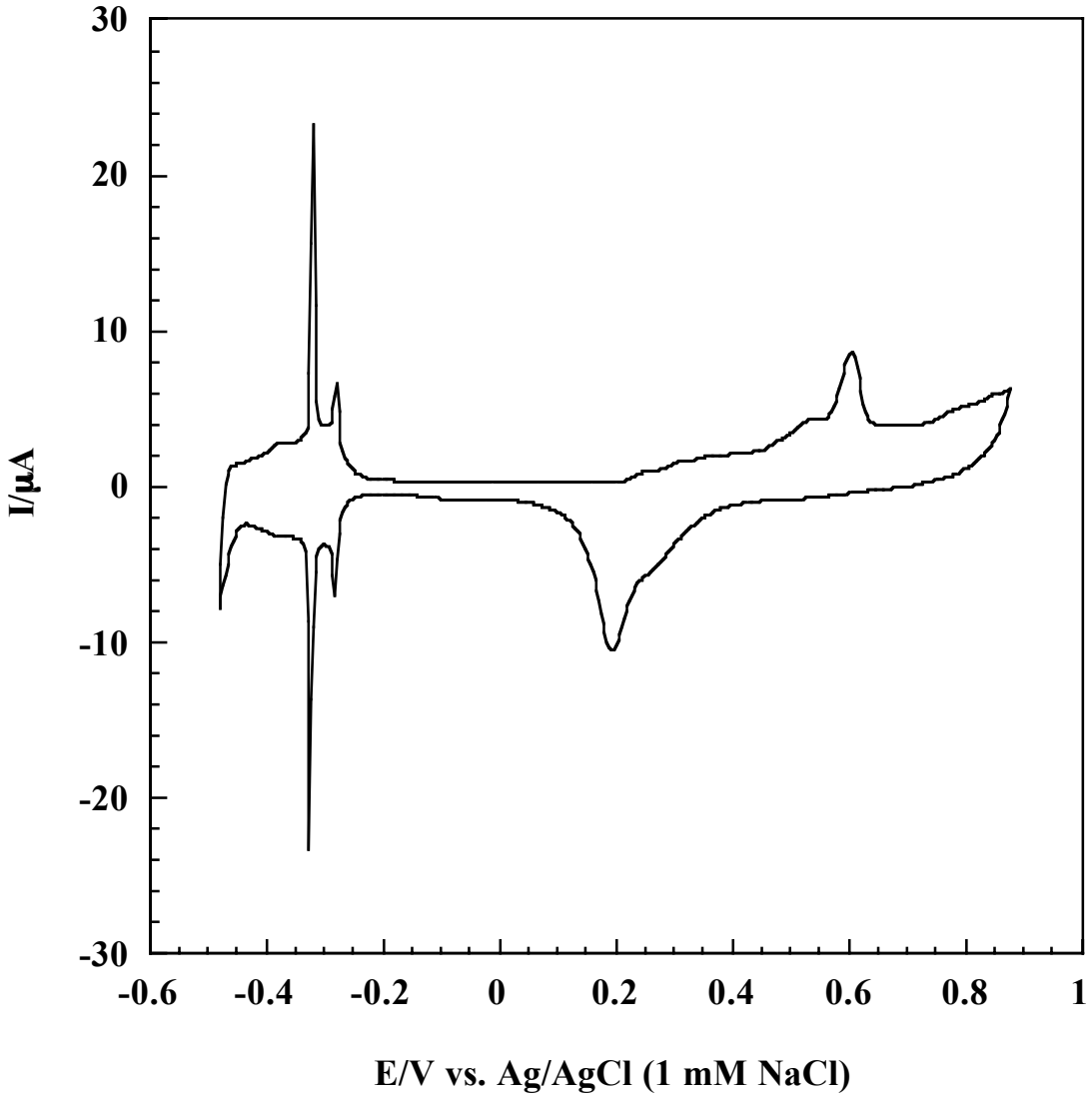

Figure 31 Continued. (D) Fifth potential cycle.

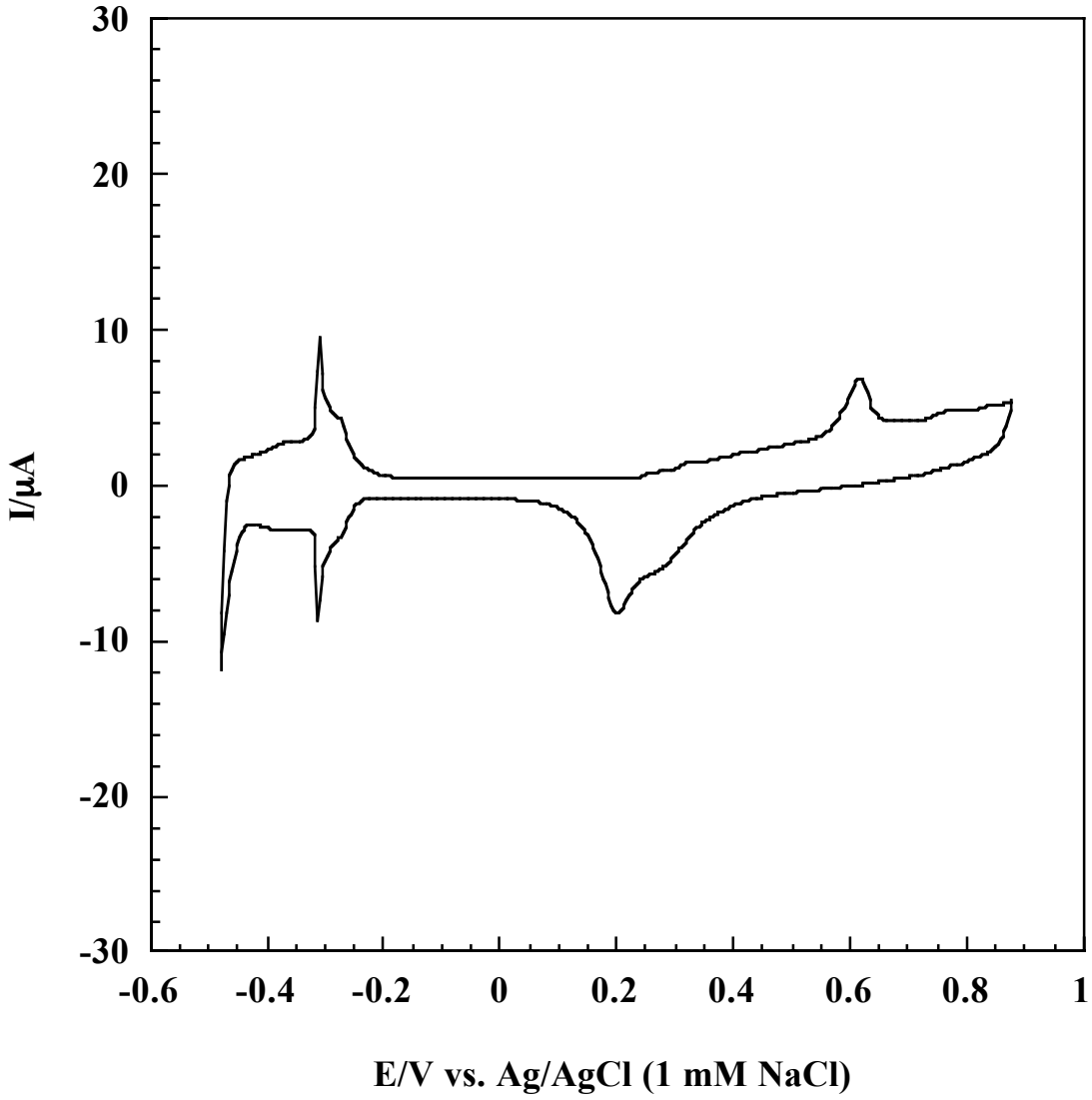

Figure 31 Continued. (E) Eighth potential cycle.

the decline in the signal intensity is much more dramatic for the already-puny step-related peak such that the two peaks begin to merge. The step Pd oxidation peak at 0.48 V disappeared in the voltammogram. The Pt oxidation peak observed at 0.24 V appears larger than that obtained in the 5th potential cycle.

Parallel studies on the effect of electrochemical annealing between the HER and Pd surface oxidation regions were conducted using 4 ML Pd_{PSD} films. The 1st potential cycle (Figure 32 (A)) shows very large terrace H_{upd} adsorption/desorption peaks at 0.34 V and large terrace Pd oxidation peak at 0.58 V. Very small step H_{upd} adsorption/desorption peaks appears at 0.30 V while a small broad step Pd oxidation peak registers at 0.48 V. Pd reduction peak appears at 0.18 V. All peaks appear slightly smaller during the 2nd potential cycle (Figure 32 (B)).

The decrease in peak sizes continues in the 3rd and 4th potential cycles, as shown in Figure 32 (C) and (D) respectively. The terrace H_{upd} adsorption/desorption peaks are noticeably much smaller. The step H_{upd} adsorption/desorption peaks appear like tiny spikes against the sloping background. The step Pd oxidation peak remains absent in both cycles. A broad peak due to Pt reduction emerged at 0.24 V. The same voltammetric features are observed during the 5th potential cycle (Figure 32 (E)) except that the peaks become expectedly smaller.

To understand the evolution of Pd voltammetric features upon potential cycling, the Auger electron spectrum of the surface was analyzed. Figure 33 reveals the dwindling of the Pd peak intensity as the number of potential cycle increases. At the end of the 8th potential cycle, submonolayer coverages (less than 0.3 ML) of Pd remain on

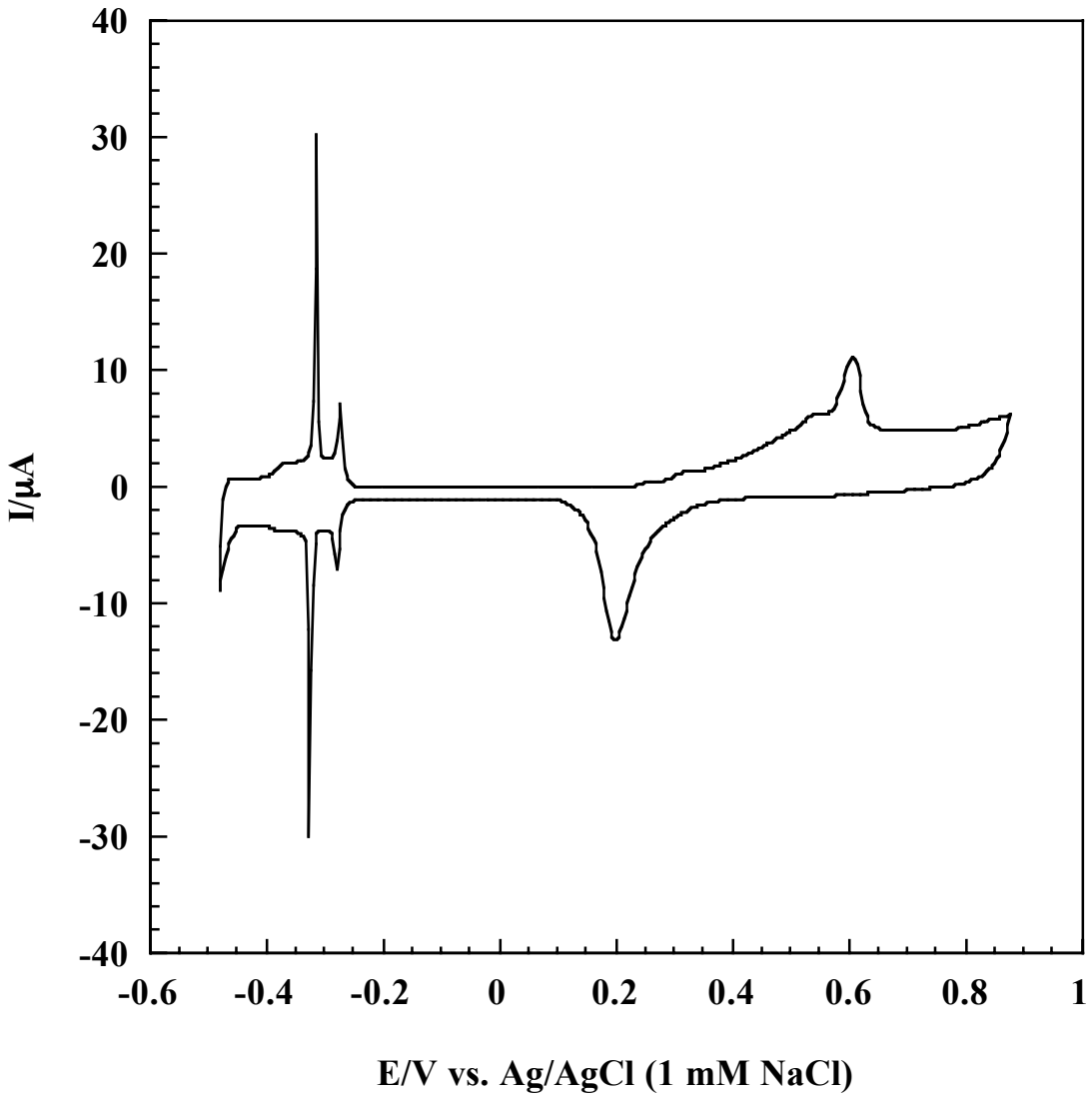

Figure 32. Cyclic voltammogram for 4 ML Pd_{PSD} film on Pt(111) in 100 mM H_2SO_4. Potential was cycled between the hydrogen evolution and Pd oxidation regions. (A) First potential cycle. Pd film was prepared by potentiodynamic deposition. Sweep rate = 2 mV/sec. Electrode area = 1.12 cm^2.

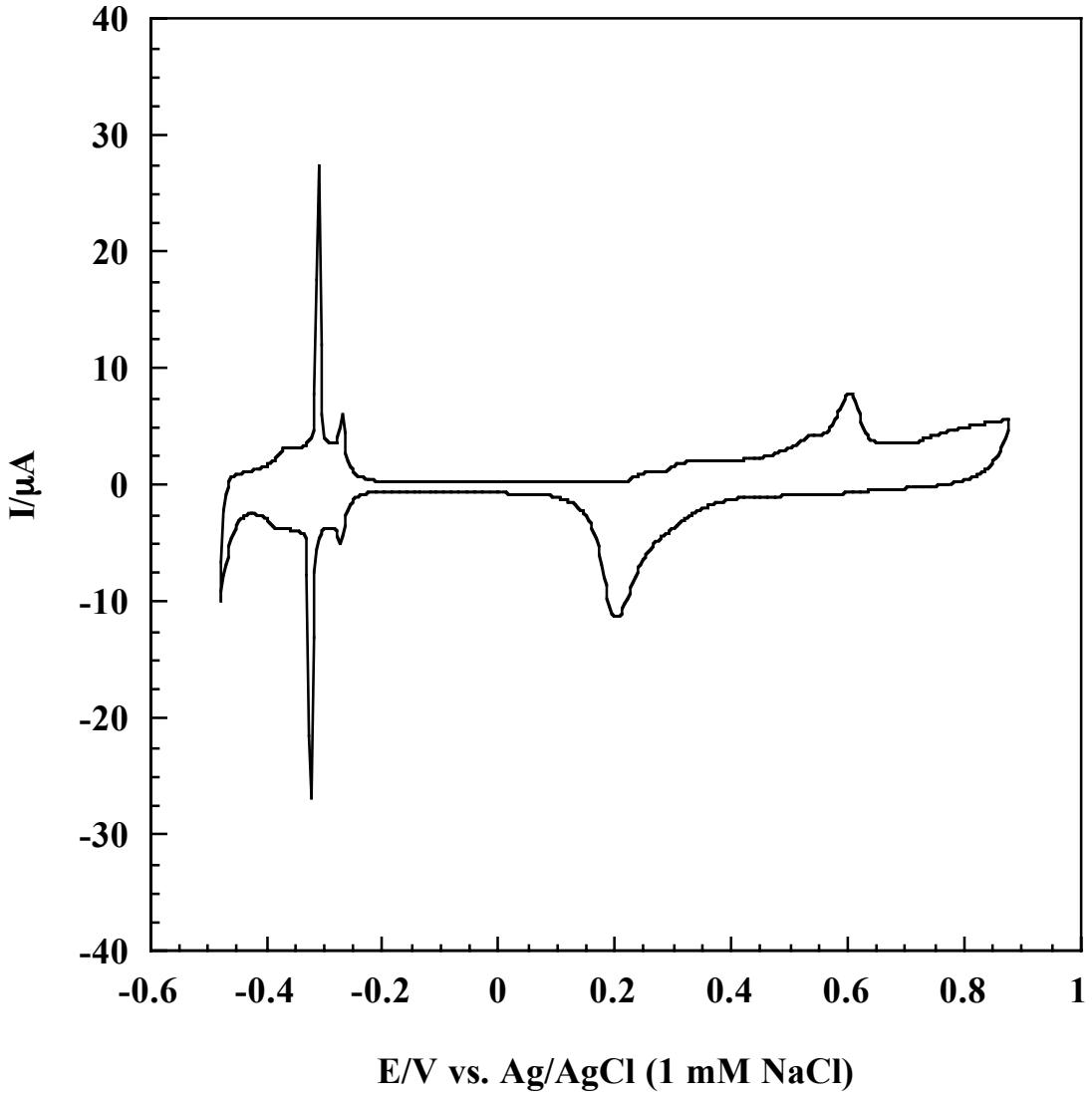

Figure 32 Continued. (B) Second potential cycle.

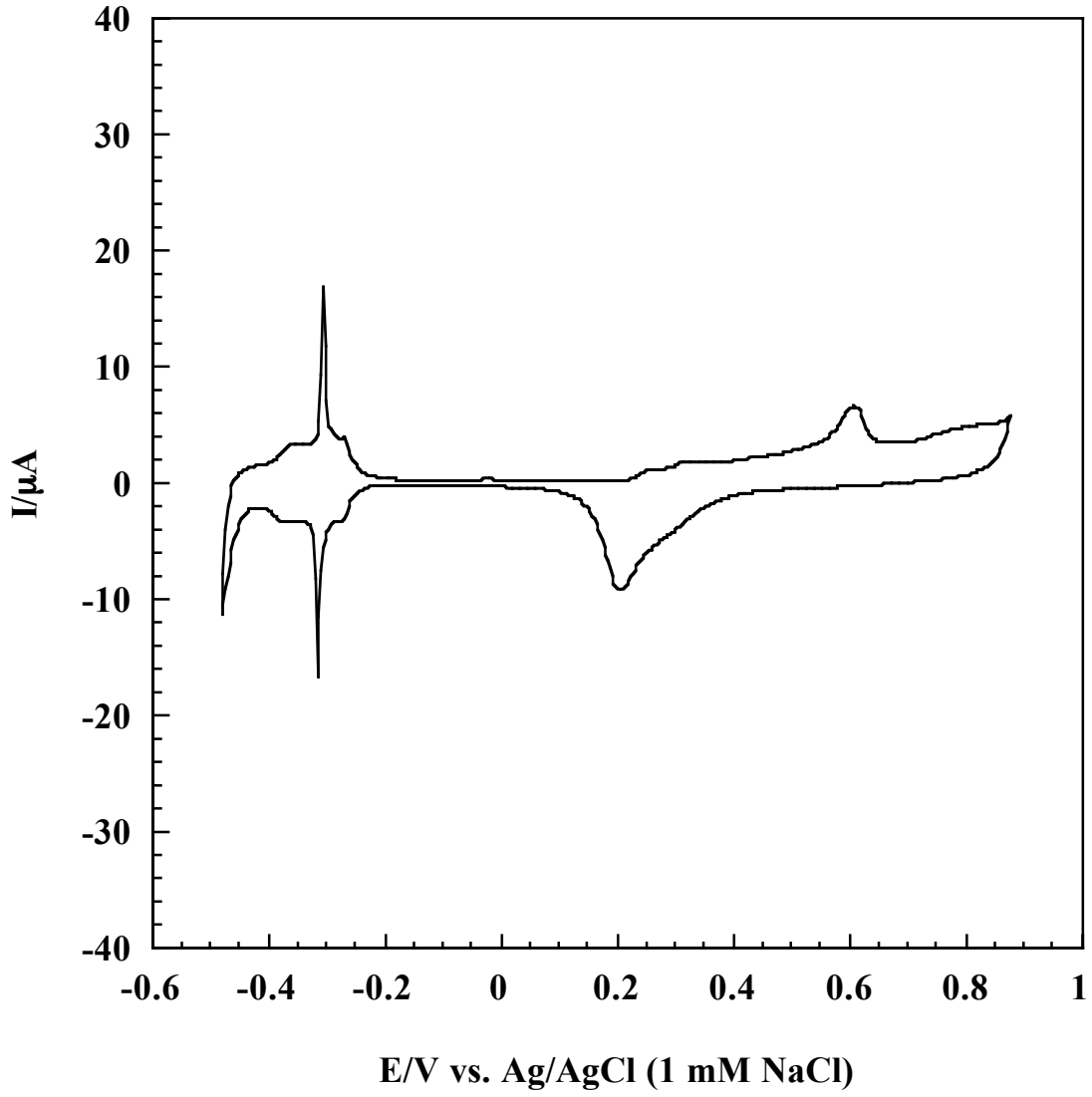

Figure 32 Continued. (C) Third potential cycle.

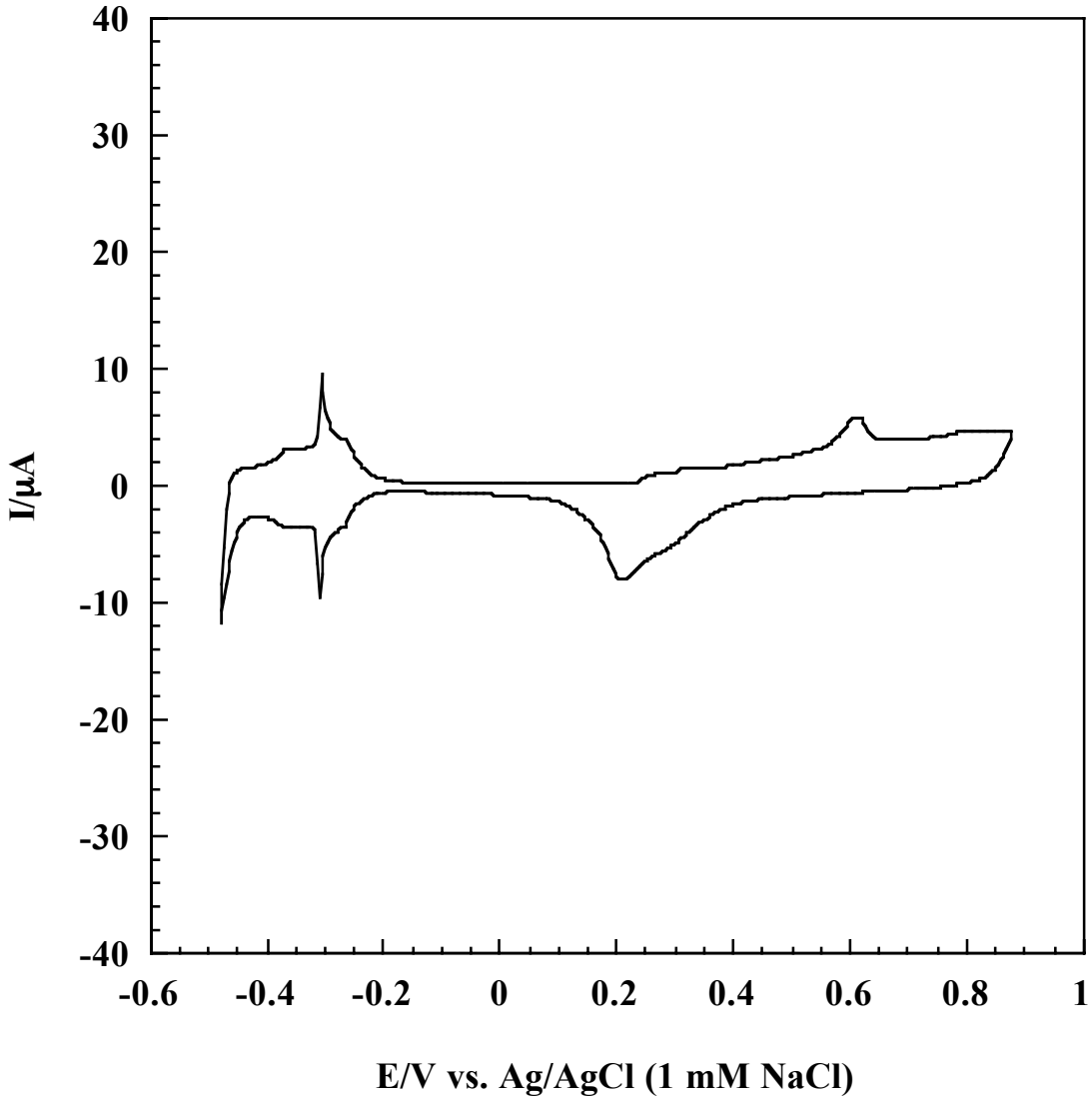

Figure 32 Continued. (D) Fourth potential cycle.

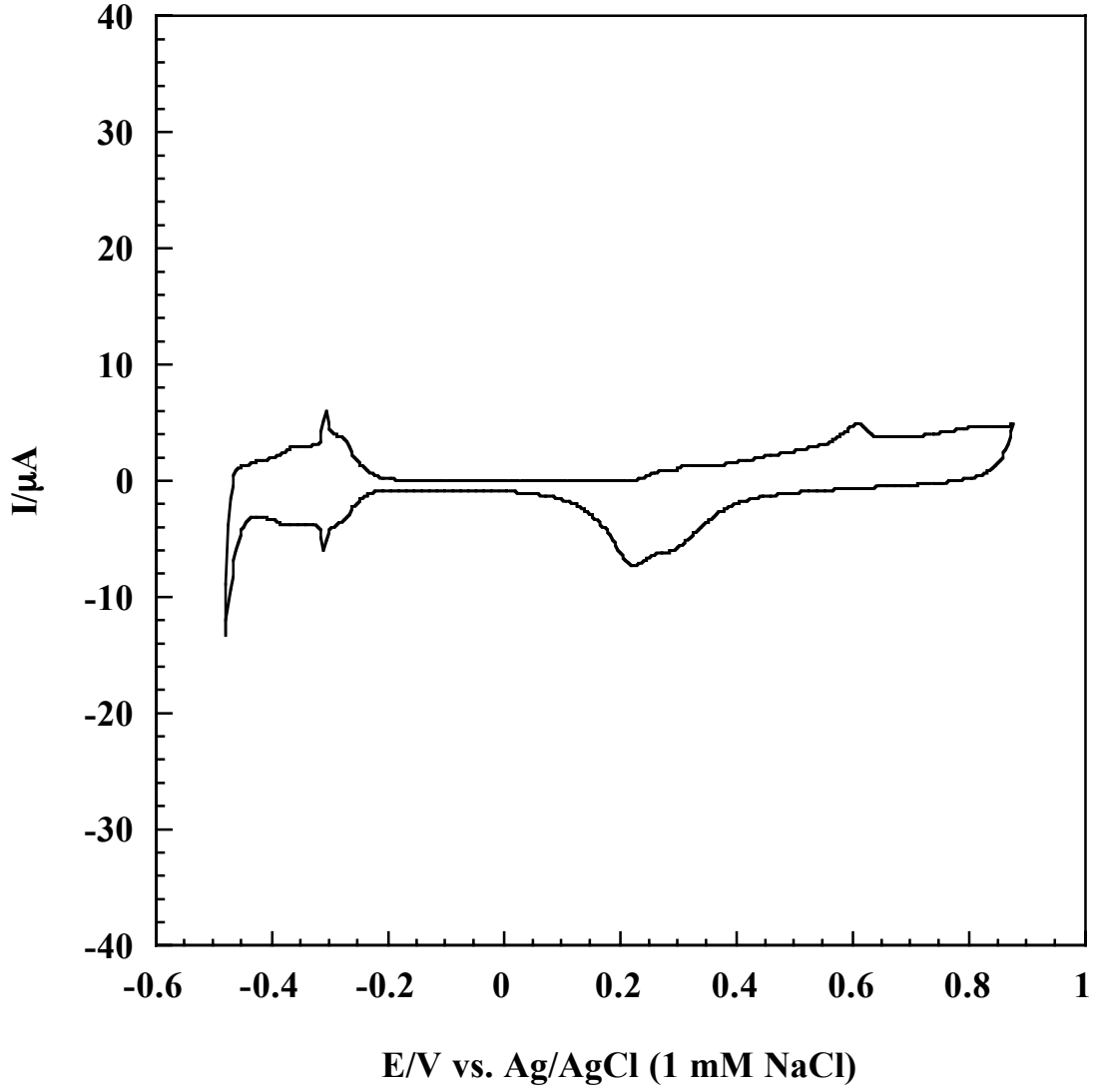

Figure 32 Continued. (E) Fifth potential cycle.

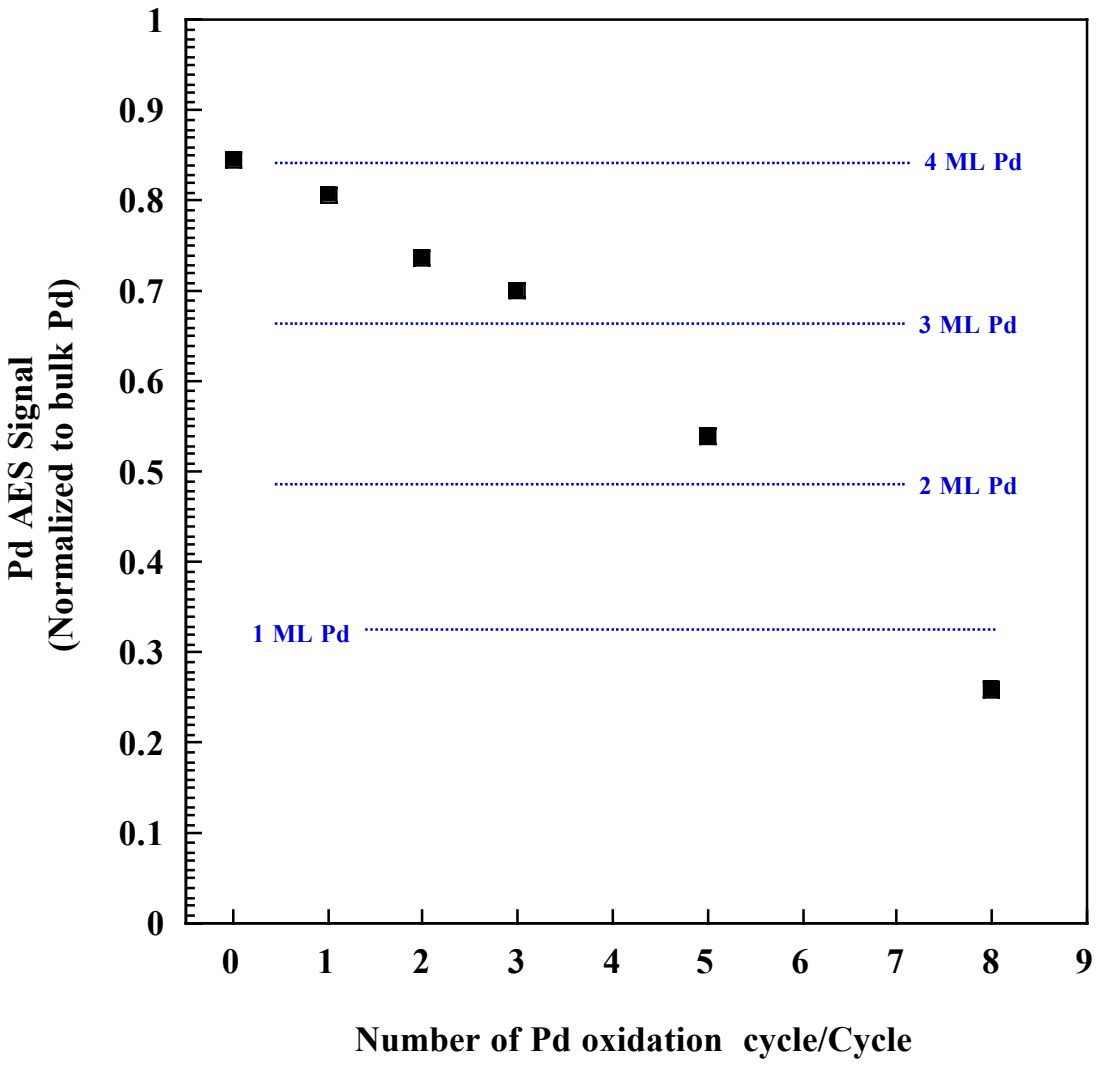

Figure 33. Change in Pd intensity as a function of the number of Pd oxidation cycles. The Pd intensity was obtained from Auger electron spectra of 4 ML Pd_{CPD} film after each potential cycle between –0.48 V and 0.88 V. Incident beam energy = 2 keV; beam current = 1 μA.

the Pt(111) surface. Potential cycling between the HER and Pd oxidation regions removes significant amounts of Pd, altering the morphology and reactivity of the remnant Pd adlayer.

Interaction of Ultrathin Pd Films with Bromide Electrolyte

The occurrence of H_{upd} adsorption on ultrathin Pd films, but not on the bulk state, is a fascinating illustration of the emergence of unique interfacial properties as the thickness (expressed as surface coverage) of a metal adlayer is intentionally decreased. This fact suggests the existence of a wealth of interesting interactions between well-characterized ultrathin Pd films and strongly adsorbed species, such as halides.

In this investigation, the bromide ion is used as a probe species that can be readily chemisorbed onto and removed from Pd film surfaces under potential control. The use of 100 mM sodium fluoride (NaF) solution, adjusted to pH 4 with tetrafluoroacetic acid (TFA), as the supporting electrolyte solution (hereafter referred as *NaF (pH 4)*) ensures a wide potential window for the formation of ordered bromine adlayers [27]. Both NaF and TFA are known not to chemisorb on Pd surfaces under the present experimental conditions. Using NaF (pH 4) as supporting electrolyte also allows direct comparison of results from the present study with those obtained from previous works utilizing bulk Pd(111).

Electrochemistry in Bromide-free NaF Solution

Figure 34 displays typical features of a cyclic voltammogram of Pt(111) in 100 mM NaF (pH 4): (i) a broad nondescript H_{upd} adsorption/desorption region between –0.33 and –0.66V; (ii) a broad Pt oxidation region stretching from –0.12 to 0.78 V which includes relatively large oxidation peaks at 0.35 and 0.65 V; and (iii) a Pt reduction peak at 0.07 V.

The cyclic voltammogram of 1 ML Pd_{CPD} film in 100 mM NaF (pH 4) is given in Figure 35. A pair of relatively sharp H_{upd} adsorption/desorption peaks is observed at –0.43 V; such features are absent on bulk Pd(111) [28] and Pt(111) substrate. Broad voltammetric features for Pd oxidation can be discerned between –0.10 and 0.70 V. Just slightly negative to the Pt reduction peak at 0.07 V is the Pd reduction peak at –0.01 V.

A very similar current-potential profile (Figure 36) is obtained from 1 ML Pd_{PSD} film, except that the H_{upd} adsorption/desorption peaks appear slightly smaller.

Electrochemistry in Bromide-containing NaF Solution

A noticeable feature in the cyclic voltammogram of 1 ML Pd_{CPD} film (Figure 37) immersed in a solution of 1 mM NaBr and 100 mM NaF (pH 4) is a reversible set of sharp H_{upd} adsorption/desorption peaks at –0.45 V. The position of these peaks is negatively shifted compared to the one observed in bromide-free solution. The Pd oxidation peak also becomes more visible at 0.35 V. The emergence of a broad reduction peak associated with the Pt substrate at 0.18 V suggests the occurrence bromide-induced stripping of Pd during the anodic scan. At 0.55 V, a large voltammetric wave ascribed to

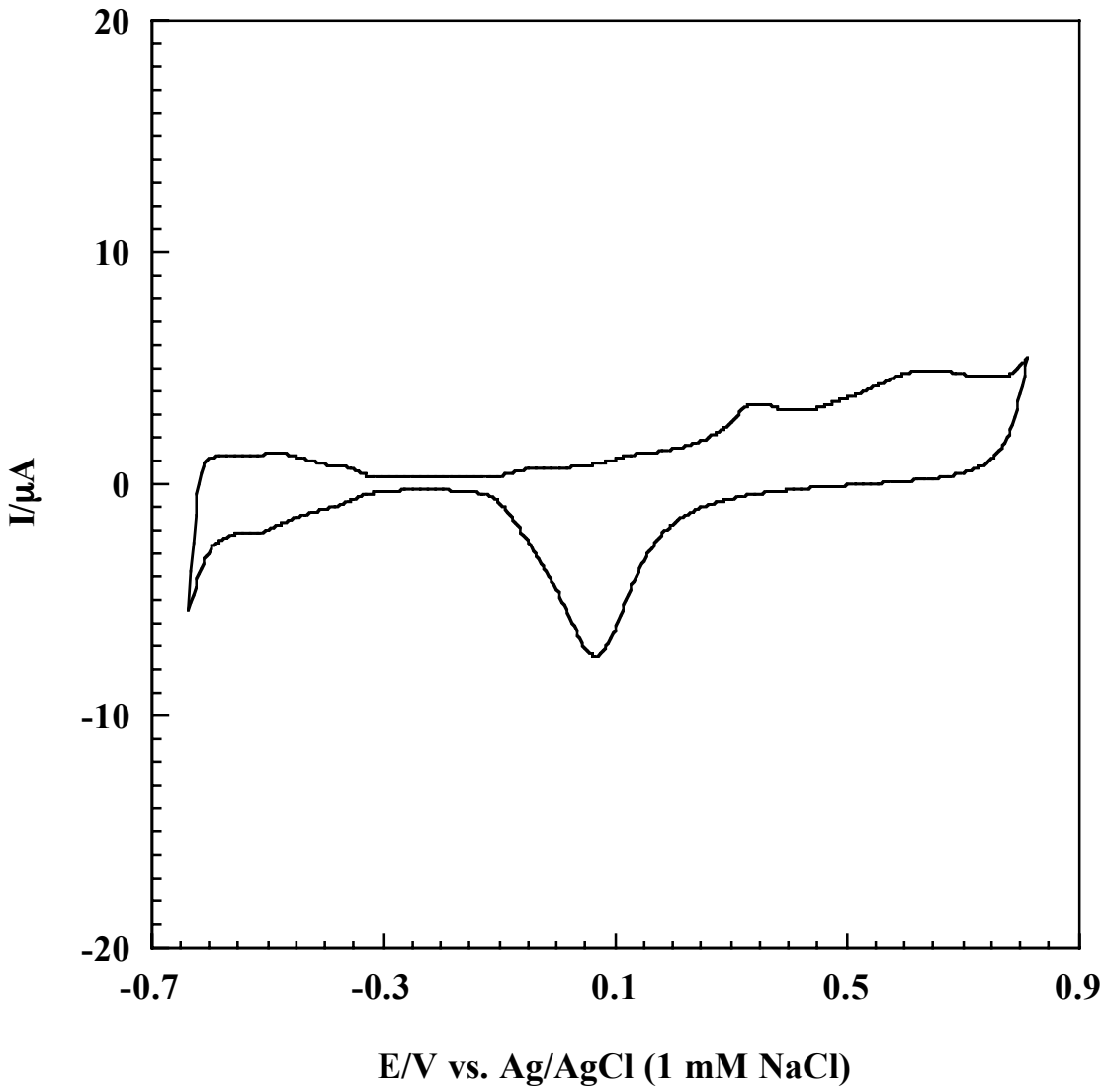

Figure 34. Cyclic voltammogram for a Pt(111) disc electrode in 100 mM NaF solution adjusted to pH 4 with tetrafluoroacetic acid. Sweep rate = 2 mV/sec. Electrode area = 1.12 cm^2.

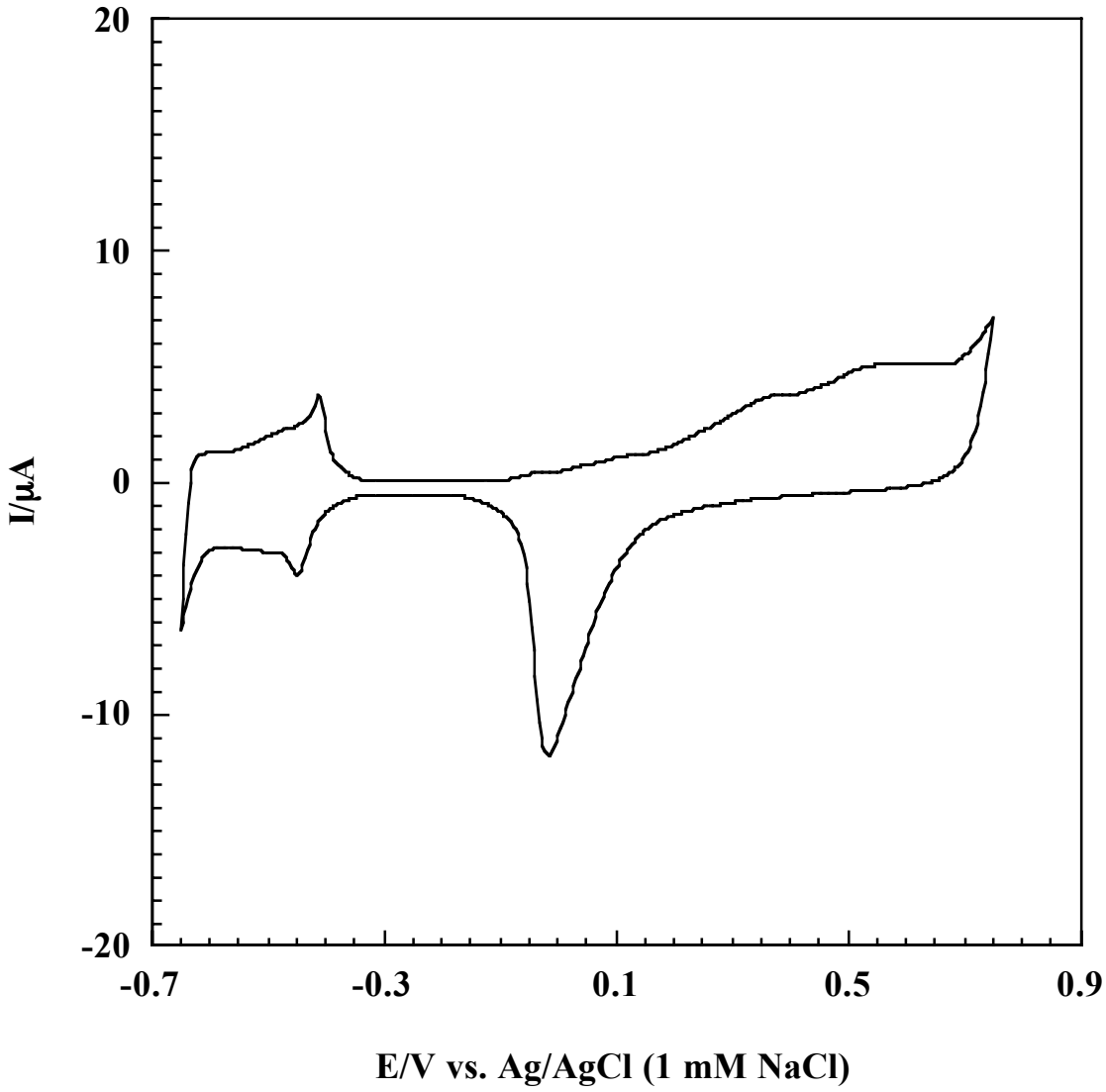

Figure 35. Cyclic voltammogram for 1 ML Pd_{CPD} film on Pt(111) in 100 mM NaF solution adjusted to pH 4 with tetrafluoroacetic acid. Pd film was prepared by potentiostatic deposition. Sweep rate = 2 mV/sec. Electrode area = 1.12 cm^2.

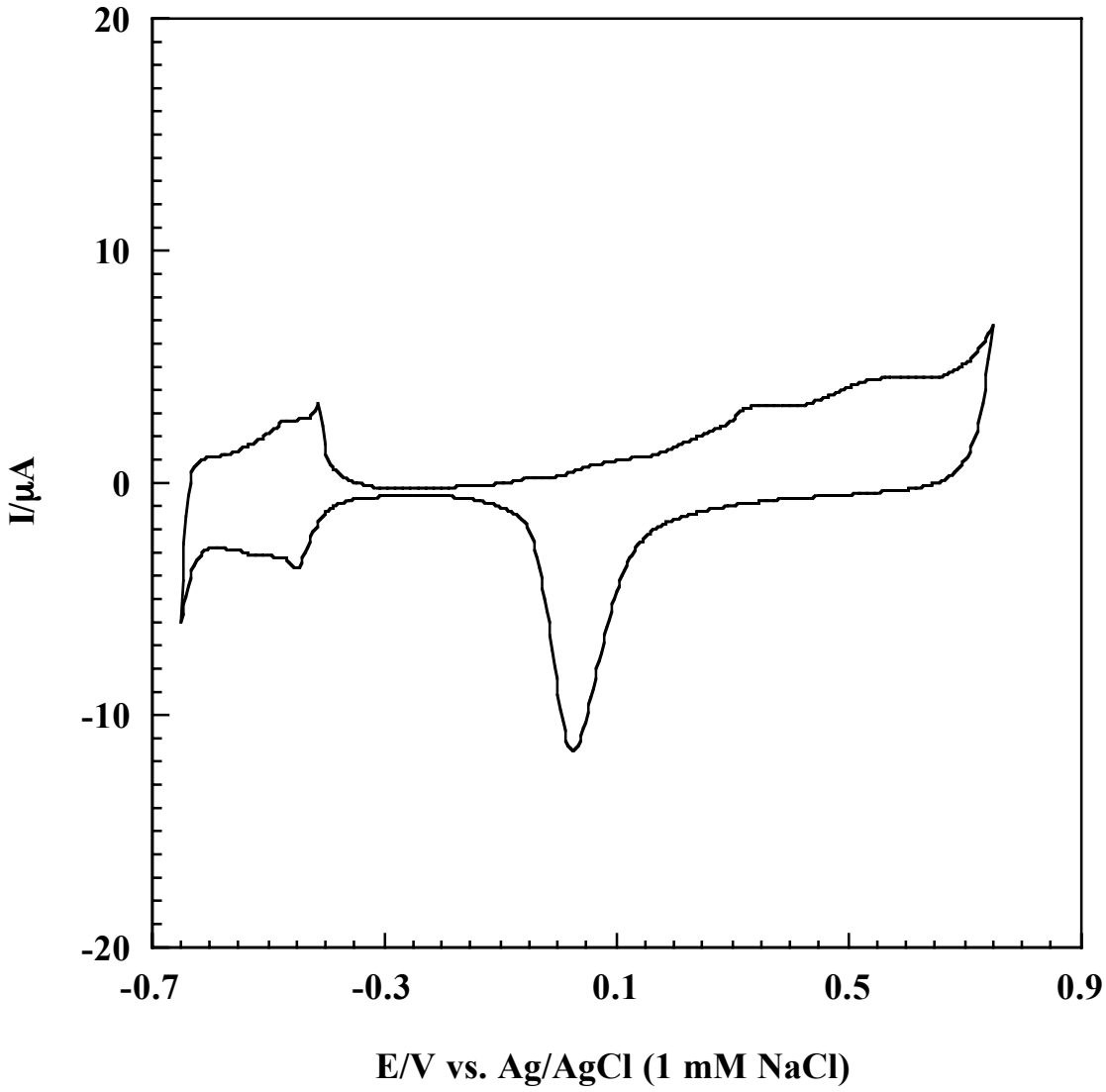

Figure 36. Cyclic voltammogram for 1 ML Pd_{PSD} film on Pt(111) in 100 mM NaF solution adjusted to pH 4 with tetrafluoroacetic acid. Pd film was prepared by potentiodynamic deposition. Sweep rate = 2 mV/sec. Electrode area = 1.12 cm^2.

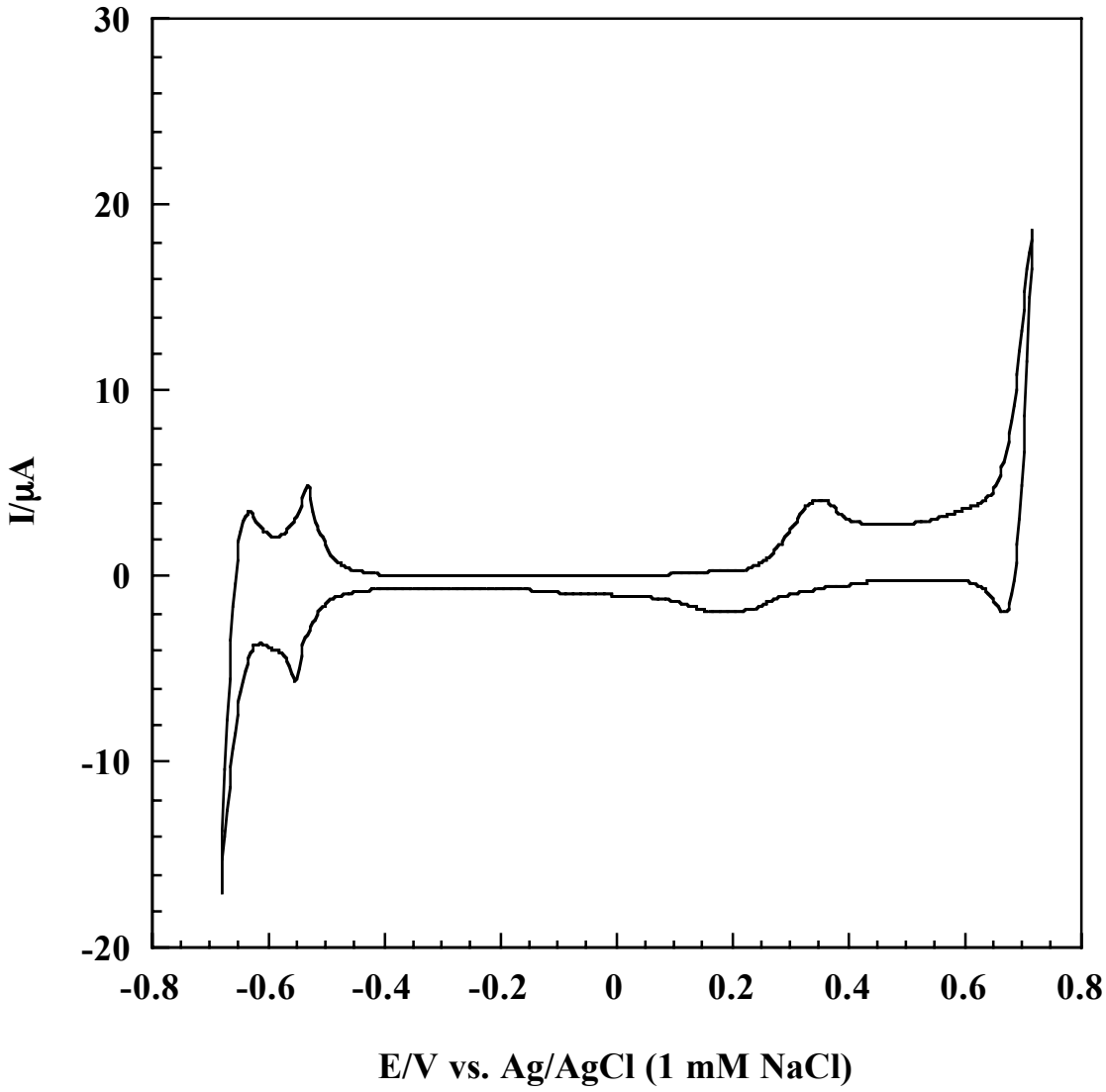

Figure 37. Cyclic voltammogram for 1 ML Pd_{CPD} film on Pt(111) in 1 mM NaBr and 100 mM NaF adjusted to pH 4 with tetrafluoroacetic acid. Pd film was prepared by potentiostatic deposition. Sweep rate = 2 mV/sec. Electrode area = 1.12 cm^2.

bromide-to-bromate oxidation begins to develop; reversing the potential in the negative direction gives rise to a small peak at 0.67 V due to bromate-to-bromide reduction [31].

The cyclic voltammogram of 1 ML Pd_{PSD} film (Figure 38) resembles that of 1 ML Pd_{CPD} film, except for the slightly smaller H_{upd} adsorption/desorption and Pd-oxidation peaks.

Bromine Chemisorption

Bromine was adsorbed onto 1 ML Pd films from a solution of 1 mM NaBr and 100 mM NaF (pH 4) at various constant potentials. The resulting surface was characterized using LEED and AES.

Auger electron spectra in Figure 39 indicate that the surface of 1 ML Pd_{CPD} film remains bromine-free if the immersion is carried out at –0.20 V. The spectrum obtained after immersion at 0.22 V shows the characteristic Br peak at 102 eV. The same trend is observed for 1 ML Pd_{PSD} films (Figure 40). Under the present experimental conditions, bromine adsorption onto ultrathin Pd films occurs at –0.10 V or higher.

Figure 41 is a plot of bromine coverage on 1 ML Pd_{CPD} film as a function of adsorption potential. Bromine coverage at –0.10 V is ca. 0.30 ML. It increases slightly with adsorption potential and crested at a value of 0.33 ML at 0.22 V (open circuit potential). Excursions to more positive potentials lead to a gradual decrease in bromine coverage until at 0.60 V a minimum value of 0.16 ML is reached. Above 0.60 V, the bromine coverage increases again and reaches a value of 0.23 ML at 0.80 V.

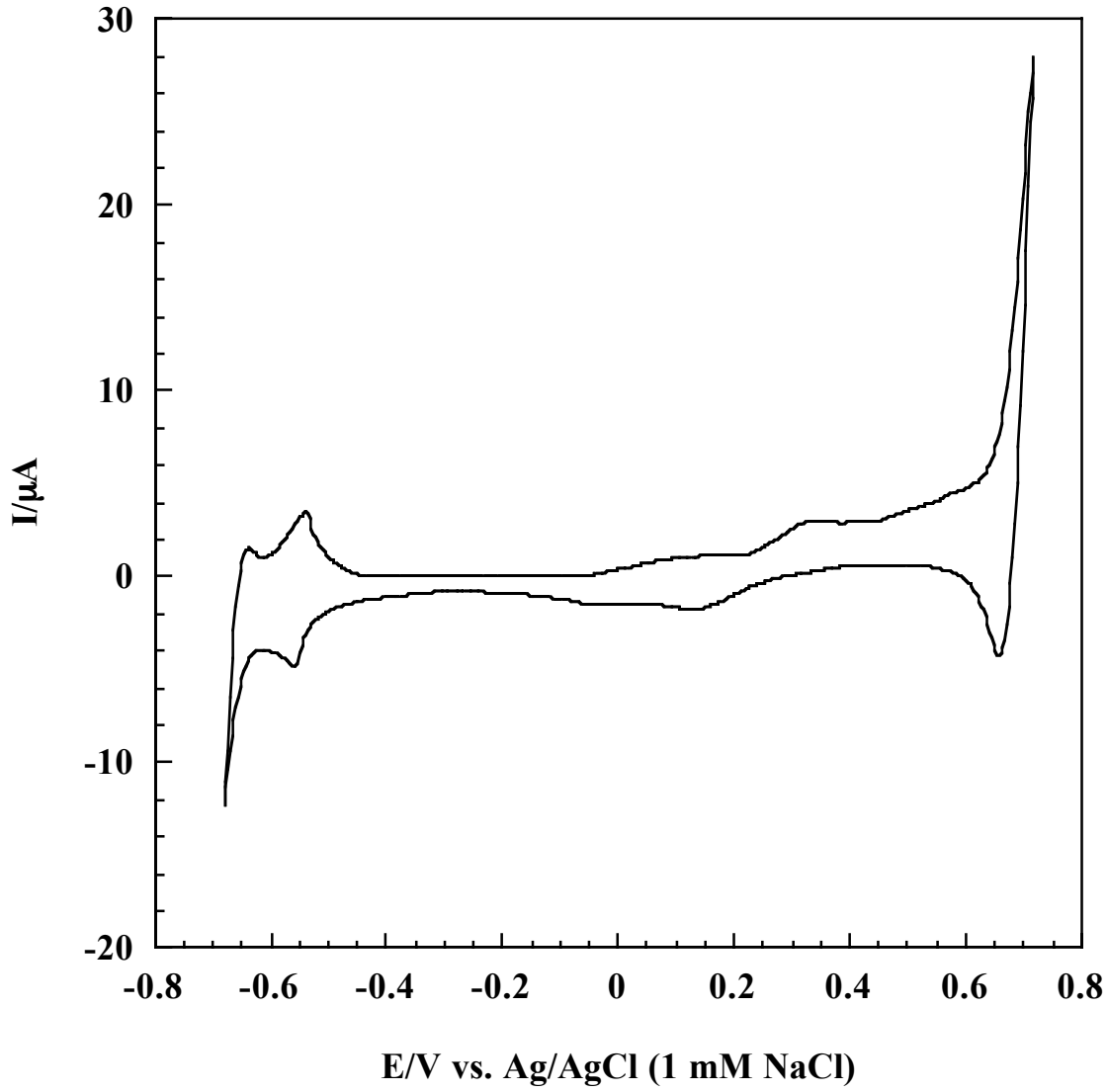

Figure 38. Cyclic voltammogram for 1 ML Pd_{PSD} film on Pt(111) in 1 mM NaBr and 100 mM NaF adjusted to pH 4 with tetrafluoroacetic acid. Pd film was prepared by potentiodynamic deposition. Sweep rate = 2 mV/sec. Electrode area = 1.12 cm^2.

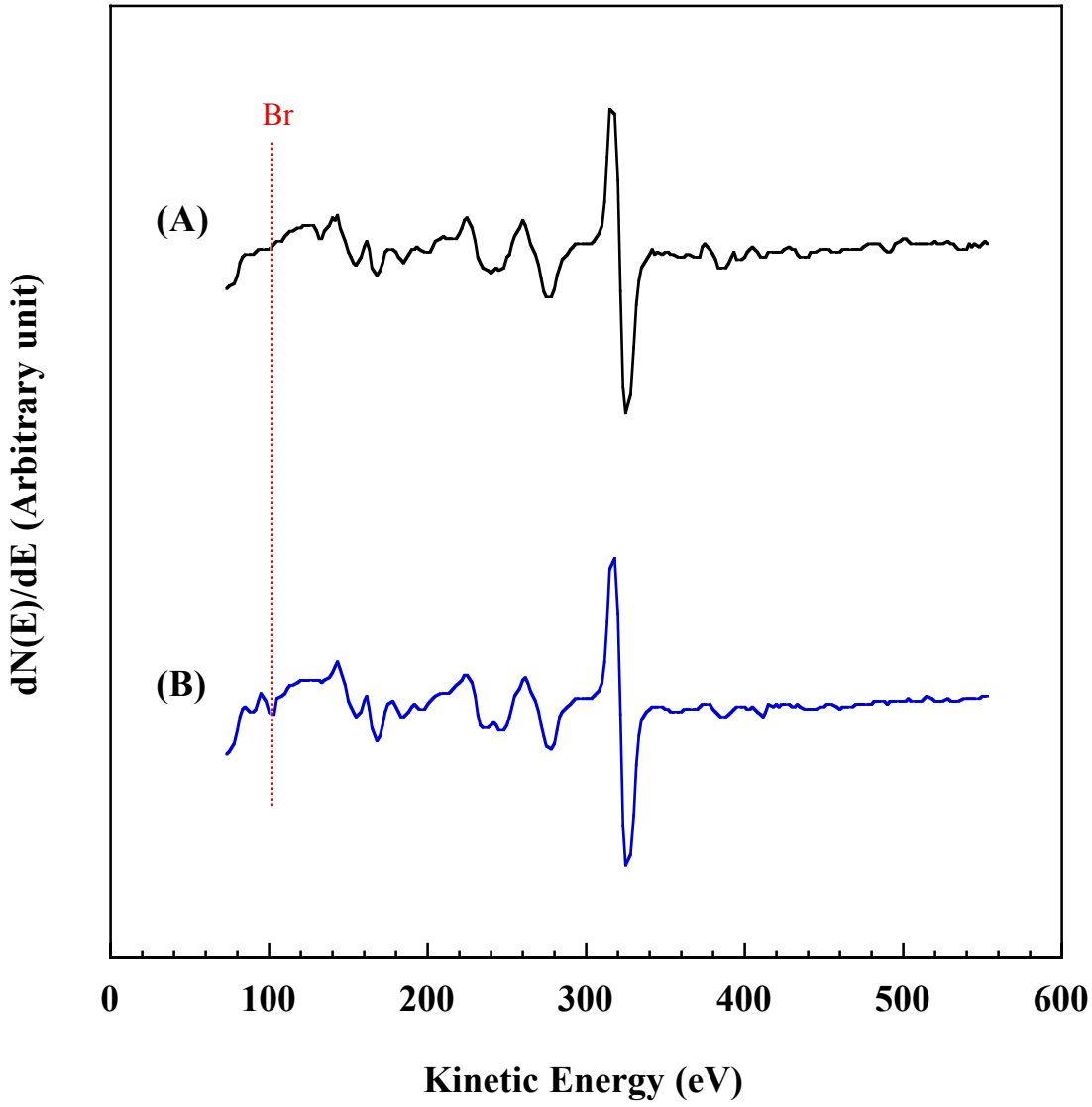

Figure 39. Auger electron spectra for 1 ML Pd_{CPD} film on Pt(111) obtained after applying potentials at (A) –0.20 and (B) 0.22 V in 1 mM NaBr and 100 mM NaF adjusted to pH 4 with tetrafluoroacetic acid. Pd film was prepared by potentiostatic deposition. Incident beam energy = 2 keV; beam current = 1 μA.

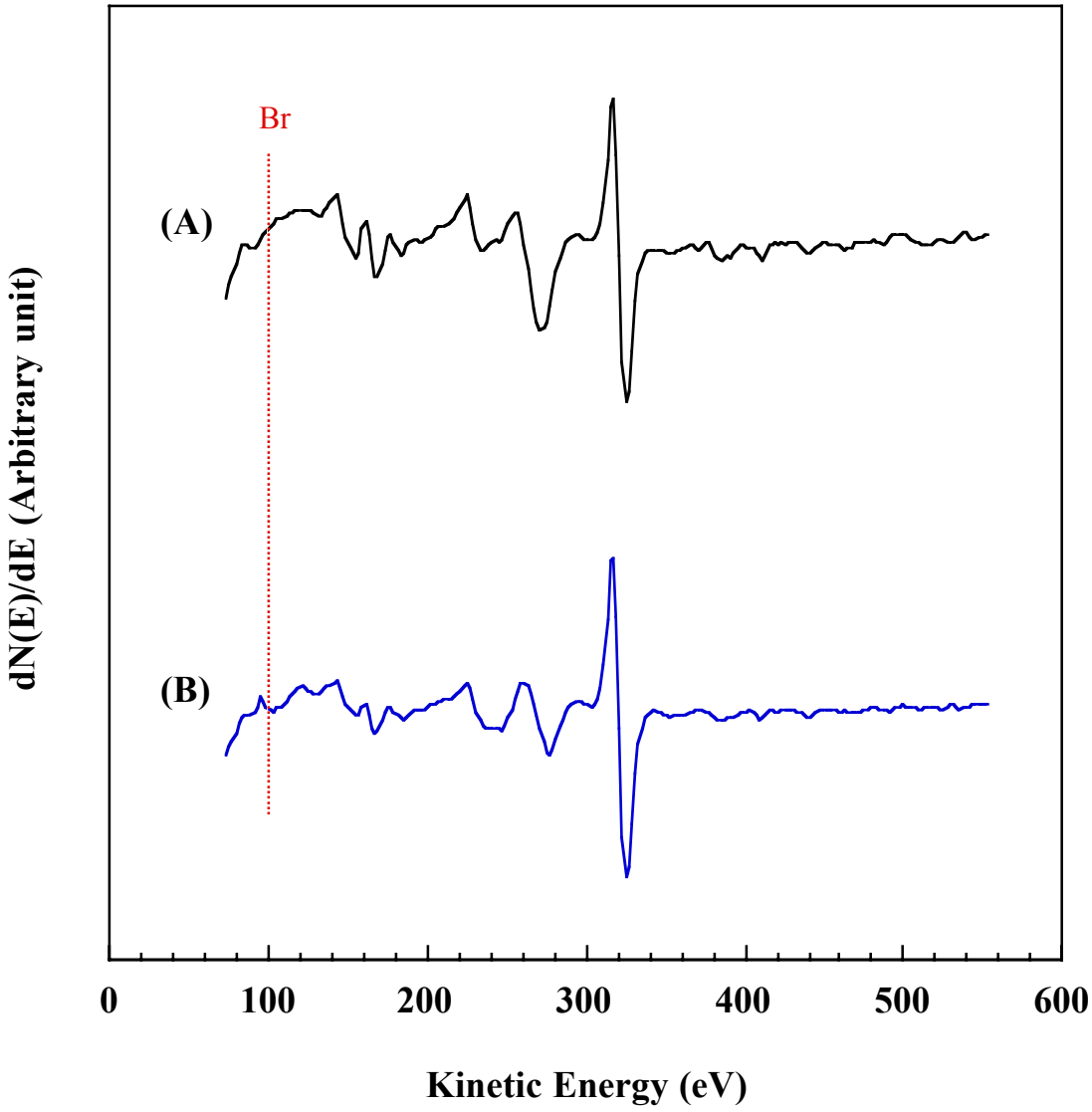

Figure 40. Auger electron spectra for 1 ML Pd_{PSD} film on Pt(111) after applying potentials at (A) –0.20 and (B) 0.22 V in 1 mM NaBr and 100 mM NaF adjusted to pH 4 with tetrafluoroacetic acid. Pd film was prepared by potentiodynamic deposition at 0.1 mV/s. Incident beam energy = 2 keV; beam current = 1 μA.

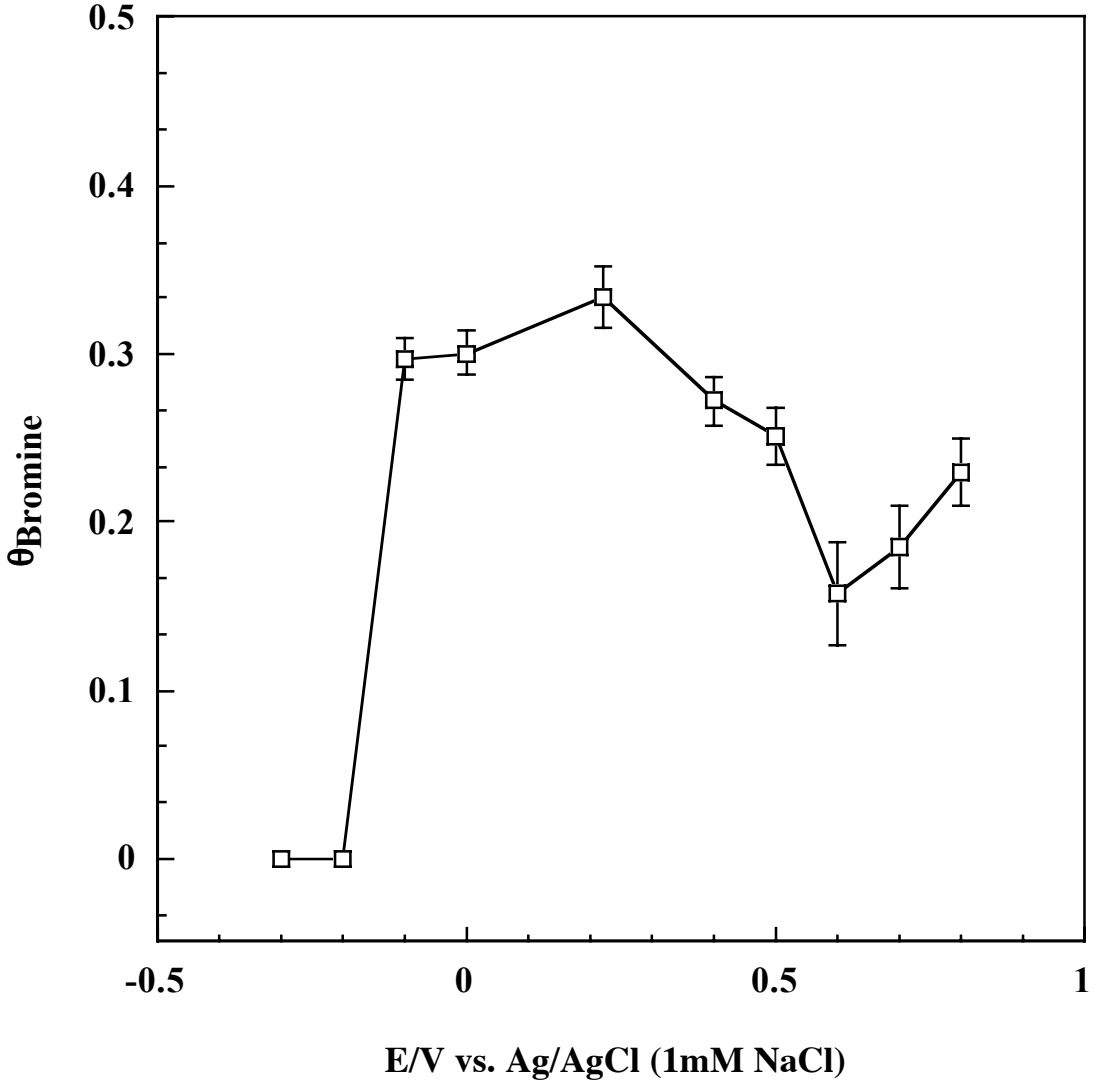

Figure 41. Bromine coverage on 1 ML Pd_{CPD} film as a function of bromine adsorption potential. Pd film was prepared by potentiostatic deposition. Bromine was adsorbed from 1 mM NaBr in 100 mM NaF adjusted to pH 4 with tetrafluoroacetic acid. Bromine adsorption time = 3 minutes.

For 1 ML Pd_{PSD} film, essentially the same adsorption potential dependence of bromine coverage is observed (Figure 42). Bromine adsorption occurs above –0.20 V. Akin to the results obtained from CPD films, bromine coverage reaches a maximum value of 0.33 ML at 0.22 V, plummets to a minimum of 0.12 ML at 0.60 V, and then rises gradually to a final value 0.22 ML at 0.80 V.

Figure 43 shows LEED patterns for 1 ML Pd_{CPD} film obtained after bromine adsorption at various potentials. Depending on bromine adsorption potential, different LEED patterns were obtained: (i) At –0.20 V or lower, a (1×1) pattern indicative of a clean and ordered Pd film on Pt(111) was observed; the absence of bromine adsorption is implied. (ii) Between –0.10 and 0.50 V, the characteristic (√3×√3)R30°-Br pattern was obtained. (iii) At 0.60 V or higher, a diffuse (1×1) pattern was detected. LEED spectra for 1 ML Pd_{PSD} films (Figure 44) show the same adsorption-potential dependence of bromine coverages.

Auger electron spectra in Figure 45 reveal the Pd peak intensity profile after bromine adsorption on 1 ML Pd_{CPD} films. The Pd peak intensity remains unchanged up to 0.40 V, but tapers off from 80% to 40% as the potential is switched from 0.50 V to 0.60 V. No oxygen peak is observed. These observations confirm that bromine-induced Pd stripping at 0.50 V or higher is not accompanied by oxide formation.

Similar spectral behavior is observed from 1 ML Pd_{PSD} film (Figure 46).

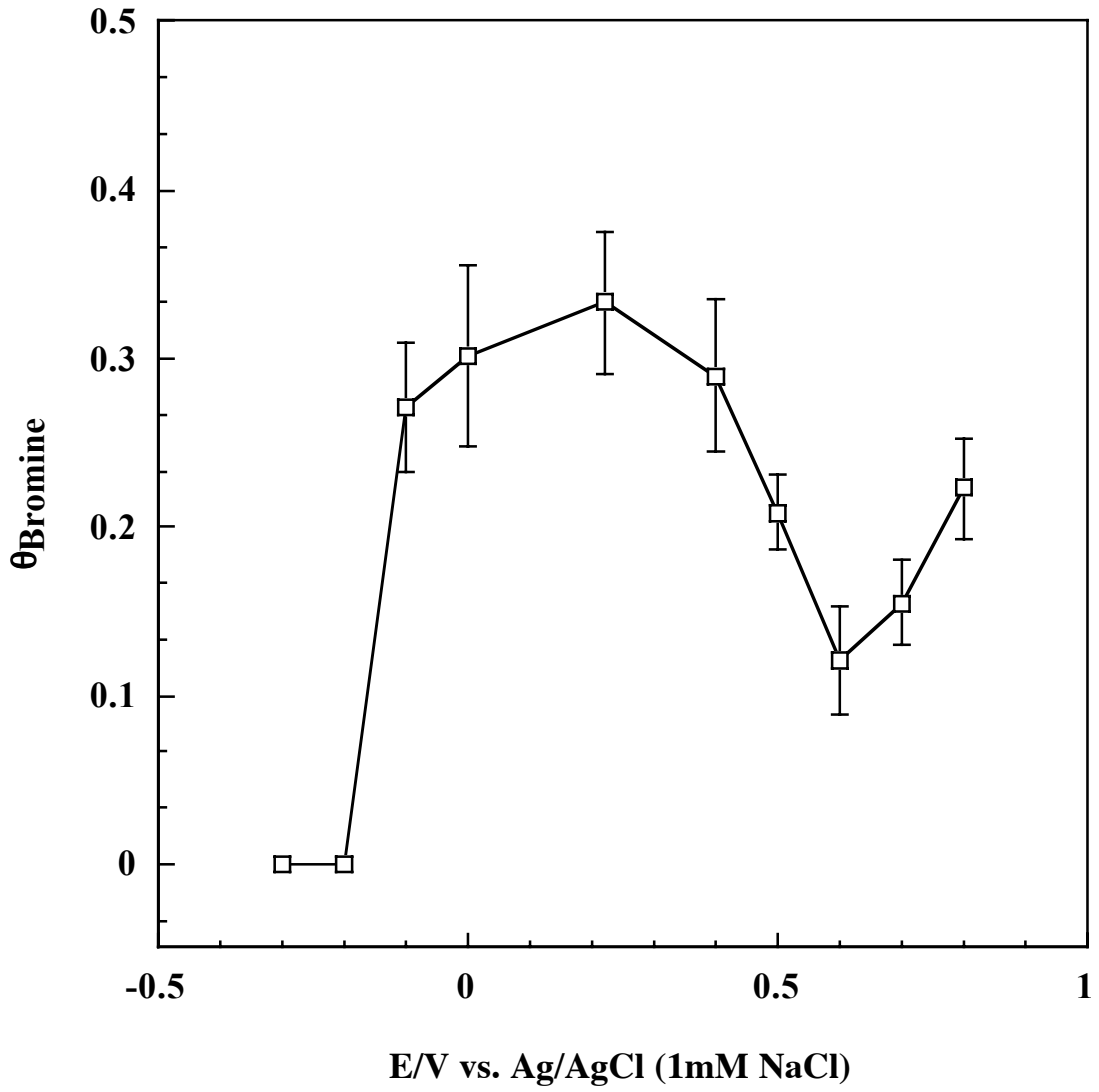

Figure 42. Bromine coverage on 1 ML Pd_{PSD} film as a function of bromine adsorption potential. Pd film was prepared by potentiodynamic deposition. Bromine was adsorbed from 1 mM NaBr in 100 mM NaF adjusted to pH 4 with tetrafluoroacetic acid. Bromine adsorption time = 3 minutes.

(A) Br adsorption at -0.40 V

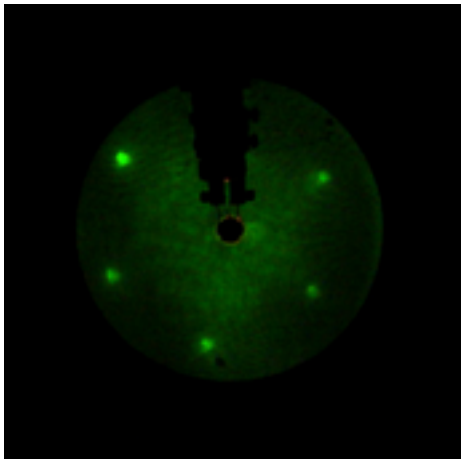

(B) Br adsorption at 0.22 V

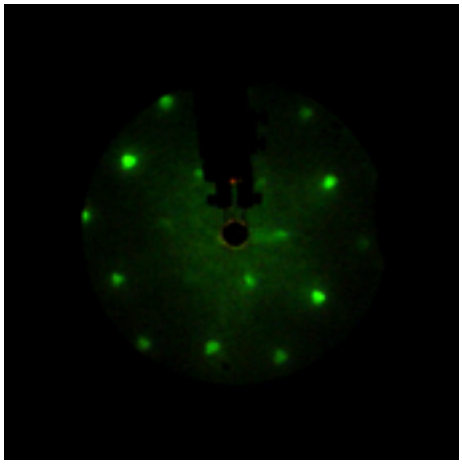

(C) Br adsorption at 0.60 V

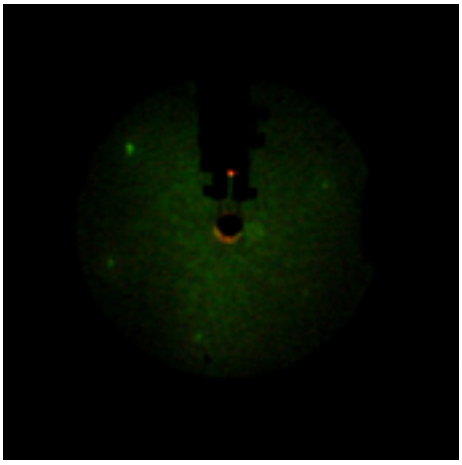

Figure 43. LEED patterns for 1 ML Pd_{CPD} film obtained after applying potentials at (A) –0.40, (B) 0.22, (C) 0.60 V in 1 mM NaBr and 100 mM NaF adjusted to pH 4 with tetrafluoroacetic acid. Pd film was prepared by potentiostatic deposition. Beam energy = 62.0 eV; beam current = 2 μA.

(A) Br adsorption at -0.40 V

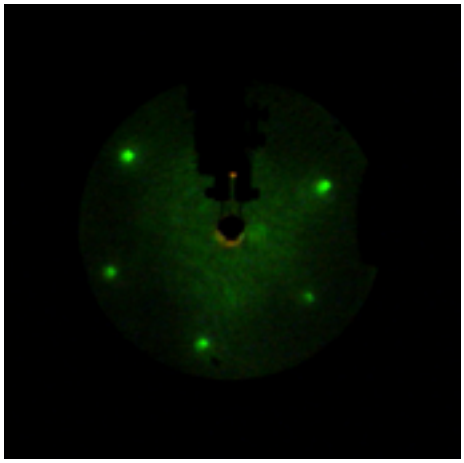

(B) Br adsorption at 0.22 V

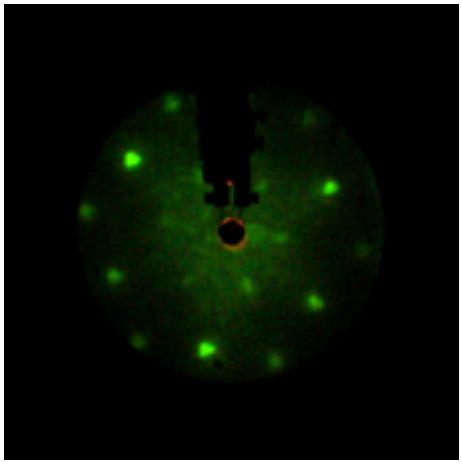

(C) Br adsorption at 0.60 V

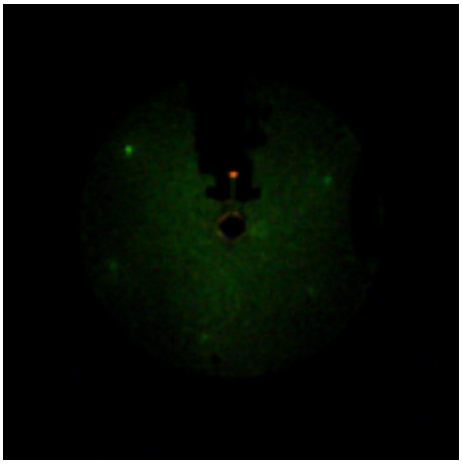

Figure 44. LEED patterns for 1 ML Pd_{PSD} film obtained after applying potentials at (A) –0.40, (B) 0.22, (C) 0.60 V in 1 mM NaBr and 100 mM NaF adjusted to pH 4 with tetrafluoroacetic acid. Pd film was prepared by potentiodynamic deposition. Beam energy = 62.0 eV; beam current = 2 μA.

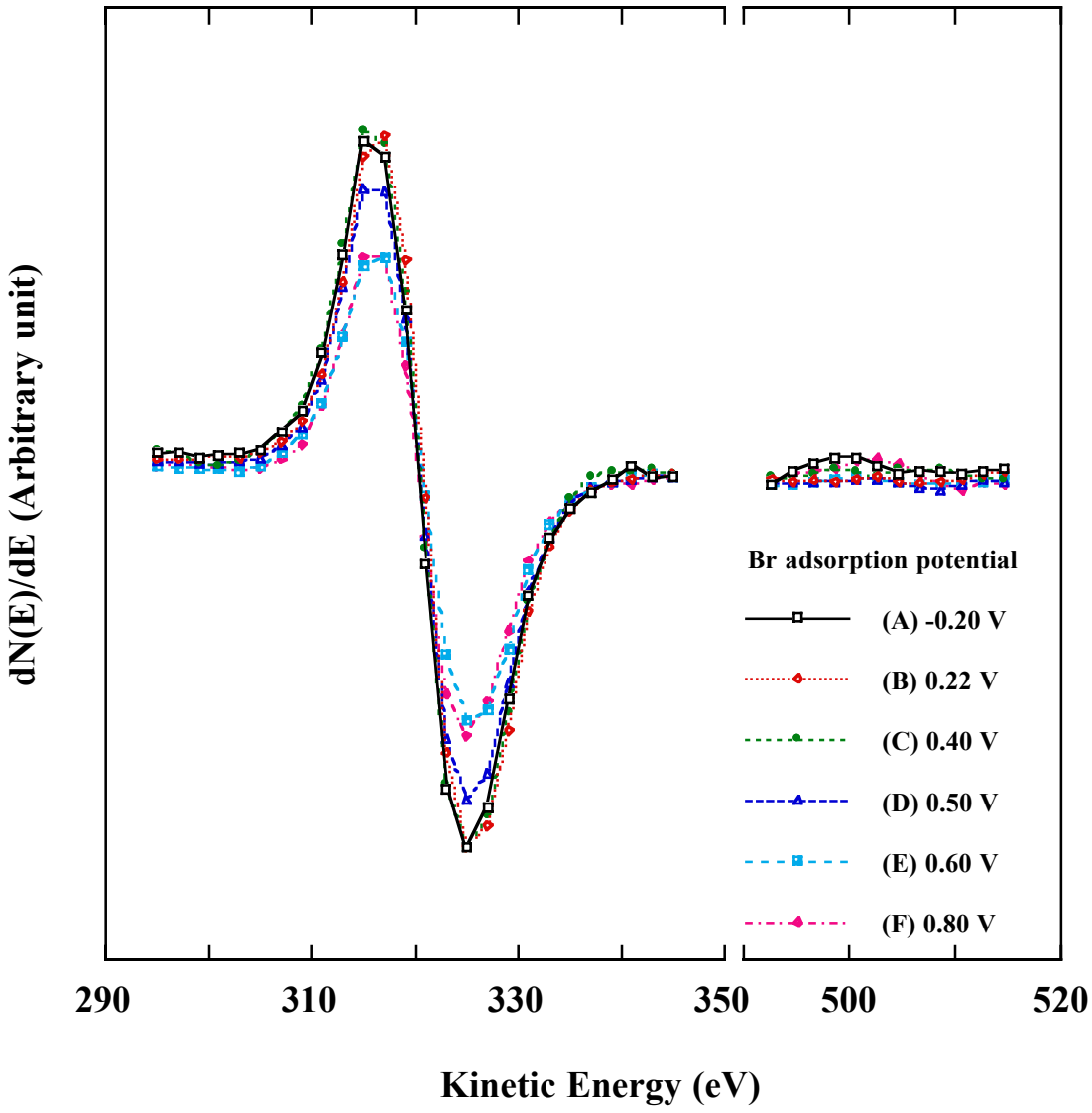

Figure 45. Auger electron spectra showing changes in Pd and O signals after bromine adsorption onto 1 ML Pd_{CPD} film on Pt(111) at various potentials. Pd film was prepared by potentiostatic deposition. Incident beam energy = 2 keV; beam current = 1 μA.

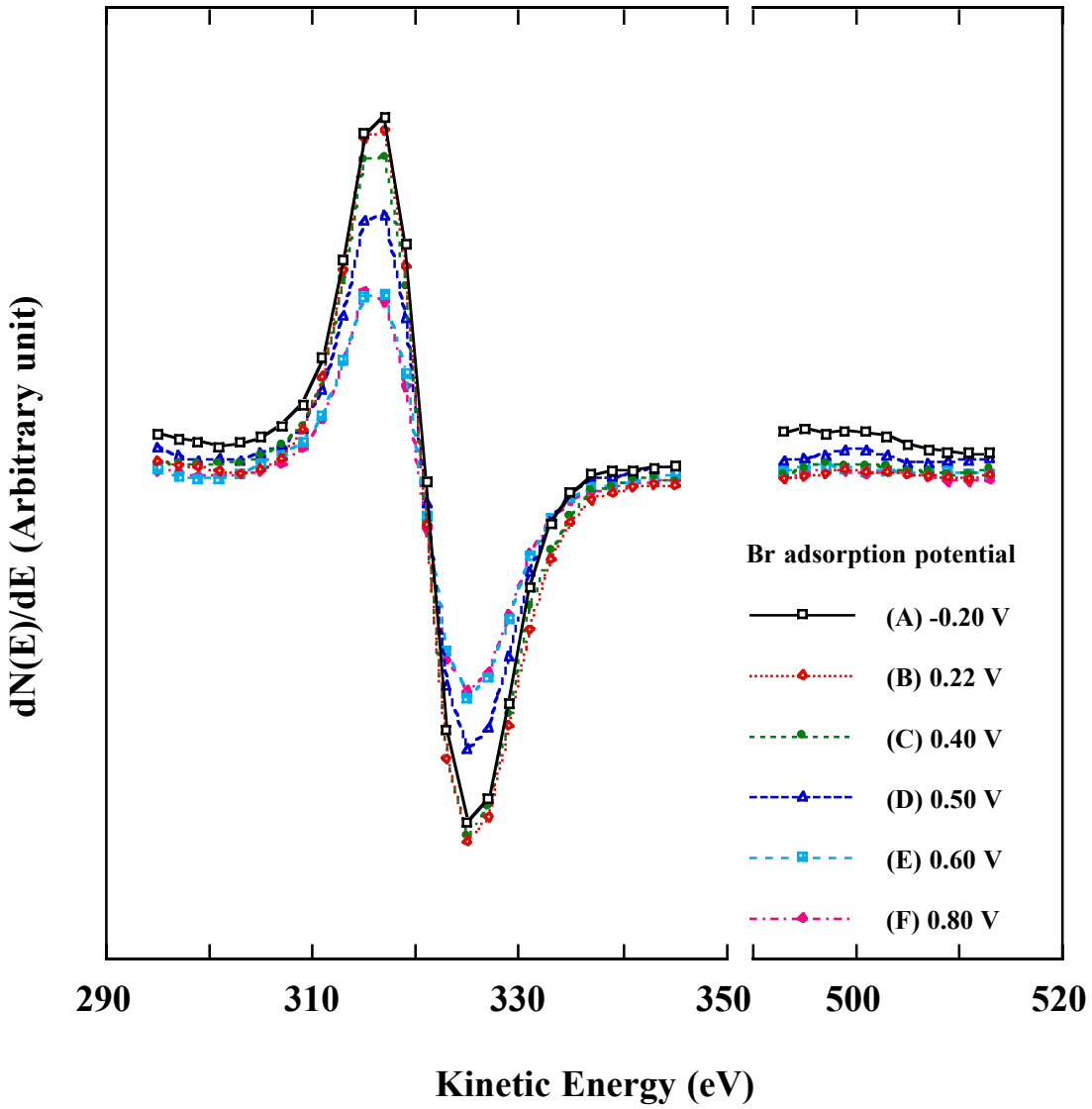

Figure 46. Auger electron spectra showing changes in Pd and O signals after bromine adsorption onto 1 ML Pd_{PSD} film on Pt(111) at various potentials. Pd film was prepared by potentiodynamic deposition. Incident beam energy = 2 keV; beam current = 1 μA.

Electrochemical Annealing of Ultrathin Pd Films in Bromide Solution

It is well documented that chemisorbed iodine induces surface ordering of ion-bombarded or electrochemically roughened Pd surfaces [32-34]. Removal of chemisorbed iodine without disturbing the Pd surface is, however, very difficult because iodine catalyzes Pd corrosion at a relatively broad potential window. Chemisorbed iodine can be reductively desorbed near the HER region under appropriate pH control. Bromine adsorption/desorption, on the other hand, occurs around -0.20 V, which is well positive than the hydrogen evolution potential (ca. –0.40 V). Thus, the prospect of using chemisorbed bromine in obtaining a clean and ordered Pd film surface remains to be fully explored.

To investigate the effects of bromine adsorption/desorption on the electrochemical annealing of ultrathin Pd films, potential cycling between –0.65 and 0.22 V was carried out using a solution of 1 mM NaBr in 100 mM NaF (pH 4) at a sweep rate 2 mV/s. A typical electrochemical annealing *in the presence of bromide* (hereafter referred as *EC annealing*) consisted of five cycles of bromine adsorption/desorption.

Figure 47 reveals a slight decrease in the double layer charge for 1 ML Pd_{CPD} film after EC annealing. The increase in signal intensity for the terrace H_{upd} adsorption/desorption peaks, accompanied by the disappearance of step H_{upd} adsorption/desorption peaks, suggests an improvement in the surface order. Bromine-induced surface-smoothening effects after electrochemical annealing are further demonstrated by the enhanced sharpness of the LEED patterns for 1 ML Pd_{CPD} (Figure

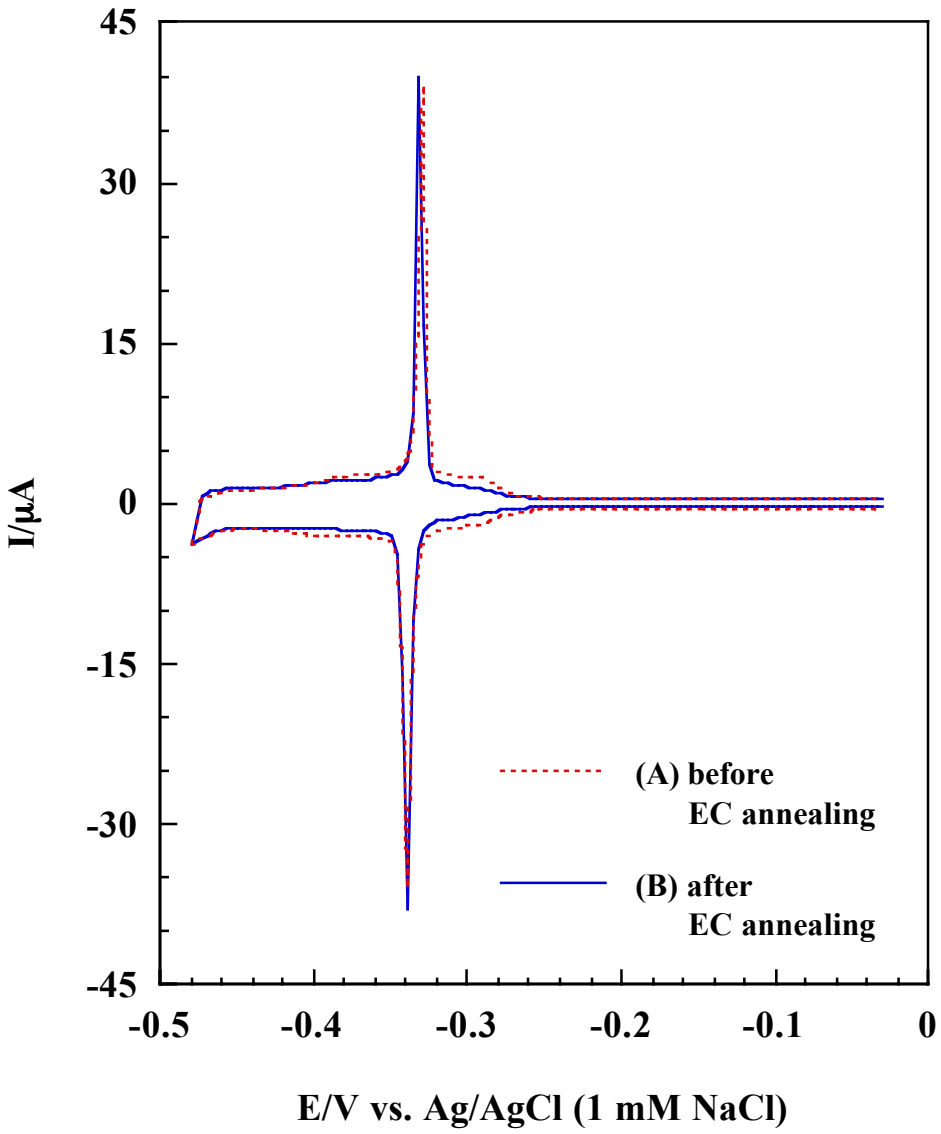

Figure 47. Voltammograms for 1 ML Pd_{CPD} film on Pt(111) in 100 mM H_2SO_4 obtained (A) before and (B) after EC annealing. EC annealing consisted of 5 cycles of potential cycling between –0.65 and 0.22 V in 1 mM NaBr and 100 mM NaF adjusted to pH 4 with tetrafluoroacetic acid. Pd film was prepared by potentiostatic deposition. Sweep rate = 2 mV/sec. Electrode area = 1.12 cm^2.

(A) Before EC annealing

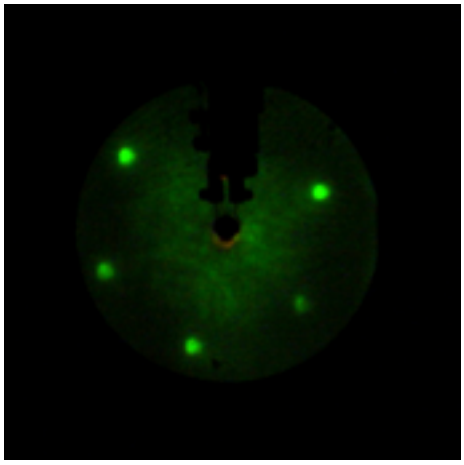

(B) After EC annealing

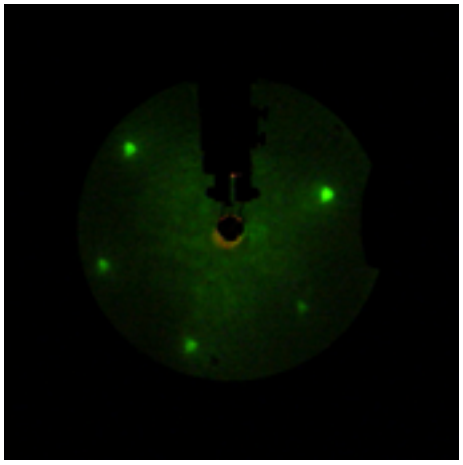

Figure 48. LEED patterns for 1 ML Pd_{CPD} film on Pt(111) obtained (A) before and (B) after EC annealing. Pd film was prepared by potentiostatic deposition. EC annealing protocols were the same as in Figure 47. Beam energy = 62.0 eV; beam current = 2 μA.

48).

The same surface-smoothening effects can be gleaned from the voltammograms (Figure 49) and LEED patterns (Figure 50) of 2 ML Pd_{CPD} films.

A Pd coverage of 3 ML represents a critical transition in the observed thin-film behavior of the electrodeposited Pd adlayer. It is worthwhile to note that the pre-EC-annealed Pd film exhibits step features, along with terrace-related peaks which appear smaller than those obtained from 2 ML Pd_{CPD} films. The post-EC-annealed 3 ML Pd_{CPD} film (Figure 51) exhibits a sudden decrease in the terrace and step H_{upd} adsorption/desorption peaks as well the double-layer charge. The existence of minuscule step H_{upd} adsorption/desorption peaks after EC annealing implies that the pre-defined number of potential cycles was inadequate in making the 3 ML Pd_{CPD} film surface *completely* smooth. LEED patterns after EC annealing (Figure 52), however, still remain sharp.

Voltammetric features associated with step sites continue to become more prominent at a Pd coverage of 4 ML Pd_{CPD}. As shown in Figure 53, EC annealing leads to a decrease in the intensity of both the step- and terrace-related peaks; the terrace H_{upd} peaks appear much smaller than the step H_{upd} peaks. The acquisition of sharp LEED patterns (Figure 54) indicates that the surface remains ordered after EC annealing.

Figure 55 unveils the dramatic disappearance of terrace and step H_{upd} adsorption/desorption peaks after EC annealing a 5 ML Pd_{CPD} film. LEED patterns (Figure 56) before and after EC annealing exhibit the same sharpness.

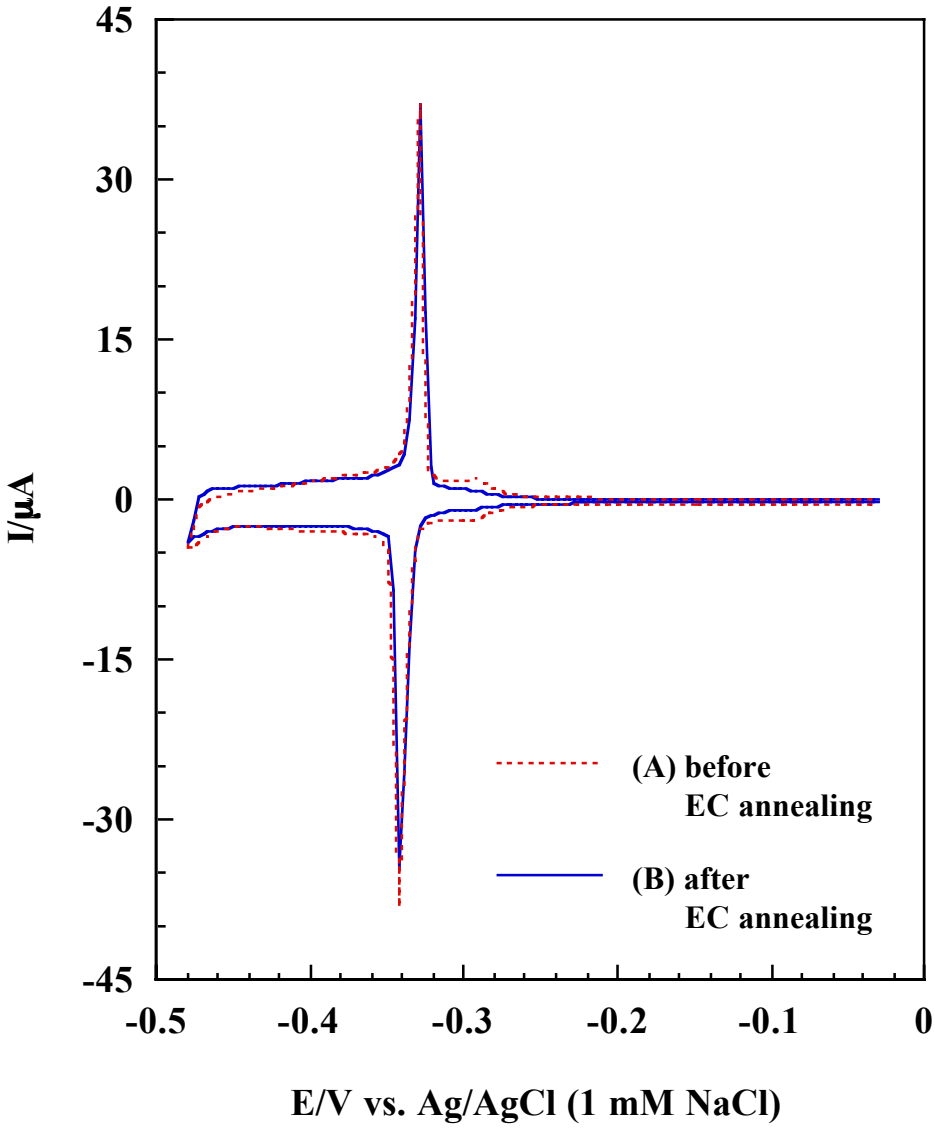

Figure 49. Voltammograms for 2 ML Pd_{CPD} film on Pt(111) in 100 mM H_2SO_4 obtained (A) before and (B) after EC annealing. Pd film was prepared by potentiostatic deposition. Experimental conditions were as in Figure 47.

(A) Before EC annealing

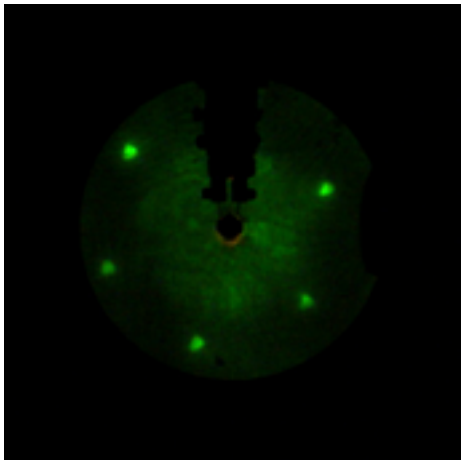

(B) After EC annealing

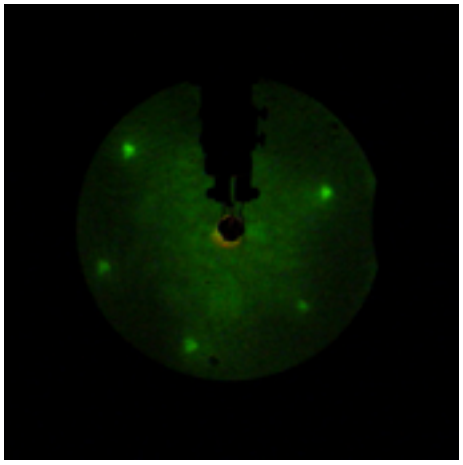

Figure 50. LEED patterns for 2 ML Pd_{CPD} film on Pt(111) obtained (A) before and (B) after EC annealing. Pd film was prepared by potentiostatic deposition. Experimental conditions were as in Figure 48.

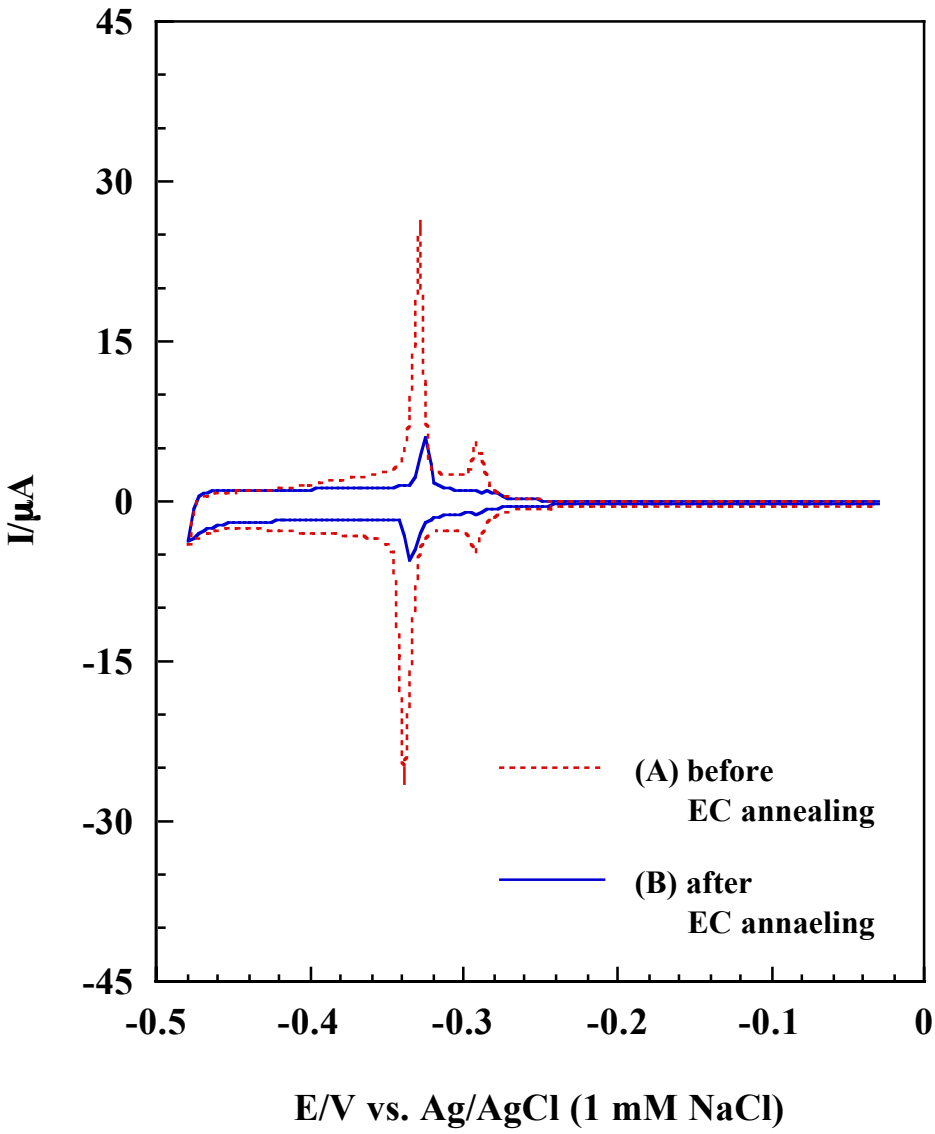

Figure 51. Voltammograms for 3 ML Pd_{CPD} film on Pt(111) in 100 mM H_2SO_4 obtained (A) before and (B) after EC annealing. Pd film was prepared by potentiostatic deposition. Experimental conditions were as in Figure 47.

(A) Before EC annealing

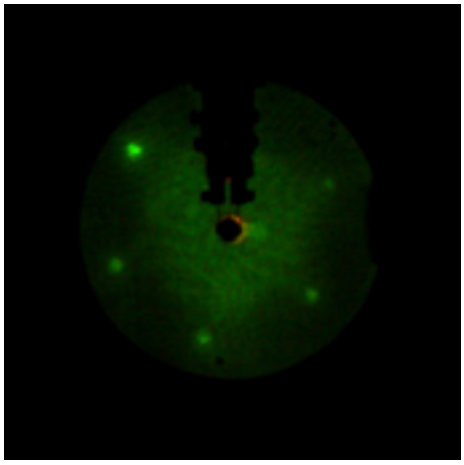

(B) After EC annealing

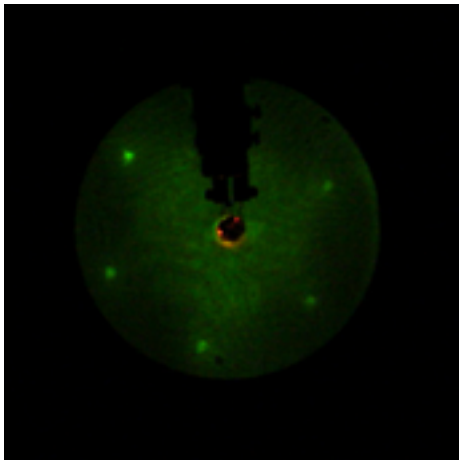

Figure 52. LEED patterns for 3 ML Pd_{CPD} film on Pt(111) obtained (A) before and (B) after EC annealing. Pd film was prepared by potentiostatic deposition. Experimental conditions were as in Figure 48.

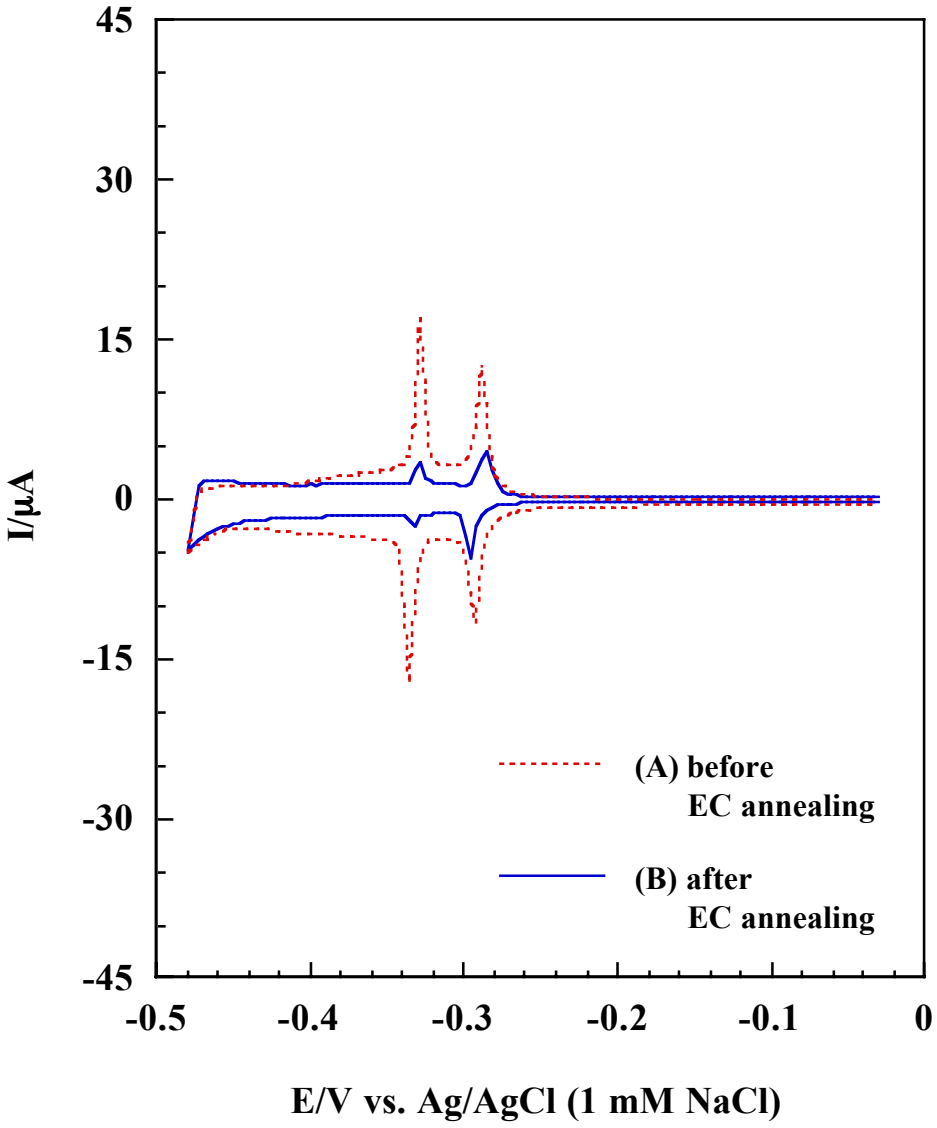

Figure 53. Voltammograms for 4 ML Pd_{CPD} film on Pt(111) in 100 mM H_2SO_4 obtained (A) before and (B) after EC annealing. Pd film was prepared by potentiostatic deposition. Experimental conditions were as in Figure 47.

(A) Before EC annealing

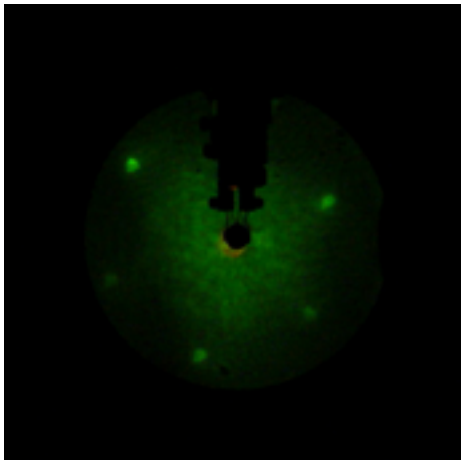

(B) After EC annealing

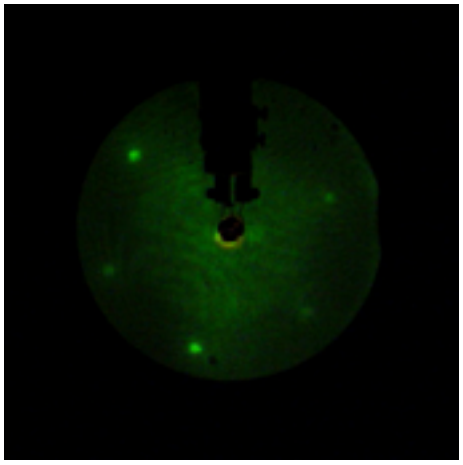

Figure 54. LEED patterns for 4 ML Pd_{CPD} film on Pt(111) obtained (A) before and (B) after EC annealing. Pd film was prepared by potentiostatic deposition. Experimental conditions were as in Figure 48.

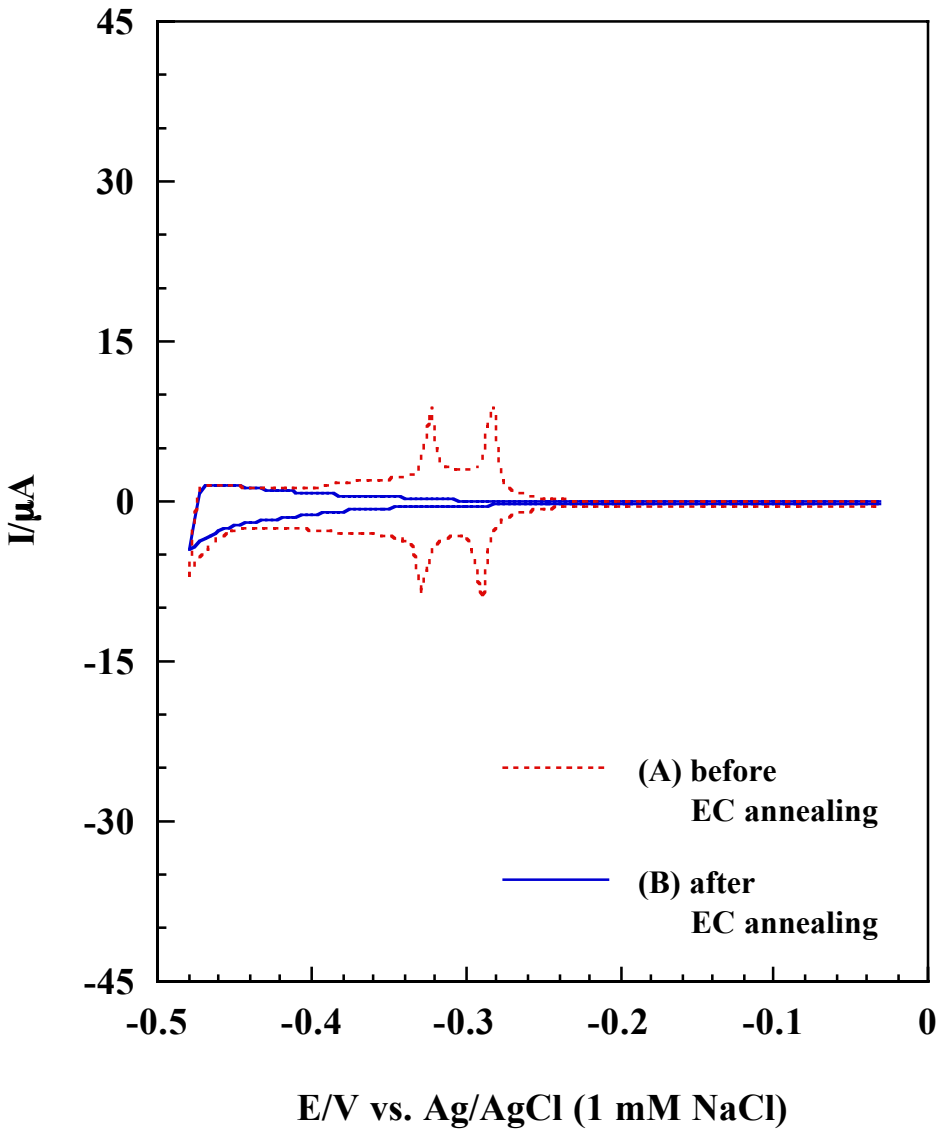

Figure 55. Voltammograms for 5 ML Pd_{CPD} film on Pt(111) in 100 mM H_2SO_4 obtained (A) before and (B) after EC annealing. Pd film was prepared by potentiostatic deposition. Experimental conditions were as in Figure 47.

(A) Before EC annealing

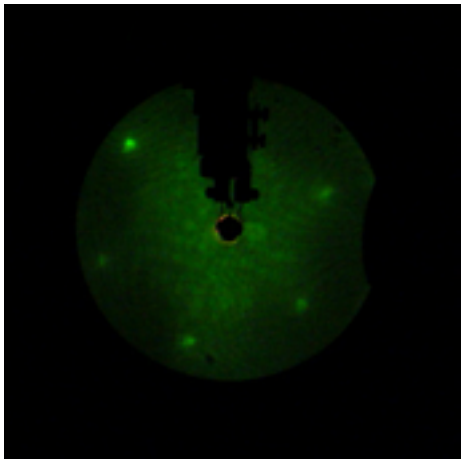

(B) After EC annealing

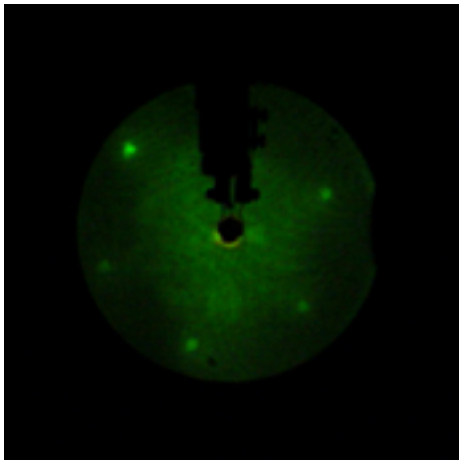

Figure 56. LEED patterns for 5 ML Pd_{CPD} film on Pt(111) obtained (A) before and (B) after EC annealing. Pd film was prepared by potentiostatic deposition. Experimental conditions were as in Figure 48.

To investigate the effect of the number of potential cycles on the Pd film surface, voltammograms and LEED patterns for 3 ML Pd_{CPD} films (Figures 57 and 58, respectively) were compared after performing a single cycle and two cycles of EC annealing. Results indicate that the differences in the voltammetric features and LEED patterns are negligible.

Auger electron spectra (Figure 59) for 4 ML Pd_{CPD} film were taken before and after EC annealing to monitor changes in the Auger Pd peak. A slight increase (less than 10 %) in the Pd intensity was observed after the EC annealing cycles.

Chemisorbed Bromine-induced Anodic Dissolution of Ultrathin Pd Films

Chemisorbed bromine (Br_{ads}), unlike I_{ads}, exerts minimal effects on the corrosion of bulk Pd [27]. Ultrathin Pd films are, however, known to be susceptible to Br_{ads}-catalyzed corrosion [31]. An in-depth investigation was launched to probe the corrosive effects of Br_{ads} on ultrathin Pd films. Bromine was adsorbed onto Pd_{CPD} films at 0.22 V for about 3 minutes. Current-potential profiles were obtained in Br^--free electrolyte by sweeping the potential from 0.22 to 0.77 V at 2 mV/s.

Figure 60 shows voltammograms of Pt(111) and ultrathin Pd films obtained after Br adsorption. The voltammogram for Br_{ads} on Pt(111) shows a very broad oxidation peak at 0.65 V while that for Br_{ads} on 0.5 ML Pd_{CPD} film has two distinctive plateaus centered at 0.45 and 0.65 V. At higher Pd coverages (4ML), a large oxidation peak is observed at 0.45 V. The peak at 0.45 V is possibly related with the oxidation of Pd

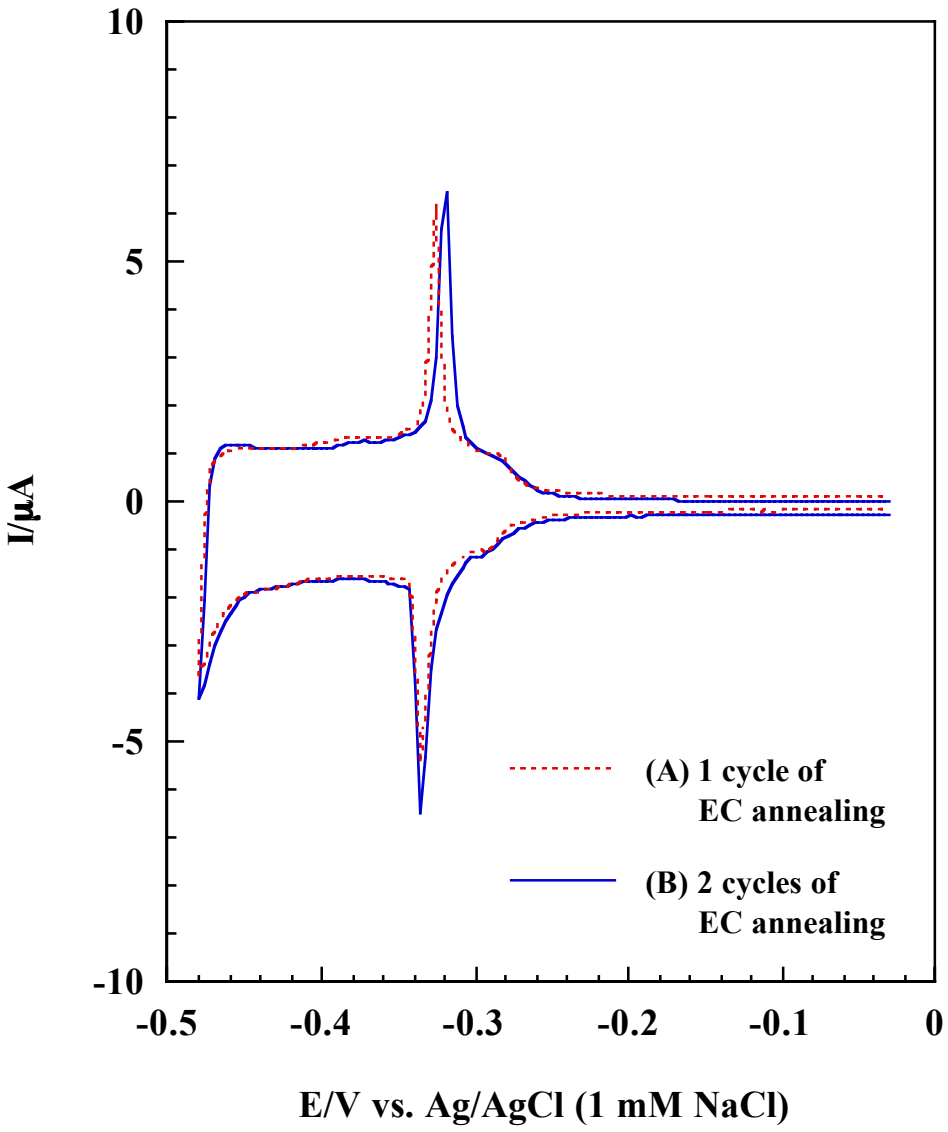

Figure 57. Voltammograms for 3 ML Pd_{CPD} film on Pt(111) in 100 mM H_2SO_4 obtained after (A) one cycle and (B) two cycles of EC annealing. Pd film was prepared by potentiostatic deposition. Experimental conditions were as in Figure 47.

(A) Before one cycle of EC annealing

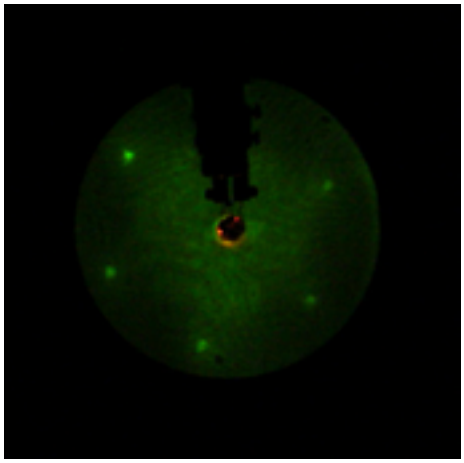

(B) After two cycles of EC annealing

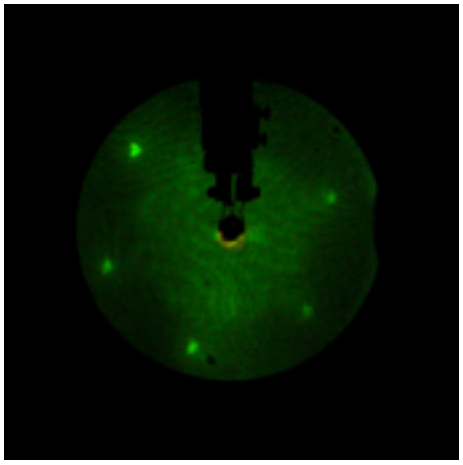

Figure 58. LEED patterns for 3 ML Pd_{CPD} film on Pt(111) obtained after (A) one cycle and (B) two cycles of EC annealing. Pd film was prepared by potentiostatic deposition. Experimental conditions were as in Figure 48.

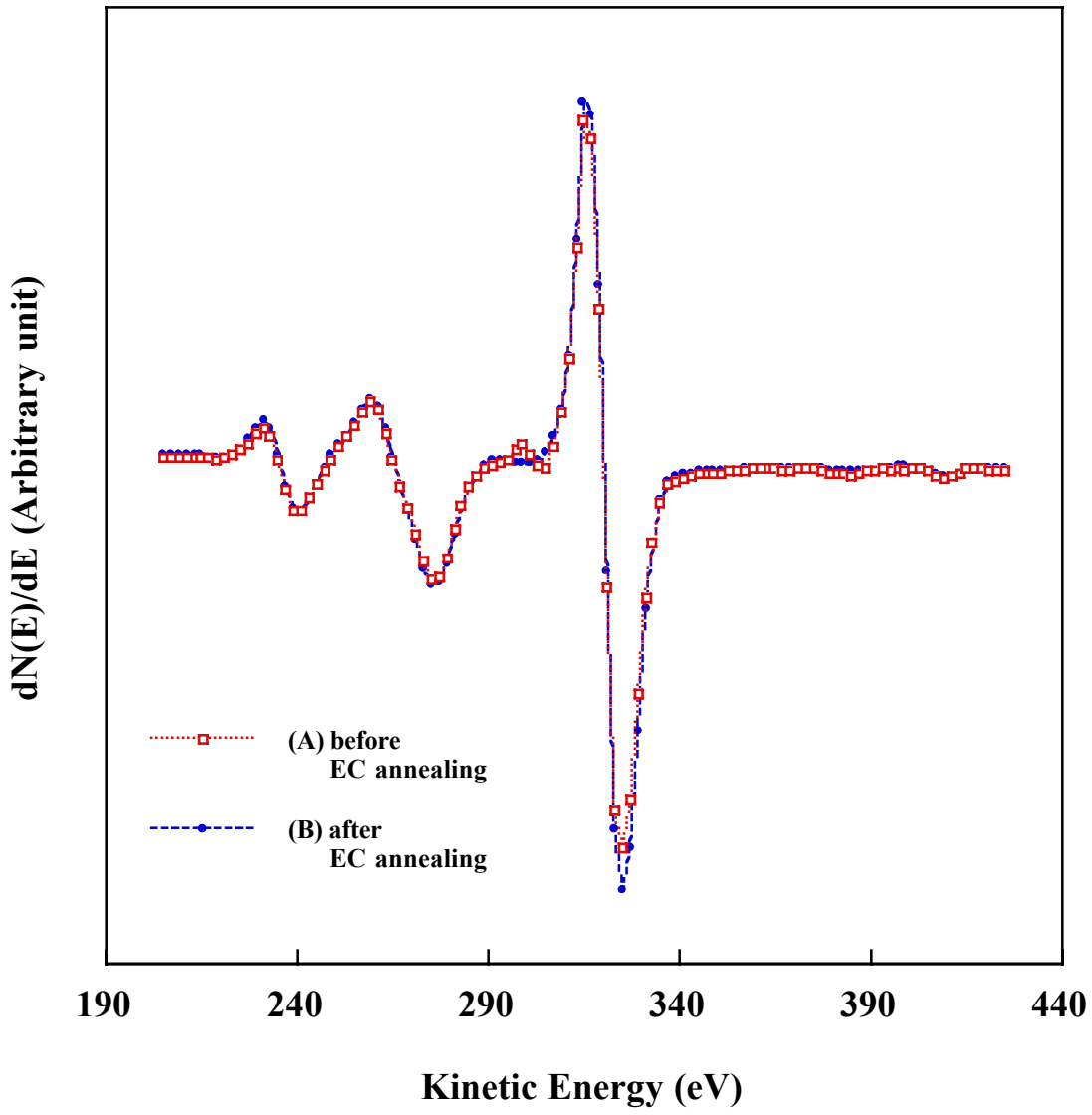

Figure 59. Auger electron spectra for 4 ML Pd_{CPD} film on Pt(111) obtained (A) before and (B) after EC annealing. Pd film was prepared by potentiostatic deposition. EC annealing protocols were the same as in Figure 47. Incident beam energy = 2 keV; beam current = 1 μA.

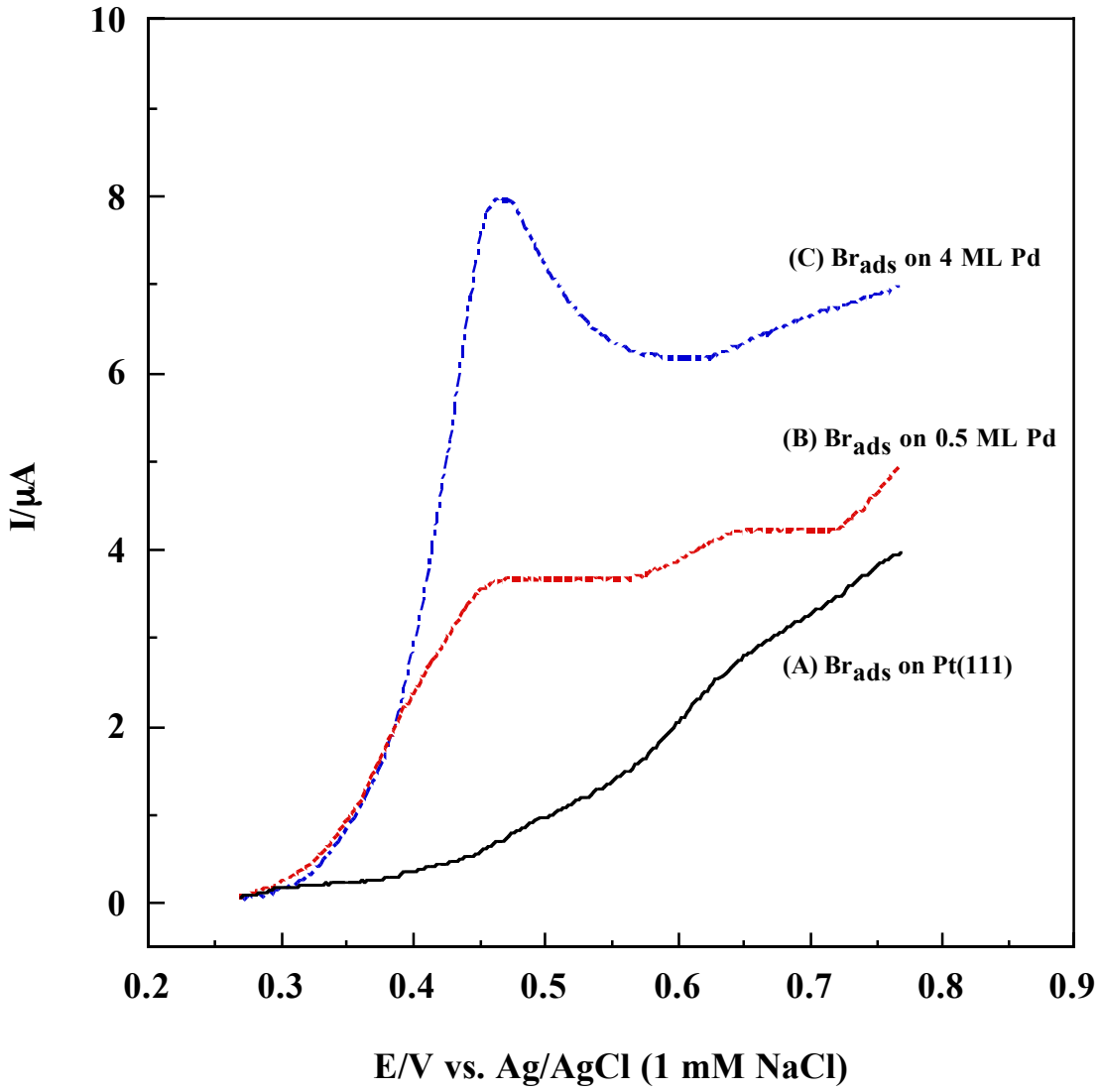

Figure 60. Voltammograms for Br_{ads} on (A) Pt(111), (B) 0.5 ML Pd_{CPD} film, and (C) 4 ML Pd_{CPD} film in 100 mM H_2SO_4. Pd films were prepared by potentiostatic deposition. Bromine adsorption conditions were as in Figure 41. Sweep rate = 2 mV/sec. Electrode area = 1.12 cm^2.

and/or Br_{ads} on Pd film while the peak at 0.65 V represents the oxidation of Br_{ads} on Pt and/or Pd film surface.

The Auger electron spectra (Figure 61) for (A) Br_{ads} on Pt(111), (B) Br_{ads} on 0.5 ML Pd film, and (C) Br_{ads} on 1 ML Pd film reveal very small Br peaks at 102 and 108 eV. No O peak is discernible at 503 eV. The Br surface coverage on Pt(111) was estimated to be 0.03 ML; both 0.5 ML and 1 ML Pd films have approximately the same Br surface coverage of 0.05 ML. As shown in Figure 62, diffuse (1×1) LEED patterns are obtained from Br_{ads} on Pt(111), Br_{ads} on 0.5 ML Pd, and Br_{ads} on 1 ML Pd.

Br_{ads}-induced corrosion of Pd thin film with higher Pd coverages was explored. Bromine was chemisorbed onto a 5 ML Pd_{CPD} film at 0.22 V in bromide-containing 100 mM NaF (pH4). The resulting film was transferred to Br^--free 100 mM H_2SO_4; the potential was scanned from the open circuit potential to the potential which marks the completion of the Br_{ads}-induced Pd corrosion (typically 0.58 – 0.52 V). Bromine was then re-adsorbed to the film before another corrosion cycle was conducted. A total of five Br_{ads}-induced Pd corrosion cycles was performed.

The voltammograms in Figure 63 reveal that the Pd stripping peak at ca. 0.44 V is largest during the first cycle. The intensity of the Pd stripping peak gradually decreases as more corrosion cycles are carried out. During the second cycle, a small anodic peak is observed at ca. 0.55 V; the peak develops into a broad shoulder as the number of corrosion cycles increases.

The amount of remnant Pd and stripped Pd (expressed in terms of ML) after each cycle is plotted in Figure 64. The amount of Pd that remains on the Pt substrate

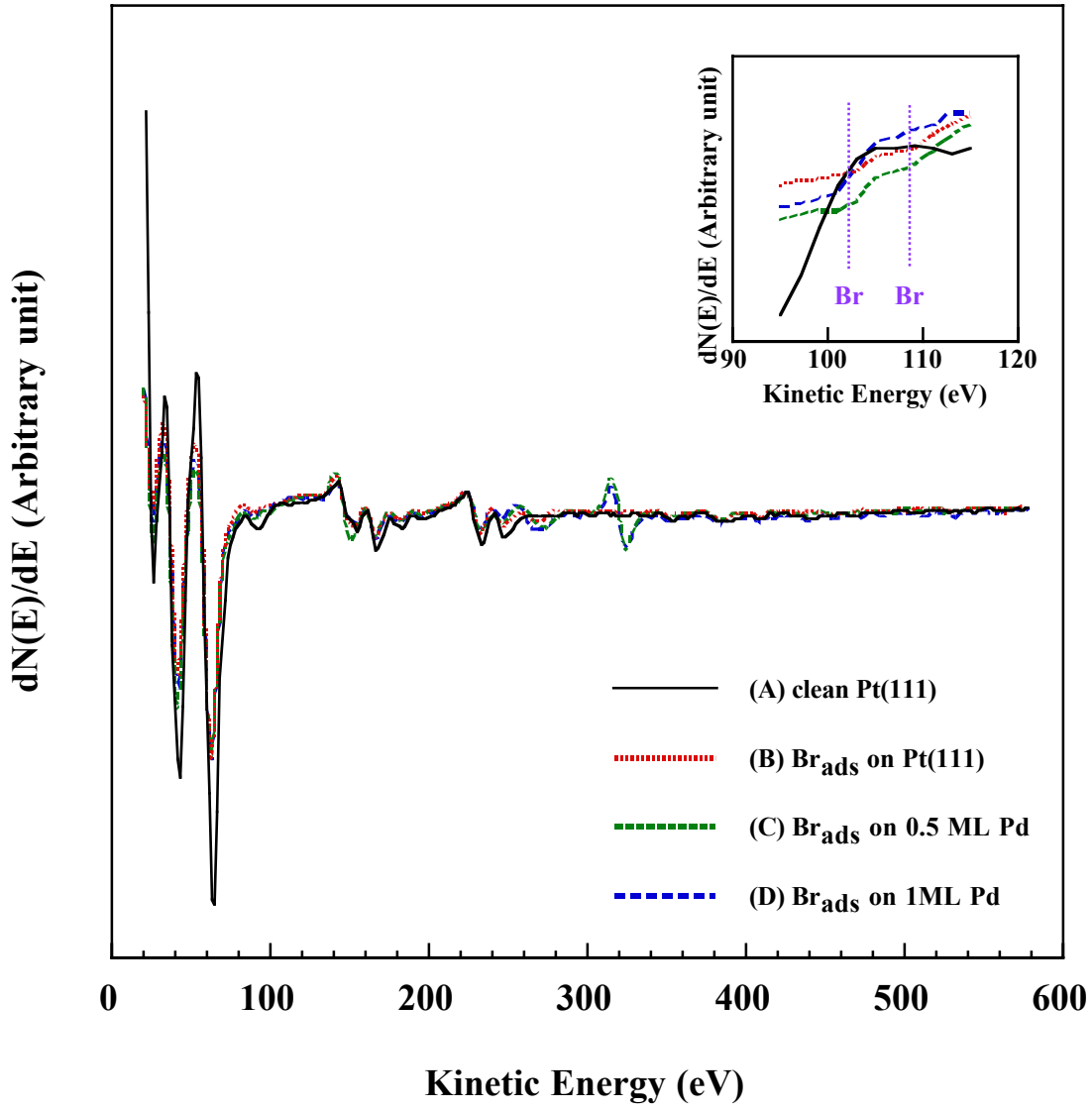

Figure 61. Auger electron spectra for (A) Pt(111), (B) Br_{ads} on Pt(111), (C) Br_{ads} on 0.5 ML Pd_{CPD} film, and (D) Br_{ads} on 1 ML Pd_{CPD} film obtained after potential scan in 100 mM H_2SO_4 from 0.22 to 0.77 V at 2 mV/s. Pd film was prepared by potentiostatic deposition. Bromine adsorption conditions were as in Figure 41. Incident beam energy = 2 keV; beam current = 1 μA. Insert: magnified Auger electron spectra showing Br signal.

(A) Br_{ads} on Pt(111)

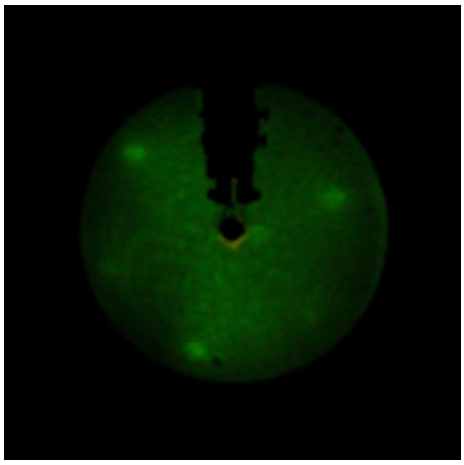

(B) Br_{ads} on 0.5 ML Pd

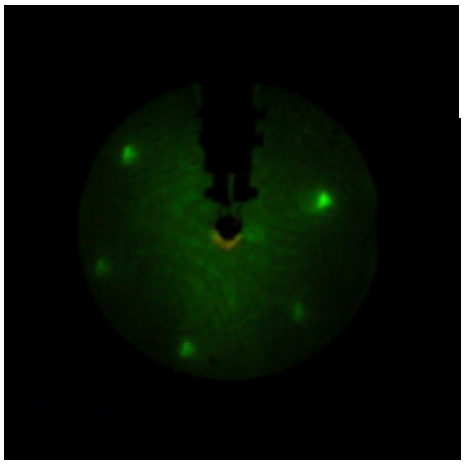

(C) Br_{ads} on 1 ML Pd

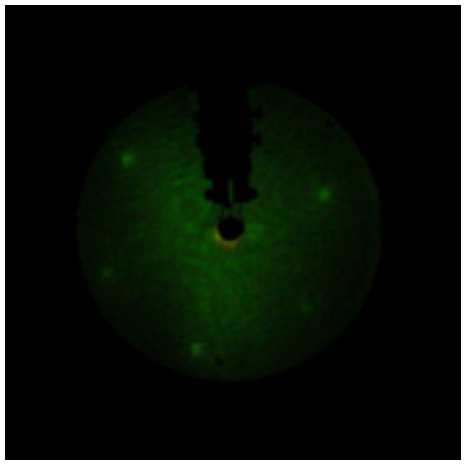

Figure 62. LEED patterns for (A) Br_{ads} on Pt(111), (B) Br_{ads} on 0.5 ML Pd_{CPD} film, and (C) Br_{ads} on 1 ML Pd_{CPD} film obtained after potential scan in 100 mM H_2SO_4 from 0.22 to 0.77 V at 2 mV/s. Pd films were prepared by potentiostatic deposition. Bromine adsorption conditions were as in Figure 41.Beam energy = 62.0 eV; beam current = 2 μA.

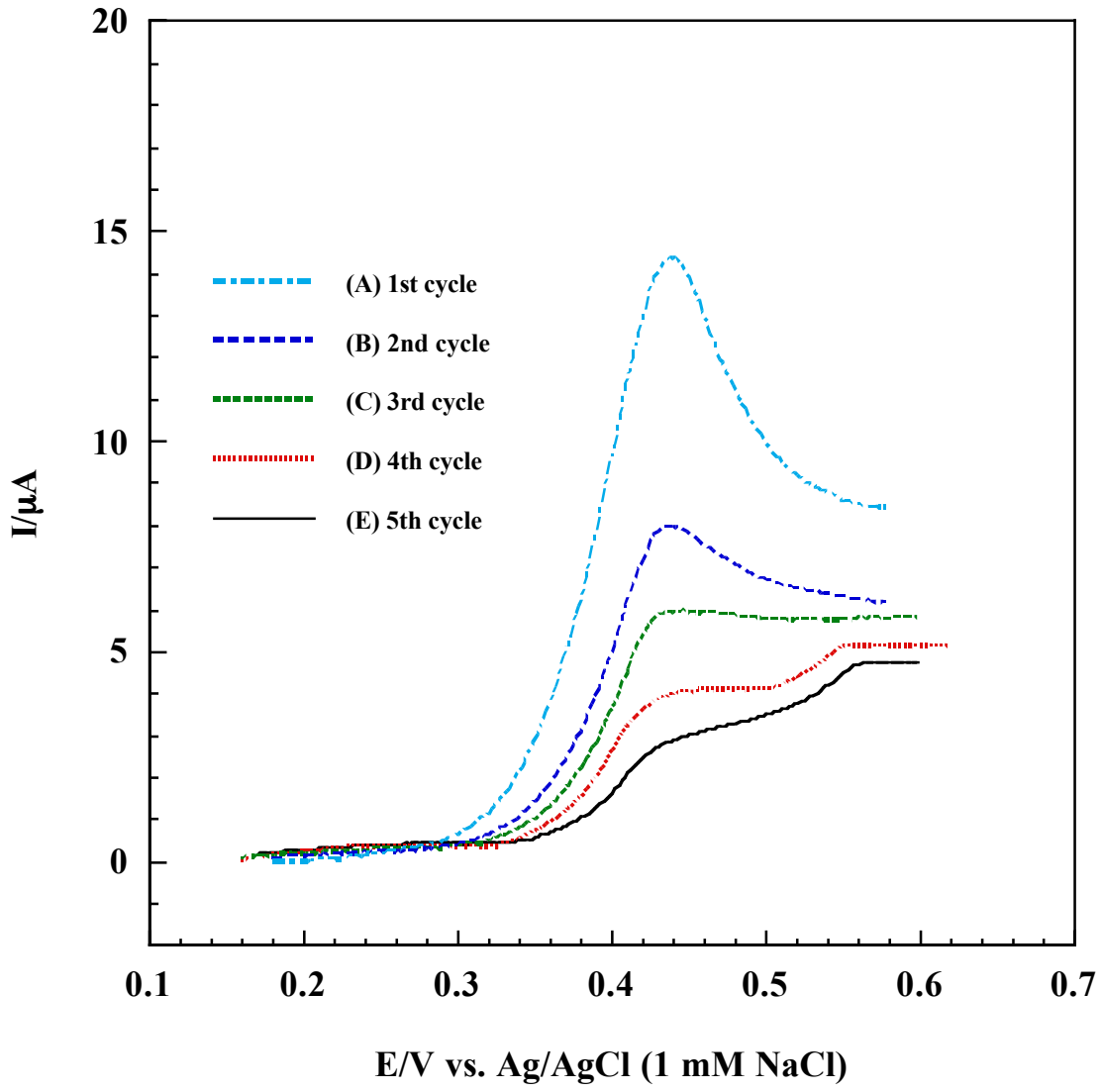

Figure 63. Voltammograms for Br_{ads}-induced corrosion of 5 ML Pd_{CPD} film on Pt(111) in 100 mM H_2SO_4. Bromine was adsorbed before each corrosion cycle. Pd film was prepared by potentiostatic deposition. Bromine adsorption conditions were as in Figure 41. Sweep rate = 2 mV/sec. Electrode area = 1.12 cm^2.

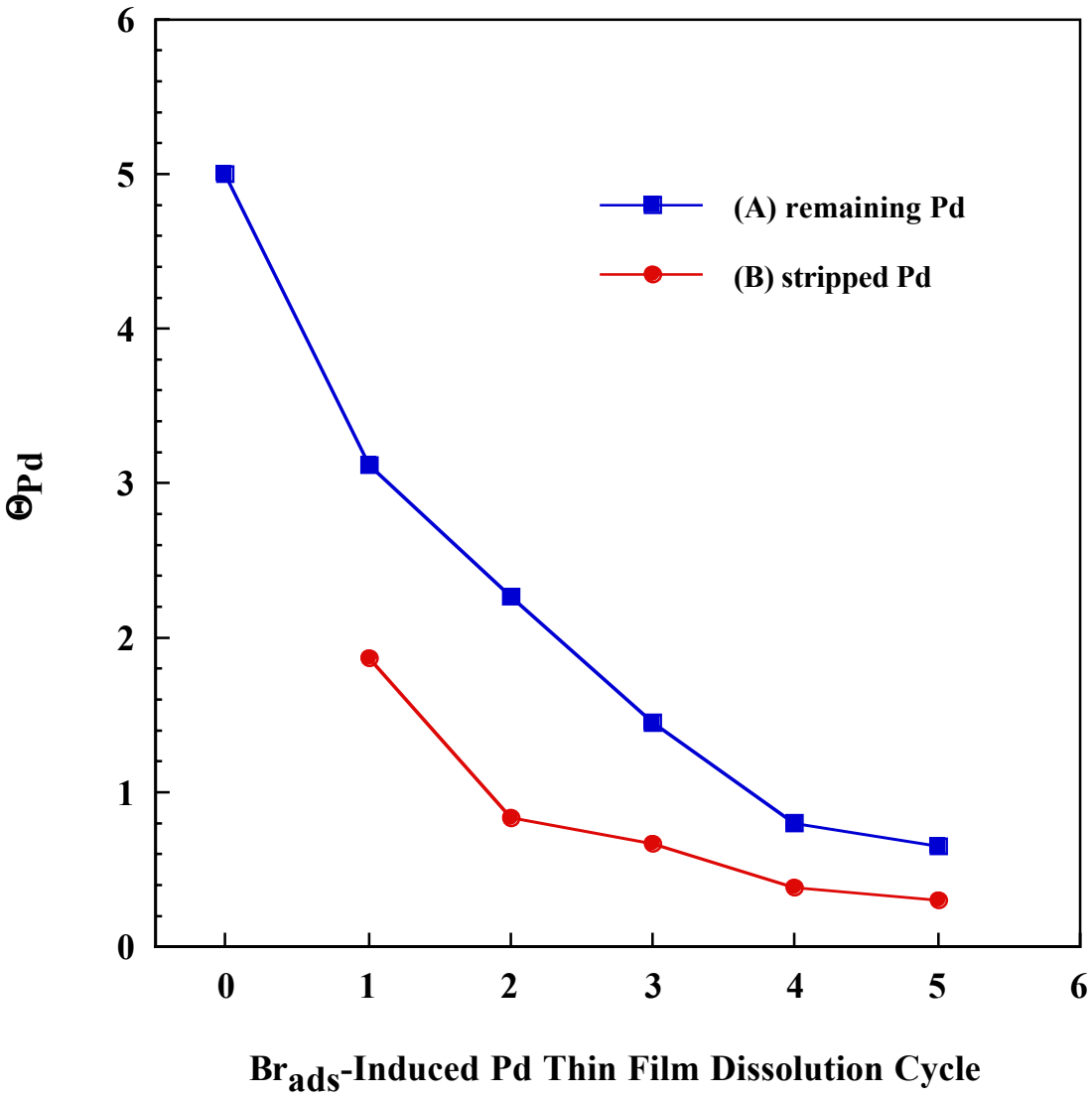

Figure 64. Changes in Pd coverage during the process of 5 cycles of Br_{ads}-induced Pd film corrosion. Experimental conditions were as in Figure 63.

decreases with the number of corrosion cycle. On the other hand, the amount of stripped Pd is largest after the first cycle and then gradually decreases with number of corrosion cycles. This observation suggests that it is increasingly more difficult to strip off Pd adatoms as the Pd film becomes thinner.

Figure 65 shows the LEED spectra for 5 ML Pd_{CPD} film on Pt(111) obtained after each Br_{ads}-induced Pd corrosion cycle. Diffuse $(\sqrt{3}\times\sqrt{3})R30°$ patterns indicative of Br adlayers can be seen. Auger electron spectra in Figure 66 show a decrease in Pd peak intensity as the number of the corrosion cycle increases. It is interesting to note that the surface remains oxide-free after each corrosion cycle.

Bromine stays on the surface at the end of each cycle at a fairly constant coverage (0.18 ML), except for the 4^{th} and 5^{th} cycles at which values drop to 0.12 and 0.07 ML, respectively. About 55 % of the bromine chemisorbed during the initial stage of the cycle remains on the surface after the first three cycles. At the end of the 4^{th} and 5^{th} cycle, only 35% and 20 % of the original bromine adatoms are retained, respectively. AES and LEED data suggest that the remaining Br_{ads} exhibit significant long-range surface order.

Current-transient analysis was employed to further examine the origin of the observed surface order of the remnant bromine after each corrosion cycle. Br_{ads} on 5 ML Pd_{CPD} films were subjected to a potential scan from 0.22V (open circuit potential) to 0.41 V which is 0.03 V more negative than the peak potential for the Br_{ads}-induced Pd corrosion. Figure 67 depicts an exponential decay of Br_{ads}-induced Pd corrosion current with time upon holding the potential at 0.41 V for 2 minutes.

(A) Br_{ads} on 5 ML Pd_{CPD} film

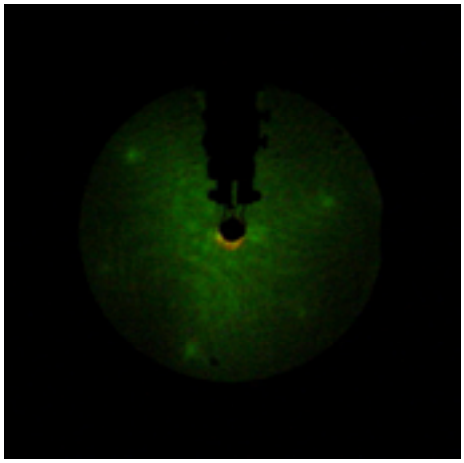

(B) After 1st corrosion cycle

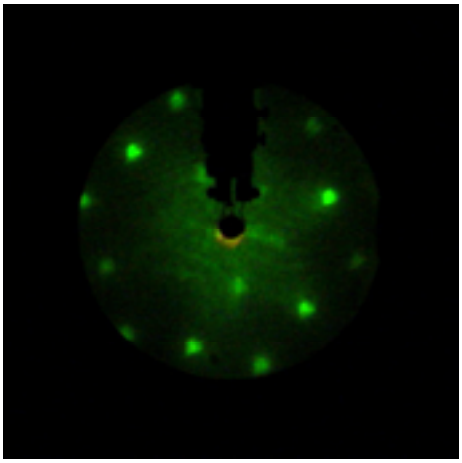

(C) After 3rd corrosion cycle

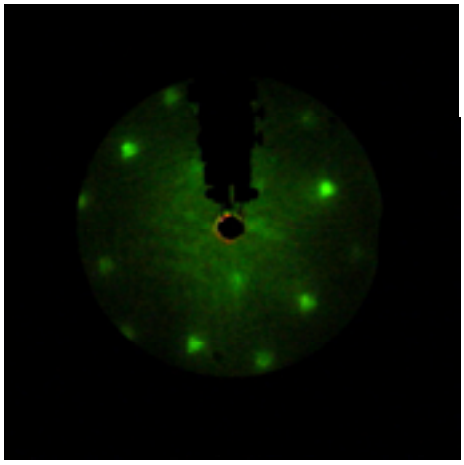

(D) After 5th corrosion cycle

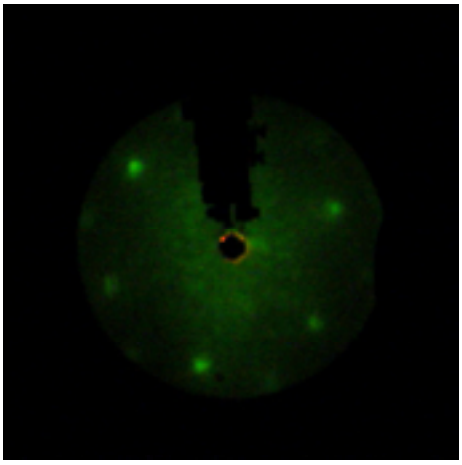

Figure 65. LEED patterns for Br_{ads} on 5 ML Pd_{CPD} film obtained (A) before and after the (B) 1st, (C) 3rd, and (D) 5th Br_{ads}-induced Pd film corrosion cycles. Bromine was adsorbed before each cycle. Pd film was prepared by potentiostatic deposition. Br adsorption conditions were as in Figure 41. Beam energy = 62.0 eV; beam current = 2 μA.

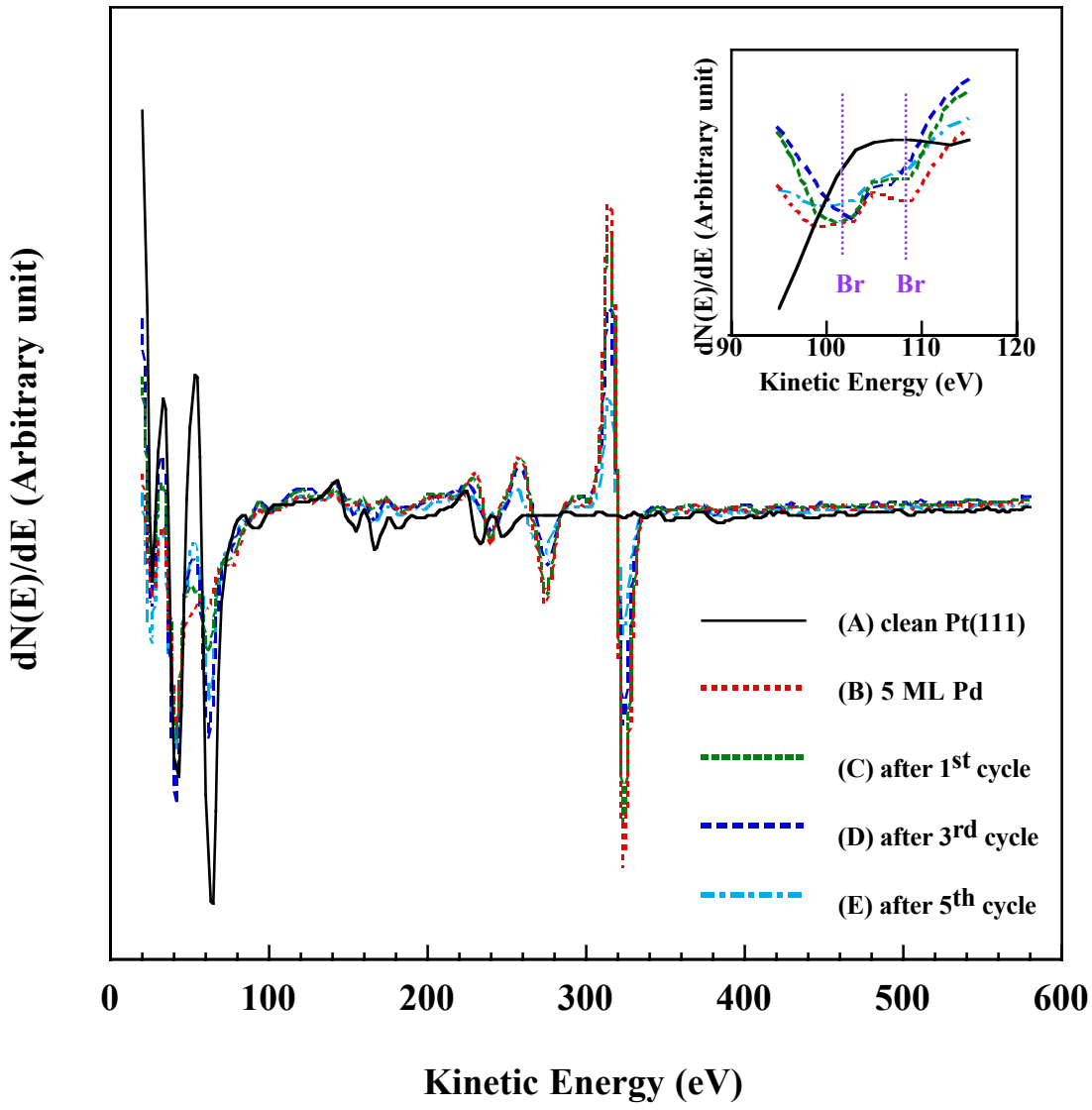

Figure 66. Auger electron spectra for (A) Pt(111) and Br_{ads} on 5 ML Pd_{CPD} film (B) before and after the (C) 1st, (D) 3rd, and (E) 5th Br_{ads}-induced Pd film corrosion cycle. Pd film was prepared by potentiostatic deposition. Bromine adsorption conditions were as in Figure 41. Incident beam energy = 2 keV; beam current = 1 μA.

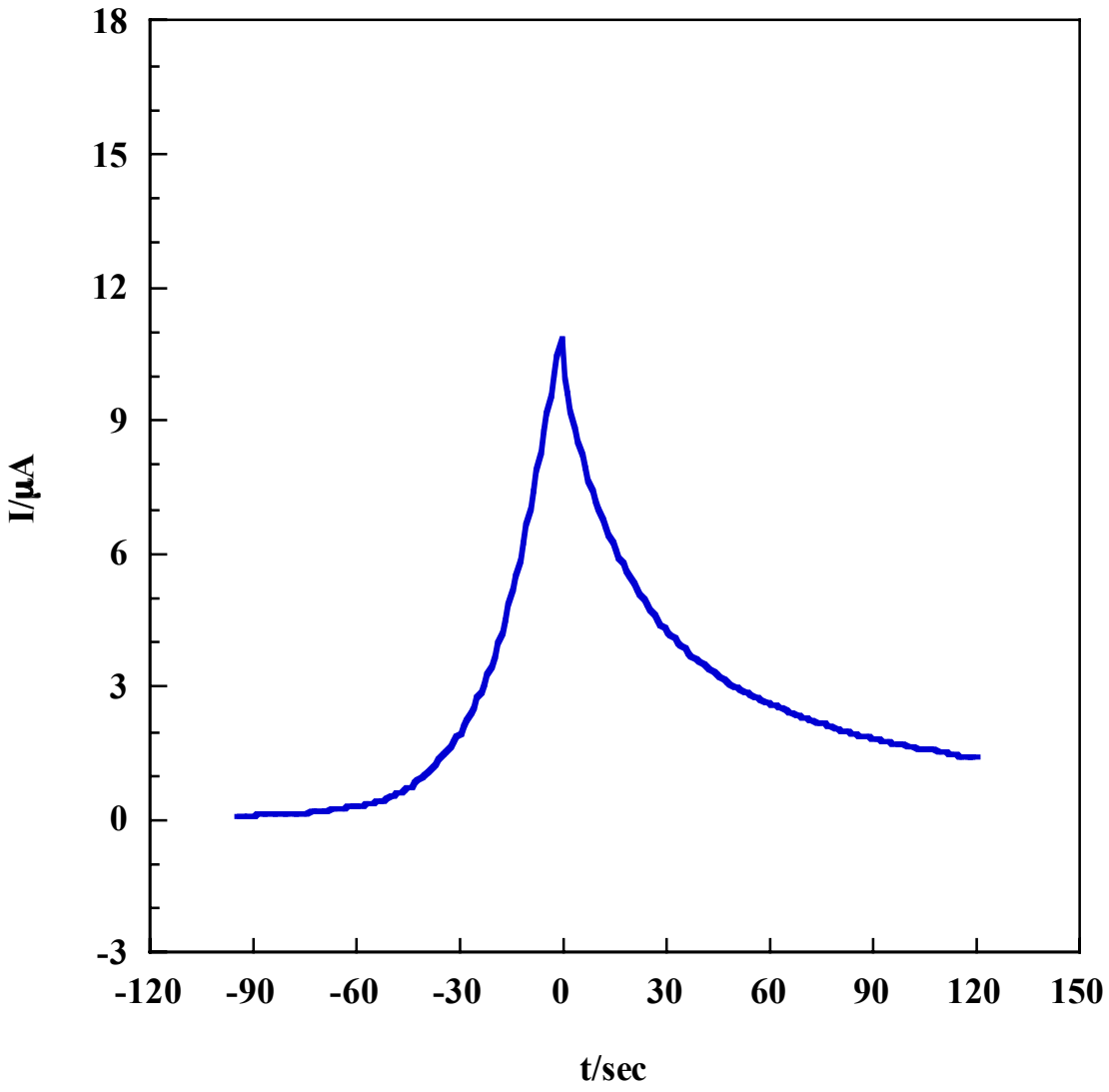

Figure 67. Current transient of Br_{ads} on 5 ML Pd_{CPD} film after the potential was scanned from 0.22 to 0.41 V, at 2 mV/s, and then fixed at 0.41 V for 2 minutes in 100 mM H_2SO_4. Pd film was prepared by potentiostatic deposition. Bromine adsorption conditions were as in Figure 41.

Very diffuse (1x1) LEED patterns were acquired from 5 ML Pd_{CPD} film after the potential scan was terminated at 0.41V and the final potential was kept for 2 and 7 minutes (Figures 68 (A) and (B), respectively). Holding the final potential for 2 minutes during 2^{nd} Pd corrosion cycle did not alter the diffuse nature of the LEED patterns (Figure (C)). A diffuse (1×1) LEED pattern (Figures 68 (D)) was also obtained when 1 ML Pd_{CPD} film was treated with the same potential excursion undergone by the sample in Figure 68(A).

Changes in Br and Pd coverages brought about by equilibration of the films at 0.41 V after the programmed potential scans are reflected in the Auger electron spectra (Figure 69). After potentiodynamic cycling and then holding the potential constant at 0.41 V from 2 to 7 minutes, both Pd and Br peaks experience a decrease in signal intensity. However, under the present experimental conditions, the decrease in the Pd signal intensity is much more drastic compared to the diminution of the Br signal intensity: from 5 ML Pd to 2.9 ML Pd viz-a-vis from 0.33 ML to 0.22 ML after 2 minutes; from 5 ML Pd to 2.5 ML Pd viz-a-vis from 0.33 ML to 0.15 ML after 7 minutes. The surface remains oxide-free as evidenced by the absence of O peak in the Auger electron spectra.

(A) 5 ML Pd, 2 minutes

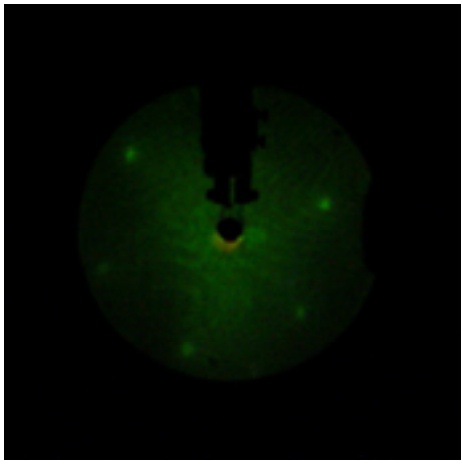

(B) 5 ML Pd, 7 minutes

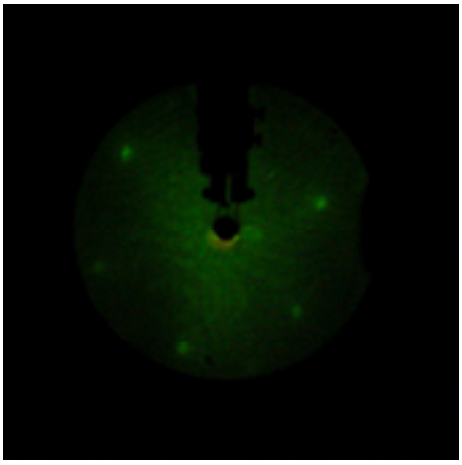

(C) 5 ML Pd after 1st cycle, 2 minutes

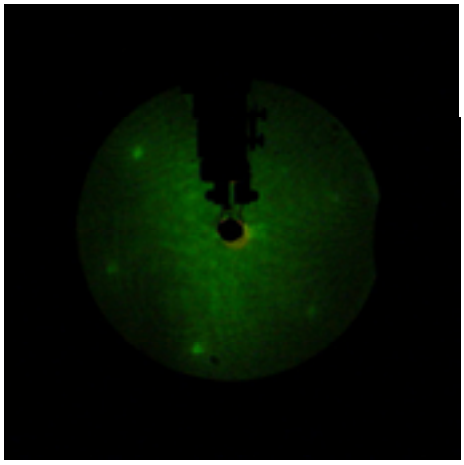

(D) 1 ML Pd, 2 minutes

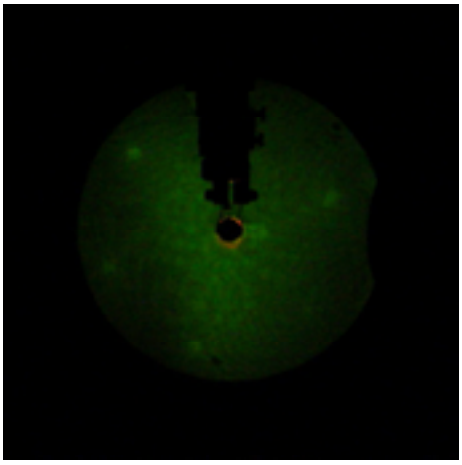

Figure 68. LEED patterns for Br_{ads} on *n* ML Pd_{CPD} films obtained after potential was scanned from 0.22 to 0.41 V, at 2 mV/s, and then fixed at 0.41 V for different durations, *t*: (A) *n* = 5, *t* = 2 minutes, (B) *n* = 5, *t* = 7 minutes, (C) *n* = 5 after 1st Pd corrosion cycle, *t* = 2 minutes, and (D) *n* =1, *t* = 2 minutes. Other experimental conditions were as in Figure 67. Beam energy = 62.0 eV; beam current = 2 μA.

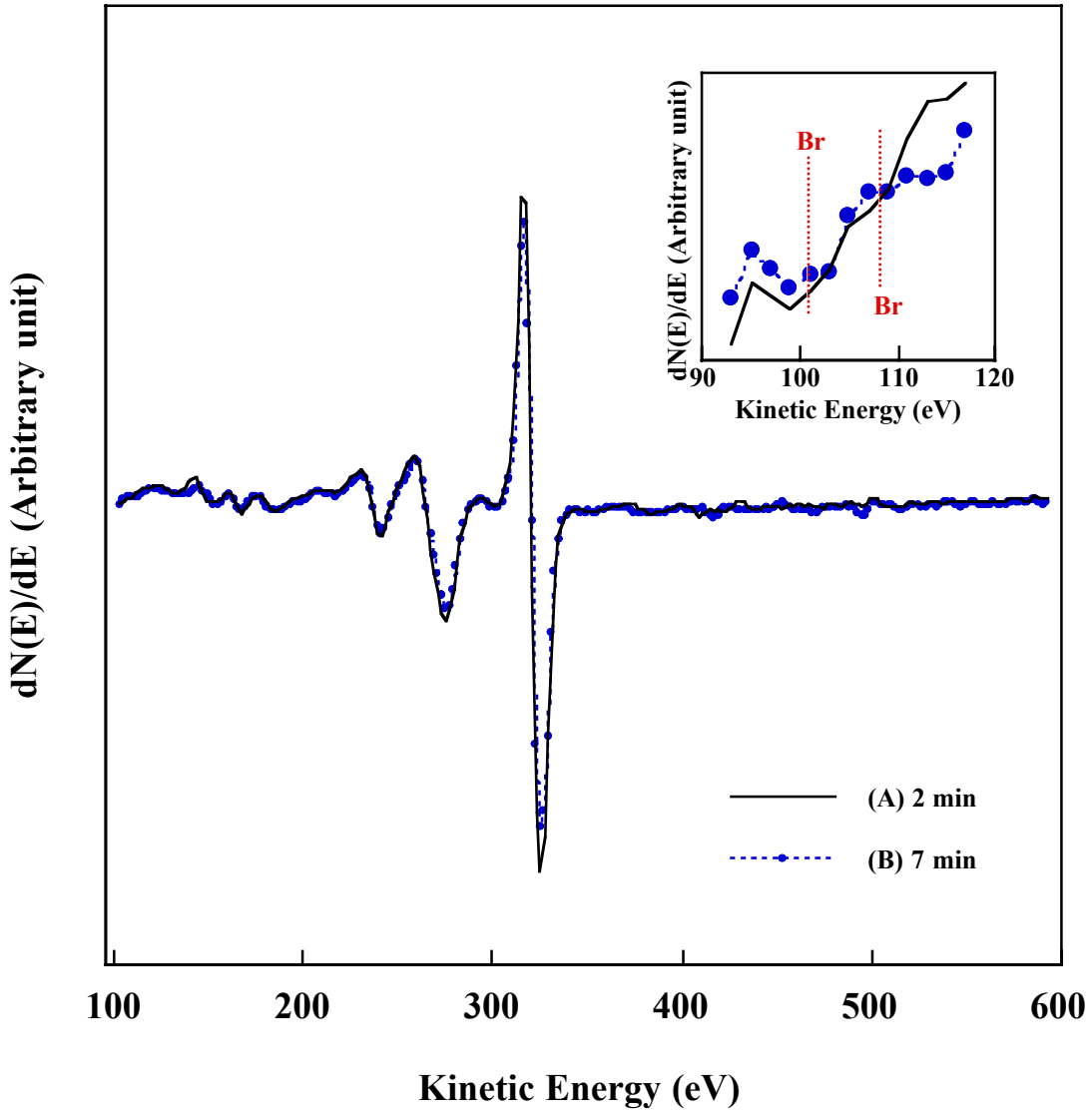

Figure 69. Auger electron spectra of Br_{ads} on 5 ML Pd_{CPD} film obtained after potential was scanned from 0.22 to 0.41 V, at 2 mV/s, and then fixed at 0.41 V for (A) 2 and (B) 7 minutes in 100 mM H_2SO_4. Pd film was prepared by potentiostatic deposition. Bromine adsorption condition was as in Figure 41. Incident beam energy = 2 keV; beam current = 1 μA.

DISCUSSION

Ultrathin Pd Films

Potentiostatic Deposition of Pd

Controlled potential deposition (CPD) is a feasible method in systematically controlling ultrathin Pd film coverages, from submonolayer to multilayer regimes, on Pt(111) surfaces. For a given electrolysis time, at low overpotentials η_{Pd}, the charge increases linearly until a near-exhaustive electrolysis occurs. Electrodeposition at large η_{Pd} (i. e., $E_{Pd\ deposition} < 0.00$ V), however, breaks down the linear trend. Potential excursions to extremely negative values lead to the inhibition of Pd deposition since a greater portion of the applied potential goes to the hydrogen evolution reaction (HER).

Pd_{CPD} Films

Surface evolution during potentiostatic electrodeposition of Pd films has been partly mapped out using a combination of LEED and AES. The deposition of 1 ML Pd leads to the formation of large, highly ordered Pd domains that fully cover the Pt(111) substrate. Two evidences support this fact: (i) the acquisition of sharp, bright LEED spots (Figure 18 (B)) and (ii) the disappearance of the Pt AES signal at 168 eV (Figure 19(C)). The slight, yet reproducible, decrease in the brightness of the LEED pattern obtained after the deposition of 2 ML suggests the onset of three-dimensional island formation on top of the first conformal layer.

As more Pd is deposited, it is interesting to note that the LEED spot sharpness virtually remains the same even up to 8 ML while there is a progressive decline in the spot brightness. It can be surmised that island growth ensues at 3 ML and becomes most prominent at 4 ML as can be gleaned from alterations in spot brightness of the LEED patterns and features in the cyclic voltammograms (*vide infra*). Based on the LEED and AES data alone, no definitive descriptions can be made on the surface structural changes as the Pd coverage increases from 3 ML to 8 ML. Further characterization of the island growth and nucleation, at 3 ML and higher, would have been possible by LEED spot-intensity-vs-beam-energy analysis which, unfortunately, could not be carried out.

The evidence suggests that the growth of the ultrathin Pd_{CPD} films proceeds via the Stranski-Krastanov mechanism; i.e., the completion of the first full monolayer is followed by three-dimensional island formation. The observed growth mode is dictated by the interplay of the relative surface energy of the Pd film and Pt(111) substrate (σ_{Pd} and σ_{Pt}, respectively) and the specific free interfacial energy, σ_i. The relation, in its simplest form, can be expressed as $\Delta = \sigma_{Pd} + \sigma_i - \sigma_{Pt}$, where edge-, shape- and size-effects on the reported surface energies are neglected [47]. Three-dimensional island growth is observed when $\Delta > 0$ while layer-by-layer growth is expected when $\Delta \leq 0$.

Taking the specific surface free energies [48] of Pd (111) and Pt (111), as 1382 and 1656 ergs/cm^2, respectively, and considering the similarity in lattice parameter of both metals (hence, $\sigma_i \approx 0$ ergs/cm^2 for 1 ML or lower Pd coverage), it is expected that complete 1 ML Pd film is formed initially, followed by a uniform second layer. At 2 ML or higher, island formation occurs, suggesting that the contribution of σ_i exceeds 274

ergs/cm^2. The Stranski-Krastanov growth mode of Pd on Pt substrate has been supported by previous studies using X-ray diffraction (XRD) [6], surface X-ray scattering [49], electrochemical-scanning tunneling microscopy (EC-STM) [21], and electrochemistry [6,21].

The prepared ultrathin Pd_{CPD} films under investigation show H_{upd} adsorption/desorption. Bulk Pd exhibits no H_{upd} adsorption/desorption peaks due to interfacial transformation of the surface H_{upd} into the bulk [50]. Surface H_{upd} facilitates hydrogen absorption in which a stable Pd-H phase is formed [51]; ultimately, bulk Pd lattice relaxation leads to a reduction in the hydrogen absorption energy barrier [52,53]. As the Pd film thickness decreases, both the hydrogen diffusion coefficient and the hydrogen solubility in Pd are notably decreased [50]; thus it is not unexpected to observe H_{upd} adsorption/desorption *without absorption* in ultrathin Pd films.

Voltammetric signatures of H_{upd} adsorption/desorption can be used to consolidate the morphological changes of the Pd film surface initially monitored by LEED and AES. Specifically, the growth of terraces and steps can be electrochemically monitored as a function of Pd coverage. Terrace- and step-site peaks appear at –0.34 V and –0.29 V, respectively.

At 1 ML Pd coverage, the surface is predominantly made up of large terraces as indicated by the very intense terrace H_{upd} adsorption/desorption peaks. The close agreement between the experimentally determined charge (213 μC) and the theoretical charge (212 μC) for a pseudomorphic Pd film on Pt(111) supports the assertion that the 1 ML Pd completely covers the Pt substrate. The disappearance of the characteristic

broad voltammetric features of Pt(111) between –0.17 and 0.0 V renders further evidence to this claim. Additional voltammetric evidence is also provided by the fact that only Pd-related Cu UPD signals are observed at a Pd coverage of 1 ML.

Surface imperfections, typified by step sites, can be detected by voltammetry. The first Pd monolayer conforms to any pre-existing step sites of the Pt(111) electrode; thus, it is not surprising to see very small step-related peaks.

Based on the changes in the voltammetric terrace- and step-peak size and charge from 1 to 3 ML Pd, the following surface events are deemed to transpire: The growth of three-dimensional islands occurs at the expense of the diminution of the surface area associated with ordered terraces. When Pd coverage increases from 3 to 4 ML, the number of islands on the film surface increases, thereby a substantial fraction of the terraces disappears.

It is interesting to note that at a considerably high Pd coverage of 8 ML, H_{upd} adsorption/desorption peaks are still observed. Similar results have been reported in the literature [21] suggesting the pervasiveness of highly-stepped thin-film structures (manifested by H_{upd}) even up to 10 ML under various deposition conditions and anion effects. In the present investigation, the step H_{upd} desorption charge at 8 ML is comparable to that of a 3 ML Pd_{CPD} film, suggesting that the Pd island density of the 8 ML Pd_{CPD} film is at least comparable to that of the 3 ML Pd_{CPD} film.

As the Pd coverage increases, the influence of Pt(111) substrate on the voltammetric features of Pd adlayers dramatically decreases. Peaks for Pt oxidation and reduction at 0.78 and 0.24 V, respectively, become negligible at 3 ML or higher.

Pd_{PSD} Films

Ultrathin Pd films prepared by different electrochemical methods are expected to show different structural and electrochemical properties. Under the present conditions of PSD, the potential is swept at a scan rate of 0.1 mV/s; i.e., the electrode surface potential is perturbed every 10 s, leading to the formation of Pd electrodeposits with non-equilibrium surface structures. In this regard, the interfacial electrochemical properties of Pd_{PSD} films were compared with those of Pd_{CPD} films.

Pd_{PSD} films, just like Pd_{CPD} films, exhibit Pd coverage-dependent surface order. Pd_{PSD} films initially show sharp, bright (1×1) patterns but yield diffuse (1×1) patterns at Pd coverages ≥ 4 ML. LEED spots for Pd_{PSD} films appear sharper but less brighter than their CPD counterparts. It is essential to recall that in order for sharp LEED patterns to be observed, well-ordered domains have to exist with a surface area of at least 100 $Å^2$; domains with surface area lower than this value leads to beam broadening. On the other hand, spot brightness is, in part, a function of the number of well-ordered domains that effectively contribute to coherent interference. In view of this analysis, it can be argued that Pd_{PSD} films have larger, yet fewer, Pd domains, compared with Pd_{CPD} films with corresponding coverages.

Auger electron spectra for Pd_{PSD} films are very similar to those for Pd_{CPD} films of the same Pd coverage. The intensity of the Pd peak at 330 eV increases gradually with Pd coverage while that of the Pt signal at 168 eV decreases. The Pt peak intensity for Pd_{PSD} films is no longer discernible at 3 ML; in this respect, Pd_{CPD} films are different

because at 2 ML the Pt peak is already indistinguishable from the background. The reason for this disparity remains unclear and necessitates further studies.

PSD films display a host of unexpected, idiosyncratic behavior: (i) Results indicate that PSD produces *step-free* 1 ML Pd films that completely cover the Pt(111) substrate. (ii) Pd adatoms are readily stripped off, giving rise to a Pt reduction peak (0.24 V) which is larger than the Pd reduction peak (0.18 V). (iii) Step density increases with Pd coverage, from 1 to 4 ML, and reaches a maximum at 8 ML. (iv) As the Pd coverage increases from 1 to 4 ML, a concomitant increase in the total H_{upd} desorption charge is observed.

The aforestated trends are not concordant with the behavior of Pd_{CPD} films of corresponding coverages. The reason for some of the counterintuitive behavior of Pd_{PSD} films remains to be uncovered in future studies.

The intrinsic smoothness of the prepared films can be compared using terrace-to-step charge ratios ($Q_{Hupd,terrace}/ Q_{Hupd,step}$) for H_{upd} desorption. A decrease in the charge ratio, such as the one shown in the transition from 1 M to 4 ML (Figure 70), signifies that the Pd_{CPD} film surface becomes increasingly roughened up to 4 ML. A caveat to the interpretation of the terrace-to-step charge ratios is the fact that the decrease in the terrace- and step-site charges can also be brought about by the increasing dominance of bulk-like behavior at higher coverages. This case is illustrated by comparing the terrace-to-step charge ratios of 4 ML and 8 ML. It is very unlikely that the surface of an 8 ML film becomes smoother than that of a 4 ML film; this claim is supported by the fact the LEED pattern for an 8 ML film is more diffuse than that of a 4 ML film.

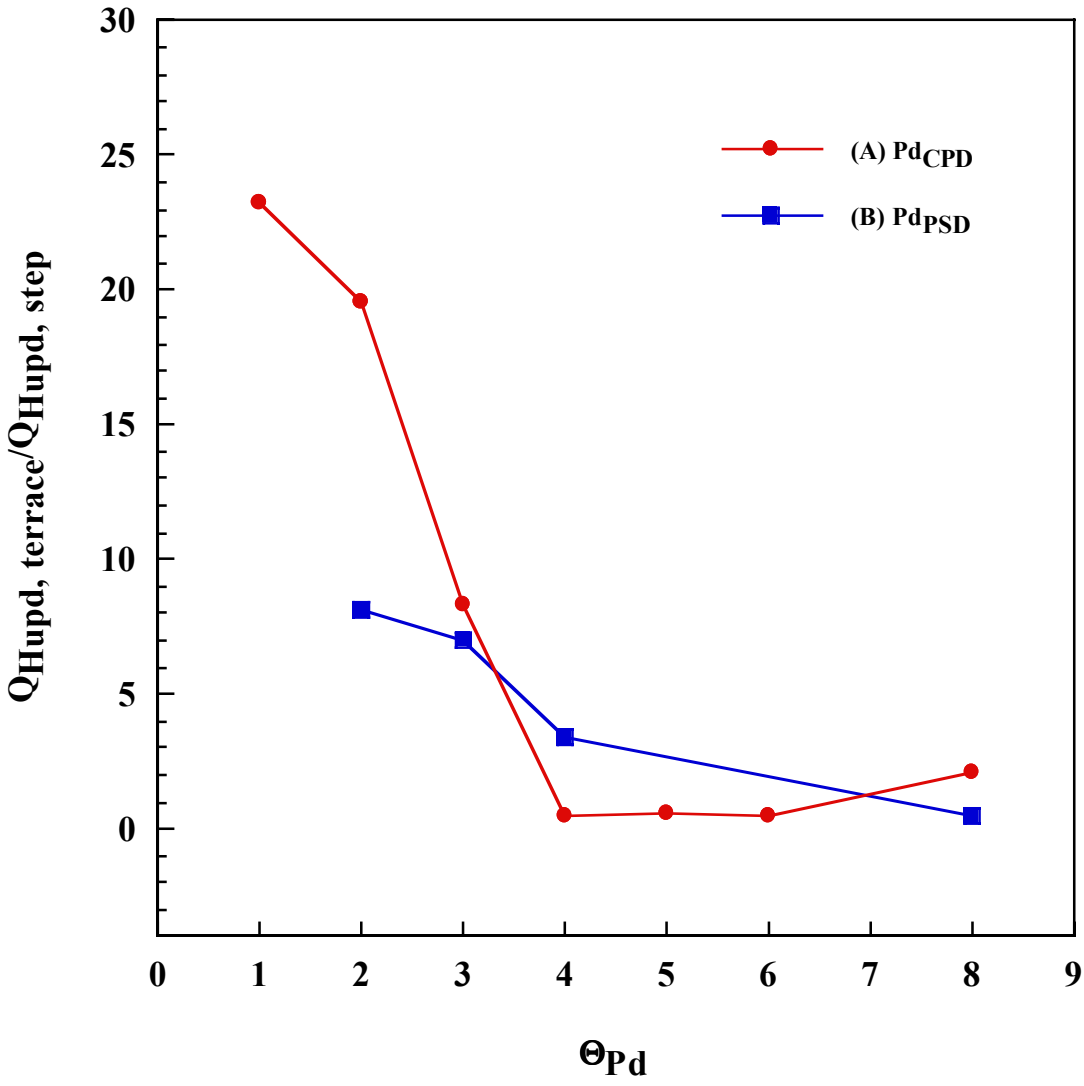

Figure 70. Ratio of terrace to step H_{upd} desorption charges versus Pd coverage. The charges were obtained from Figures 21 and 25.

The charge ratio for Pd_{PSD} films monotonically drops as the Pd coverage increases, implying a progression in the extent of surface roughening.

A quick comparison of the terrace-to-step charge ratios for PSD and CPD reveals that Pd_{CPD} films have smoother surfaces than Pd_{PSD} films up to 3 ML Pd. At 4 ML, Pd_{PSD} films are smoother than Pd_{CPD} films. At high coverages (8 ML), both yield rough surfaces.

Thermal Annealing of Ultrathin Pd Films

Smoothening effects by thermal annealing on the electrodeposited Pd_{CPD} films (0.5 - 8 ML) are manifestly evidenced by the enhanced brightness and sharpness of LEED spots and the absence of step-related voltammetric peaks after thermal treatment.

By carefully annealing island-strewn Pd surfaces at 250 ^{o}C, smooth Pd adlayers of varying coverages can be prepared. The annealing temperature employed in this investigation is low enough to minimize interfacial mingling of Pt and Pd. Hence, the initial Pd coverage remains nominally the same after thermal annealing; the adlattice, at least for low coverages, also keeps its registry with the substrate as evidenced by the attainment of bright and sharp (1×1) LEED patterns.

An interesting ramification of the surface smoothening effect is the emergence of a diffuse $(\sqrt{3}\times\sqrt{3})R30°$ LEED pattern, starting at a Pd coverage of 3 ML, after thermal annealing. This pattern is associated with the formation of $PdSO_4$ whose genesis can be traced from the sulfate ions in the electrolyte solution. The precipitation of $PdSO_4$ is typically not a nuisance side-reaction for relatively smooth surfaces (like 1 ML or 2 ML)

since the physisorbed precipitate can be readily removed by multiple rinsing. Surfaces teeming with steps (typified by 3 ML) can, however, effectively retain $PdSO_4$, thereby circumventing its removal by rinsing. Thermal annealing removes these surface imperfections and puts forth the precipitate onto the surface in an orderly array. The formation of $PdSO_4$ is evidenced by the presence of small sulfur and oxygen peaks in the post-annealing AES spectra. This hypothesis can be further tested by rinsing the surface after thermal treatment, in order to probe the possible removal of the ordered surface-segregated $PdSO_4$. Surface smoothening also allows access to island-free Pd coverages greater than 1 ML. These smoothened surfaces can be used to investigate the threshold Pd coverage at which thin-film behavior (represented by H_{upd} adsorption/desorption) can still be observed, without having to distinguish step and terrace signals. A Pd coverage of 3 ML marks the inception of bulk-like behavior as manifested by the disappearance of H_{upd} adsorption/desorption peaks.

Electrochemical Annealing of Ultrathin Pd Films

Potential cycling can be considered a form of non-thermal annealing that induces surface smoothening of Pd films. Two different potential windows were investigated: (i) between the inception of the HER and double-layer charging and (ii) between HER and Pd-film oxidation.

Potential cycling between the HER and double-layer regions induces only slight surface smoothening of Pd films, regardless of film preparation methods. For both 4 ML Pd_{CPD} and 4 ML Pd_{PSD} films, the first potential cycle yields slightly sharper terrace and

step H_{upd} adsorption/desorption peaks. Further potential cycling brings about only minimal changes in voltammetric features, implying little morphological changes in the Pd film surface.

Potential cycling between the HER and Pd-surface oxidation regions was examined. Using 4 ML Pd_{CPD} film as a prototypical island-rich system, the 1st potential cycle increases the number of surface steps as indicated by the fact that the step-related voltammetric peaks (–0.30 V and 0.48 V) are much larger than terrace-related peaks. At the 2nd potential cycle, changes in the voltammetric peaks suggest a competition between the growth of terraces and steps. The occurrence of Pd stripping exposes a surface with slightly more Pd islands and thinner Pd terraces than during the first cycle as indicated by the increase in the step Pd oxidation peak size. Between the 3rd and 5th potential cycles, step-related peaks continue to diminish while the peaks associated with the terraces become more pronounced. At the 8th potential cycle, both terrace and step H_{upd} adsorption/desorption peaks decrease dramatically while the step Pd oxidation peak is not observed. These results imply the existence of a very low coverage of Pd film.

As the number of potential cycle increases, more Pd adatoms are removed. Evidence is provided by the progressive decline in the Pd reduction peak at 0.18 V and the concomitant increase in the Pt reduction peak at 0.24 V. Analysis of the Pd Auger peak intensity corroborates this Pd stripping phenomenon. Figure 33 shows the dwindling Pd peak intensity as more potential cycles are performed. At the end of the 8th potential cycle, only submonolayer coverages of Pd remain on the Pt(111) surface.

Similar smoothening and stripping effects are observed during the electrochemical annealing of 4 ML Pd_{PSD} films. Interestingly, voltammetric features of 4 ML Pd_{CPD} film at the 8^{th} potential cycle resemble those of 4 ML Pd_{PSD} film at the 4^{th} potential cycle. Pd stripping is, therefore, more facile in 4 ML Pd_{PSD} films than in 4 ML Pd_{CPD} film. These results point to the fact that the imposition of a fixed potential during electrodeposition yields stable adlattices that approximate equilibrium structures, in contrast to potentiodynamically deposited films wherein surfaces are constantly perturbed by the ramped potential.

Interaction of Ultrathin Pd film with Bromide Electrolyte

The current investigation attempts to use bromide ions to interrogate the thin-film behavior of Pd adlayers electrodeposited via CPD and PSD.

Voltammetric features of both 1 ML Pd_{CPD} and 1 ML Pd_{PSD} films in 100 mM NaF (pH 4) are very similar to those of bulk Pd(111) [28], except for the existence of H_{upd} adsorption/desorption peak. The Pd redox peak sizes associated with thin films are about 3 times smaller than those of bulk Pd(111) [28]. The peak size difference stems from the smaller amount of Pd present on ultrathin Pd films.

In bromide-containing 100 mM NaF (pH 4), both 1 ML Pd_{CPD} and 1 ML Pd_{PSD} films share similar voltammetric features: (i) a pair of sharp H_{upd} adsorption/desorption peaks at –0.45 V; (ii) Pd oxidation peak at 0.35 V; (iii) a large voltammetric wave, starting at 0.55 V, corresponding to bromide-to-bromate oxidation; (iv) a small bromate-to-bromide reduction peak at 0.67 V; and (v) a broad Pt reduction peak at 0.18 V.

Subtle differences exist between the voltammetric features of thin films (1 ML Pd_{CPD} and 1 ML Pd_{PSD}) and bulk Pd(111) in the presence of bromide ions [28]. Bulk Pd typically exhibits a large Pd reduction peak at 0.10 V but does not show H_{upd} adsorption/desorption. The observance of Pd reduction peak current about 10 times larger than that of ultrathin Pd films is a natural consequence of the fact that bulk Pd offers a much larger supply of Pd atoms available for redox reactions than thin films do.

The notable enhancement of the Pd oxidation peak, along with the emergence of broad Pt reduction peak, in the presence of aqueous bromide, strongly suggests a bromide-induced Pd stripping phenomenon during the anodic scan.

Bromine Chemisorption

Bromine chemisorption was carried out by immersing 1 ML Pd films in bromide-containing 100 mM NaF (pH 4) at various constant potentials. Resulting adlayers were characterized using LEED and AES.

Under the present experimental conditions, bromine adsorption on 1 ML Pd film occurs at $E_{deposition} \geq -0.10$ V, regardless of the deposition method employed. Bromine adsorption is confirmed by the appearance of Auger Br peak at 102 eV and the observation of the characteristic $(\sqrt{3}\times\sqrt{3})R30°$-Br LEED pattern.

Bromine coverage strongly depends on the chemisorption potential. Potential-controlled chemisorption between –0.10 and 0.50 V yields the same characteristic $(\sqrt{3}\times\sqrt{3})R30°$-Br LEED pattern. Since Br chemisorption on Pd surfaces is known to be an oxidative process, potential excursions to positive regions are expected to increase

bromine coverage; it is, therefore, not surprising to see such trend within the chemisorption potential range of –0.10 to 0.22 V (Figure 41).

It can be seen in Figures 71 and 72 that the open circuit potential (0.22 V) corresponds to the inception of Pd dissolution into Pd^{2+} (Pd stripping). The drop in bromine coverage, from 0.22 V to 0.60 V, indicates that the adsorbed Br departs along with the stripped Pd. That the subsequent voltammetric Pd stripping peak is really small suggests that the amount of stripped Pd is also minuscule; hence, AES only detects a decrease in the Pd peak intensity at ca. 0.50 V or higher (Figures 45 and 46). As the Auger electron spectra would reveal, bromide-induced Pd stripping occurs without the formation of surface oxides.

To understand the Br coverage upturn at 0.60 V, it is essential to underscore two experimental observations: (i) This potential marks the onset of the oxidation of aqueous bromide to aqueous bromate. (ii) The Auger Pd signal intensity essentially remains the same from 0.60 to 0.80 V. It is believed that an increase in Br coverage leads to the accumulation of Br as part of a passivating $PdBr_2$ film in a manner akin to what has been previously observed in bulk Pd(111) [27,28]. The highly diffuse (1×1) LEED pattern probably emanates from the Pd film covered with the passivating $PdBr_2$ layer. It is also important to note that the measured Br coverage at 0.80 V would have given rise to the usual $(\sqrt{3}\times\sqrt{3})R30°$ pattern, but its absence indicates that the bromine is incorporated, in a disordered fashion, into the passivating film. The nature of this passivating film requires further elucidation.

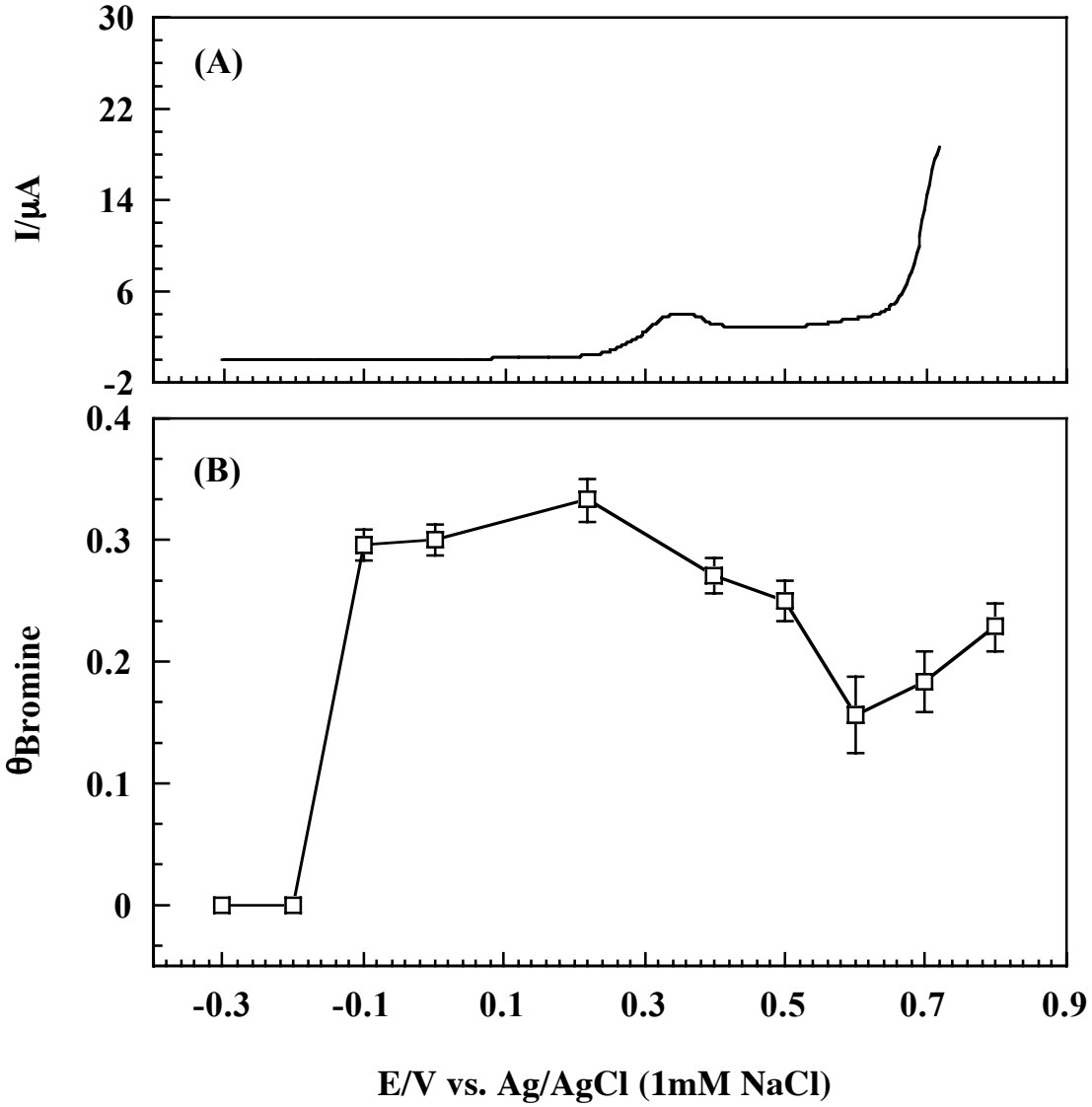

Figure 71. Correlation between Br coverage and voltammetric features of 1 ML Pd_{CPD} film in bromide-containing electrolyte. (A) is a segment of Figure 37 and (B) is a reproduction of Figure 41.

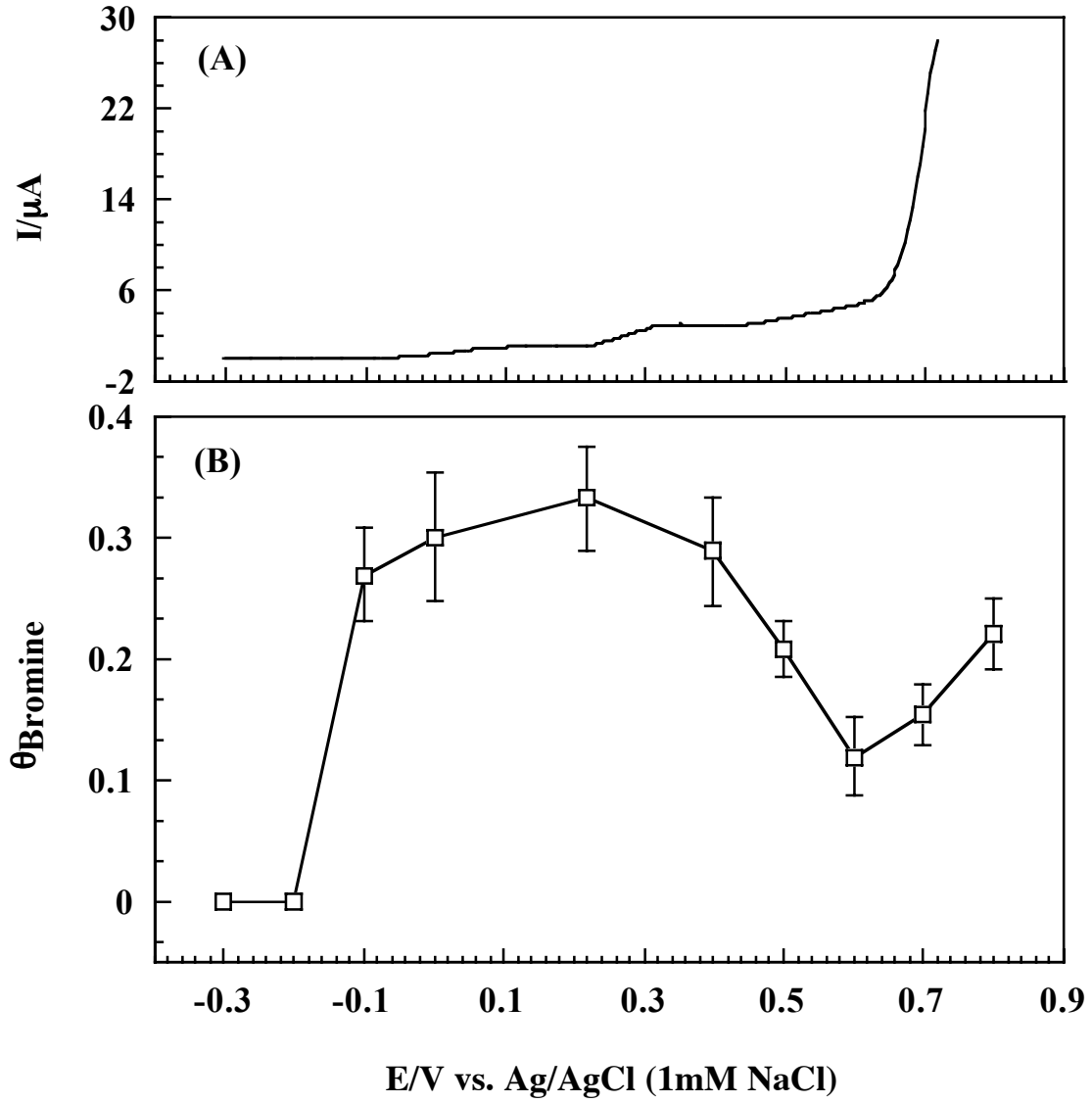

Figure 72. Correlation between Br coverage and voltammetric features of 1 ML Pd_{PSD} film in bromide-containing electrolyte. (A) is a segment of Figure 38 and (B) is a reproduction of Figure 42.

Electrochemical Annealing of Ultrathin Pd Films in Bromide Solution

Iodine chemisorption induces spontaneous disorder-to-order reconstruction of Pd surface, most probably due to the formation of interfacial clustered structures, facilitated by the unusual mobility of interfacial Pd atoms [54]. Reordering extensively roughened Pd surface requires multiple cycles of iodine adsorption-desorption at potentials within the double-layer region. Bromine has chemical properties similar to iodine and forms well-ordered adlayers on Pd surface. It can, therefore, be surmised that bromine chemisorption can induce Pd surface smoothening by enhancing the surface diffusion of the Pd island atoms to sites of minimum surface free energy. Considering that the adsorption energy of bromine on Pd is lower than that of iodine on Pd [54], bromine adsorption-desorption would be expected to require more numerous potential cycles than that by iodine adsorption-desorption to achieve optimal surface smoothening effects.

Chemisorbed bromine-induced surface-smoothening effects were scrutinized by electrochemically annealing Pd_{CPD} films in bromide-containing 100 mM NaF (pH 4). Smoothening effects are adjudged based on: (i) the widening of terraces and the disappearance of step sites and (ii) the enhancement of surface order evaluated by LEED.

Surface imperfections are readily removed from 1 and 2 ML Pd_{CPD} films. The relative ease of smoothening is a consequence of the fact that the pre-annealed surfaces bear only very few step sites. 3 ML and 4 ML Pd_{CPD} films are initially strewn with three-dimensional islands; thus, a single potential cycle is inadequate to effectuate complete smoothening. Two cycles of EC annealing produce the same effect as the first one,

suggesting that more EC annealing cycles provide minimal changes in the surface order of Pd films.

EC annealing of a 5 ML Pd_{CPD} film leads to the formation of a completely smooth surface, as evidenced by the absence of step H_{upd} adsorption/desorption peaks. This result is not unexpected because the Pd island density in the 5 ML Pd_{CPD} film is initially low, as indicated by the small pre-EC-annealing terrace H_{upd} and step H_{upd} adsorption/desorption peaks. EC annealing induces the adatoms of small Pd islands to fill the gaps between them, resulting in a completely smooth film of high Pd coverage.

The emergence of bulk-like properties is monitored by the extinction of the voltammetric H_{upd} dsorption/desorption peaks. Step-related H_{upd} adsorption/desorption peaks are not useful for this purpose since their diminution may also imply surface smoothening. The post-annealing decrease in the signal intensity of terrace-related H_{upd} peaks is a more useful signpost for the onset of bulk-like properties.

Pd_{CPD} films begin to manifest bulk-like properties, after EC annealing, at a Pd coverage of 3 ML. If the post-EC-annealed 3 ML Pd_{CPD} film were to behave purely like thin films, the terrace H_{upd} adsorption/desorption peaks would have increased due to the lowering of Pd island density; however, a decrease in the terrace H_{upd} adsorption/desorption peak intensity is noted, signifying the start of bulk-like behavior.

Chemisorbed Bromine-Induced Anodic Dissolution of Ultrathin Pd Films

Ultrathin Pd films, unlike bulk Pd, readily undergoes anodic dissolution in the presence of chemisorbed bromine [27,31]. Such corrosive effects are examined using a 5

ML Pd_{CPD} film coated with bromine that is chemisorbed at 0.22 V for 3 minutes. The resulting film is then transferred to a Br^--free 100 mM H_2SO_4. The potential is scanned from the open circuit potential to the potential tail-end of the Br_{ads}-induced Pd dissolution wave (typically ranging from 0.58 to 0.62 V). Before another dissolution cycle is launched, bromine is re-adsorbed to the Pd film.

Br_{ads}-induced dissolution cycles promote the removal of both Pd and Br_{ads} (Figure 73). Pd coverage decreases drastically (1.9 ML) at the 1st cycle and then decreases gradually in almost linear fashion (0.8 ML/cycle) between 2nd and 4th cycles. The 5th cycle, however, results only in a slight decrease in Pd coverage, compared to the 4th cycle.

After each dissolution cycle, the remnant Br_{ads} adlayer is less than a full coverage of 0.33 ML; this case is unlike the I_{ads}-induced dissolution where the remnant I_{ads} adlayer retains its original structure and coverage. The remnant Br_{ads} coverage is practically the same between 1st and 3rd cycles, but it decreases gradually thereafter. It is interesting to note that, after one cycle, the resulting surface remains oxide-free and exhibits significant long-range order. A significant degree of surface order is still preserved after the 5th cycle as evidenced by the acquisition of a diffuse $(\sqrt{3}\times\sqrt{3})R30°$-Br pattern.

Interestingly, after the 1st cycle, LEED pattern changes from very diffuse to slightly diffuse $(\sqrt{3}\times\sqrt{3})R30°$-Br adlayer structure and Pd coverage decreases a lot. Between 2nd and 4th cycles, however, Pd coverage decreases almost linearly with cycle while maintaining LEED patterns similar to that of the 1st cycle. Remnant Br_{ads} coverage is practically the same between 1st and 3rd cycles while it shows further gradual decrease

with cycle, as Pt(111) substrate surface is exposed more, between 4th and 5th cycles. These observations suggest that (i) Br_{ads} desorption occurs from the step Pd atoms; no Br desorption takes place from the terrace Pd atoms, (ii) Br_{ads}-induced dissolution of smooth Pd proceeds in layer-by-layer fashion, and (iii) only after all of the Pd is dissolved will the Br_{ads}, which then resides on the Pt(111) substrate, be oxidatively desorbed.

Br_{ads} desorption starts at the early stage of Pd film corrosion. This finding is derived from the fact that both Auger Pd and Br peak intensities decrease upon fixing the potential of the bromine-coated 5 ML Pd_{CPD} film at 0.41 V for 2 to 7 minutes after potential scanning from 0.22 to 0.41 V. The rate of Pd stripping is higher than the rate of Br desorption as can be gleaned from the time-dependent changes of the Pd and Br coverages. When the potential was held at 0.41 V, a very rough surface is obtained, experiment does not induce oxide formation, as evidenced by the absence of the Auger O peak.

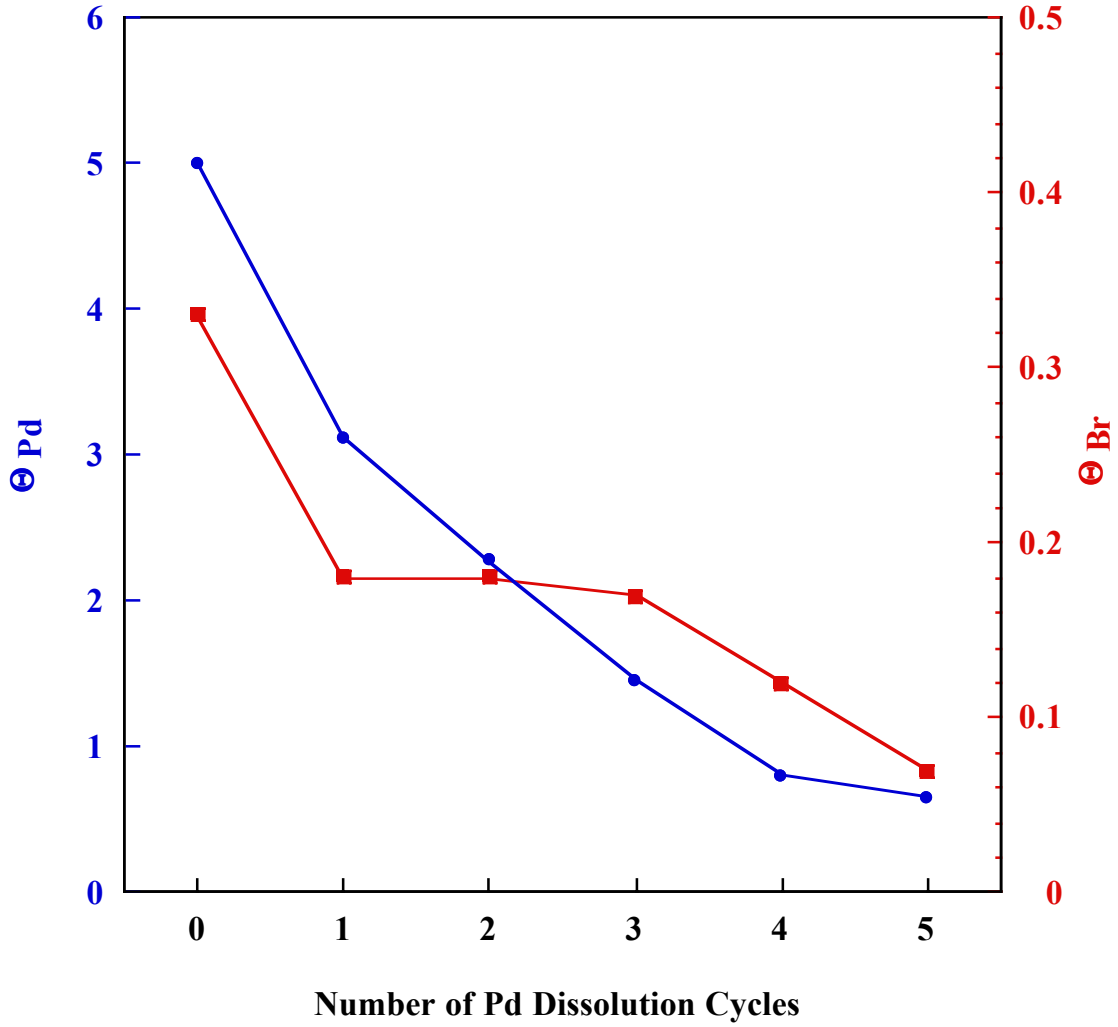

Figure 73. Changes in Pd and Br coverages during the process of 5 cycles of Br_{ads}-induced Pd film dissolution. Experimental conditions were as in Figure 63.

CONCLUSIONS

The present research has established experimental protocols in the electrochemical preparation of ultrathin Pd films on Pt(111). The preparation of various Pd coverages, ranging from submonolayer to multilayer quantities, has been effectively fine-tuned by employing spontaneous deposition, constant potential deposition (CPD) and potential-sweep deposition (PSD). The tandem use of surface science tools and conventional electrochemical techniques allowed the formulation of atomic-level descriptions of the interfacial structure and electrochemistry of the prepared films in sulfuric acid and in aqueous bromide solutions. The accumulated spectroscopic, voltammetric and coulometric data lead to the following conclusions:

(i) CPD and PSD produce Pd thin films that manifest different degrees of surface order, stability toward potential cycling and halide-induced corrosion, and ultrathin-film-to-bulk transitional behavior.

(ii) At a Pd coverage (Θ_{Pd}) of 1 ML, the electrodeposited film completely covers the Pt(111) substrate and conforms to its initial surface morphology.

(iii) At Θ_{Pd} higher than 1 ML, three-dimensional island formation and growth are indicated. The electrodeposited Pd films assume a Stranski-Krastanov growth mode.

(iv) Voltammetric peaks associated with H_{upd} adsorption/desorption on terrace- and step-sites are surface-sensitive indicators of the thin-film-to-bulk

transition, as well as the extent of surface order; bulk Pd is deprived of such surface processes.

(v) Thermal annealing, at temperatures below Pt-Pd interfacial diffusion, allows access to smooth, step-free thick films (1 ML < Θ_{Pd} ≤ 8 ML) which are erstwhile dotted with islands during electrodeposition.

(vi) Almost paralleling the diagnostic ability of LEED in UHV conditions, signal intensity diminution of step-related H_{upd} adsorption/desorption voltammetric peaks is a useful *in situ* criterion for assessing surface smoothness during electrochemical annealing.

(vii) In contrast to thermal annealing, electrochemical annealing at potentials between the hydrogen evolution and the double-layer regions, or Pd film oxidation regions, has minimal smoothening effects on the electrodeposited Pd films.

(viii) Room-temperature electrochemical cycling within the double-layer region, in the presence of surface-active aqueous Br^-, promotes smoothening of ultrathin Pd surfaces just like thermal annealing.

(ix) Based on voltammetric peaks associated with H_{upd} adsorption/desorption on terrace sites, Pd films begin to manifest bulk-like properties at a Pd coverage of 3 ML provided the film is atomically smooth and essentially defect-free; for non-annealed surfaces, non-bulk like behavior is shown even at higher coverages,

(x) The presence of aqueous bromide catalyzes the anodic oxidation of ultrathin Pd films.

(xi) The potential dependence of Br coverage on ultrathin Pd films is not as of straightforward as what has been observed on bulk-state Pd. The onset of the anodic stripping (dissolution) of Pd creates a spike in the adsorption isotherm because, as the stripping progresses, bromine desorption accompanies the dissolution of the step Pd atoms. The decrease in bromine coverage is not monotonic since the formation of a passivating $PdBr_2$ precipitate causes the bromine coverage to increase.

(xii) Auger electron spectroscopy reveals that the aqueous-bromide-induced anodic stripping of Pd occurs without the formation of surface oxides. The constancy in the Auger Pd signal intensity marks the formation of the passivating $PdBr_2$ film.

(xiii) In bromide-free solution, chemisorbed bromine (Br_{ads}) induces the anodic dissolution of Pd.

(xiv) Both Pd and Br_{ads} are removed by Br_{ads}-induced anodic dissolution cycles. Bromine desorption occurs during the early stage of Pd stripping due to dissolution of step Pd atoms. At the end of the dissolution of the step Pd atoms, a significant amount of Br_{ads} ($\theta_{Br} < 0.33$ ML) still remains on the film terrace. This scenario is similar to that of I_{ads}-induced corrosion in which the chemisorbed iodine retains both the original structure and coverage although,

in contrast, iodine desorption does not accompany the dissolution of the step Pd.

(xv) Atomically smooth, well-defined ultrathin Pd films can be prepared by CPD followed by multiple electrochemical cycles at double-layer region and reductive removal of Br_{ads}, by simple emersion at $E_{HER} < E < E_{DL}$, in dilute Br^- solution. Similar smoothening effects were previously demonstrated using the chemisorption of iodine onto ultrathin Pd_{CPD} films, from dilute I^- solution, followed by reductive desorption of I_{ads} in iodide-free solution at pH 10 and potential just before E_{HER}.

REFERENCES

[1] A.J. Bard, L.R. Faulkner, Electrochemical Methods: Fundamentals and Applications, John Wiley & Sons, New York, 1980.

[2] J.H. Sinfelt, Bimetallic Catalysts: Discoveries, Concepts, and Applications, John Wiley and Sons, New York, 1983.

[3] D.W. Goodman, J.A. Rodriguez, Science 257 (1992) 897.

[4] G.A. Somorjai, Introduction to Surface and Catalysis, John Wiley, New York, 1994.

[5] M. Han, P. Mrozek, A. Wieckowski, Phys. Rev. B 48 (1993) 8329.

[6] M.J. Ball, C.A. Lucas, N.M. Markovic, V. Stamenkovic, P.N. Ross, Surf. Sci. 518 (2002) 201.

[7] F.R. Hartley, The Chemistry of Platinum and Palladium, John Wiley and Sons, New York, 1973.

[8] A.R. West, Solid State Chemistry and Its Applications, John Wiley and Sons Pte. Ltd., Singapore, 1989.

[9] W.R. Tyson, Canadian Metal Q. 14(1975) 307.

[10] M.J. Llorca, J.M. Feliu, A. Aldaz, J. Clavilier, J. Electroanal. Chem. 351 (1993) 299.

[11] G.A. Attard, R. Price, A. Al-Akl, Electrochim. Acta 39 (1994) 1525.

[12] G.A. Attard, R. Price, Surf. Sci. 335 (1995) 63.

[13] N.M. Markovic, C.A. Lucas, V. Climent, V. Stamenkovic, N.R. Ross, Surf. Sci. 465 (2000) 103.

[14] M. Arenz, V. Stamenkovic, T.J. Schmidt, K. Wandelt, P.N. Ross, N.M. Markovic, Surf. Sci. 506 (2002) 287.

[15] B. Alvarez, V. Climent, A. Rodes, J.M. Felieu, J. Electroanal. Chem. 497 (2001) 125.

[16] N.M. Markovic, T.J. Schmidt, B.N. Grgur, H.A. Gasteiger, R.J. Behm, P.N. Ross, J. Phys. Chem. B 103 (1999) 8568.

[17] G.-Q. Lu, A. Crown, A. Wieckowski, J. Phys. Chem. B 103 (1999) 9700.

[18] D.A.J. Rand, R. Wood, J. Electroanal. Chem. and Inter. Electrochem. 44 (1973) 83.

[19] G.A. Attard, A. Bannister, J. Electroanal. Chem. 300 (1991) 467.

[20] J. Clavilier, M.J. Llorca, J.M. Feliu, A. Aldaz, J. Electroanal. Chem. 310 (1991) 429.

[21] R. Hoyer, L.A. Kibler, D.M. Kolb, Electrcochim. Acta 49 (2003) 63.

[22] R. Hoyer, L.A. Kibler, D.M. Kolb, Surf. Sci. 562 (2004) 275.

[23] M.J. Llorca, J.M. Feliu, A. Aldaz, J. Clavilier, J. Electroanal. Chem. 376 (1994) 151.

[24] M. Baldauf, D.M. Kolb, J. Phys. Chem. 100 (1996) 11375.

[25] V. Clement, N.M. Morkovic, P.N. Ross, J. Phys. Chem. B 104 (2000) 3116.

[26] A. Al-Akl, G.A. Attard, J. Phys. Chem. B 101 (1997) 4597.

[27] A. Carrasquillo, Jr., Ph.D. Dissertation, Texas A&M University, 1995.

[28] R.J. Barriga, Ph.D. Dissertation, Texas A&M University, 1998.

[29] M.P. Soriaga, J.A. Schimpf, A. Carrasquillo, Jr., J.B. Abreu, W. Temesghen, R.J. Barriga, J.-J. Jeng, K. Sashikata, K. Itaya, Surf. Sci. 335 (1995) 273.

[30] Y.-G. Kim, M.P. Soriaga, J. Phys. Chem. B 102 (1998) 6188.

[31] E.A. Lafferty, Ph.D. Dissertation, Texas A&M University, 1999.

[32] J.F. Rodriguez, M.E. Bothwell, G.I. Cali, M.P. Soriaga, J. Am. Chem. Soc. 112 (1990) 7392.

[33] M.E. Bothwell, G.J. Cali, G.M. Berry, M.P. Soriaga, Surf. Sci. 249 (1991) L322.

[34] Y.-G. Kim, J.H. Baricuatro, M.P. Soriaga, D.W. Suggs, J. Electroanal. Chem. 509 (2001) 170.

[35] E.A. Lafferty, Y.-G. Kim, M.P. Soriaga, Electrochim. Acta 44 (1998) 1031.

[36] M.P. Soriaga, Prog. in Surf.Sci. 39 (1992) 325.

[37] B. Shardt, Computation LEED patterns. Unpublished. M.P. Soriaga Laboratories, Texas A&M University, College Station, TX.

[38] E.A. Wood, J. Appl. Phys. 35 (1964) 1306.

[39] P. Auger, Compt. Rend. 180 (1925) 1939.

[40] D. Briggs, M.P. Seah (Eds.), Practical Surface Analysis by Auger and X-ray Photoelectron Spectroscopy, John Wiley & Sons, New York, 1983.

[41] L.B. Leder and J.A. Simpson, Rev. Sci. Inst. 29 (1958) 571.

[42] M.P. Seah, Surf. Interface Anal. 1 (1979) 86.

[43] J. Schimpf, M.S. Thesis, Texas A&M University, 1991.

[44] R.M. Lambert, Surf. Sci. 27 (1971) 653.

[45] A. Capon, R. Parsons, J. Electroanal. Chem. 65 (1975) 285.

[46] F. Kadirgan, B. Beden, J.M. Leger, C. Lamy, J. Electroanal. Chem. 125 (1981) 89.

[47] E. Bauer, Appl. Surf. Sci. 11/12 (1982) 479.

[48] J.-M. Zhang, F. Ma, K. Xu, Appl. Surf. Sci. 229 (2004) 34.

[49] J.M. Ball, C.A. Lucas, N.M. Markovic, V. Stamenkovic, P.N. Ross, Surf. Sci. 540 (2003) 295.

[50] Y. Li, Y.-T. Cheng, Int. J. Hydrogen Energy 21 (1996) 281.

[51] G.E. Gdowski, T.E. Felter, R.H. Stulen, Surf. Sci. 181 (1987) L147.

[52] K. Nobuhara, H. Kasai, H. Nakanishi, A. Okiji, J. Appl. Phys. 92 (2002) 5704.

[53] W. Dong, V. Ledentu, P. Sautet, A. Eichler, J. Hafner, Surf. Sci. 411 (1998) 123.

[54] M.P. Soriaga, Y.-G. Kim, J.E. Soto, in: A. Wieckowski (Ed.), Interfacial Electrochemistry: Theory, Experiment, and Applications, Marcel Dekker, New York, 1999, pp. 249-267.

VITA

YEON SU PARK
202-18 Onchon-2-dong,
Asan, Choongnam 336-012, Korea
yspman@hotmail.com

EDUCATION

Ph.D., Analytical Chemistry, Texas A&M University, May 2005.
M.S., Physical Chemistry, Korea University, February 1993.
B.S., Chemistry, Korea University, February 1991.

EXPERIENCE

Texas A&M University (September 1998 - present)

Research assistant

Electrochemical preparation of Pd thin films on Pt(111) surfaces, characterization of Pd film-bromine interfaces, and investigation of effects of chemisorbed bromine on Pd film corrosion by utilizing electrochemical and spectroscopic techniques

Teaching assistant

Instructor of undergraduate general chemistry and instrumental analysis laboratories

Hankook Tire R&D Center, Korea (February 1993 - June 1998)

Researcher/senior researcher

Qualitative, quantitative, and instrumental analyses of inorganic, organic, and polymer materials for batteries

Korea University, Korea (March 1991 - February 1993)

Research assistant

Investigation of electrochemical behavior of and catalytic O_2-reduction by self-assembled viologen layers on various electrode surfaces.

Teaching assistant

Instructor of undergraduate general chemistry and physical chemistry laboratories

HONORS

Martell Travel Award, Chemistry Department, Texas A&M University, Oct. 2002
Best Research Award of '97, Hankook Tire R&D Center, Korea, Dec. 1997
Top Professional Award, Hankook Tire R&D Center, Korea, Feb. 1995
Yangyoung Foundation Scholarship, Yangyoung Foundation, Korea, 1990